

INVESTIGATIONS OF C-H ACTIVATION AND THE CONVERSION OF  
METHANOL TO TRIPTANE

Thesis by

Valerie J. Scott

In Partial Fulfillment of the Requirements for the  
degree of

Doctor of Philosophy

CALIFORNIA INSTITUTE OF TECHNOLOGY

Pasadena, California

2011

(Defended February 14, 2011)

© 2011

Valerie J. Scott

All Rights Reserved

## ACKNOWLEDGEMENTS

I need to thank first and foremost my advisors John Bercaw and Jay Labinger. I really couldn't have asked for better people to learn from. Thanks for both allowing me to figure things out on my own and also for being there when I needed help. Not only are you both great chemists and advisors—you're also wonderful people and I consider myself incredibly lucky to have had the opportunity to work with you.

Thank you also to the rest of my committee: Harry Gray, Brian Stoltz, and Jackie Barton. You have each pushed me, given me valuable critiques, and I'm glad to have been able to get your help and input throughout my graduate career. Thank to Harry for many helpful chats, particularly in my last year here—thanks for cheering me on.

To the Bercaw group, past and present, I leave now with high standards for a working environment. Each and every one of you has contributed to my Caltech experience and made it all the more cheery, fun, and enlightening. I'm happy that I met all of you and hope to cross paths with you all in the future. I could write pages about how wonderful everyone in the group is and I will miss all of you very much.

I really need to thank Steve Baldwin—thanks for putting up with me over the last few years! I'm glad we had our little less-than-serious corner in the office—I could always count on you to poke me with a joke, a cartoon strip, or a funny article. To make it even better, I couldn't have asked for a better person to sit next to—thanks for always being willing to talk chemistry with me, read drafts of anything, and putting up with my endless questions. You've been a great friend and I've learned a lot from you.

To Nilay Hazari, thanks for giving me the chance to work with you during my first year in the Bercaw group. You were a great mentor and I took a lot from the time that we worked together. I can say with real confidence that you are, and will continue to be, an incredible advisor.

I'd also like to thank my undergraduate advisor, Oleg Ozerov. My time at Brandeis was ridiculously cool, mainly because of getting to work with you—I know most people don't get the experiences that I was able to get and I'll always be grateful. Thank you for continuing to be a presence in my life after Brandeis—your continued support has been of real value to me.

For my stay in the Peters' group, I'd like to thank Jonas and the rest of the group. In particular, Christine Thomas and Caroline Saouma made that stay intensely more fun than it would have been otherwise and have continued to be good friends.

Anna Beck, Mike Shearn, Tony Roy, Kristin Gleitsman, Matt Eichenfield, Sameer Walavalkar, Jess and Peter Clark—you guys are what makes Caltech awesome. You're the best and that's really all there is to it.

My family (all of it!) has been a huge support system for me throughout my entire education. They've always been there for me through every experience and I know I can count on them to be there for me in the future. My parents have always been my #1 cheerleaders in everything I do and it means a lot that they've been there with me through everything. There is nothing I can think of that accurately expresses my gratitude to them for everything they've ever done for me.

Last, but certainly not least, I'd like to thank my husband, Kent Kristof. Sitting next to me in the Crellin basement while I collected data on Daytona, having bottles of champagne prepped and ready for every obstacle I've had to cross, listening to me jabber about everything going on in the lab, actually being interested in what I'm saying, and being up for anything, you are my best friend. I couldn't have asked for more in a partner-in-crime; you've always got my back and I love you and can't thank you enough.

## ABSTRACT

Broadly speaking, this thesis represents research towards understanding the mechanisms and important species related to small molecule conversion, namely methane to methanol and methanol to higher hydrocarbons. The first section is on understanding the catalytic formation of methanol from methane, with specific interest in using gold (Au). While this transformation is known to occur catalytically, very little is understood about how it happens. To study this reaction, well-defined Au-complexes were synthesized and reactions relevant to the possible catalytic cycles were examined. In doing so, the first simple Au(III)-monoalkyl complex was generated and characterized: (Idipp)AuI<sub>2</sub>Me, where Idipp = 1,3-bis(2,6-diisopropylphenyl)imidazol-2-ylidene). Kinetics experiments demonstrated that the complex reductively eliminates methyl iodide, which is relevant to the functionalization step in CH activation. At low concentrations of iodide, the reductive elimination happens faster, from an unobserved 3-coordinate intermediate. However, at high iodide concentrations, the pathway is still consistent with reductive elimination, but from a 5-coordinate intermediate. This is in contrast to the related platinum-system, as well as to density functional theory calculations done on the Au-system.

The second section studies the C-H activation step alone by close examination of the microscopic reverse: protonation of a metal-alkyl. It had previously been noted that the observed kinetic isotope effects (KIEs) were unusually high for the protonolysis of a few Pd complexes and one Pt complex. It was hypothesized that these high KIEs and involvement of quantum mechanical tunneling may indicate a change in the mechanism of the protonolysis reaction, from protonation at the metal center and reductive coupling to

direct protonation of the M-Me bond. The experiments described here were designed to explicitly test this theory and demonstrated that no correlation can be made between mechanism and tunneling.

The third section is focused on the study of the conversion of methanol to highly branched alkanes that make good fuel additives, namely 2,2,3-trimethylbutane (triptane), amidst other alkanes, olefins, and aromatics. Catalyzed by  $\text{ZnI}_2$  or  $\text{InI}_3$  at high temperatures, the reaction is hydrogen deficient: aromatics are formed as unsaturated by-products necessary for alkane generation. While the product distributions are somewhat different for the two different catalysts, the general mechanism is the same. While typical  $\text{InI}_3$  reactions generate more alkanes, more aromatics, and fewer olefins than  $\text{ZnI}_2$  reactions, longer reaction times and higher temperatures make the  $\text{ZnI}_2$  reaction look like the  $\text{InI}_3$  profile. Furthermore,  $\text{InI}_3$  can activate alkanes; it was found that  $\text{InI}_3$  can “upgrade” other alkanes with methanol. Notably, a 1:1 mixture of 2,3-dimethylbutane and methanol can be converted into triptane with good selectivity and little aromatic formation;  $\text{ZnI}_2$  can carry out similar chemistry at higher temperatures. Quantification of the iodine-containing products in each reaction mixture was attempted because of its relevance to the system’s industrial viability and found that these concentrations were significantly higher than would be acceptable in an industrial setting.

## TABLE OF CONTENTS

Chapter 1 .....	1
Synthesis and characterization of Au(III)-monoalkyl complexes.....	1
1.1 Abstract.....	1
1.2 Introduction .....	1
1.3 Results and Discussion.....	4
1.3.1 Formation and characterization of (Idipp)AuI <sub>2</sub> Me .....	4
1.3.2 Other oxidants .....	9
1.4 Conclusions .....	12
1.5 Experimental Section .....	12
General considerations. ....	12
(Idipp)AuMe (A). ....	13
(Idipp)Au <sup>13</sup> CH <sub>3</sub> (A*). ....	13
(Idipp)AuEt (E).....	14
(Idipp)AuPh (F). ....	14
(Idipp)AuI <sub>2</sub> Me (B). ....	15
1.6 References .....	16
Chapter 2.....	20
Mechanism of reductive elimination methyl iodide from a novel gold(III)-monomethyl complex.....	20
2.1 Abstract.....	20



2.2 Introduction .....	20
2.3 Results and Discussion.....	23
2.3.1 Qualitative effects on the formation and decomposition of (Idipp)AuI <sub>2</sub> Me	23
2.3.2 Mechanistic alternatives .....	25
2.3.3 Kinetic studies on (Idipp)AuI <sub>2</sub> Me decomposition.....	28
2.4 Conclusions .....	32
2.5 Experimental Section .....	33
General considerations. ....	33
Kinetics experiments. ....	33
2.6 References .....	34
Chapter 3 .....	39
Investigations into the possible correlation of mechanism and tunneling for the protonolysis of M-Me complexes .....	39
3.1 Abstract.....	39
3.2 Introduction .....	39
3.3 Results and Discussion.....	43
3.4 Conclusions .....	54
3.5 Experimental Section .....	55
General considerations. ....	55
Kinetic isotope effect measurements. ....	55
NMR technique.....	56

<sup>1</sup> H NMR spectral data for protonation reactions. ....	57
3.6 References .....	58
Chapter 4.....	62
Understanding the mechanism of conversion of methanol to triptane by ZnI <sub>2</sub> and InI <sub>3</sub> .....	62
4.1 Abstract.....	62
4.2 Introduction .....	62
4.2.1 Methanol conversion and surprising selectivity for ZnI <sub>2</sub> -catalyzed conversion.....	62
4.2.2 Early mechanistic studies on ZnI <sub>2</sub> -catalyzed methanol conversion .....	63
4.2.3 Relative rates of methylation versus hydride transfer and selectivity for triptane .....	68
4.3 Results and Discussion.....	71
4.3.1 Investigating the differences between ZnI <sub>2</sub> and InI <sub>3</sub> catalyzed reactions.....	71
4.3.2 Quantifying iodine-containing products .....	76
4.4 Conclusions .....	79
4.5 Experimental .....	80
General considerations. ....	80
Standard reaction protocols. ....	80
4.6 References .....	81
Chapter 5.....	83
Alkane homologation with methanol catalyzed by InI <sub>3</sub> and ZnI <sub>2</sub> .....	83

5.1 Abstract.....	83
5.2 Introduction .....	83
5.3 Results and Discussion.....	87
5.3.1 Homologation of 2,3-dimethylbutane .....	87
5.3.2 Variation of reaction conditions .....	93
5.3.3 Effect of added adamantane on homologation.....	98
5.3.4 Mechanism .....	100
5.3.5 ZnI <sub>2</sub> -catalyzed alkane homologation.....	104
5.4 Conclusions .....	106
5.5 Experimental .....	107
General considerations. ....	107
Standard reaction protocols. ....	107
5.6 References .....	108

## TABLE OF CONTENTS

APPENDIX A .....	112
Crystallographic data.....	112
A.1 (Idipp)AuMe (A).....	112
A.2 (Idipp)AuEt (E) .....	118
A.3 (Idipp)AuPh (F).....	124
A.4 (Idipp)AuI <sub>2</sub> Me (B) .....	135
A.5 (Idipp)AuMeI(C <sub>4</sub> H <sub>4</sub> NO <sub>2</sub> ).....	145
A.6 (Idipp)AuBr <sub>2</sub> OTf.....	152
A.7 (VW <sup>OE<sub>t</sub></sup> )AuCl.....	160
A.8 (VW <sup>NMe<sub>2</sub></sup> )AuCl.....	165
A.9 (VW <sup>OE<sub>t</sub></sup> )AuBr <sub>3</sub> .....	171
A.10 [(VW <sup>OE<sub>t</sub></sup> ) <sub>2</sub> AuBr <sub>2</sub> ][PF <sub>6</sub> ] .....	176
A.11 [Ir(CO)(O,C-CHONMeCH <sub>2</sub> )Cl <sub>2</sub> I][AsPh <sub>4</sub> ] .....	183
A.12 [Ir(CO)I <sub>5</sub> ][AsPh <sub>4</sub> ] <sub>2</sub> .....	189
APPENDIX B.....	205
Rate law derivations for kinetic studies on (Idipp)AuI <sub>2</sub> Me .....	205
APPENDIX C.....	208
NMR and mass spectral data for (Idipp)Au-complexes.....	208
C.1 (Idipp)AuMe (A) <sup>1</sup> H, <sup>13</sup> C .....	208
C.2 (Idipp)AuEt (E) <sup>1</sup> H, <sup>13</sup> C .....	210
C.3 (Idipp)Au <sup>13</sup> CH <sub>3</sub> <sup>1</sup> H, <sup>13</sup> C.....	212

C.4 (Idipp)AuPh (F) $^1\text{H}$ , $^{13}\text{C}$ .....	214
C.5 $^1\text{H}$ spectrum of A + $\text{I}_2$ .....	216
C.6 HMBC spectrum for A + $\text{I}_2$ + KI .....	218
C.7 HMBC spectrum for A + $\text{Br}_2$ .....	219
C.8 HMBC spectrum for A + $\text{Cl}_2$ .....	220
C.9 HMBC spectrum for A + $\text{ICl}$ .....	221
C.10 FAB $\text{MS}^+$ spectrum of monomethyl species from A + $\text{Br}_2$ .....	222
C.11 FAB $\text{MS}^+$ spectrum of monomethyl species from A + $\text{Cl}_2$ .....	223
C.12 FAB $\text{MS}^+$ spectrum of monoalkyl species from E + $\text{Cl}_2$ .....	224
C.13 FAB $\text{MS}^+$ spectrum of F+ $\text{Cl}_2$ .....	225
APPENDIX D .....	226
Table of raw kinetic isotope effect data and Arrhenius plots and equations	226
D.1 Table of raw kinetic isotope effect data.....	226
D.2 General Considerations for Arrhenius plots .....	227
D.3 Arrhenius plot and equation for (cod)PtMe <sub>2</sub> .....	228
D.4 Arrhenius plot for (dppe)PdMe <sub>2</sub> with TFA .....	229
D.5 Arrhenius plot for <sup>t</sup> Bu <sub>2</sub> Cp <sub>2</sub> ZrMe <sub>2</sub> .....	230
D.6 Arrhenius plot for ZnMe <sub>2</sub> .....	231
D.7 Arrhenius plot for (Idipp)AuMe .....	232
APPENDIX E .....	233
Attempts to observe C-H activation using NHC-supported Au-complexes	233
E.1 Abstract .....	233

E.2 Introduction.....	233
E.3 Results and Discussion .....	235
E.3.1 Oxidation .....	235
E.3.2 Investigations into C-H activation .....	235
E.4 Conclusions.....	241
E.5 Experimental .....	241
General considerations. ....	241
E.6 References.....	242
APPENDIX F .....	245
Synthesis of novel (NHC)Au-complexes .....	245
F.1 Abstract .....	245
F.2 Introduction .....	245
F.3 Results and Discussion .....	246
F.4 Conclusions .....	253
F.5 Experimental Section.....	253
General considerations. ....	253
(VW <sup>OE<sub>t</sub></sup> )Br. ....	253
(VW <sup>NMe<sub>2</sub></sup> )Cl.....	254
(VW <sup>OE<sub>t</sub></sup> )AuCl. ....	254
(VW <sup>NMe<sub>2</sub></sup> )AuCl.....	255
(VW <sup>OE<sub>t</sub></sup> )AuBr <sub>3</sub> .....	255
F.6 References .....	255

APPENDIX G .....	257
Competitive activation of a methyl C-H bond of dimethylformamide at an Ir center	257
G.1 Abstract.....	257
G.2 Introduction .....	257
G.3 Results and Discussion.....	258
G.4 Conclusions .....	261
G.5 Experimental Section .....	261
General considerations. ....	261
[AsPh <sub>4</sub> ][Ir(CO) <sub>2</sub> I <sub>2</sub> ] (1). ....	262
[AsPh <sub>4</sub> ][Ir(CO)(κ <sup>2</sup> -(O,C)-CH <sub>2</sub> NMeCHO)Cl <sup>2</sup> I] (6) and [AsPh <sub>4</sub> ] <sub>2</sub> [Ir(CO) <sub>4</sub> X]	
where X = Cl or I (5).....	262
Structural data for 6. ....	262
G.6 References .....	263
APPENDIX H .....	265
Attempts to increase triptane yields in metal-iodide catalyzed methanol conversion by	
addition of an external hydride source .....	265
H.1 Abstract.....	265
H.2 Introduction .....	265
H.3 Results and Discussion.....	267
H.3.1 ZnI <sub>2</sub> -catalyzed reactions in glass vessels with substoichiometric amount of	
Ir.....	267
H.3.2 ZnI <sub>2</sub> -catalyzed reactions in the Zr-Parr reactor .....	270

H.3.3 Notes on working with a Zr-Parr reactor .....	272
H.3.4 Addition of an external hydrogen source to $\text{InI}_3$ -catalyzed MeOH conversion.....	273
H.4 Conclusions .....	275
H.5 Experimental Section .....	276
General considerations. ....	276
Glass bomb protocols. ....	276
Zr Parr reactor protocols.....	277
H.6 References .....	278
APPENDIX I .....	279
Synthesis and characterization of Fe and Co complexes of a new sterically demanding $\text{BP}_2\text{pz}$ ligand.....	279
I.1 Abstract .....	279
I.2 Introduction .....	279
I.3 Results and Discussion .....	284
I.3.1 Ligand synthesis .....	284
I.3.2 $[\text{PhBP}^{\text{tBu}}_2(\text{pz}^{\text{tBu}})]\text{Metal(II)-Halide}$ complexes .....	288
I.3.3 $[\text{PhBP}^{\text{tBu}}_2(\text{pz}^{\text{tBu}})]\text{Metal(I) Complexes}$ .....	291
I.3.4 Investigations toward an Fe-carbyne complex .....	297
I.3.5 Metal(III)-imide synthesis.....	300
I.3.6 Synthesis of $[\text{PhBP}^{\text{tBu}}_2(\text{pz}^{\text{tBu}})]\text{FeOSiPh}_3$ .....	302
I.3.7 Cationic complexes .....	304



I.4 Conclusions .....	306
I.5 Experimental Section.....	307
General considerations. ....	307
$\text{Ti}[\text{PhBP}^t\text{Bu}_2(\text{pz}^{t\text{Bu}})]$ (1). ....	308
$[\text{PhBP}^t\text{Bu}_2(\text{pz}^{t\text{Bu}})]\text{FeCl}$ (2).....	309
$[\text{PhBP}^t\text{Bu}_2(\text{pz}^{t\text{Bu}})]\text{CoI}$ (3).....	310
$[\text{PhBP}^t\text{Bu}_2(\text{pz}^{t\text{Bu}})]\text{CoCl}$ (4). ....	310
$[\text{PhBP}^t\text{Bu}_2(\text{pz}^{t\text{Bu}})]\text{FePMe}_3$ (5).....	311
$[\text{PhBP}^t\text{Bu}_2(\text{pz}^{t\text{Bu}})]\text{CoPMe}_3$ (6). ....	311
$[\text{PhBP}^t\text{Bu}_2(\text{pz}^{t\text{Bu}})]\text{CoNaI}$ (7).....	312
$[\text{PhBP}^t\text{Bu}_2(\text{pz}^{t\text{Bu}})]\text{CoN}^t\text{Bu}$ (8). ....	312
$[\text{PhBP}^t\text{Bu}_2(\text{pz}^{t\text{Bu}})]\text{FeOSiPh}_3$ (9).....	313
$\{[\text{PhBP}^t\text{Bu}_2(\text{pz}^{t\text{Bu}})]\text{Fe}(\text{THF})\} \{\text{BArF-24}\}$ (10).....	313
$[\text{PhBP}^t\text{Bu}_2(\text{pz}^{\text{Me}_2})]\text{CoI}$ (11).....	313
I.6 References .....	314

## LIST OF ILLUSTRATIONS

Figure 1.1 Anisotropically refined structure of (Idipp)AuMe (A). A benzene molecule and all protons have been omitted for clarity. Selected bond lengths and angles: Au-C1 2.038(5) Å, Au-C15 2.039(5) Å, C1-Au-C15 180.000(2)° .....	4
Figure 1.2 Anisotropically refined structure of (Idipp)AuEt (E). A benzene molecule and all protons have been omitted for clarity. Selected bond lengths and angles: Au-C1 2.0322(16) Å, Au-C28 2.0605(17) Å, C1-Au-C28 177.86(7)° .....	5
Figure 1.3 Anisotropically refined structure of (Idipp)AuEt (F). A benzene molecule and all protons have been omitted for clarity. Selected bond lengths and angles: Au-C1 2.0322(16) Å, Au-C28 2.0605(17) Å, C1-Au-C28 177.86(7)° .....	5
Figure 1.4 <sup>1</sup> H NMR spectrum of the reaction mixture formed from A + I <sub>2</sub> in CD <sub>3</sub> CN yielding (Idipp)AuI (D), MeI, and the proposed monomethyl species B.....	6
Figure 1.5 HMBC of the reaction of A with 10 KI and 10 I <sub>2</sub> in CD <sub>3</sub> CN.....	7
Figure 1.6 Overlay of <sup>13</sup> C NMR spectra resulting from labeled (blue) and unlabeled (red) reaction mixtures of (Idipp)AuMe + I <sub>2</sub> + xs KI. The doublet identified as B* corresponds to the NHC carbene signal, coupled to <sup>13</sup> CH <sub>3</sub> .....	8
Figure 1.7 Anisotropically refined structure of (Idipp)AuI <sub>2</sub> Me (B). A second molecule of B in the unit cell, co-crystallized I <sub>2</sub> , and all protons have been omitted for clarity. Selected bond lengths and angles: Au-C1A 2.116(11) Å, Au-C28A 2.185(11) Å, Au-I1A 2.5917(10) Å, Au-I2A 2.6092(10) Å, C1A-Au-C28A 177.9(4)°, C1A-Au-	

I2A 96.2(3) <sup>o</sup> , C1A-Au-I1A 90.3(3) <sup>o</sup> , C28A-Au-I2A 83.2(3) <sup>o</sup> , C28A-Au-I1A 90.4(3) <sup>o</sup> , I1A-Au-I2A 173.30(3) <sup>o</sup> .....	9
--	---

Figure 1.8 Anisotropically refined structure of (Idipp)AuMeI(NC<sub>4</sub>H<sub>4</sub>O<sub>2</sub>). All protons and

two molecules of acetonitrile have been omitted for clarity. Selected bond lengths

and angles: Au-C1A 2.128(3) Å, Au-C32 2.086(3) Å, Au-N3 2.051(2) Å, Au-I

2.5597(2) Å, C1-Au-N3 99.53(9)<sup>o</sup>, C1-Au-C32 177.37(10)<sup>o</sup>, C1A-Au-I 89.84(6)<sup>o</sup>,

C32-Au-N3 82.51(11)<sup>o</sup>, C32-Au-I 88.41(10)<sup>o</sup>, N3-Au-I 167.03(6)<sup>o</sup> ..... 11

Figure 2.1 Reaction monitored over time for (Idipp)AuMe + 1.06 eq. I<sub>2</sub>..... 23

Figure 2.2 Effect of [I<sub>2</sub>] on rate of decomposition of B..... 29

Figure 2.3 Effect of [I<sup>-</sup>] on rate of decomposition of B. ▲ = added LiI, ■ = buffered

experiments (I<sub>2</sub> + LiI)..... 30

Figure 2.4 Effect of [I<sup>-</sup>] (high [I<sup>-</sup>]) on rate of decomposition of B. ▲ = added LiI, ■ =

buffered experiments (I<sub>2</sub> + LiI)..... 31

Figure 2.5 Effect of [I<sup>-</sup>] (low [I<sup>-</sup>]) on rate of decomposition of B. ▲ = added LiI, ■ =

buffered experiments (I<sub>2</sub> + LiI)..... 31

Figure 3.1 Complexes for which KIEs of protonolysis were measured ..... 44

Figure 3.2 Arrhenius plot of (cod)PtMe<sub>2</sub> protonolysis ..... 53

Figure 4.1 Yield of 2-methyl-2-butene over time for ZnI<sub>2</sub> catalyzed methanol conversion at

200 °C. Each data point represents a separate experiment..... 74

Figure 4.2 Yield of aromatics over time for ZnI<sub>2</sub> catalyzed methanol conversion at 200 °C.

Each data point represents a separate experiment..... 75

Figure 4.3 Yield of 2-methyl-2-butene over time for $\text{InI}_3$ catalyzed methanol conversion at 170 °C. Each point represents a separate experiment. ....	76
Figure 4.4 GC trace of a reaction of $\text{ZnI}_2$ (7.52 mmol), MeOH (24.7 mmol), and $i\text{PrOH}$ (0.65 mmol) at 200 °C for 3 hours. A. ECD signal. B. FID signal. ....	78
Figure 5.1 Triptane selectivity against number of mmol of 2,3-dimethylbutane. Each point represents a separate experiment. ....	88
Figure 5.2 MS of DMB fraction from reaction between $\text{InI}_3$ , $^{13}\text{C}$ -labeled MeOH and DMB; 71 ((P-Me) $^+$ , $^{12}\text{C}_5\text{H}_{11}$ ), 72 ((P-Me) $^+$ , $^{12}\text{C}_4^{13}\text{CH}_{11}$ ), 76 ((P-Me) $^+$ , $^{13}\text{C}_5\text{H}_{11}$ ), 86 (P $^+$ , $^{12}\text{C}_6\text{H}_{13}$ ). ....	90
Figure 5.3 MS of the triptane fraction from a reaction between $\text{InI}_3$ , $^{13}\text{C}$ -labeled MeOH and DMB; 91 ((P-Me) $^+$ , $^{13}\text{C}_6\text{H}_{13}$ ), 86 (P $^+$ , $^{12}\text{C}_6\text{H}_{13}$ ) ....	90
Figure 5.4 Triptane yield and selectivity over time for a reaction containing 1:1 DMB:MeOH catalyzed by $\text{InI}_3$ . Each data point represents a different experiment. ....	94
Figure 5.5 Combined yield of 2-methyl and 3-methylpentane over time for a reaction containing 1:1 DMB:MeOH catalyzed by $\text{InI}_3$ . Each data point represents a different experiment. ....	95

## LIST OF ILLUSTRATIONS

Figure E.1 $^1\text{H}$ NMR spectra of the reaction of (Idipp)AuBr <sub>3</sub> and AgOTf in C <sub>6</sub> D <sub>6</sub> over time (red = 15 min, green = 5 days, blue = 9 days); blue spectrum (top) matches resonances for pure (Idipp)AuBr <sub>3</sub> and (Idipp)AuBr while green and red spectra do not. ....	238
Figure E.2 Anisotropically refined thermal ellipsoid representation of (Idipp)AuBr <sub>2</sub> OTf; hydrogen atoms have been omitted for clarity. Au-C1 Å; Au-Br1 Å; Au-Br2 Å; Br1-Au-C1 180.000°; Br2-Au-C1 180.000°; O2-Au-C1 180.000°; O2-Au-Br1 180.000°; Br2-Au-O2 180.000° .....	239
Figure F.1 (VW <sup>OE<sub>t</sub></sup> )Br and (VW <sup>NMe<sub>2</sub></sup> )Cl.....	246
Figure F.2 Anisotropically refined thermal ellipsoid representation of (VW <sup>OE<sub>t</sub></sup> )AuCl; hydrogen atoms have been omitted for clarity. Au-Cl1 2.2863 Å; Au-C1 1.9753 Å; Cl1-Au-C1 180.000° .....	247
Figure F.3. Anisotropically refined thermal ellipsoid representation of (VW <sup>NMe<sub>2</sub></sup> )AuCl with H <sub>2</sub> O molecule shown; hydrogen atoms other than those on H <sub>2</sub> O have been omitted for clarity with the exception of water hydrogen. Au-Cl1 2.2872 Å; Au-C1 1.9689 Å; C1-Au-Cl1 177.059° .....	248
Figure F.4. Anisotropically refined thermal ellipsoid representation of (VW <sup>OE<sub>t</sub></sup> )AuBr <sub>3</sub> ; hydrogen atoms have been omitted for clarity. Au-C2 2.0075 Å; Au-Br1 2.4208 Å; Au-Br2 2.4264 Å; Au-Br3 2.4455 Å; C2-Au-Br1 85.774°; C2-Au-Br2 90.227°; Br1-Au-Br3 92.913°; Br2-Au-Br3 91.004° .....	251

Figure F.5.	Anisotropically refined thermal ellipsoid representation of $[(VW^{OEt})_2AuBr_2][PF_6]$ ; hydrogen atoms and $PF_6$ have been omitted for clarity. Au-Br2 2.4254 Å; Au-C4 2.0410 Å; C4-Au-Br2 88.288 °; C4-Au-Br1 91.712 ° .....	252
Figure G.1	Anisotropically refined thermal ellipsoid representation of $[Ir(CO)(\kappa^2-CH_2N(CH_3)CHO)Cl_2I]^-$ , the anion of 6. The $[AsPh_4]^+$ cation is not shown, and phenyl and methyl hydrogen atoms have been removed for clarity. Selected bond distances and angles: Ir-C1 1.8221(12) Å; Ir-C3 2.0651(11) Å; Ir-I 2.76746(12) Å; C1-Ir-C3 95.23(5)°; C3-Ir-I 171.68(3)° .....	261
Figure I.1.	Ligands and the abbreviations used to denote them .....	280
Figure I.2.	Fe(IV)-imides supported by $[PhBP^{tBu}_2(pz')]^-$ .....	282
Figure I.3	New ligand design .....	283
Figure I.4.	3,5-di- <i>tert</i> -butylpyrazole .....	284
Figure I.5.	MM2 energy minimization of $[PhBP^{tBu}_2(pz^{tBu2})]^-$ and steric clash between 5- <i>tert</i> -butyl on the pyrazole and the phenyl substituent on the borane .....	285
Figure I.6.	Variable temperature NMR of $Tl[PhBP^{tBu}_2(pz)]^{19}$ .....	287
Figure I.7.	$^{31}P$ NMR spectra of $Tl[PhBP^{tBu}_2(pz^{tBu})]$ at room temperature .....	288
Figure I.8.	Anisotropically refined thermal ellipsoid representation of $[PhBP^{tBu}_2(pz^{tBu})]FeCl$ ; 2 molecules of toluene and hydrogen atoms omitted for clarity. Fe-N 2.1057(0.0020) Å; Fe-P1 2.4900(0.0009) Å; Fe-P2 2.4787(0.0011) Å; Fe-Cl 2.2645(0.0010) Å; N1-Fe-Cl 141.87(0.06)°; P1-Fe-P2 112.44(0.04)°; P1-Fe-N1 88.11(0.06)°; N1-Fe-P2 87.20(0.06)° .....	290

- Figure I.9. Isotropically refined thermal ellipsoid representation of  $\kappa^2$ -  
 $[\text{PhBP}^{\text{tBu}}_2(\text{pz}^{\text{tBu}})]\text{CoNaI}$ ; hydrogen atoms have been omitted for clarity. No bond  
length and angles are reported due to poor quality of the data set.....292
- Figure I.10.  $\{\kappa^2\text{-}[\text{PhBP}^{\text{tBu}}_2(\text{pz})]\text{CoNH}(\text{anthr})\}\{\text{Na}(\text{THF})_3\}^{25}$  .....293
- Figure I.11. Cyclic voltammetry of A)  $[\text{PhBP}^{\text{tBu}}_2(\text{pz}^{\text{tBu}})]\text{FePMe}_3$  and B)  
 $[\text{PhBP}^{\text{tBu}}_2(\text{pz}^{\text{tBu}})]\text{CoPMe}_3$  in THF containing 0.4 M TBAPF<sub>6</sub> using a glassy carbon  
electrode as the working electrode, a Pt wire as the auxiliary electrode, and  
Ag/AgNO<sub>3</sub> in THF as the reference electrode; plotted vs Fc/Fc<sup>+</sup>.....295
- Figure I.12. Anisotropically refined thermal ellipsoid representation of  
 $[\text{PhBP}^{\text{tBu}}_2(\text{pz}^{\text{tBu}})]\text{CoPMe}_3$ ; hydrogen atoms have been omitted for clarity. Co-N1  
2.0736(0.0057) Å; Co-P1 2.4260(0.0020) Å; Co-P2 2.4300(0.0020) Å; Co-P3  
2.2693(0.0021) Å; N1-Co-P3 134.38 (0.15)°; P1-Co-P2 113.00(0.07)°; P1-Co-N1  
89.83(0.15)°; N1-Co-P2 90.51 (0.15)°.....296
- Figure I.13. <sup>1</sup>H NMR spectra of  $[\text{PhBP}^{\text{tBu}}_2(\text{pz}^{\text{tBu}})]\text{CoPMe}_3$  at 25 °C (C<sub>6</sub>D<sub>6</sub>) and -40 °C  
(toluene-*d*<sub>8</sub>) .....297
- Figure I.14. Anisotropically refined thermal ellipsoid representation of  $\kappa^2$ -  
 $[\text{PhBP}^{\text{tBu}}_2(\text{pz}^{\text{tBu}})]\text{Co}(\text{PMe}_3)(\text{CN}^{\text{tBu}})$ ; 2 molecules of pentane and hydrogen atoms  
have been omitted for clarity. Co-C35 1.8707(0.0100) Å; Co-P1 2.3151(0.0032) Å;  
Co-P2 2.3515(0.0033) Å; Co-P3 2.2884(0.0033) Å; C35-Co-P1 103.08(0.32)°;  
C35-Co-P2 109.32(0.31)°; C35-Co-P3 91.86(0.33)°; P1-Co-P2 100.45(0.12)°; P1-  
Co-P3 115.02(0.12)°; P2-Co-P3 133.28(0.11)° .....299

- Figure I.15. Anisotropically refined thermal ellipsoid representation of  $[\text{PhBP}^{\text{tBu}}_2(\text{pz}^{\text{tBu}})]\text{FeN}^{\text{tBu}}$ ; solvent and hydrogen atoms have been omitted for clarity. Fe-N3 1.7312(0.0040) Å; Fe-N2 2.0327(0.0040) Å; Fe-P2 2.5931(0.0034) Å; Fe-P3 2.3986(0.0038) Å; C10-N3-Fe1 168.79(0.31)°; N2-Fe-N3 140.66(0.15)°; N2-Fe-P2 90.85(0.12)°; P2-Fe-P3 103.86(0.09)°; P3-Fe-N2 88.60(0.12)° ..... 301
- Figure I.16. Anisotropically refined thermal ellipsoid representation of  $[\text{PhBP}^{\text{tBu}}_2(\text{pz}^{\text{tBu}})]\text{FeOSiPh}_3$ ; solvent and hydrogen atoms have been omitted for clarity. Fe-O1 1.9710(0.0060) Å; Fe-N1 2.0832(0.0067) Å; Fe-P1 2.5432(0.0043) Å; Fe-P2 2.5457(0.0033) Å; Fe-O1-Si 162.25(0.39)°; N1-Fe-O1 133.32(0.25)°; N1-Fe-P1 88.04(0.19)°; P1-Fe-P2 109.93(0.12)°; P2-Fe-N1 89.04(0.19)° ..... 303
- Figure I.17. Anisotropically refined thermal ellipsoid representation of  $\{[\text{PhBP}^{\text{tBu}}_2(\text{pz}^{\text{tBu}})]\text{Fe}(\text{THF})\} \{\text{B}(\text{Ar}_\text{F})_4\}$ ; hydrogen atoms and  $\{\text{B}(\text{Ar}_\text{F})_4\}$  have been omitted for clarity. Fe-O 2.1441(0.0040) Å; Fe-N1 2.0604(0.0037) Å; Fe-P1 2.4921(0.0020) Å; Fe-P2 2.4829(0.0021) Å; O-Fe-N1 138.40(0.13)°; N1-Fe-P1 90.67(0.12)°; P1-Fe-P2 115.31(0.05)°; P2-Fe-N1 89.17(0.12)° ..... 306



## CHAPTER 1

### Synthesis and characterization of Au(III)- monoalkyl complexes

#### 1.1 Abstract

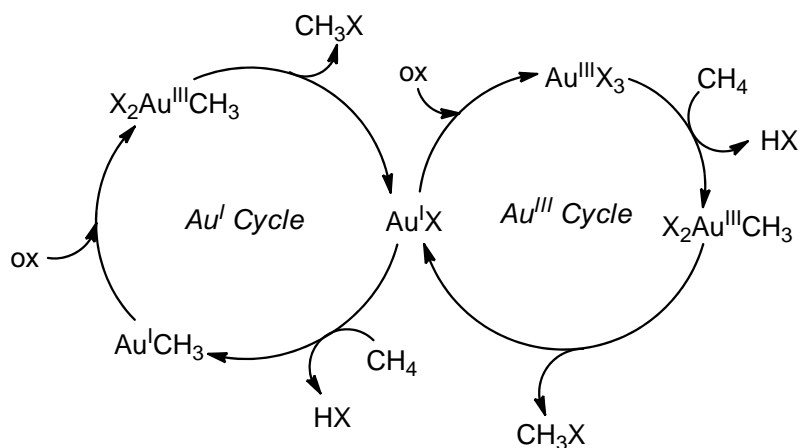
Oxidation of (Idipp)AuMe (Idipp = 1,3-bis(2,6-diisopropylphenyl)imidazol-2-ylidene) with various oxidants yields monomethyl Au(III) complexes. Namely, with I<sub>2</sub>, *trans*-(Idipp)AuI<sub>2</sub>Me is generated, which decomposes cleanly to MeI and (Idipp)AuI. Other oxidants demonstrate similar reactivity, however the transformations are not as clean. These complexes have been characterized by a series of 2-D NMR experiments, labeling studies, and X-ray crystallography.

#### 1.2 Introduction

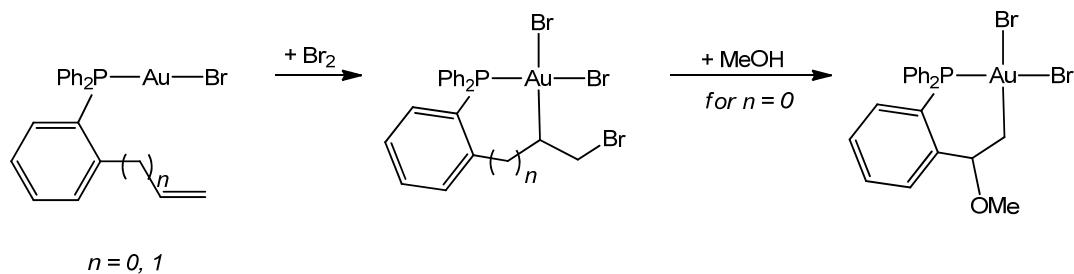
C-H activation has been an area of intense interest for many decades. Past work has focused largely on Pt- and Pd-based systems,<sup>1-8</sup> but recently the ability to use other metals has come to light, with Au-based catalysts among them.<sup>9-25</sup> These systems tend to be difficult to study mechanistically, so it has become commonplace for catalytic cycles to be proposed with little or no evidence for them. Two possible catalytic cycles based on redox chemistry are shown in Scheme 1.1; the Au(I)-cycle is analogous to Pt(II)-based C-H activation and the Au(III) cycle is analogous to what is generally proposed for Pd(II)-based C-H activation. It is notable that it is also possible to draw schemes that do not involve redox chemistry at the metal center. A commonly proposed intermediate in the activation of alkyl C-H bonds is a Au(III)-monoalkyl species. While this is a logical proposal, very few Au(III) complexes containing only one C-sp<sup>3</sup> bond are present in the literature so the

corresponding reactivity is uncharted; those that are known require special ligand frameworks (described below). Several Au(III)-monoaryl species are known,<sup>26-30</sup> but to the best of our knowledge, no simple Au(III)-monoalkyls are known<sup>24, 31-36</sup> and so their corresponding reactivity is unknown.

**Scheme 1.1**



From what is apparent in the literature, only a few special cases of Au(III)-alkyls have been reported, utilizing chelates and the perfluorinated  $-CF_3$  ligand over  $-CH_3$ . In 1971, an unusual example was reported by Bennet et al.,<sup>34</sup> upon reaction of  $LAuBr$  with  $Br_2$ , where  $L = 2$ -vinylphenyldiphenylphosphine or 2-allylphenyldiphenylphosphine, the Au species was oxidized to generate a chelating  $C-sp^3$  bond, with preference for forming the smaller possible ring (Scheme 1.2). Upon further reaction with methanol, the 5-membered ring undergoes expansion forming a new complex with a  $C-sp^3$  bond as part of the chelate.<sup>37</sup> Related complexes containing one  $Au-C-sp^3$  bond within a chelate have since been reported.<sup>24, 38</sup>

**Scheme 1.2**

Others based on the trifluoromethyl moiety have been reported;  $(\text{PR}_3)\text{Au}(\text{CF}_3)\text{X}_2$ , where  $\text{R} = \text{Me, Et, or Ph}$  and  $\text{X} = \text{I or Br}$ , are formed by oxidative addition of the halogen to the trifluoromethyl Au(I)-phosphine complex.<sup>35</sup> The related methyl complexes have been suggested as possible intermediates in reactions of Au(I)-halides with MeI, Au(I)-methyls with halogens, and Au(I)-acetate with alkyl halides, but again, no direct evidence was obtained.<sup>39, 40</sup>

The use of N-heterocyclic carbenes (NHCs) has grown immensely for a wide variety of complexes.<sup>41</sup> These species are frequently air stable and so are easily manipulated without the use of oxygen and water-free techniques. They tend to be thermally robust as compared with other ligand scaffolds, such as phosphines, which has often allowed for the isolation of complexes that otherwise could not have been observed. They have also demonstrated increased catalytic activities for many different systems. These characteristics are generally attributed to the fact that NHCs are exceptionally strong  $\sigma$ -donors, a trait that helps in the stabilization of many metal complexes. The generation of a Au(III)-monomethyl complex with an NHC ligand is described herein,  $(\text{Idipp})\text{AuI}_2\text{Me}$  ( $\text{Idipp} = 1,3\text{-bis}(2,6\text{-diisopropylphenyl})\text{imidazol-2-ylidene}$ ).<sup>42</sup> The characterization of this

complex was done by a series of 1- and 2-D NMR experiments, labeling studies, and X-ray diffraction experiments. Related reactions using other oxidants are also discussed.

### 1.3 Results and Discussion

#### 1.3.1 Formation and characterization of (Idipp)AuI<sub>2</sub>Me

(Idipp)AuMe (**A**) was prepared from (Idipp)AuCl and ZnMe<sub>2</sub> in benzene, and characterized by <sup>1</sup>H NMR spectroscopy, FAB<sup>+</sup> MS, and X-ray crystallography (Figure 1.1). (Idipp)AuEt (**E**, Figure 1.2) and (Idipp)AuPh (**F**, Figure 1.3) were prepared similarly. Zn-based reagents consistently gave better yields than other alkylating/aryllating reagents.

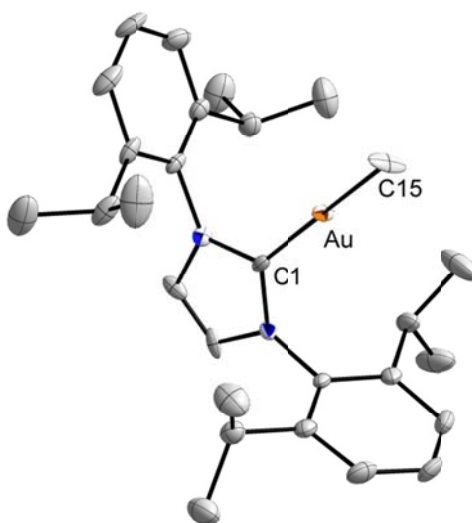


**Figure 1.1** Anisotropically refined structure of (Idipp)AuMe (**A**). A benzene molecule and all protons have been omitted for clarity. Selected bond lengths and angles: Au-C1 2.038(5) Å, Au-C15 2.039(5) Å, C1-Au-C15 180.000(2)°

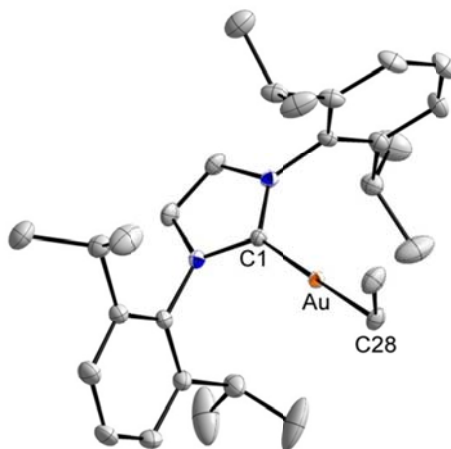


**Figure 1.2** Anisotropically refined structure of (Idipp)AuEt (**E**). A benzene molecule and all protons have been omitted for clarity. Selected bond lengths and angles: Au-C1 2.0322(16) Å, Au-C28 2.0605(17) Å, C1-Au-C28 177.86(7)°

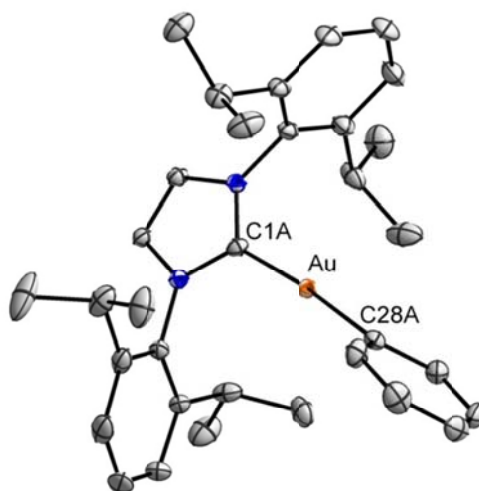


**Figure 1.3** Anisotropically refined structure of (Idipp)AuEt (**F**). A benzene molecule and all protons have been omitted for clarity. Selected bond lengths and angles: Au-C1 2.0322(16) Å, Au-C28 2.0605(17) Å, C1-Au-C28 177.86(7)°

Oxidation of **A** with  $I_2$  led to formation of two new (Idipp)Au species in addition to MeI (by  $^1H$  NMR spectroscopy; Figure 1.4). Over time, one of the two products converted into the other, shown by  $^1H$  NMR spectroscopy and  $FAB^+$  MS to be (Idipp)AuI (**D**). The  $^1H$  NMR ligand resonances of the unstable product **B** appeared at chemical shifts similar to those of (Idipp)AuBr<sub>3</sub>,<sup>43</sup> and quite different from those typical of (Idipp)Au(I) complexes. A singlet at  $\delta$  1.43 which disappeared with the other resonances attributed to **B** suggests a methyl-gold complex; furthermore, when no excess  $I_2$  was present, the reaction mixture was initially yellow, typical for Au(III), becoming clear and colorless (characteristic of Au(I)) over time. All these observations suggest that **B** is a monomethyl Au(III) complex.

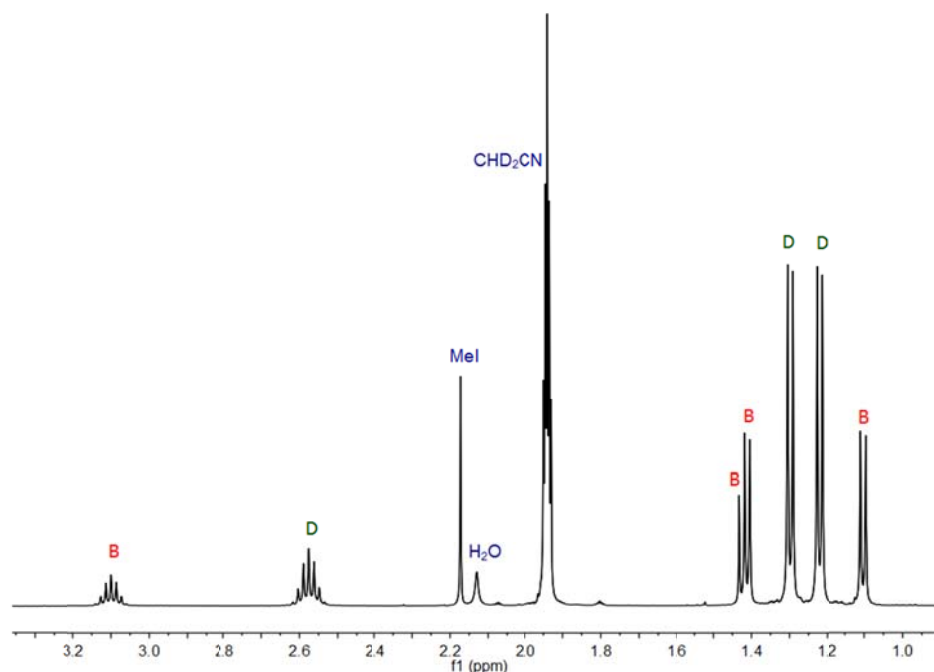


**Figure 1.4**  $^1H$  NMR spectrum of the reaction mixture formed from **A** +  $I_2$  in  $CD_3CN$  yielding (Idipp)AuI (**D**), MeI, and the proposed monomethyl species **B**

Further NMR support for this formulation was obtained from 2-D and isotopic labeling experiments. An HMBC experiment (Figure 1.5) carried out on a reaction mixture clearly showed two different carbene signals: one corresponded to **D** ( $\delta$  184.0), while the other ( $\delta$  182.3) showed 3-bond coupling to the  $^1\text{H}$  signal at  $\delta$  1.43. Isotopically labeled (Idipp)Au $^{13}\text{CH}_3$  was prepared from (Idipp)AuCl using the Grignard reagent obtained (in situ) from Mg(0) and  $^{13}\text{CH}_3\text{I}$ ; the carbene carbon signal appears as a doublet at  $\delta$  201, with  $^2J_{\text{CC}} = 32.5$  Hz. Upon oxidation with  $\text{I}_2$  in the presence of excess  $\text{I}^-$  to retard decomposition (see Chapter 2), the carbene signal for **B** could be identified by overlaying the spectra from the labeled and unlabeled reactions (Figure 1.6); here  $^2J_{\text{CC}} = 46.3$  Hz for coupling of the NHC carbon to the methyl C.  $^1J_{\text{CH}}$  is 120 Hz and 105 Hz in labeled **A** and **B**, respectively, for the methyl protons to the methyl carbon.

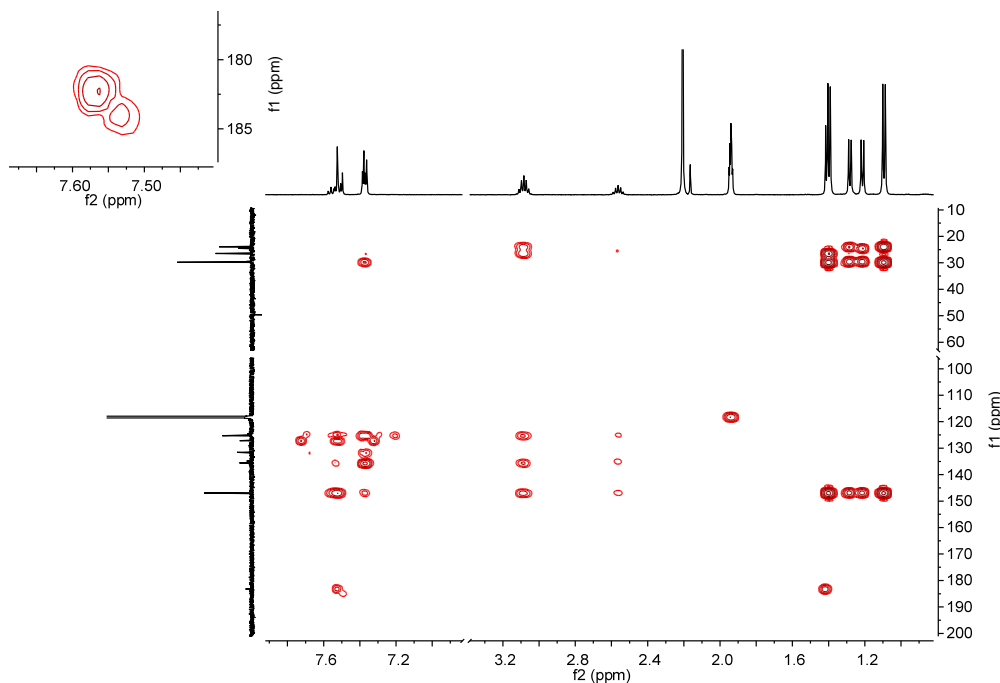


**Figure 1.5** HMBC of the reaction of **A** with 10 KI and 10  $\text{I}_2$  in  $\text{CD}_3\text{CN}$

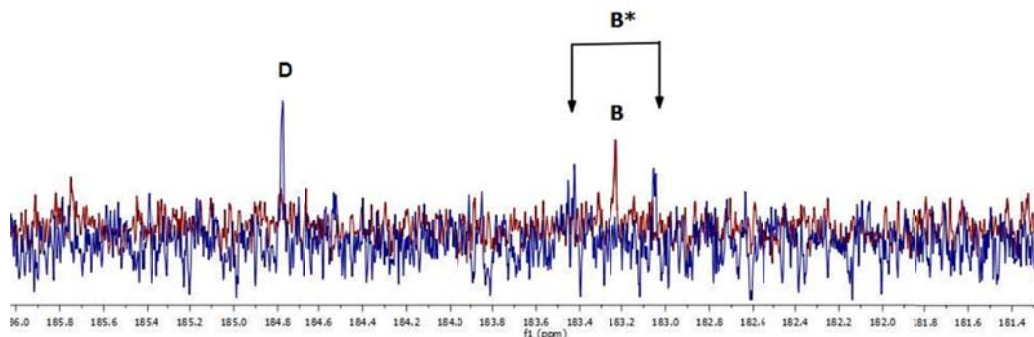


**Figure 1.6** Overlay of  $^{13}\text{C}$  NMR spectra resulting from labeled (blue) and unlabeled (red) reaction mixtures of (Idipp)AuMe +  $\text{I}_2$  + xs KI. The doublet identified as **B\*** corresponds to the NHC carbene signal, coupled to  $^{13}\text{CH}_3$ .

While yellow crystals, apparently of **B**, could be obtained on several occasions, crystallographic analysis never gave a structure corresponding to a pure species. In most cases the structures appeared to refine as *trans*-(Idipp)AuI<sub>2</sub>Me co-crystallized with small amounts of (Idipp)AuI, resulting in some iodide population in all 3 non-NHC positions; furthermore, the crystals were both temperature and X-ray sensitive. Crystals that were more thermally stable were grown from a concentrated solution of **B** and  $\text{I}_2$ , and these exhibited co-crystallization of  $\text{I}_2$  instead of **A**. Although they were also sensitive to X-rays, these crystals yielded a data set good enough to clearly identify **B** as *trans*-(Idipp)AuI<sub>2</sub>Me (Figure 1.7), although angles and bond lengths could not be determined with high precision.



Selected bond lengths and angles: Au-C1A 2.116(11) Å, Au-C28A 2.185(11) Å, Au-I1A 2.5917(10) Å, Au-I2A 2.6092(10) Å, C1A-Au-C28A 177.9(4)°, C1A-Au-I2A 96.2(3)°, C1A-Au-I1A 90.3(3)°, C28A-Au-I2A 83.2(3)°, C28A-Au-I1A 90.4(3)°, I1A-Au-I2A 173.30(3)°

Oxidation of **A** with Cl<sub>2</sub>, Br<sub>2</sub>, ICl, and N-iodosuccinimide (NIS) appears to proceed similarly to that with I<sub>2</sub>, although less cleanly. Cl<sub>2</sub>, Br<sub>2</sub>, and ICl all gave four products, including in all cases (Idipp)AuX and (Idipp)AuX<sub>3</sub>. The latter, presumably formed by

oxidation of (Idipp)AuX by these stronger oxidants, is not observed in the reaction with I<sub>2</sub>; in fact, the reaction of (Idipp)AuBr<sub>3</sub> with excess KI to replace the halogens gave only the reduced product **D**. The other two species in these oxidation reactions appear to be *cis* and *trans* isomers of a Au(III)-monomethyl species. FAB<sup>+</sup> MS experiments support the existence of the monomethyl species in these reaction mixtures; (Idipp)AuBrMe<sup>+</sup> and (Idipp)AuClMe<sup>+</sup> were both observed. HMBC data for the reactions with Cl<sub>2</sub> and Br<sub>2</sub> likewise show coupling of the presumed methyl protons to the NHC carbene carbon (see Appendix C). X-ray diffraction studies were not definitive: in the case of Cl<sub>2</sub>, disorder in the crystal and the similarity in size of Cl and Me made it impossible to distinguish between a monomethyl species, *cis*-(Idipp)AuCl<sub>2</sub>Me, with disorder in packing, or a dimethyl species co-crystallized with (Idipp)AuCl<sub>3</sub>. With Br<sub>2</sub>, it appeared that the *cis* and *trans* isomers co-crystallized, resulting in calculated populations of halide that again made a definitive identification impossible. With ICl, the crystals were X-ray sensitive, leading to yet another poor structure. In support of these assignments, a related complex was recently reported from Mankad et al.; when (Idipp)AuMe is allowed to react with XeF<sub>2</sub>, the observed product in solution is *cis*-(Idipp)AuF<sub>2</sub>Me, however only a dimeric form could be observed by X-ray crystallography.<sup>44</sup>

Oxidation of (Idipp)AuEt (**E**) with Cl<sub>2</sub> gave a reaction that was less clean and crystals that were unsuitable for X-ray diffraction experiments, but analysis by FAB<sup>+</sup> MS showed (Idipp)AuClEt<sup>+</sup>. In a similar experiment with (Idipp)AuPh (**F**), the only product seen by <sup>1</sup>H NMR and FAB<sup>+</sup> MS was (Idipp)AuCl (see Appendix C).

In the case of NIS, while the overall reaction was not as clean as with  $I_2$ , only two major ligand-containing products (in addition to MeI) were observed. Crystals grown from this reaction mixture refined as (Idipp)AuMeI(C<sub>4</sub>H<sub>4</sub>NO<sub>2</sub>), with the methyl group located *trans* to the NHC (Figure 1.8). Such a species might be an intermediate in the recently reported catalytic conversion of benzene to PhX (X = Cl, Br, I) by NXS in the presence of AuCl<sub>3</sub>.<sup>11</sup>

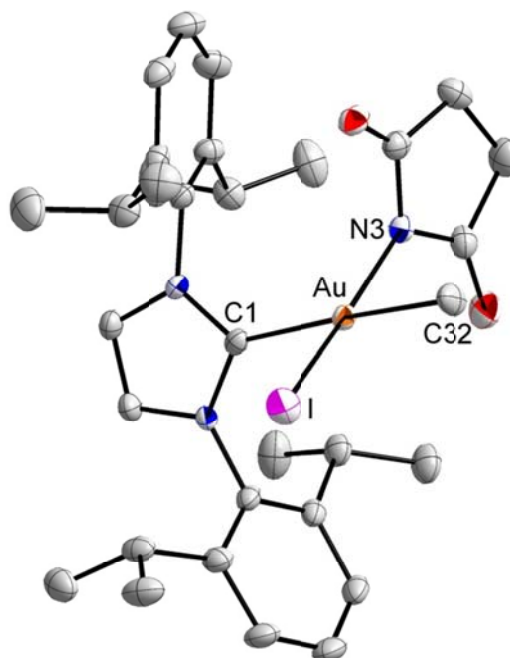


**Figure 1.8** Anisotropically refined structure of (Idipp)AuMeI(NC<sub>4</sub>H<sub>4</sub>O<sub>2</sub>). All protons and two molecules of acetonitrile have been omitted for clarity. Selected bond lengths and angles: Au-C1A 2.128(3) Å, Au-C32 2.086(3) Å, Au-N3 2.051(2) Å, Au-I 2.5597(2) Å, C1-Au-N3 99.53(9)°, C1-Au-C32 177.37(10)°, C1A-Au-I 89.84(6)°, C32-Au-N3 82.51(11)°, C32-Au-I 88.41(10)°, N3-Au-I 167.03(6)°

## 1.4 Conclusions

An unusual Au(III)-monoalkyl complex was synthesized by the reaction of (Idipp)AuMe with I<sub>2</sub> and characterized by a variety of methods that demonstrated that the methyl group is located in the unexpected *trans* position to the strong NHC  $\sigma$ -donor. Other oxidants demonstrate similar chemistry, however the transformations are generally not as clean. N-iodosuccinamide also generates a *trans* product that yielded high quality X-ray diffraction data. Br<sub>2</sub> appears to give a mixture of *cis* and *trans* products while Cl<sub>2</sub> only forms *cis*-(Idipp)AuMeCl<sub>2</sub>.

## 1.5 Experimental Section

**General considerations.** (Idipp)AuCl was purchased from Sigma-Aldrich or prepared by the methods described in the literature.<sup>45</sup> LiI, I<sub>2</sub>, Mg, and ZnCl<sub>2</sub> were purchased from Sigma-Aldrich; LiI was dried overnight under vacuum then stored in a vial in an N<sub>2</sub>-atmosphere glovebox away from light. Deuterated solvents were purchased from Cambridge Isotope Laboratories. Before use, each was subjected to three freeze-pump-thaw cycles, then stored over alumina overnight. Benzene and diethyl ether were dried by the method described in the literature by Pangborn et al.<sup>46</sup> All other chemicals and solvents were used as received, without further purification. X-ray diffraction experiments were carried out in the Beckman Institute Crystallographic Facility on a Bruker KAPPA APEXII X-ray diffractometer. <sup>1</sup>H and <sup>13</sup>C NMR spectra were obtained on both Varian 500 and 600 MHz instruments.

**(Idipp)AuMe (A).** In a N<sub>2</sub>-atmosphere glovebox, (Idipp)AuCl (179 mg, 0.288 mmol) was dissolved in 18 mL of dry, degassed C<sub>6</sub>H<sub>6</sub> and placed into a 20 mL vial equipped with a stir bar. 159  $\mu$ L of a 2.0 M solution of ZnMe<sub>2</sub> in toluene (0.317 mmol) was added to the solution and the vial was sealed with a Teflon coated cap. The vial was brought outside of the glovebox and stirred overnight. A black precipitate was filtered off (in the air) and the resulting colorless solution was lyophilized to give a flocculent white powder in 65% yield. <sup>1</sup>H NMR (CD<sub>3</sub>CN):  $\delta$  7.53 (t, <sup>3</sup>J<sub>HH</sub> = 9 Hz, 2H, *p*-ArH), 7.37 (d, <sup>3</sup>J<sub>HH</sub> = 9 Hz, 4 H, *m*-ArH), 7.34 (s, 2H, NHC backbone), 2.64 (sep, <sup>3</sup>J<sub>HH</sub> = 6 Hz, 4H, CH(CH<sub>3</sub>)<sub>2</sub>), 1.32 (d, <sup>3</sup>J<sub>HH</sub> = 3 Hz, 6H, CH(CH<sub>3</sub>)<sub>2</sub>), 1.21 (d, <sup>3</sup>J<sub>HH</sub> = 3 Hz, 6H, CH(CH<sub>3</sub>)<sub>2</sub>), -0.41 (s, 3H, CH<sub>3</sub>). <sup>13</sup>C NMR (CD<sub>3</sub>CN):  $\delta$  201.4 (carbene), 147.1 (Ar), 136.1 (Ar), 131.1 (Ar), 124.9 (NHC backbone), 124.2 (Ar), 29.5 (<sup>i</sup>Pr), 24.5 (<sup>i</sup>Pr), 23.9 (<sup>i</sup>Pr), -0.8 (Me). Anal. Calcd for C<sub>28</sub>H<sub>39</sub>AuN<sub>2</sub>: C, 55.99; H, 6.55; N, 4.66. Found: C, 55.11; H, 6.46; N, 4.61.

**(Idipp)Au<sup>13</sup>CH<sub>3</sub> (A\*).** In a N<sub>2</sub>-atmosphere glovebox, Mg metal (87.9 mg, 3.62 mmol) and <sup>13</sup>CH<sub>3</sub>I (45.0  $\mu$ L, 0.722 mmol) were added to 5 mL Et<sub>2</sub>O in a vial and stirred for 5 hours. The resulting cloudy gray solution was decanted from the excess Mg into a vial containing a solution of (Idipp)AuCl (150 mg, 0.242 mmol in 10 mL THF). This reaction mixture was allowed to stir overnight. The resulting white precipitate was filtered off (in air) and the volatiles removed in vacuo. The white solids were dissolved in approximately 12 mL of C<sub>6</sub>H<sub>6</sub> and filtered again. The clear, colorless solution was lyophilized to give a white powder in 59% yield. <sup>1</sup>H NMR (CD<sub>3</sub>CN):  $\delta$  7.53 (t, *J* = 9 Hz, 2H, *p*-ArH), 7.37 (d,

$^3J_{HH} = 9$  Hz, 4 H, *m*-ArH), 7.34 (s, 2H, NHC backbone), 2.64 (sep,  $^3J_{HH} = 6$  Hz, 4H,  $CH(CH_3)_2$ ), 1.32 (d,  $^3J_{HH} = 3$  Hz, 6H,  $CH(CH_3)_2$ ), 1.21 (d,  $^3J_{HH} = 3$  Hz, 6H,  $CH(CH_3)_2$ ), -0.41 (d,  $^1J_{CH} = 120$  Hz, 3H,  $CH_3$ ).  $^{13}C$  NMR ( $CD_3CN$ ):  $\delta$  201.4 ( $^2J_{CC} = 32.5$  Hz, carbene), 147.1 (Ar), 136.1 (Ar), 131.1 (Ar), 124.9 (NHC backbone), 124.2 (Ar), 29.5 ( $i$ Pr), 24.5 ( $i$ Pr), 23.9 ( $i$ Pr), -0.8 (Me).

**(Idipp)AuEt (E).** In a  $N_2$ -atmosphere glovebox, (Idipp)AuCl (100 mg, 0.161 mmol) was dissolved in 18 mL of dry, degassed  $C_6H_6$  and placed into a 20 mL vial equipped with a stir bar. 17.5  $\mu$ L of  $ZnEt_2$  (0.171 mmol) was added to the solution and the vial was sealed with a Teflon coated cap. The vial was brought outside of the glovebox and stirred overnight. A black precipitate was filtered off (in the air) and the resulting colorless solution was lyophilized to give a flocculent white powder in 76% yield. Crystals suitable for X-ray diffraction were grown from a  $CH_3CN$  solution layered with  $H_2O$ .  $^1H$  NMR ( $CD_3CN$ ):  $\delta$  7.52 (t,  $J = 9$  Hz, 2H, *p*-ArH), 7.35 (d,  $J = 9$  Hz, 4 H, *m*-ArH), 7.32 (s, 2H, NHC backbone), 2.62 (sep,  $J = 6$  Hz, 4H,  $CH(CH_3)_2$ ), 1.31 (d,  $J = 3$  Hz, 6H,  $CH(CH_3)_2$ ), 1.20 (d,  $J = 3$  Hz, 6H,  $CH(CH_3)_2$ ), 0.82 (t,  $J = 8$  Hz, 3H,  $CH_2CH_3$ ), 0.43 (q,  $J = 8$  Hz, 2H,  $CH_2CH_3$ ).  $^{13}C$  NMR ( $CD_3CN$ ):  $\delta$  201.6 (carbene), 147.1 (Ar), 136.1 (Ar), 131.1 (Ar), 124.9 (NHC backbone), 124.2 (Ar), 29.6 ( $i$ Pr), 24.6 ( $i$ Pr), 24.0 ( $i$ Pr), 17.3 (Et), 13.9 (Et). Anal. Calcd for  $C_{29}H_{41}AuN_2$ : C, 56.67; H, 6.72; N, 4.56. Found: C, 56.11; H, 5.54; N, 4.28.

**(Idipp)AuPh (F).** In a  $N_2$ -atmosphere glovebox,  $ZnCl_2$  (18.9 mg, 0.139 mmol) was dissolved in 3 mL  $Et_2O$ . Solid PhLi (24.4 mg, 0.290 mmol) was added and the mixture was stirred for one hour. The resulting cloudy white solution was filtered into a vial

containing (Idipp)AuCl (78.3 mg, 0.126 mmol) dissolved in 15 mL of dry, degassed C<sub>6</sub>H<sub>6</sub> and stirred overnight. Outside of the glovebox, the solution was lyophilized. The resulting solids were extracted with 10 mL of CH<sub>3</sub>CN and this solution was layered with H<sub>2</sub>O to give colorless crystals suitable for X-ray diffraction studies in 44% yield. <sup>1</sup>H NMR (CD<sub>3</sub>CN):  $\delta$  7.52 (t,  $J$  = 9 Hz, 2H, *p*-ArH), 7.42 (s, 2H, NHC backbone), 7.37 (d,  $^3J_{HH}$  = 6 Hz, 4 H, *m*-ArH), 6.90-6.70 (m, Ph), 2.66 (sep,  $^3J_{HH}$  = 6 Hz, 4H, CH(CH<sub>3</sub>)<sub>2</sub>), 1.36 (d,  $^3J_{HH}$  = 6 Hz, 6H, CH(CH<sub>3</sub>)<sub>2</sub>), 1.23 (d,  $^3J_{HH}$  = 6 Hz, 6H, CH(CH<sub>3</sub>)<sub>2</sub>). <sup>13</sup>C NMR (CD<sub>3</sub>CN):  $\delta$  147.1, 141.0, 131.7, 131.2, 127.5, 125.3, 125.0, 124.6, 124.2 (Ar and NHC backbone); 26.7, 24.8, 24.0 (<sup>*i*</sup>Pr); the carbene signal was unresolved. Anal. Calcd for C<sub>33</sub>H<sub>41</sub>AuN<sub>2</sub>: C, 59.81; H, 6.24; N, 4.23. Found: C, 58.41; H, 5.73; N, 4.09.

**(Idipp)AuI<sub>2</sub>Me (B).** (Idipp)AuMe (53.0 mg, 0.0882 mmol) was dissolved in approximately 5 mL CH<sub>3</sub>CN and I<sub>2</sub> (24.7 mg, 0.0973 mmol) was dissolved separately in 5 mL CH<sub>3</sub>CN. The solution containing the Au complex was frozen on dry ice and the I<sub>2</sub> solution was layered on top. The mixture was allowed to thaw slowly with mixing and once it was completely melted, the resulting yellow solution was put under vacuum to concentrate. When yellow solids began to form on the sides of the vial, the solution was capped and stored at -36 °C overnight. The orange, X-ray sensitive, temperature sensitive crystals were transported in a -50 °C bath and were quickly mounted on the diffractometer. Yields and elemental analyses were not determined due to the instability of the complex. Spectra were taken in the presence of extra LiI or KI and (Idipp)AuI was always a contaminant. <sup>1</sup>H NMR (CD<sub>3</sub>CN):  $\delta$  7.58-7.36 (m, NHC backbone and ArH), 3.20 (sep,  $^3J_{HH}$

= 6 Hz, 4H,  $\text{CH}(\text{CH}_3)_2$ ), 1.43 (s, 3H,  $\text{CH}_3$ ), 1.41 (d,  $^3J_{\text{HH}} = 6$  Hz, 6H,  $\text{CH}(\text{CH}_3)_2$ ), 1.11 (d,  $^3J_{\text{HH}} = 6$  Hz, 6H,  $\text{CH}(\text{CH}_3)_2$ ).  $^{13}\text{C}$  NMR ( $\text{CD}_3\text{CN}$ ):  $\delta$  183.2 (carbene), 146.9, 135.6, 131.6, 127.2, 125.3, 29.8 ( $^i\text{Pr}$ ), 26.5 ( $^i\text{Pr}$ ), 23.9 ( $^i\text{Pr}$ ), -7.47 (Me).

## 1.6 References

1. Shilov, A. E.; Shul'pin, G. B., *Usp. Khim.*, **1987**, 56, 754-792.
2. Labinger, J. A.; Bercaw, J. E., *Nature*, **2002**, 417, 507-514.
3. Geletii, Y. V.; Shilov, A. E., *Kinet. Catal.*, **1983**, 24, 413-416.
4. Luinstra, G. A.; Wang, L.; Stahl, S. S.; Labinger, J. A.; Bercaw, J. E., *J. Organomet. Chem.*, **1995**, 504, 75-91.
5. Johansson, L.; Tilset, M.; Labinger, J. A.; Bercaw, J. E., *J. Am. Chem. Soc.*, **2000**, 122, 10846-10855.
6. Lin, M. R.; Shen, C. Y.; Garcia-Zayas, E. A.; Sen, A., *J. Am. Chem. Soc.*, **2001**, 123, 1000-1001.
7. Sen, A.; Benvenuto, M. A.; Lin, M. R.; Hutson, A. C.; Basicckes, N., *J. Am. Chem. Soc.*, **1994**, 116, 998-1003.
8. Periana, R. A.; Taube, D. J.; Gamble, S.; Taube, H.; Satoh, T.; Fujii, H., *Science*, **1998**, 280, 560-564.
9. de Graaf, P. W. J.; Boersma, J.; van der Kerk, G. J. M., *J. Organomet. Chem.*, **1976**, 105, 399-406.
10. Frúctos, M. R.; de Frémont, P.; Nolan, S. P.; Díaz-Requejo, M. M.; Perez, P. J., *Organometallics*, **2006**, 25, 2237-2241.



11. Mo, F. Y.; Yan, J. M.; Qiu, D.; Li, F.; Zhang, Y.; Wang, J. B., *Angew. Chem. Int. Ed.*, **2010**, *49*, 2028-2032.
12. Hashmi, A. S. K.; Salathe, R.; Frost, T. M.; Schwarz, L.; Choi, J. H., *Applied Catalysis A-General*, **2005**, *291*, 238-246.
13. Hashmi, A. S. K.; Schafer, S.; Wolfe, M.; Gil, C. D.; Fischer, P.; Laguna, A.; Blanco, M. C.; Gimeno, M. C., *Angew. Chem. Int. Ed.*, **2007**, *46*, 6184-6187.
14. Höffmann-Roder, A.; Krause, N., *Org. Biomol. Chem.*, **2005**, *3*, 387-391.
15. Jones, C. J.; Taube, D.; Ziatdinov, V. R.; Periana, R. A.; Nielsen, R. J.; Oxgaard, J.; Goddard, W. A., *Angew. Chem. Int. Ed.*, **2004**, *43*, 4626-4629.
16. Kar, A.; Mangu, N.; Kaiser, H. M.; Tse, M. K., *J. Organomet. Chem.*, **2009**, *694*, 524-537.
17. Kharasch, M. S.; Beck, T. M., *J. Am. Chem. Soc.*, **1934**, *56*, 2057-2060.
18. Kharasch, M. S.; Isbell, H. S., *J. Am. Chem. Soc.*, **1931**, *53*, 3053-3059.
19. Levchenko, L. A.; Kartsev, V. G.; Sadkov, A. P.; Shestakov, A. F.; Shilova, A. K.; Shilov, A. E., *Dokl. Chem.*, **2007**, *412*, 35-37.
20. Levchenko, L. A.; Sadkov, A. P.; Lariontseva, N. V.; Koldasheva, E. M.; Shilova, A. K.; Shilov, A. E., *J. Inorg. Biochem.*, **2002**, *88*, 251-253.
21. Li, Z. G.; Capretto, D. A.; Rahaman, R. O.; He, C., *J. Am. Chem. Soc.*, **2007**, *129*, 12058-12059.
22. Shul'pin, G. B.; Shilov, A. E.; Süß-Fink, G., *Tetrahedron Lett.*, **2001**, *42*, 7253-7256.

23. Vicente, J.; Bermúdez, M. D.; Chicote, M. T.; Sanchez-Santano, M. J., *J. Chem. Soc. Chem. Comm.*, **1989**, 141-142.
24. Vicente, J.; Chicote, M. T.; Lozano, M. I.; Huertas, S., *Organometallics*, **1999**, *18*, 753-757.
25. Xiao, Y. P.; Liu, X. Y.; Che, C. M., *J. Organomet. Chem.*, **2009**, *694*, 494-501.
26. Oña-Burgos, P.; Fernandez, I.; Rocas, L.; Fernandez, L. T.; García-Granda, S.; Ortíz, F. L., *Organometallics*, **2009**, *28*, 1739-1747.
27. Shaik, N.; Martinez, A.; Augustin, I.; Giovinozzo, H.; Varela-Ramirez, A.; Sanau, M.; Aguilera, R. J.; Contel, M., *Inorg. Chem.*, **2009**, *48*, 1577-1587.
28. Uson, R.; Laguna, A.; Delaorden, M. U.; Parish, R. V. D.; Moore, L. S., *J. Organomet. Chem.*, **1985**, *282*, 145-148.
29. Vicente, J.; Chicote, M. T.; Bermúdez, M. D.; García-García, M., *J. Organomet. Chem.*, **1985**, *295*, 125-130.
30. Vicente, J.; Chicote, M. T.; Bermúdez, M. D., *J. Organomet. Chem.*, **1984**, *268*, 191-195.
31. Ahmed, E.; Clark, R. J. H.; Tobe, M. L.; Cattalini, L., *J. Chem. Soc. Dalton*, **1990**, 2701-2706.
32. Parish, R. V. D., *Gold Bull.*, **1997**, *30*, 3-12.
33. Bennett, M. A., *J. Organomet. Chem.*, **1986**, *300*, 7-19.
34. Bennett, M. A.; Hoskins, K.; Kneen, W. R.; Nyholm, R. S.; Hitchcock, P.; Mason, R.; Robertson, G.; Towl, D. C., *J. Am. Chem. Soc.*, **1971**, *93*, 4591-4592.

35. Sanner, R. D.; Satcher, J. H.; Droege, M. W., *Organometallics*, **1989**, 8, 1498-1506.
36. Cinellu, M. A.; Cocco, F.; Minghetti, G.; Stoccoro, S.; Zucca, A.; Manassero, M., *J. Organomet. Chem.*, **2009**, 694, 2949-2955.
37. Bennett, M. A.; Hoskins, K.; Kneen, W. R.; Nyholm, R. S.; Mason, R.; Hitchcock, P.; Robertson, G.; Towl, A. D. C., *J. Am. Chem. Soc.*, **1971**, 93, 4592-4593.
38. Monaghan, P. K.; Puddephatt, R. J., *Inorg. Chim. Acta.*, **1975**, 15, 231-234.
39. Nichols, D. I.; Charlest.As, *J. Chem. Soc. A*, **1969**, 2581-2583.
40. Tamaki, A.; Kochi, J. K., *J. Organomet. Chem.*, **1974**, 64, 411-425.
41. Herrmann, W. A., *Angew. Chem. Int. Ed.*, **2002**, 41, 1290-1309.
42. Scott, V. J.; Labinger, J. A.; Bercaw, J. E., *Organometallics*, **2010**, 29, 4090-4096.
43. de Frémont, P.; Singh, R.; Stevens, E. D.; Petersen, J. L.; Nolan, S. P., *Organometallics*, **2007**, 26, 1376-1385.
44. Mankad, N. P.; Toste, F. D., *J. Am. Chem. Soc.*, **2010**, 132, 12859-12861.
45. de Frémont, P.; Marion, N.; Nolan, S. P., *J. Organomet. Chem.*, **2009**, 694, 551-560.
46. Kuch, P. L.; Tobias, R. S., *J. Organomet. Chem.*, **1976**, 122, 429-446.

## CHAPTER 2

### Mechanism of reductive elimination methyl iodide from a novel gold(III)- monomethyl complex

#### 2.1 Abstract

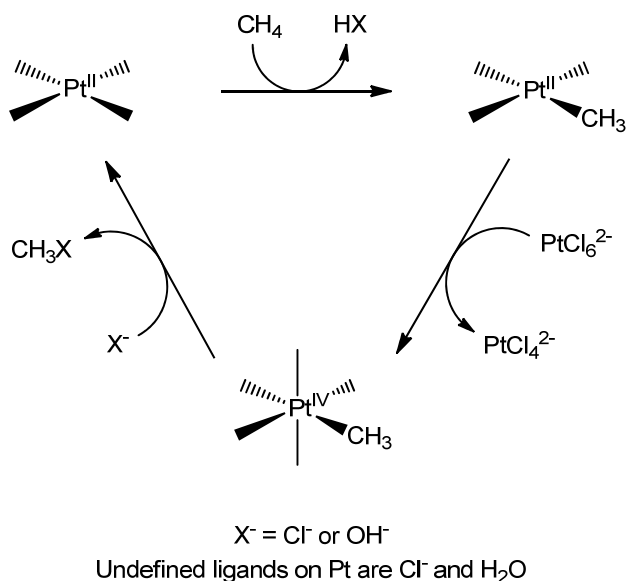
Oxidation of (Idipp)AuMe (Idipp = 1,3-bis(2,6-diisopropylphenyl)imidazol-2-ylidene) with I<sub>2</sub> gives a monomethyl Au(III) complex, (Idipp)AuI<sub>2</sub>Me, which decomposes cleanly to MeI and (Idipp)AuI. Kinetics experiments show that this transformation occurs primarily via 3-coordinate, cationic [(Idipp)AuI<sub>2</sub>Me]<sup>+</sup> which undergoes intramolecular reductive elimination rather than nucleophilic attack by external I<sup>-</sup>.

#### 2.2 Introduction

C-H activation by transition metal complexes has been a significant area of research for several decades, with particular interest in its applicability to the conversion of methane to methanol. The stability of these bonds typically renders them inert to chemical reactions but advances in organometallic chemistry over the last several decades have demonstrated the ability to access these reactions, particularly with Pt- and Pd-based complexes.<sup>1-8</sup> Conversion of methane to methanol is useful from an industrial point of view; natural gas is abundant and cheap and methanol is easier to transport and store and is additionally the starting point for many chemical syntheses. While the activation of a C-H bond is already a difficult task, there is an additional selectivity complication with this proposed transformation: the C-H bonds in methanol are weaker than those in methane and so are easier to activate, resulting in typical over-oxidation.

The most well-known (and most studied) example of a system that is capable of carrying out this difficult chemistry is the Shilov system,<sup>1,4</sup> where methane is catalytically converted to methanol using a Pt(II)-catalyst with high selectivity. Significant work has focused on elucidating the mechanism of the Shilov system and related Pt- and Pd based complexes.<sup>1-8</sup> The mechanism of the catalytic system (Scheme 2.1) has been determined to be the following: 1) Pt(II) electrophilically activates a C-H bond, resulting in the formation of a Pt(II)-alkyl, 2), this species is then oxidized to give a Pt(IV)-alkyl, and 3) the Pt(IV)-alkyl undergoes nucleophilic attack by either water or chloride in the system to give  $\text{CH}_3\text{X}$  and regenerate the Pt(II) species. One of the major downfalls to this system is that the stoichiometric oxidant is  $[\text{Pt}(\text{IV})\text{Cl}_6]^{2-}$ , which is expensive and not readily regenerated, rendering this particular system commercially impractical.

**Scheme 2.1**



Despite the masses of work done using Pt, a viable catalytic system for commercial use has yet to be found. However, other metals have been shown to effect such chemistry as

well, notably including gold;<sup>9-25</sup> gold-based catalysis in general has been a topic of intense recent activity.<sup>26</sup> In nature, Au is proposed to take methane to methanol in the “Au-containing protein” isolated from *M. luteus* which has been proposed to proceed through a Au(I)/(III) couple.<sup>19, 20</sup> This reactivity is not exclusive to nature; NaAuCl<sub>4</sub> and ClAu(PPh<sub>3</sub>) can oxidize alkanes in the presence of H<sub>2</sub>O<sub>2</sub>, where an unusual Au-oxo species is proposed to be involved.<sup>22</sup> In 2004 Periana and coworkers reported the stoichiometric conversion of methane to methanol by Au<sub>2</sub>O<sub>3</sub> dissolved in H<sub>2</sub>SO<sub>4</sub> and showed it could be made catalytic under the same conditions (starting with Au(0)) in the presence of H<sub>2</sub>SeO<sub>4</sub>.<sup>15</sup> While the Au species responsible for C-H activation was not identified, both the reaction conditions and DFT calculations suggested electrophilic substitution by Au(III) to give a Au(III)-methyl species (See Scheme 1.1). Subsequent functionalization to give methanol was proposed to involve an S<sub>N</sub>2 type mechanism, as reductive elimination was calculated to be significantly higher in energy. No experimental evidence was obtained, however.

Here the generation of a Au(III)-monomethyl complex with an N-heterocyclic carbene (NHC) ligand, (Idipp)AuI<sub>2</sub>Me (Idipp = 1,3-bis(2,6-diisopropylphenyl)imidazol-2-ylidene) is reported.<sup>27</sup> While several Au(III)-monoaryl species are known,<sup>28-34</sup> to the best of our knowledge no simple Au(III)-monoalkyl has been previously reported.<sup>24,28, 35-39</sup> (Idipp)AuI<sub>2</sub>Me decomposes to (Idipp)AuI and MeI over time, primarily via a reductive elimination pathway, in contrast to the behavior of the Shilov system as well as the mechanism predicted by DFT calculations on the Periana system.<sup>15</sup>

## 2.3 Results and Discussion

### 2.3.1 Qualitative effects on the formation and decomposition of (Idipp)AuI<sub>2</sub>Me

Oxidation of (Idipp)AuMe (**A**) with I<sub>2</sub> led to formation of two new (Idipp)Au species in addition to MeI (by <sup>1</sup>H NMR spectroscopy; Figure 2.1). Over time, one of the two products converted into the other, shown by <sup>1</sup>H NMR spectroscopy and FAB<sup>+</sup> MS to be (Idipp)AuI (**D**). As discussed in Chapter 1, the second product (**B**) was shown to be *trans*-(Idipp)AuI<sub>2</sub>Me.

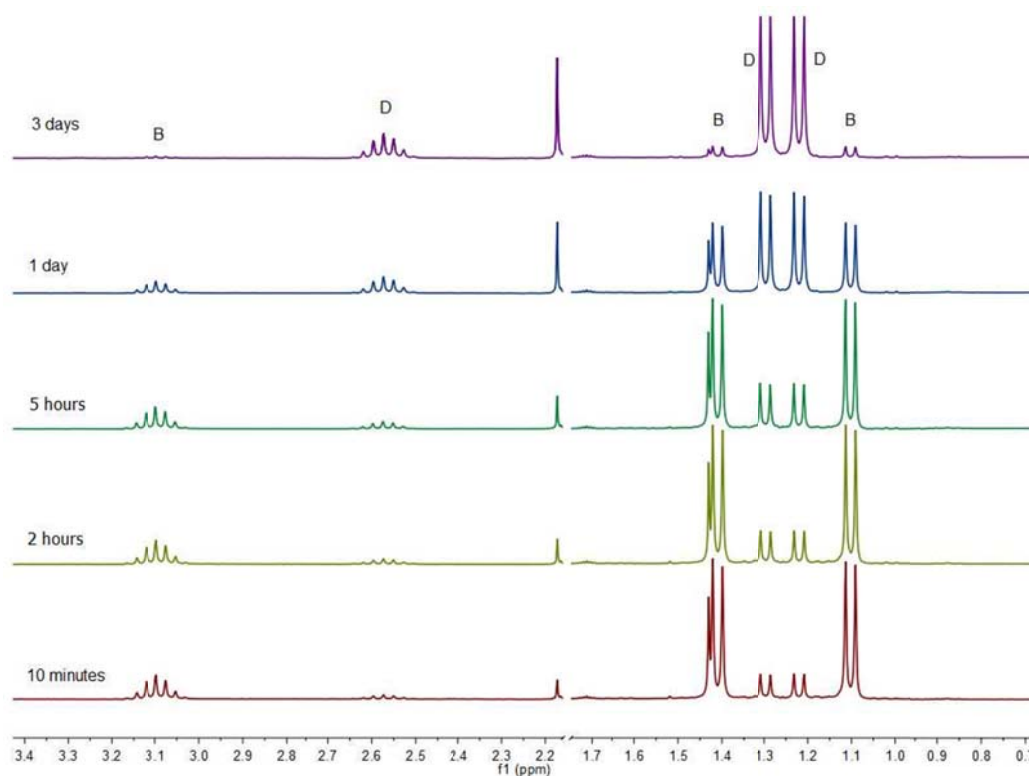


**Figure 2.1** Reaction monitored over time for (Idipp)AuMe + 1.06 eq. I<sub>2</sub>

Initial studies examined the effects of solvent and the presence of excess I<sub>2</sub> or I<sup>-</sup>. Oxidation of **A** by I<sub>2</sub> in benzene, toluene, bromobenzene, acetonitrile, methanol, methylene

chloride, and acetone all lead to the same products, but the initial ratio of **D** to **B** depends on the solvent, decreasing in the order  $\text{CD}_2\text{Cl}_2 \sim \text{C}_6\text{D}_5\text{Br}$  (trace) < benzene  $\sim$  toluene < acetone < acetonitrile (very low solubility in methanol makes it difficult to determine where it would fall on the scale) at room temperature. This change in ratio does not appear to be an effect of coordination: a reaction run in  $\text{CD}_2\text{Cl}_2$  with 10 equivalents of  $\text{CD}_3\text{CN}$  displayed the same initial distribution of products as in neat  $\text{CD}_2\text{Cl}_2$ ; nor did the presence of  $\text{PPh}_3$  (which reacts reversibly with  $\text{I}_2$ ) have any effect.

Reactions carried out in the presence of excess KI (in  $\text{CD}_3\text{CN}$ ) show an increase in both the initial concentration and the lifetime of **B**. The initial product ratio also depends strongly on temperature and  $[\text{I}_2]$ : at room temperature in  $\text{CD}_3\text{CN}$ , with no added  $\text{I}^-$  and only a small excess of  $\text{I}_2$ , **B** constitutes only about 30% of the initial product; but addition of up to 10 equiv  $\text{I}^-$  increases that proportion to 65%, and running the reaction at  $-20\text{ }^\circ\text{C}$  gives >95% **B** as initially formed product. Conversely, reactions run with higher excesses of  $\text{I}_2$  or at elevated temperature give less **B**; with 3 equiv  $\text{I}_2$  at  $50\text{ }^\circ\text{C}$  less than 10% of the initial product was **B** (Table 2.1).



**Table 2.1** Effect of  $[I^-]$ ,  $[I_2]$  and temperature on the initial concentration of **B**

Experiment	Temp (°C)	$I_2$ (equivalents in excess)	$I^-$ (equivalents)	% (Idipp)AuI <sub>2</sub> Me in 1 <sup>st</sup> FID <sup>a</sup>
1	-20	0.25	10	>95
2	-20	0.25	0	>95
3	25	0.25	0	32
4	25	0.25	0	32
5	22	0.06	0	32
6	22	0.06	0.25	41
7	22	0.06	1	56
8	22	0.06	2	54
9	22	0.06	5	65
10	22	0.06	10	66
11	22	1	0	33
12	22	1	0	36
13	22	4	0	33
14	22	4	0	32
15	22	9	0	21
16	22	9	10	81
17	22	9	5	60
18	22	9	1	42
19	22	0	0	41
20	35	0.25	0	27
21	50	0.25	0	21
22	50	0.25	0	19
23	50	1	0	13
24	50	1	0	15
25	50	3	0	9
26	50	3	0	8
27	50	0.25	0.25	28
28	50	0.25	0.25	27
29	50	0.25	0.5	31
30	50	0.25	0.5	28
31	50	0.25	1	38
32	50	0.25	1	35

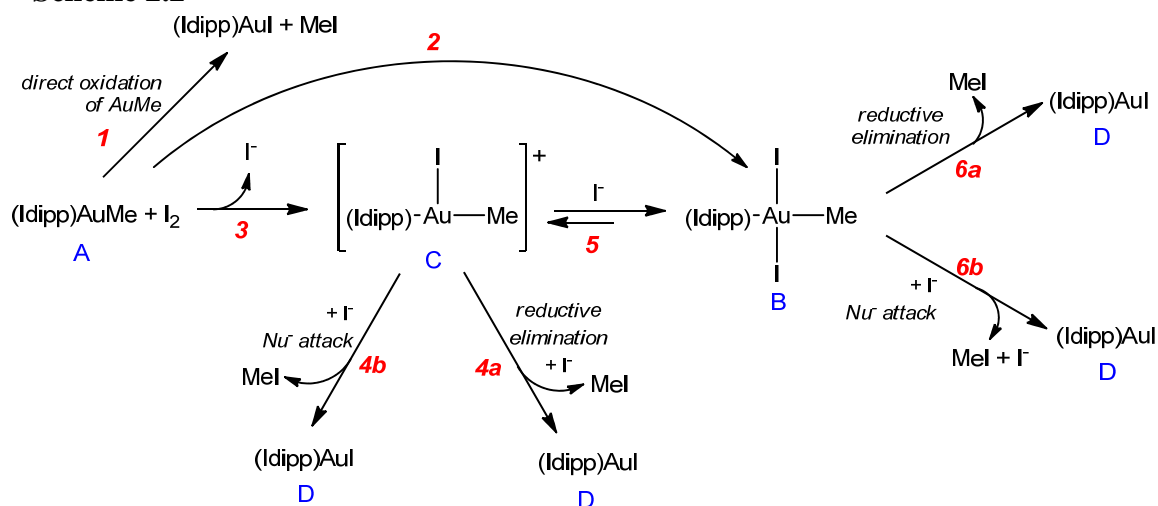
<sup>a</sup> First FID was taken within 5 minutes of mixing (time to mix, lock, and shim the instrument).

### 2.3.2 Mechanistic alternatives

Several plausible mechanistic alternatives for the oxidation of **A** to **B** and subsequent decomposition to MeI and **D** are shown in Scheme 2.2. In pathway **1**,  $I_2$  directly cleaves the Au-Me bond without going through any Au(III)-species. In **2**, **A** is oxidized in one step

to a Au(III)-monomethyl (although this would be expected initially to give a *cis*-configuration). Neither of these pathways would account for the change in initial distribution of the two Au complexes upon the addition of excess  $I^-$ ; stepwise addition of  $I_2$  via **C** thus seems to be most likely. The fact that some **D** was always observed immediately upon oxidation, no matter how quickly the first NMR spectrum was taken, could be interpreted in terms of either some contribution of pathway **I** or to the trapping of **C** by  $I^-$  in pathway **3** being relatively slow, allowing decomposition by **4a** or **4b** to compete. When the oxidation was carried out at  $-20\text{ }^\circ\text{C}$ , only trace amounts of **D** were observed; that may support the latter interpretation, if the rate of loss of MeI from **C** is more strongly temperature-dependent than the capture of  $I^-$ . ( $[(\text{Idipp})\text{Au}(\text{NCMe})]^+$ , which is a known species,<sup>40</sup> is never observed by  $^1\text{H}$  NMR, so if a Au(I) cation forms at any point it must be rapidly and irreversibly trapped by  $I^-$ .)

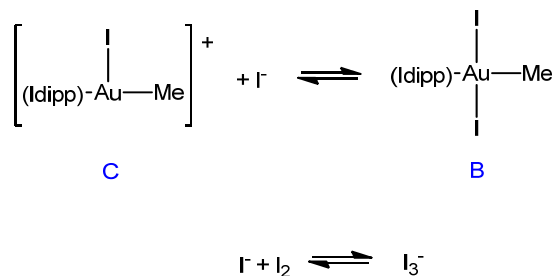
**Scheme 2.2**



Qualitatively, it was found that the subsequent conversion of **B** to **D** and MeI is strongly slowed in the presence of added  $I^-$ , and strongly accelerated when larger excesses of  $I_2$  are

used. Scheme 2.2 shows four plausible routes for that process: direct reductive elimination from **B** (**6a**); nucleophilic attack of  $\text{I}^-$  on **B** followed by loss of  $\text{I}^-$  (**6b**); or reversible dissociation of  $\text{I}^-$  from **B** to give 3-coordinate **C**, which undergoes either nucleophilic attack (**4b**) or reductive elimination (**4a**). Only the last of those is consistent with the observed trends, as changing  $[\text{I}^-]$ , either by addition or by virtue of the equilibrium formation of  $\text{I}_3^-$  from  $\text{I}_2$  and  $\text{I}^-$ , would shift the equilibrium between **B** and **C** (Scheme 2.3). That would result in an inverse dependence on  $[\text{I}^-]$  in the rate law; **6a** and **6b** would predict no such inverse term, while it would be canceled by a positive term in **4b** (for rate law derivations, see Appendix B). In contrast, the Shilov cycle is known to follow a pathway analogous to **4a**, in which nucleophilic attack of  $\text{X}^-$  on a coordinatively unsaturated  $\text{Pt(IV)-Me}$  species gives  $\text{MeX}$  and  $\text{Pt(II)}$ ,<sup>3</sup> as was also proposed, based on calculations, for the  $\text{Au}/\text{H}_2\text{SO}_4$  system. On the other hand, reductive elimination of  $\text{R-R}$  from dialkyl- $\text{Au(III)}$ <sup>41-45</sup> was demonstrated to occur through 3-coordinate intermediates.<sup>45</sup> To the best of our knowledge, reductive elimination of  $\text{RX}$  from  $\text{Au(III)}$  has not been directly observed for  $\text{R} = \text{alkyl}$ , probably because no monoalkyl- $\text{Au(III)}$  species has been previously characterized; the known  $\text{Au(III)}$  dialkyls apparently prefer to reductively eliminate alkane.

Scheme 2.3



### 2.3.3 Kinetic studies on (Idipp)AuI<sub>2</sub>Me decomposition

More quantitative kinetics experiments were carried out in two modes: either mixing solutions of **A** and I<sub>2</sub> at the desired reaction temperature, or adding a solution of I<sub>2</sub> to a frozen solution of **A** at -78 °C, thawing and mixing thoroughly, then bringing to reaction temperature; the latter procedure was designed in order to start with a maximum amount of **B**. LiI was added to adjust [I<sup>-</sup>]. In order to measure the rates at very low concentrations of I<sup>-</sup>, “buffered” reactions were run, utilizing the known K<sub>eq</sub> for I<sub>2</sub> + I<sup>-</sup> ⇌ I<sub>3</sub><sup>-</sup> in acetonitrile<sup>46</sup> to control the amount of free I<sup>-</sup> in solution. As would be expected, rates determined from one method were comparable to those from the other and in complete agreement with the qualitative trends discussed above. However, there was more scatter in the observed rates than would be expected, as can be seen in Figure 2.2 showing the effect of [I<sub>2</sub>]. The cause of the scatter is not clear: the presence of added LiOTf (to determine if the ionic strength of the solution had any effect on the measured rates), water or oxygen had no apparent effect on the rates; starting material **A** was also shown to be completely unreactive towards the products **D**, **B**, and MeI individually. (The stability to MeI is in contrast to the related phosphine complexes LAuMe, which oxidatively add MeI to give LAuMe<sub>2</sub>I and, depending on the phosphine, LAuI and ethane.<sup>43, 44</sup>).

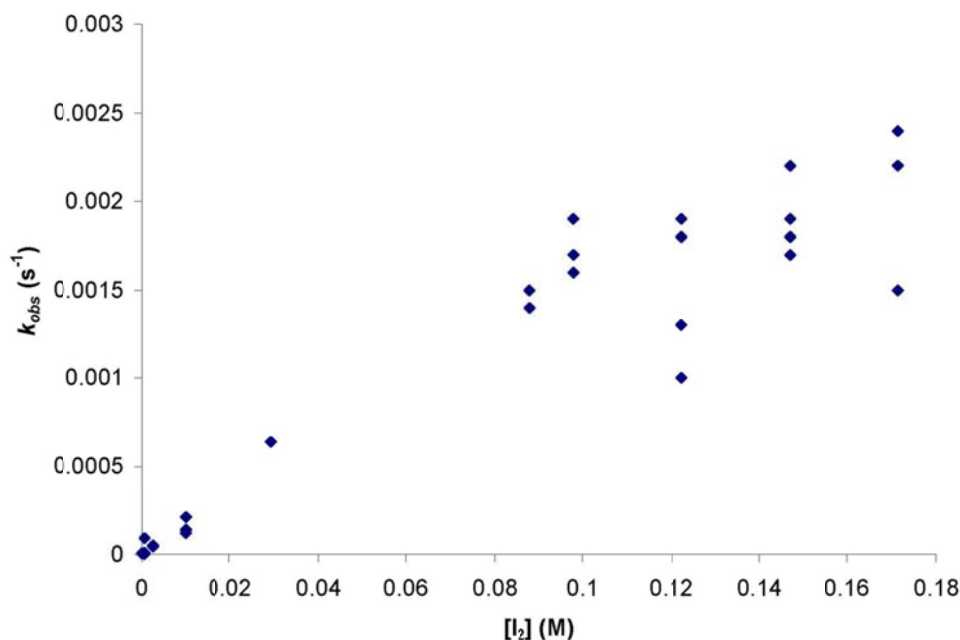


**Figure 2.2** Effect of  $[I_2]$  on rate of decomposition of **B**

Figures 2.3-2.5 show the effect of  $[I^-]$  overall and at high and low values respectively. Clearly even small concentrations of added  $I^-$  slow the decomposition rate markedly, but adding more does not slow it down further; in fact, there is a small *increase* in the rate, an effect that saturates at high concentrations of  $I^-$  (Figure 2.4). A similar trend is seen at 50 °C (Entries 21-32 in Table 2.1). This observation suggests the operation of a competing pathway that is only significant at higher iodide concentrations, where the main route via **C** is effectively turned off; the saturation behavior would be most consistent with reductive elimination from 5-coordinate intermediate  $[(Idipp)AuMeI_3]^-$  (Scheme 2.4). Unsuccessful attempts to make 5-coordinate Au(III) species are in the literature and their reactivity is unstudied.<sup>47-49</sup>

Scheme 2.4

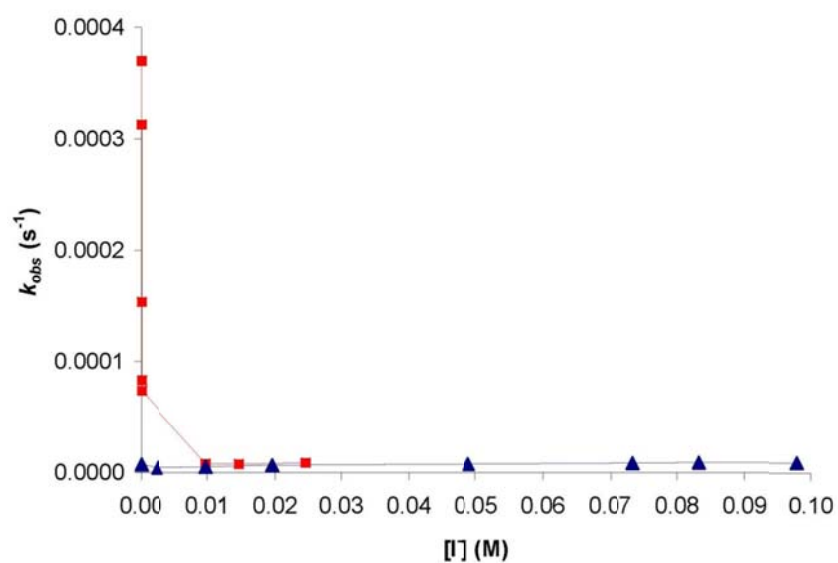
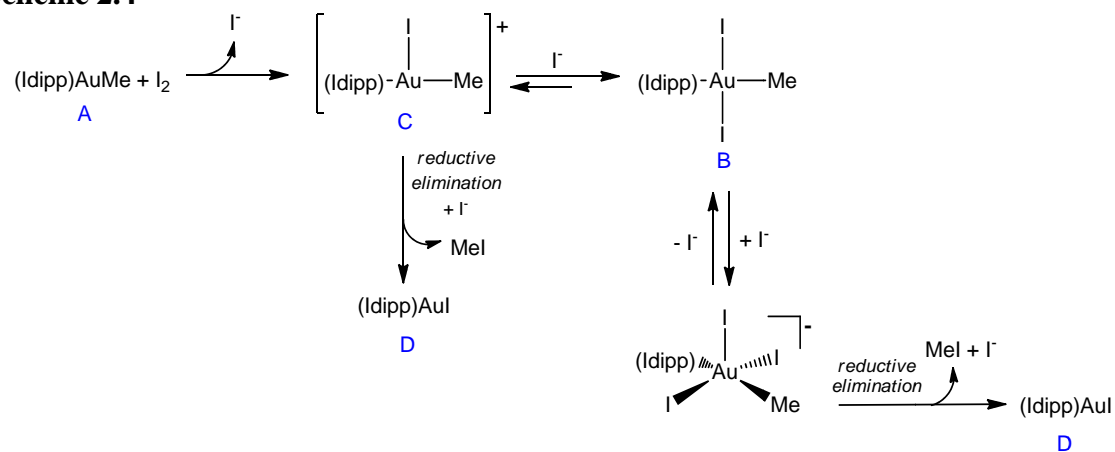


**Figure 2.3** Effect of [I<sup>-</sup>] on rate of decomposition of **B**. ▲ = added LiI, ■ = buffered experiments (I<sub>2</sub> + LiI)

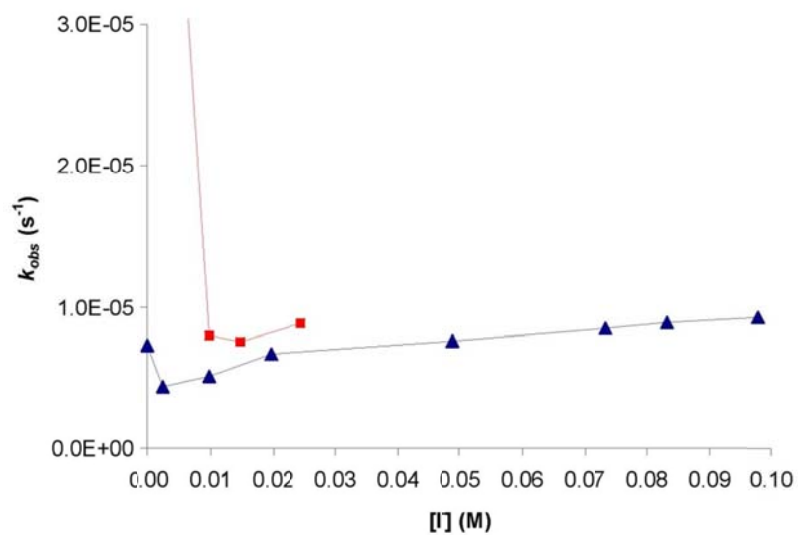


**Figure 2.4** Effect of  $[I^-]$  (high  $[I^-]$ ) on rate of decomposition of B.  $\blacktriangle$  = added LiI,  $\blacksquare$  = buffered experiments ( $I_2 + LiI$ )

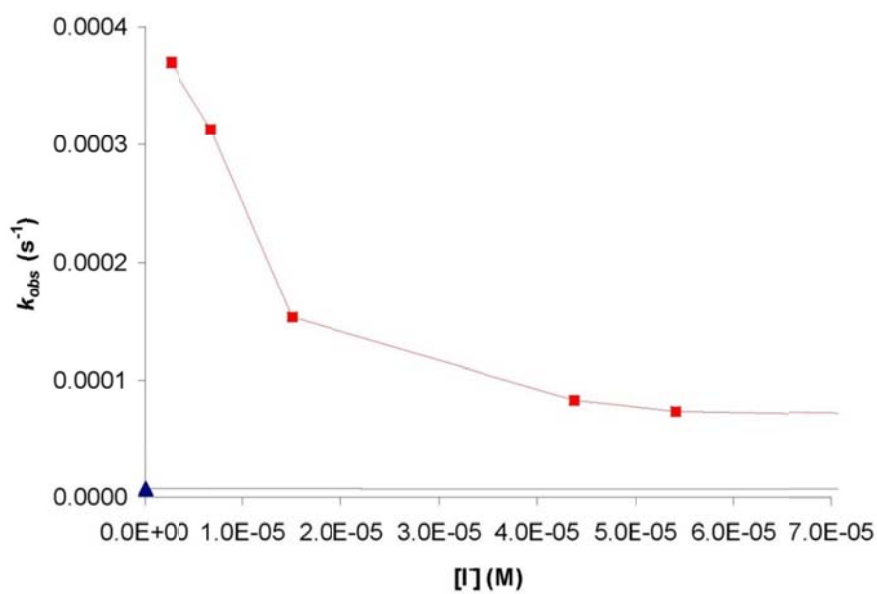


**Figure 2.5** Effect of  $[I^-]$  (low  $[I^-]$ ) on rate of decomposition of B.  $\blacktriangle$  = added LiI,  $\blacksquare$  = buffered experiments ( $I_2 + LiI$ )

In principle it should be possible to fit the data in Figures 2.2 and 2.3 to a rate law predicted from the equilibria in Scheme 2.3, utilizing the known  $K_{eq}$  for  $I_2 + I^- \rightleftharpoons I_3^-$  in acetonitrile;<sup>46</sup> however, a consistent set of equilibrium and rate constants could not be obtained. In particular, the rates for reactions with nominally equal  $[I^-]$  obtained by adding  $I^-$  or buffering were close but not identical: the buffered reactions were consistently faster than the corresponding added iodide experiments. Also the rate law predicts that the dependence on  $[I_2]$  should show saturation behavior at concentrations considerably lower than the maximum values in Figure 2.2; saturation *may* be beginning at the high end but it is not completely clear. (Higher concentrations could not be examined because of solubility limits.) Most probably these quantitative discrepancies may be attributed to the experimental uncertainties, although the possibility of additional mechanistic complications becoming significant at extreme ends of the range of conditions cannot be ruled out. Nonetheless, the qualitative and semiquantitative dependences show clearly that the dominant route for loss of MeI to generate **D** is intramolecular reductive elimination from 3-coordinate cationic **C** (pathway **4a**), rather than the external nucleophilic attack route (pathway **4b**) more commonly observed for analogous Pt systems and proposed for the Periana gold-based catalyst.

## 2.4 Conclusions

The reaction of (Idipp)AuMeI<sub>2</sub> to generate (Idipp)AuI and MeI shows complex dependence on concentrations of  $I^-$  and  $I_2$  in the reaction solution. Kinetics studies demonstrate that without excess  $I^-$ , the complex decomposes via reductive elimination from



an unobserved 3-coordinate species. At higher concentrations of  $\Gamma^-$ , the preferred pathway is reductive elimination from a 5-coordinate complex, accounting for the saturation kinetics observed for  $\Gamma^-$  rate dependence.  $I_2$  complicates the rate equation by adding an additional equilibrium that forms  $I_3^-$  from  $I_2$  and  $\Gamma^-$ .

## 2.5 Experimental Section

**General considerations.** (Idipp)AuCl was purchased from Sigma-Aldrich or prepared by the methods described in the literature.<sup>50</sup> (Idipp)AuMe was prepared by the method described in Chapter 1. LiI,  $I_2$ , Mg, and  $ZnCl_2$  were purchased from Sigma-Aldrich; LiI was dried overnight under vacuum then stored in a vial in an  $N_2$ -atmosphere glovebox away from light. Deuterated solvents were purchased from Cambridge Isotope Laboratories. Before use, each was subjected to three freeze-pump-thaw cycles, then stored over alumina overnight. Benzene and diethyl ether were dried by the method described in the literature by Pangborn et al.<sup>51</sup> All other chemicals and solvents were used as received, without further purification. Infrared spectra were recorded on a Nicolet 6700 by ThermoFisher Scientific using OMNIC software. X-ray diffraction experiments were carried out in the Beckman Institute Crystallographic Facility on a Bruker KAPPA APEXII X-ray diffractometer.  $^1H$  NMR spectra for kinetics experiments were obtained on both Varian 300 and 500 MHz instruments.

**Kinetics experiments.** In a  $N_2$  atmosphere glovebox, a stock solution of  $I_2$  in  $CD_3CN$  (22.2–44.4 mg/mL) was prepared and for each reaction, the desired volume was added to a vial equipped with a Teflon cap. (For amounts of  $I_2$  in excess of 11 equiv per Au, the solid

was weighed out individually.) (Idipp)AuMe (5.0 mg, 8.3  $\mu\text{mol}$ ) was dissolved in enough  $\text{CD}_3\text{CN}$  so that the total volume once the desired amount of  $\text{I}_2$  solution was added was 850  $\mu\text{L}$ . The Au solution was added to an NMR tube and both the NMR tube and the vial containing the  $\text{I}_2$  solution were brought outside of the glovebox. For reactions starting at RT, the  $\text{I}_2$  solution was added quickly to the NMR tube at the same time as a timer was started, mixed thoroughly, and put immediately into the probe. NMR spectra were recorded at intervals to follow the concentrations of complexes over time. For reactions started cold, the NMR tube containing the Au solution was frozen in a dry ice/acetone bath. The  $\text{I}_2$  solution was layered on top then the whole solution was allowed to thaw with inverting. NMR spectra were then recorded at intervals to follow the concentrations of complexes over time. The NMR probe was kept at 23  $^\circ\text{C}$ ; for lengthy reactions, the NMR tubes were kept in an oil bath at 23  $^\circ\text{C}$  between spectrum acquisitions.

For reaction with added  $\text{I}^-$ , a stock solution of  $\text{LiI}$  in  $\text{CD}_3\text{CN}$  (17.6 mg/mL) was prepared, and the (Idipp)AuMe (5.0 mg, 8.3  $\mu\text{mol}$ ) dissolved in the appropriate amount of  $\text{LiI}$  solution; otherwise the same procedure as above was followed.

## 2.6 References

1. Geletii, Y. V.; Shilov, A. E., *Kinet. Catal.*, **1983**, 24, 413-416.
2. Labinger, J. A.; Bercaw, J. E., *Nature*, **2002**, 417, 507-514.
3. Luinstra, G. A.; Wang, L.; Stahl, S. S.; Labinger, J. A.; Bercaw, J. E., *J. Organomet. Chem.*, **1995**, 504, 75-91.
4. Shilov, A. E.; Shul'pin, G. B., *Usp. Khim.*, **1987**, 56, 754-792.

5. Johansson, L.; Tilset, M.; Labinger, J. A.; Bercaw, J. E., *J. Am. Chem. Soc.*, **2000**, *122*, 10846-10855.
6. Lin, M. R.; Shen, C. Y.; Garcia-Zayas, E. A.; Sen, A., *J. Am. Chem. Soc.*, **2001**, *123*, 1000-1001.
7. Periana, R. A.; Taube, D. J.; Gamble, S.; Taube, H.; Satoh, T.; Fujii, H., *Science*, **1998**, *280*, 560-564.
8. Sen, A.; Benvenuto, M. A.; Lin, M. R.; Hutson, A. C.; Basicckes, N., *J. Am. Chem. Soc.*, **1994**, *116*, 998-1003.
9. Frúctos, M. R.; de Frémont, P.; Nolan, S. P.; Díaz-Requejo, M. M.; Perez, P. J., *Organometallics*, **2006**, *25*, 2237-2241.
10. Mo, F. Y.; Yan, J. M.; Qiu, D.; Li, F.; Zhang, Y.; Wang, J. B., *Angew. Chem. Int. Ed.*, **2010**, *49*, 2028-2032.
11. de Graaf, P. W. J.; Boersma, J.; van der Kerk, G. J. M., *J. Organomet. Chem.*, **1976**, *105*, 399-406.
12. Hashmi, A. S. K.; Salathe, R.; Frost, T. M.; Schwarz, L.; Choi, J. H., *Applied Catalysis A-General*, **2005**, *291*, 238-246.
13. Hashmi, A. S. K.; Schafer, S.; Wolfe, M.; Gil, C. D.; Fischer, P.; Laguna, A.; Blanco, M. C.; Gimeno, M. C., *Angew. Chem. Int. Ed.*, **2007**, *46*, 6184-6187.
14. Höffmann-Roder, A.; Krause, N., *Org. Biomol. Chem.*, **2005**, *3*, 387-391.
15. Jones, C. J.; Taube, D.; Ziatdinov, V. R.; Periana, R. A.; Nielsen, R. J.; Oxgaard, J.; Goddard, W. A., *Angew. Chem. Int. Ed.*, **2004**, *43*, 4626-4629.

16. Kar, A.; Mangu, N.; Kaiser, H. M.; Tse, M. K., *J. Organomet. Chem.*, **2009**, 694, 524-537.
17. Kharasch, M. S.; Beck, T. M., *J. Am. Chem. Soc.*, **1934**, 56, 2057-2060.
18. Kharasch, M. S.; Isbell, H. S., *J. Am. Chem. Soc.*, **1931**, 53, 3053-3059.
19. Levchenko, L. A.; Kartsev, V. G.; Sadkov, A. P.; Shestakov, A. F.; Shilova, A. K.; Shilov, A. E., *Dokl. Chem.*, **2007**, 412, 35-37.
20. Levchenko, L. A.; Sadkov, A. P.; Lariontseva, N. V.; Koldasheva, E. M.; Shilova, A. K.; Shilov, A. E., *J. Inorg. Biochem.*, **2002**, 88, 251-253.
21. Li, Z. G.; Capretto, D. A.; Rahaman, R. O.; He, C., *J. Am. Chem. Soc.*, **2007**, 129, 12058-12059.
22. Shul'pin, G. B.; Shilov, A. E.; Süß-Fink, G., *Tetrahedron Lett.*, **2001**, 42, 7253-7256.
23. Vicente, J.; Bermúdez, M. D.; Chicote, M. T.; Sanchez-Santano, M. J., *J. Chem. Soc. Chem. Comm.*, **1989**, 141-142.
24. Vicente, J.; Chicote, M. T.; Lozano, M. I.; Huertas, S., *Organometallics*, **1999**, 18, 753-757.
25. Xiao, Y. P.; Liu, X. Y.; Che, C. M., *J. Organomet. Chem.*, **2009**, 694, 494-501.
26. Hutchings, G. J., *Catal. Today*, **2007**, 122, 196-200.
27. Scott, V. J.; Labinger, J. A.; Bercaw, J. E., *Organometallics*, **2010**, 29, 4090-4096.
28. Ahmed, E.; Clark, R. J. H.; Tobe, M. L.; Cattalini, L., *J. Chem. Soc. Dalton*, **1990**, 2701-2706.
29. Liddle, K. S.; Parkin, C., *J. Chem. Soc. Chem. Comm.*, **1972**, 26-&.

30. Oña-Burgos, P.; Fernandez, I.; Roces, L.; Fernandez, L. T.; García-Granda, S.; Ortiz, F. L., *Organometallics*, **2009**, *28*, 1739-1747.
31. Shaik, N.; Martinez, A.; Augustin, I.; Giovinazzo, H.; Varela-Ramirez, A.; Sanau, M.; Aguilera, R. J.; Contel, M., *Inorg. Chem.*, **2009**, *48*, 1577-1587.
32. Uson, R.; Laguna, A.; Delaorden, M. U.; Parish, R. V. D.; Moore, L. S., *J. Organomet. Chem.*, **1985**, *282*, 145-148.
33. Vicente, J.; Chicote, M. T.; Bermúdez, M. D., *J. Organomet. Chem.*, **1984**, *268*, 191-195.
34. Vicente, J.; Chicote, M. T.; Bermúdez, M. D.; García-García, M., *J. Organomet. Chem.*, **1985**, *295*, 125-130.
35. Bennett, M. A., *J. Organomet. Chem.*, **1986**, *300*, 7-19.
36. Bennett, M. A.; Hoskins, K.; Kneen, W. R.; Nyholm, R. S.; Hitchcock, P.; Mason, R.; Robertson, G.; Towl, D. C., *J. Am. Chem. Soc.*, **1971**, *93*, 4591-4592.
37. Cinellu, M. A.; Cocco, F.; Minghetti, G.; Stoccoro, S.; Zucca, A.; Manassero, M., *J. Organomet. Chem.*, **2009**, *694*, 2949-2955.
38. Parish, R. V. D., *Gold Bull.*, **1997**, *30*, 3-12.
39. Sanner, R. D.; Satcher, J. H.; Droege, M. W., *Organometallics*, **1989**, *8*, 1498-1506.
40. de Frémont, P.; Marion, N.; Nolan, S. P., *J. Organomet. Chem.*, **2009**, *694*, 551-560.
41. Kuch, P. L.; Tobias, R. S., *J. Organomet. Chem.*, **1976**, *122*, 429-446.
42. Schouteeten, S.; Allen, O. R.; Haley, A. D.; Ong, G. L.; Jones, G. D.; Vicic, D. A., *J. Organomet. Chem.*, **2006**, *691*, 4975-4981.

43. Shiotani, A.; Schmidbaur, H., *J. Organomet. Chem.*, **1972**, 37, C24.
44. Tamaki, A.; Kochi, J. K., *J. Organomet. Chem.*, **1974**, 64, 411-425.
45. Tamaki, A.; Magennis, S. A.; Kochi, J. K., *J. Am. Chem. Soc.*, **1974**, 96, 6140-6148.
46. Crawford, E. M., J.S.; Tuck, D.G., *Can. J. Chem.*, **2006**, 84, 1607-1613.
47. Oconnor, C. J.; Sinn, E., *Inorg. Chem.*, **1978**, 17, 2067-2071.
48. Robinson, W. T.; Sinn, E., *J. Chem. Soc. Dalton*, **1975**, 726-731.
49. Vicente, J.; Chicote, M. T.; Bermúdez, M. D.; Jones, P. G.; Fittschen, C.; Sheldrick, G. M., *J. Chem. Soc. Dalton*, **1986**, 2361-2366.
50. de Frémont, P.; Scott, N. M.; Stevens, E. D.; Nolan, S. P., *Organometallics*, **2005**, 24, 2411-2418.
51. Pangborn, A. B.; Giardello, M. A.; Grubbs, R. H.; Rosen, R. K.; Timmers, F. J., *Organometallics*, **1996**, 15, 1518-1520.

## CHAPTER 3

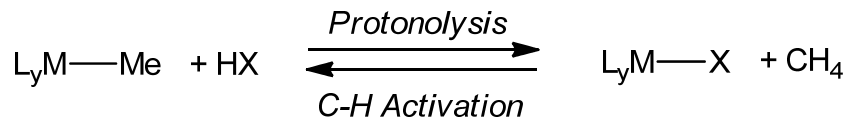
### Investigations into the possible correlation of mechanism and tunneling for the protonolysis of M-Me complexes

#### 3.1 Abstract

It has been suggested that the observation of quantum mechanical tunneling in the protonolysis reaction of metal-methyl complexes may be indicative of direct protonation of the M-Me bond, with no participation of an oxidized metal-hydride intermediate. Herein, this hypothesis is tested with examples that can only follow one pathway, and it is demonstrated that this correlation cannot be made.

#### 3.2 Introduction

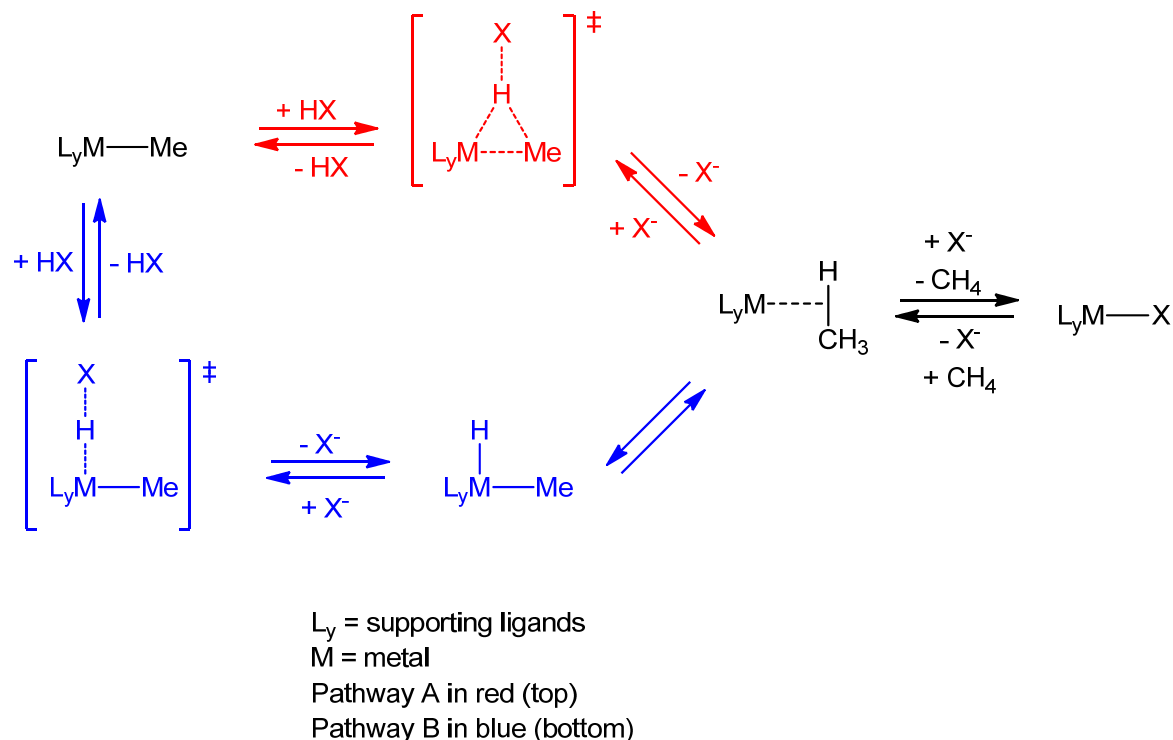
Selectively activating and functionalizing C-H bonds has been an intense area of research for several decades; the ability to do so has wide-spread applications.<sup>1-5</sup> Many transition metal complexes have been revealed over the years to carry out this partial oxidation; while much of the successes have been realized using platinum and palladium-based catalysts,<sup>1, 6-12</sup> the scope of this reaction is not limited to these metals alone.<sup>2-5</sup> Despite the numerous advances achieved in this field, C-H activation still represents a significant challenge—selectivity, turnover, and reaction conditions are frequently undesirable. If the reaction mechanism was better understood, rational catalyst design might be possible; thus, there have been significant efforts towards understanding the reaction mechanisms in these systems.

**Scheme 3.1**

Direct observation and detailed mechanistic studies on alkane C-H activation by a catalyst can be difficult to study; instead, examination of the microscopic reverse (protonolysis of a metal-alkyl bond, Scheme 3.1) has proven useful in elucidating the mechanisms that are at play.<sup>13-18</sup> Two different mechanisms for the protonolysis are generally considered (Scheme 3.2).<sup>19, 20</sup> The first (pathway A) consists of direct, concerted protonation of the metal-methyl bond. This pathway leads directly to a  $\sigma$ -adduct which is followed by loss of the alkane. The second (pathway B) involves the protonation of the metal center to generate an oxidized metal-hydride intermediate. This species can reductively eliminate the C-H bond to generate the  $\sigma$ -adduct and lose the alkane. It is important to note that any of these steps are potentially reversible. However, under protonolysis reaction conditions typically used, once the alkane is lost, it does not go back and so this step can frequently be considered irreversible; this step is generally believed to proceed by associative displacement.<sup>21-24</sup> Because all steps prior to alkane loss are reversible under the reaction conditions, the observation of a metal-hydride species may be supportive of, but is *not* conclusive evidence for the reaction proceeding through pathway B.



Scheme 3.2



Due to early successes using platinum- and palladium-based catalysts, a vast majority of the C-H activation mechanistic work has been focused on these systems.<sup>1, 6-12</sup> For Pt-Me protonolysis, the stepwise pathway B has received support (but not conclusive evidence) from the observation of Pt(IV)-H species.<sup>19, 20</sup> However, for the corresponding Pd-based systems,<sup>25-28</sup> the concerted pathway is generally preferred, both because of the lack of observed Pd(IV)-H intermediates as well as the belief that these species are less accessible.

Kinetic isotope effects (KIEs) are useful tools in the investigations of reaction mechanism,<sup>29, 30</sup> however, in the case of protonolysis, there is no obvious correlation between the measured KIE and the reaction mechanism.<sup>19, 20</sup> Recently, large kinetic isotope effects have been observed in the protonation of several Pd(II)-Me species,<sup>31</sup>

however the KIE could only be measured accurately for (dppe)PdMe<sub>2</sub> (dppe = (diphenylphosphino)ethane), due to competing reductive elimination of ethane for the other complexes examined. An unusually large KIE was likewise observed for (cod)PtMe<sub>2</sub> (cod = 1,5-cycloocatadiene).<sup>31</sup> KIEs that are greater than 10 at room temperature<sup>32-34</sup> or have Arrhenius parameters such that  $(E_a^D - E_a^H) > 1.2$  or that  $A_H/A_D$  falls outside the range of  $0.5 < A_H/A_D < 2^{1/2}$  are typically taken to demonstrate a significant amount of quantum mechanical tunneling.<sup>35-38</sup> It has been suggested that the observation of such large KIEs and tunneling may be indicative of a change in the mechanism,<sup>31, 39</sup> namely, direct protonation at the metal-methyl bond (pathway A) instead of at the metal to generate a metal-hydride species (pathway B) which can then undergo reductive elimination to give methane and the reduced metal species. The concerted pathway A was favored for both (dppe)PdMe<sub>2</sub> and (cod)PtMe<sub>2</sub> because: 1) Pd(IV)-H intermediates are not expected and 2) the presence of the electron-withdrawing cod ligand on Pt should disfavor the formation of a Pt(IV)-H. In support of this, even at low temperatures, no Pt-H is observed for this system. In contrast, past studies on other Pt-complexes that display smaller KIEs (normal and inverse, sometimes due to additional equilibrium isotope effects) do have observable Pt(IV)-H species at low temperatures.<sup>16, 19, 20, 40</sup> DFT calculations further supported the theory that the observation of tunneling may signify a mechanism change.<sup>31, 39</sup> While the few Pt and Pd species previously examined fit this notion, due to the lack of examples it was unclear whether this is a true trend or just a coincidence.

In order to determine whether this postulation was correct, the kinetic isotope effects for the protonation of several different metal-methyl species were determined. Complexes that are not capable of being oxidized further, and thus cannot form a metal-hydride, are examined as unambiguous examples for pathway A. KIEs for other complexes combined with the observation (or not) of a metal hydride species at low temperatures are also examined; the entire series of complexes should determine whether this is a mechanistic trend or a phenomenon that is not indicative of mechanism.

### 3.3 Results and Discussion

Several complexes were chosen to test the hypothesis that the observation of tunneling is a signature of following concerted pathway A (Figure 3.1).  $\text{ZnMe}_2$ ,  $\text{Cp}_2\text{ZrMeCl}$ ,  $(^t\text{Bu}_2\text{Cp})_2\text{ZrMe}_2$ , and  $(\text{Idipp})\text{AuI}_2\text{Me}$  were chosen as complexes that are unable to proceed through a metal-hydride species; if the hypothesis is correct, these complexes will display only large KIEs (Cp = cyclopentadienyl,  $^t\text{Bu}_2\text{Cp}$  = 1,3-di-*tert*-butyl cyclopentadienyl, and Idipp = 1,3-bis(2,6-diisopropylphenyl)imidazol-2-ylidene). Additionally, the reactivity of  $(\text{PONOP})\text{RhMe}$ ,  $(\text{PONOP})\text{IrMe}$ ,  $[(\text{PONOP})\text{PtMe}][\text{BAr}^{\text{F}}_4]$ , and  $(\text{Idipp})\text{AuMe}$  was examined and compared to the rest of the series (PONOP = 2,6-bis(di-*tert*butylphosphinito)pyridine,  $\text{BAr}^{\text{F}}_4 = \text{B}[3,5-(\text{CF}_3)\text{C}_6\text{H}_3]_4^-$ ).

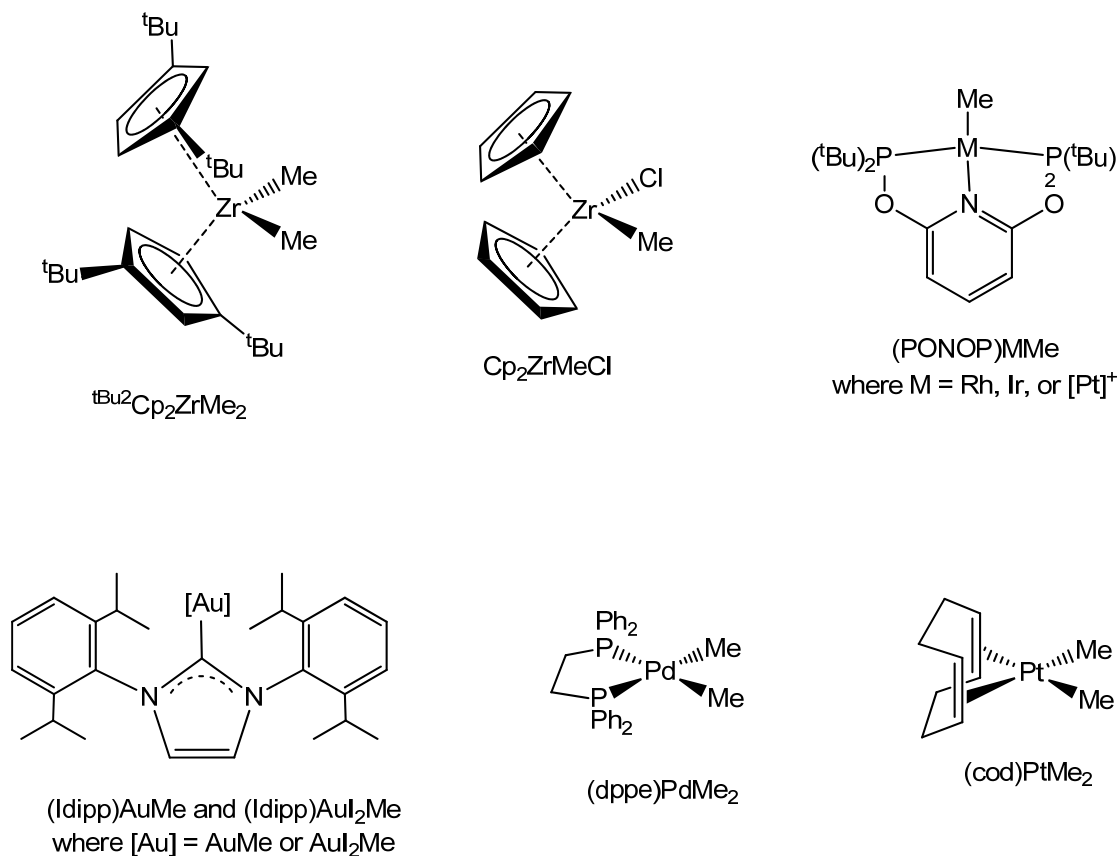
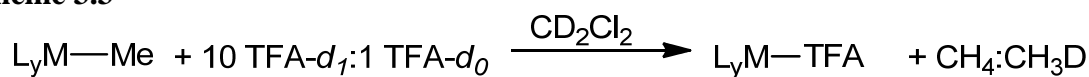


**Figure 3.1** Complexes for which KIEs of protonolysis were measured

**Scheme 3.3**



Measurements of KIEs for the protonolysis reactions were carried out using a large excess (*at least* 10 equivalents of proteo acid to methyl group) of a 10:1 mixture of TFA- $d_1$ :TFA- $d_0$  (Scheme 3.3, TFA = trifluoroacetic acid). Early on in this work, it was noted that while the observed KIEs were generally reproducible, the error was significantly higher than had been previously reported.<sup>31</sup> We were particularly concerned at our inability to reproduce the dramatic effects of temperature on the KIEs of (cod)PtMe<sub>2</sub>. It was

postulated that temperature control may not be as precise as we had originally thought- a series of experiments was designed in order to determine whether temperature control was a problem. Three different methods were examined.

Method **1**: a mixture of solvent ( $\text{CD}_2\text{Cl}_2$ ) and acid (0.5 mL and 0.2 mL, respectively) were put into a NMR tube with a septum cap. The metal complex was dissolved separately in a small amount of solvent (0.2 mL) and placed into a GC vial also equipped with a septum top. The NMR tube was placed into the appropriate temperature bath and the metal solution was added via syringe to the NMR tube, dropwise, with constant inversion (to avoid mixing problems), replacing the NMR tube in the bath between drops.

Method **2**: the acid/solvent mixture was put into a GC vial equipped with a stir bar. This vial was put into the bath and the metal solution (prepared in the same way as in method **1**) was injected dropwise with constant stirring and the acid vial remaining in the bath during the entire injection (the speed of injection—30 seconds to 2 minutes—was tested and had no effect on the observed KIE).

Method **3** was equivalent to method **1** with the exception of being run in a cold room kept at 0 °C. All NMR tubes, vials, and syringes, along with a thermometer, were allowed to equilibrate in the cold room for 1 hour before injection.

All three methods gave very similar results, but again with higher standard deviations than the previous experiments (see Table 3.1). Because of the discrepancies between this data and that previously collected,  $(\text{dppe})\text{PdMe}_2$  was also tested again, using method **2**. While these values could be reproduced within error, the standard deviation was also

higher than that reported. These discrepancies can be explained by a lack of temperature control in the original system. Qualitatively, the temperature-dependent results for the protonolysis of (cod)PtMe<sub>2</sub> are similar. Quantitatively, however, the effects appear to be somewhat smaller than previously reported (Table 3.1).

**Table 3.1** Comparison of measured and previously reported kinetic isotope effects for the protonolysis of (cod)PtMe<sub>2</sub>

Temperature (°C)	Measured KIE	Reported KIE <sup>31</sup>
-8	26.7 ± 1.4	-
0	22.7 ± 0.9	25.9 ± 0.3
23	18.0 ± 0.9	17.5 ± 0.3
40	15.5 ± 0.5	12.1 ± 0.3
60	-	9.2 ± 0.3
80	-	6.9 ± 0.3

Given these findings, we determined that method **1** was sufficient for room temperature measurements but were most comfortable with method **2** for any variable temperature measurements.

A subsequent series of experiments was performed with the complexes ZnMe<sub>2</sub>, Cp<sub>2</sub>ZrMeCl, (<sup>t</sup>Bu<sub>2</sub>Cp)<sub>2</sub>ZrMe<sub>2</sub>, and (Idipp)AuI<sub>2</sub>Me. These complexes are not expected to be able to generate intermediate metal-hydride species, as highly oxidized species such as Zn(IV), Zr(VI), and Au(V) would have to be invoked. As such, these species are expected to proceed only through the direct protonation of the metal-methyl bond and should consistently display unusually large KIEs. Thus, examination of the reactivity of these complexes may allow a correlation between tunneling and mechanism to be established.

The room temperature KIEs observed for both ZnMe<sub>2</sub> and (<sup>t</sup>Bu<sub>2</sub>Cp)<sub>2</sub>ZrMe<sub>2</sub> (yielding (<sup>t</sup>Bu<sub>2</sub>Cp)<sub>2</sub>ZrMeX) emphasize the lack of a trend between mechanism and tunneling. ZnMe<sub>2</sub>

displays a rather small KIE ( $\sim 3.1$ ) and the value for  $(^t\text{Bu}^2\text{Cp})_2\text{ZrMe}_2$  falls on the border of what is considered to be tunneling ( $\sim 10$ ). In the case of  $\text{ZnMe}_2$ , both methyl moieties react so the measured KIE is an average of the two protonolysis events. However, since the second protonolysis also occurs from a  $\text{Zn(II)}$  starting material, both events should follow the same concerted pathway so both KIEs should be large; the magnitude of the KIE is sufficiently small ( $3.1$  at  $23\text{ }^\circ\text{C}$ ) that it is unlikely that a large KIE is being masked.

In the cases of  $(\text{Idipp})\text{AuI}_2\text{Me}$  and  $\text{Cp}_2\text{ZrMeCl}$ , no protonation event was observed so a KIE could not be measured;  $\text{MeI}$  reductively eliminates over time for the  $\text{Au}$ -complex and apparently the protonation does not compete with this reaction;  $\text{Cp}_2\text{ZrMeCl}$  is seemingly stable to the acid, which is in line with the observation that  $(^t\text{Bu}^2\text{Cp})_2\text{ZrMe}_2$  only releases one equivalent of methane. Overall, this series of complexes that can only follow concerted pathway A clearly demonstrates that the observation of an unusually large KIE alone cannot be tied to this mechanism.

Recently in the Brookhart group, an unusual methane adduct was observed when  $(\text{PONOP})\text{RhMe}$  was allowed to react with  $\text{HBArF}_4 \cdot (\text{Et}_2\text{O})_2$  ( $\text{BAr}^{\text{F}}_4 = \text{B}[3,5-(\text{CF}_3)\text{C}_6\text{H}_3]_4$ ) at low temperatures ( $-110\text{ }^\circ\text{C}$ ).<sup>41</sup> Using the same ligand platform on  $\text{Ir}$  however, the reaction had been shown to proceed through an observable  $\text{Ir-H}$  at room temperature.<sup>42</sup> In fact, even at low temperatures, of the complexes examined, only  $(\text{PONOP})\text{IrMe}$  displays an observable metal-hydride species.<sup>42</sup> The lack of an observed  $\text{Rh-H}$  species does not rule out the stepwise mechanism B; likewise, the presence of an  $\text{Ir-H}$  does not conclusively show pathway B as the only functioning pathway to generate methane due to the reversible

nature of these steps. However, the evidence provided does support pathway B for the protonolysis of (PONOP)IrMe. If this premise is correct, the KIE would be expected to be smaller ( $< 10$ ). Likewise, the lack of an observable Rh-H intermediate could lead to a larger KIE, indicating pathway A.

However, the opposite was observed when (PONOP)RhMe (KIE  $\sim 6.1$ ) and (PONOP)IrMe (KIE  $\sim 10.5$ ) were allowed to react with an excess of a 10:1 mixture of  $d_1$ -TFA:TFA (TFA = trifluoroacetic acid). Additionally, in the case of (PONOP)IrMe, loss of methane is rate-determining, as demonstrated by a small amount of isotopic scrambling in the deuterolysis reaction to generate  $CD_2H_2$ . This reveals reversible reductive elimination of methane from the metal-hydride species, which in turn results in a measured KIE somewhat *higher* than its true value. Thus, caution must be used in drawing conclusions from the value obtained for this complex.<sup>42-44</sup> In further support of the lack of a trend, when the same protonation reactions were run at lower temperature, the KIE observed for (PONOP)RhMe only appears to increase a small amount, if at all; likewise, (PONOP)IrMe, only shows a small increase in KIE. It should be noted that there was insufficient material to run the low temperature experiments in duplicate using the different methods described below so these numbers are presented as qualitative data only. For complexes undergoing significant tunneling, it would be expected that the observed KIE at low temperature would increase significantly ((cod)PtMe<sub>2</sub> displays an increase in KIE from 17.5 at 21 °C to 25.9 at 0 °C).



Of the other complexes examined, [(PONOP)PtMe][BAR<sup>F</sup><sub>4</sub>] also does not protonate at room temperature; thus, no KIE could be recorded. In the case of (Idipp)AuMe, the KIEs, both at room temperature and the other temperatures examined (see Table 3.1), were difficult to reproduce as the reaction did not proceed as cleanly as the other protonolysis reactions. At present, no conclusions are being drawn from this data. From the room temperature data of the entire library of complexes alone, however, it is clear that a general correlation between tunneling and mechanism is not present.

By and large, the measured temperature dependences of the KIEs further display the lack of correlation between tunneling and mechanism; with reactions that have significant tunneling, it is expected that the KIEs will be highly temperature dependent. As discussed above, the limited data on the effect of temperature on the measured KIEs for (PONOP)MMe protonolysis with TFA was not significant when compared with that seen for the Pt and Pd complexes. ZnMe<sub>2</sub>, (<sup>t</sup>Bu<sub>2</sub>Cp)<sub>2</sub>ZrMe<sub>2</sub>, (Idipp)AuMe were examined in more detail to determine values for  $E_a^D - E_a^H$  and  $A_H/A_D$  and establish conclusively whether tunneling is occurring. The Arrhenius plots were generated using data collected via method **2** (as described above and in the Experimental Section) for the variable temperature experiments and via method **1** for room temperature data collection. Qualitatively, *none* of these complexes (except for the Pt and Pd cases) display the temperature dependence that would be expected for pathways involving significant tunneling (Table 3.2).

**Table 3.2 Measured KIEs for the protonolysis of M-Me complexes at different temperatures using different methods**

Complex	Temperature	Method	# of runs	KIE
(cod)PtMe <sub>2</sub>	-8	1	7	20.8 ± 1.0
		2	4	26.7 ± 1.4
	0	1	3	20.0 ± 2.1
		2	5	22.7 ± 0.9
		3	3	22.9 ± 1.7
	23	1	4	18.0 ± 0.9
<sup>t</sup> Bu <sub>2</sub> Cp <sub>2</sub> ZrMe <sub>2</sub>	40	1	3	16.41 ± 0.6
		2	3	15.5 ± 0.5
	-8	1	3	11.5 ± 1.8
		2	3	10.7 ± 0.2
	0	2	3	10.4 ± 0.7
	23	1	3	10.0 ± 1.1
		2	2	10.2 ± 0.11
	40	1	8	9.2 ± 0.6
		2	6	9.6 ± 1.0
(Idipp)AuMe	-8	1	3	9.1 ± 0.8
		2	3	8.1 ± 0.5
	0	2	3	7.6 ± 0.2
	23	1	5	9.5 ± 0.7
		2	3	12.8 ± 0.5
	40	2	3	9.2 ± 1.1
ZnMe <sub>2</sub>	-8	1	3	2.2 ± 0.1
		2	3	3.4 ± 0.3
	0	2	3	3.1 ± 0.3
	23	1	3	3.1 ± 0.7
	40	2	3	2.9 ± 0.3
(dppe)PdMe <sub>2</sub> - TFA	-8	2	4	9.7 ± 0.4
	0	2	4	8.1 ± 0.8
	23	2	4	6.9 ± 0.2
	40	2	4	7.2 ± 0.2
(PONOP)RhMe	-8	1	3	6.0 ± 0.9
	0	2	3	10.5 ± 3.1
	23	1	5	6.1 ± 0.4
(PONOP)IrMe	-8	1	2	13.4 ± 0.8
	23	1	6	10.5 ± 1.1

As discussed earlier, the previously reported KIEs for (dppe)PdMe<sub>2</sub> at room temperature and 0 °C could be reproduced within error, but it should be noted that the standard deviation was slightly larger than previously reported. Furthermore, the reported error in  $E_a^D - E_a^H$  and  $A_H/A_D$  was determined by the fit of the line to the Arrhenius plot alone for both of these cases, which does not take into consideration the error in each measurement. When the error is propagated all the way through, the errors in  $E_a^D - E_a^H$  and  $A_H/A_D$  increase considerably (Table 3.3).

Little information can be drawn from these experimental values; the available temperature window for experimentation is incredibly small compared to the window for an Arrhenius plot; thus, the error should be quite large, particularly for  $A_H/A_D$  (as with  $\Delta S$ ) as calculated by the value of the y-intercept. Furthermore, in Arrhenius plots where the slope is small (qualitatively demonstrating a small effect of temperature on the KIE), the error here will likewise be significant ( $E_a^D - E_a^H$  as compared to  $\Delta H$ ). These values were calculated for all experiments run here, and were recalculated for the previous results and reported standard deviations; errors here were determined here by using a linear least-squares fit with 95% confidence (Table 3.3, Figure 3.2; see Appendix D for Arrhenius plots, equations, and errors). In the case of (Idipp)AuMe, the data qualitatively demonstrates that temperature has little effect, but is shown to emphasize just how large these measured errors can be when propagated through. Measurements of temperature dependent KIEs are carried out using many different methods. While this specific method of error propagation is not always applicable, it should serve as a warning for the

importance of taking the appropriate measures for error propagation. Without accurate determination of the errors in these measurements, invalid conclusions may be drawn from these values.

**Table 3.3 Parameters and  $R^2$  values for Ahrrenius plots for complexes**

<b>Complex</b>	<b><math>E_a^D - E_a^H</math> (kcal)</b>	<b><math>A_H/A_D</math></b>	<b><math>R^2</math></b>
<b>(cod)PtMe<sub>2</sub> – fixed error on reported data</b>	$3.2 \pm 0.2$	$0.08 \pm \begin{smallmatrix} 0.03 \\ 0.02 \end{smallmatrix}$	0.99715
<b>(cod)PtMe<sub>2</sub></b>	$1.7 \pm 0.9$	$0.9 \pm \begin{smallmatrix} 3.6 \\ 0.8 \end{smallmatrix}$	0.97337
<b>(dppe)PdMe<sub>2</sub> - fixed error on reported data using TFE</b>	$2.5 \pm 0.4$	$0.3 \pm \begin{smallmatrix} 0.3 \\ 0.1 \end{smallmatrix}$	0.99715
<b>(dppe)PdMe<sub>2</sub> – using TFA</b>	$1.0 \pm 1.7$	$1.5 \pm \begin{smallmatrix} 34.0 \\ 1.4 \end{smallmatrix}$	0.74023
<b><sup>t</sup>Bu<sub>2</sub>Cp<sub>2</sub>ZrMe<sub>2</sub></b>	$0.3 \pm 0.1$	$5.6 \pm \begin{smallmatrix} 1.3 \\ 1.1 \end{smallmatrix}$	0.98651
<b>ZnMe<sub>2</sub></b>	$0.4 \pm 0.8$	$1.7 \pm \begin{smallmatrix} 5.0 \\ 1.3 \end{smallmatrix}$	0.64977
<b>(Idipp)AuMe</b>	$-0.6 \pm 3.7$	$24.8 \pm \begin{smallmatrix} 13500 \\ 24.8 \end{smallmatrix}$	0.21497

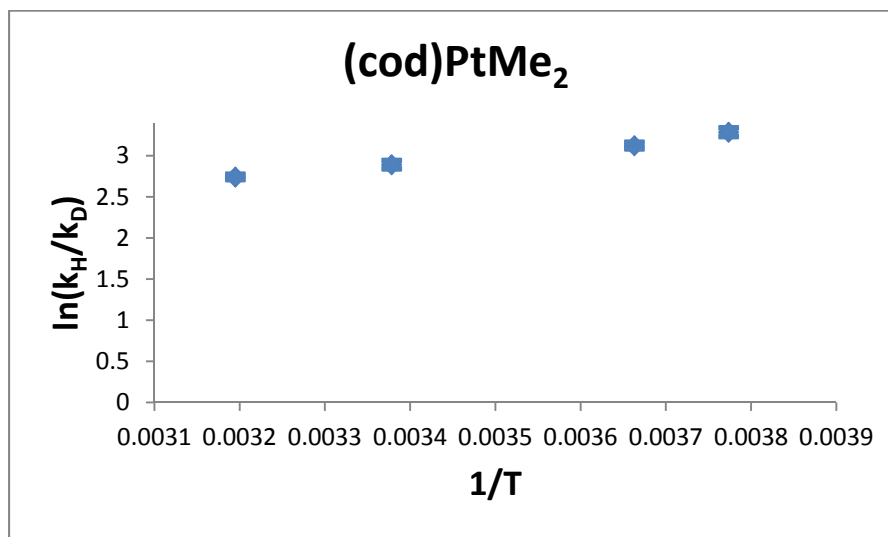


**Figure 3.2** Arrhenius plot of (cod)PtMe<sub>2</sub> protonolysis

Unexpected results were obtained when TFA is used instead of TFE in the protonolysis of (dppe)PdMe<sub>2</sub>. This reaction results in the protonolysis of both methyl moieties, as in the case of ZnMe<sub>2</sub> so the measured KIE here is again an average of the two events. The measured KIEs in this case were dramatically smaller than for the mono-protonolysis reaction with TFE (6.9 with TFA at 23 °C versus 21.4 with TFE). To accommodate a similar KIE for the first protonolysis, the second would need to be very small (inverse), which is unlikely. It may be that what is being observed in this case is a dependence of the KIE on the identity or pK<sub>a</sub> of the acid being used. For other systems, dependencies of observed KIEs on acid,<sup>45-47</sup> concentration,<sup>48</sup> pressure,<sup>49</sup> and base<sup>50</sup> have been reported. In each of these cases, however (with the exception of acid dependencies), the reliance of the KIE on each factor can be tied to the mechanism of the reaction. In the cases where the acid was observed to have an effect on the KIE, one system utilized the acid as the solvent

so the partitioning effects may be different from one acid to another.<sup>47</sup> For the other case, THF was used as the solvent<sup>45, 46</sup> and partitioning effects may be important here as well. In our case, with CD<sub>2</sub>Cl<sub>2</sub> as the main constituent of the solvent, partitioning effects are not as likely; however, the acid concentration is high enough (0.2 mL acid per 0.7 mL CD<sub>2</sub>Cl<sub>2</sub>) that it cannot be ruled out. The reason for the observed acid dependency on the KIE is not yet understood. The dramatic difference in KIE for the two different acids is intriguing and warrants further examination.

### 3.4 Conclusions

In summary, the kinetic isotope effects of the protonolysis reactions for a series of complexes were measured. The room temperature KIEs alone displayed that there is no strict correlation between the observation of tunneling and the reaction mechanism; temperature dependent KIE experiments are in agreement with this assessment. Furthermore, upon running more experiments both on the new complexes as well as the original Pd and Pt complexes, it became clear that the error in these experiments is significantly larger than originally thought, both in the direct measurements as well as propagated into the calculated values for  $E_a^D - E_a^H$  and  $A_H/A_D$ . Also, an intriguing dependence of the measured KIE on the acid used was observed with (dppe)PdMe<sub>2</sub>; further experiments will be required to fully understand this dependence.

### 3.5 Experimental Section

**General considerations.** (Idipp)AuMe,<sup>51</sup> (dppe)PdMe<sub>2</sub>,<sup>52</sup> Cp<sub>2</sub>ZrMeCl, and <sup>t</sup>Bu<sub>2</sub>Cp<sub>2</sub>ZrMe<sub>2</sub> were prepared using the reported literature procedures. (PONOP)RhMe, (PONOP)IrMe, and [(PONOP)PtMe][BAr<sup>F</sup><sub>4</sub>] were synthesized by the literature procedures<sup>41, 42</sup> by Michael Findlater. (cod)PtMe<sub>2</sub> and ZnMe<sub>2</sub> were purchased from Aldrich and used without further purification. CD<sub>2</sub>Cl<sub>2</sub> was purchased from Cambridge Isotope Laboratories. Before use, the solvent was subjected to three freeze-pump-thaw cycles and stored over alumina overnight in a N<sub>2</sub>-atmosphere glovebox. For every KIE measurement experiment, the ratio of proteo acid to methyl was *at least* 10:1 to insure that the ratio of proteo:deutero acid is the same throughout the course of the reaction.

#### **Kinetic isotope effect measurements.**

**Method 1:** In a N<sub>2</sub>-atmosphere glovebox, 0.500 mL of CD<sub>2</sub>Cl<sub>2</sub> was put into an NMR tube with a septum top along with 0.200 mL of a 10:1 mixture of TFA-*d*<sub>1</sub>:TFA. The metal complex (5 mg for solids, 0.5 μL for ZnMe<sub>2</sub>) was dissolved separately in 0.200 mL in a vial equipped with a septum top. The ratio of proteo-acid to the metal-methyl moiety was always greater than 10:1. Outside of the glovebox, the NMR tube was allowed to equilibrate with an oil bath or NaCl/ice bath for 5 minutes. The metal-complex solution was added to the NMR tube dropwise via syringe with constant inversion of the tube to prevent mixing complications.

**Method 2:** In a N<sub>2</sub>-atmosphere glovebox, a 1.5 mL vial equipped with a stirbar was charged with 0.500 mL of CD<sub>2</sub>Cl<sub>2</sub> and 0.200 mL of a 10:1 mixture of TFA-*d*<sub>1</sub>:TFA and capped with a septum. In a separate vial, the metal complex (5 mg for solids, 0.5 μL for

ZnMe<sub>2</sub>) was dissolved in 0.200 mL of CD<sub>2</sub>Cl<sub>2</sub> and capped with a septum. NMR tubes were capped with septa as well, empty, under inert atmosphere. Outside of the glovebox, the vial containing the acid mixture and stirbar was placed into the appropriate temperature bath and allowed to equilibrate for 5 minutes. The metal solution was then injected via syringe dropwise to the stirring mixture (the amount of time to add this mixture was tested from ~ 30 seconds to 2 minutes and no difference in KIE was noted). After the entire metal solution was added to the acid mixture, the reaction mixture was transferred to the septum-capped NMR tube using a gas-tight syringe.

**Method 3:** The experimental setup for this method was identical to Method 1 prior to removal from the glovebox. Once the mixtures and NMR tubes were brought outside of the glovebox, they, a syringe, and a thermometer were brought into a cold room kept at 0 °C. These were allowed to equilibrate in the cold room for 1 hour. The metal-complex solution was then added to the NMR tube dropwise via syringe with constant inversion of the tube to prevent mixing complications as in Method 1.

**NMR technique.** The NMR spectra were recorded on a 600 MHz Varian. For each reaction run, five single-scan (with an attenuation time of 5 seconds) spectra were recorded, with several minutes between scans. With the integration of CH<sub>3</sub>D set to 1, the average integration for CH<sub>4</sub> times 10 in these five spectra was taken as the KIE for that particular experiment. Every experiment was run at least three times with the exception of low temperature (PONOP)IrMe. For raw data, see Appendix D.



**$^1\text{H}$  NMR spectral data for protonation reactions.** All assignments of the final reaction products were determined by  $^1\text{H}$  NMR spectroscopy, collected on a Varian 600 MHz instrument; the  $^{19}\text{F}$  NMR spectra for all complexes were consistent with fast exchange with the excess acid present. The reaction of  $(\text{cod})\text{PtMe}_2$  with excess TFA results in the formation of  $(\text{cod})\text{PtMe}(\text{TFA})$ .  $^1\text{H}$  NMR ( $\text{CD}_2\text{Cl}_2$ ):  $\delta$  5.50-5.46 (m, 2H), 5.80-5.60 (m, 2H), 2.7-2.2 (m, 8H), 0.78 (s,  $^2J_{\text{PtH}} = 30$  Hz). The reaction of  $(\text{dppe})\text{PdMe}_2$  with excess TFE results in the formation of  $(\text{dppe})\text{PdMe}(\text{TFE})$ .  $^1\text{H}$  NMR ( $\text{CD}_2\text{Cl}_2$ ):  $\delta$  7.8-7.4 (m, 20H), 2.50-2.10 (m, 4H), 0.54 (br, 3H). The reaction of  $(\text{dppe})\text{PdMe}_2$  with excess TFA results in the formation of  $(\text{cod})\text{Pt}(\text{TFA})_2$ .  $^1\text{H}$  NMR ( $\text{CD}_2\text{Cl}_2$ ):  $\delta$  7.88-7.56 (m, 20H), 2.8-2.55 (m, 4H). The reaction of  $\text{ZnMe}_2$  with excess TFA results in the formation of  $\text{Zn}(\text{TFA})_2$ ; no  $^1\text{H}$  NMR signal other than those for the acid, solvent and methane isotopologs are observed. The reaction of  $^t\text{Bu}_2\text{Cp}_2\text{ZrMe}_2$  with excess TFA results in the formation of  $^t\text{Bu}_2\text{Cp}_2\text{ZrMe}(\text{TFA})$ .  $^1\text{H}$  NMR ( $\text{CD}_2\text{Cl}_2$ ):  $\delta$  6.7-6.3 (m, 6H), 1.30 (s, 3H), 1.28, (s, 9H), 1.25 (s, 9H). The reaction of  $(\text{PONOP})\text{IrMe}$  with excess TFA results in the formation of  $(\text{PONOP})\text{Ir}(\text{TFA})$ .  $^1\text{H}$  NMR ( $\text{CD}_2\text{Cl}_2$ ):  $\delta$  8.00 (t, 1H,  $^3J_{\text{HH}} = 12$  Hz), 7.11 (d, 2H,  $^3J_{\text{HH}} = 6$  Hz), 1.6-1.3 (m, 36H). The reaction of  $(\text{PONOP})\text{RhMe}$  with excess TFA results in the formation of  $(\text{PONOP})\text{Rh}(\text{TFA})$ .  $^1\text{H}$  NMR ( $\text{CD}_2\text{Cl}_2$ ):  $\delta$  7.56 (t, 1H,  $^3J_{\text{HH}} = 6$  Hz), 7.37 (d, 2H,  $^3J_{\text{HH}} = 6$  Hz), 1.34 (d, 18H,  $^3J_{\text{HH}} = 6$  Hz), 1.26 (d, 18H,  $^3J_{\text{HH}} = 6$  Hz). The reaction of  $(\text{Idipp})\text{AuMe}$  with excess TFA results in the formation of  $(\text{Idipp})\text{Au}(\text{TFA})$ .  $^1\text{H}$  NMR ( $\text{CD}_2\text{Cl}_2$ ):  $\delta$  7.57 (t, 2H,  $^3J_{\text{HH}} = 6$  Hz), 7.37, (2, 4H,  $^3J_{\text{HH}} = 6$  Hz), 7.33 (s, 2H), 2.60-2.51 (m, 4H), 1.34 (d, 12H,  $^3J_{\text{HH}} = 6$  Hz), 1.26 (d, 12H,  $^3J_{\text{HH}} = 6$  Hz).

### 3.6 References

1. Labinger, J. A.; Bercaw, J. E., *Nature*, **2002**, *417*, 507-514.
2. Arndtsen, B. A.; Bergman, R. G.; Mobley, T. A.; Peterson, T. H., *Accounts. Chem. Res.*, **1995**, *28*, 154-162.
3. Crabtree, R. H., *Chem. Rev.*, **1995**, *95*, 987-1007.
4. Shilov, A. E.; Shul'pin, G. B., *Chem. Rev.*, **1997**, *97*, 2879-2932.
5. Stahl, S. S.; Labinger, J. A.; Bercaw, J. E., *Angew. Chem. Int. Ed.*, **1998**, *37*, 2181-2192.
6. Geletii, Y. V.; Shilov, A. E., *Kinetics and Catalysis*, **1983**, *24*, 413-416.
7. Johansson, L.; Tilset, M.; Labinger, J. A.; Bercaw, J. E., *J. Am. Chem. Soc.*, **2000**, *122*, 108467-10855.
8. Lin, M. R.; Shen, C. Y.; Garcia-Zayas, E. A.; Sen, A., *J. Am. Chem. Soc.*, **2001**, *123*, 1000-1001.
9. Luinstra, G. A.; Wang, L.; Stahl, S. S.; Labinger, J. A.; Bercaw, J. E., *J. Organomet. Chem.*, **1995**, *504*, 75-91.
10. Periana, R. A.; Taube, D. J.; Gamble, S.; Taube, H.; Satoh, T.; Fujii, H., *Science*, **1998**, *280*, 560-564.
11. Sen, A.; Benvenuto, M. A.; Lin, M. R.; Hutson, A. C.; Basickes, N., *J. Am. Chem. Soc.*, **1994**, *116*, 998-1003.
12. Shilov, A. E.; Shul'pin, G. B., *Uspekhi Khimii*, **1987**, *56*, 754-792.
13. Hill, G. S.; Rendina, L. M.; Puddephatt, R. J., *Organometallics*, **1995**, *14*, 4966-4968.

14. Parmene, J.; Ivanovic-Burmazovic, I.; Tilset, M.; van Eldik, R., *Inorg. Chem.*, **2009**, *48*, 9092-9103.
15. Romeo, R.; Plutino, M. R.; Elding, L. I., *Inorg. Chem.*, **1997**, *36*, 5909-5916.
16. Stahl, S. S.; Labinger, J. A.; Bercaw, J. E., *J. Am. Chem. Soc.*, **1995**, *117*, 9371-9372.
17. Wik, B. J.; Ivanovic-Burmazovic, I.; Tilset, M.; van Eldik, R., *Inorg. Chem.*, **2006**, *45*, 3613-3621.
18. Wik, B. J.; Lersch, M.; Tilset, M., *J. Am. Chem. Soc.*, **2002**, *124*, 12116-12117.
19. Romeo, R.; D'Amico, G., *Organometallics*, **2006**, *25*, 3435-3446.
20. Stahl, S. S.; Labinger, J. A.; Bercaw, J. E., *J. Am. Chem. Soc.*, **1996**, *118*, 5961-5976.
21. Johansson, L.; Ryan, O. B.; Romming, C.; Tilset, M., *J. Am. Chem. Soc.*, **2001**, *123*, 6579-6590.
22. Johansson, L.; Tilset, M., *J. Am. Chem. Soc.*, **2001**, *123*, 739-740.
23. Procelewska, J.; Zahl, A.; van Eldik, R.; Zhong, H. A.; Labinger, J. A.; Bercaw, J. E., *Inorg. Chem.*, **2002**, *41*, 2808-2810.
24. Zhong, H. A.; Labinger, J. A.; Bercaw, J. E., *J. Am. Chem. Soc.*, **2002**, *124*, 1378-1399.
25. Ackerman, L. J.; Sadighi, J. P.; Kurtz, D. M.; Labinger, J. A.; Bercaw, J. E., *Organometallics*, **2003**, *22*, 3884-3890.
26. Kapteijn, G. M.; Dervisi, A.; Grove, D. M.; Kooijman, H.; Lakin, M. T.; Spek, A. L.; Vankoten, G., *J. Am. Chem. Soc.*, **1995**, *117*, 10939-10949.
27. Kim, Y. J.; Osakada, K.; Sugita, K.; Yamamoto, T.; Yamamoto, A., *Organometallics*, **1988**, *7*, 2182-2188.

28. Kim, Y. J.; Osakada, K.; Takenaka, A.; Yamamoto, A., *J. Am. Chem. Soc.*, **1990**, *112*, 1096-1104.
29. Jones, W. D., *Accounts. Chem. Res.*, **2003**, *36*, 140-146.
30. Ryabov, A. D., *Chem. Rev.*, **1990**, *90*, 403-424.
31. Bercaw, J. E.; Chen, G. S.; Labinger, J. A.; Lin, B. L., *J. Am. Chem. Soc.*, **2008**, *130*, 17654-17655.
32. Bell, R. P., *Chem. Soc. Rev.*, **1974**, *3*, 513-544.
33. Bell, R. P., *The Proton in Chemistry*. Cornell University Press: Ithaca, NY, 1973.
34. Bell, R. P., *The Tunnel Effect in Chemistry*. Chapman and Hall: London, 1980.
35. Caldin, E. F., *Chem. Rev.*, **1969**, *69*, 135-156.
36. Kwart, H., *Accounts. Chem. Res.*, **1982**, *15*, 401-408.
37. Limbach, H. H.; Lopez, J. M.; Kohen, A., *Philos. Trans. Roy. Soc. B*, **2006**, *361*, 1399-1415.
38. Melander, L.; Saunders, W. H., *Reaction Rates of Isotopic Molecules*. Krieger: Malabar, FL, 1987.
39. Bercaw, J. E.; Chen, G. S.; Labinger, J. A.; Lin, B. L., *Organometallics*, **2010**, *29*, 4354-4359.
40. Crumpton-Bregel, D. M.; Goldberg, K. I., *J. Am. Chem. Soc.*, **2003**, *125*, 9442-9456.
41. Bernskoetter, W. H.; Schauer, C. K.; Goldberg, K. I.; Brookhart, M., *Science*, **2009**, *326*, 553-556.

42. Bernskoetter, W. H.; Hanson, S. K.; Buzak, S. K.; Davis, Z.; White, P. S.; Swartz, R.; Goldberg, K. I.; Brookhart, M., *J. Am. Chem. Soc.*, **2009**, *131*, 8603-8613.
43. Chen, G. S.; Labinger, J. A.; Bercaw, J. E., *Proc. Nat. Acad. Sci. USA*, **2007**, *104*, 6915-6920.
44. Owen, J. S.; Labinger, J. A.; Bercaw, J. E., *J. Am. Chem. Soc.*, **2006**, *128*, 2005-2016.
45. Basallote, M. G.; Duran, J.; Fernandez-Trujillo, M. J.; Manez, M. A., *J. Chem. Soc. Dalt. Trans.*, **1998**, 2205-2210.
46. Basallote, M. G.; Duran, J.; Fernandez-Trujillo, M. J.; Manez, M. A., *J. Organomet. Chem.*, **2000**, *609*, 29-35.
47. Bennett, B. L.; Hoerter, J. M.; Houlis, J. F.; Roddick, D. M., *Organometallics*, **2000**, *19*, 615-621.
48. Castillo, I.; Tilley, T. D., *J. Am. Chem. Soc.*, **2001**, *123*, 10526-10534.
49. Rosini, G. P.; Soubra, S.; Vixamar, M.; Wang, S. Y.; Goldman, A. S., *J. Organomet. Chem.*, **1998**, *554*, 41-47.
50. Sandoval, C. A.; Ohkuma, T.; Muniz, K.; Noyori, R., *J. Am. Chem. Soc.*, **2003**, *125*, 13490-13503.
51. Scott, V. J.; Labinger, J. A.; Bercaw, J. E., *Organometallics*, **2010**, *29*, 4090-4096.
52. Degraaf, W.; Boersma, J.; Smeets, W. J. J.; Spek, A. L.; Vankoten, G., *Organometallics*, **1989**, *8*, 2907-2917.

## CHAPTER 4

### Understanding the mechanism of conversion of methanol to triptane by $\text{ZnI}_2$ and $\text{InI}_3$

#### 4.1 Abstract

$\text{ZnI}_2$  and  $\text{InI}_3$  both catalytically convert methanol to a mixture of hydrocarbons, olefins, and aromatic products, with particular selectivity for 2,2,3-trimethylbutane (*triptane*). The mechanisms of these transformations are further probed, specifically examining the differences between the two catalytic systems. Finally, the iodide contents of the final reaction mixtures for several methanol conversion reactions are inspected. This research represents part of a larger collaborative body of work done with Nilay Hazari that has been previously published.<sup>1</sup>

#### 4.2 Introduction

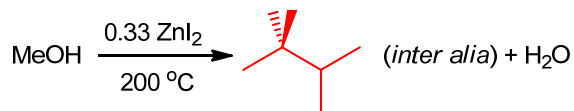
##### 4.2.1 Methanol conversion and surprising selectivity for $\text{ZnI}_2$ -catalyzed conversion

Given the forecasted depletion in oil reserves and the rising cost of oil, it appears likely that methanol will play an increasingly important role as both a direct energy source and a petrochemical feedstock.<sup>2, 3</sup> One common approach to methanol conversion into hydrocarbons involves acid-catalyzed dehydrative condensation;<sup>4</sup> different classes of hydrocarbons can be obtained depending on the nature of the catalyst and the temperature (typically 200–450 °C). The most familiar examples are the methanol-to-gasoline (MTG) and methanol-to-olefins (MTO) processes, which operate at temperatures above 300 °C over zeolitic and aluminophosphate catalysts yielding mainly  $\text{C}_{2-4}$  paraffins and olefins, respectively, among arene byproducts.<sup>5-7</sup> Another related process is the Pearson system,<sup>8</sup>

which generates alkanes and arenes from methanol at high temperatures (190 °C) over a polyphosphoric acid catalyst. This system gives a highly complex product mixture implicative of a thermodynamically controlled system.

In 1978, the reaction of methanol with  $\text{ZnI}_2$  at 200 °C was reported to give quite different results: the hydrocarbon product mixture consisted primarily of highly branched alkanes and highly methylated benzenes, with striking selectivity for one particular alkane, 2,2,3-trimethylbutane (triptane). This  $\text{C}_7$  alkane, which has a research octane number of 112, was obtained in overall yields of up to 20% (based on moles of carbon), corresponding to as much as half of the gasoline-range fraction (Scheme 4.1).<sup>9</sup> Besides the obvious practical advantages that would result from development of a convenient synthetic route to a potentially highly valuable fuel, there is a fundamental question of considerable interest: how can we account for the unusual selectivity in mechanistic terms?

#### Scheme 4.1



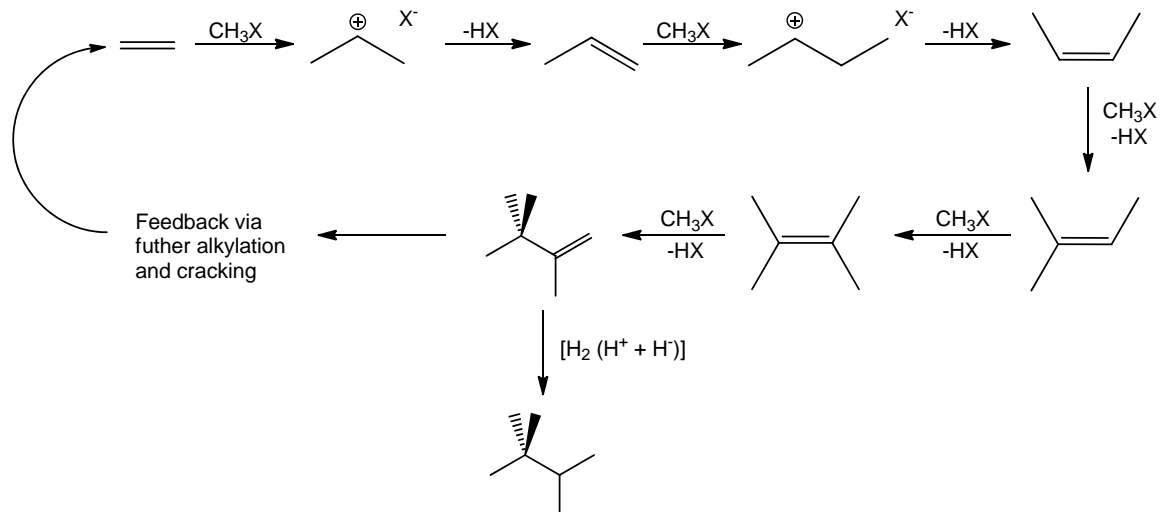
#### 4.2.2 Early mechanistic studies on $\text{ZnI}_2$ -catalyzed methanol conversion

The chemistry here appears to be significantly different from that of the MTG and MTO reactions, which take place at considerably higher temperatures and give very different product distributions. Their mechanism(s) have inspired lengthy debate, but consensus seems to be coalescing about a “hydrocarbon pool” route, which involves polymethylbenzenes as key intermediates. These undergo rearrangements and

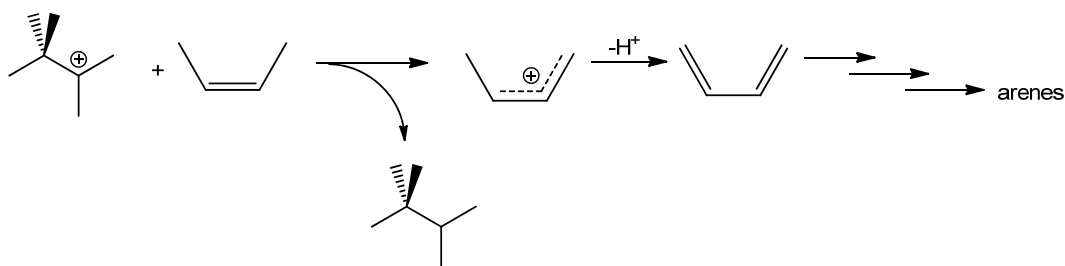
fragmentations to split off small ( $C_2$ - $C_4$ ) olefins, generating less-substituted benzenes which are remethylated by methanol. For MTG the main products are  $C_{2-4}$  paraffins, obtained via hydrogen transfer processes, and  $C_{7-10}$  methylbenzenes; the shape-selective properties of the catalyst ensure that larger arenes are unable to exit the cages.<sup>10</sup> In the case of MTO *no* arenes can get out, and the products consist of  $C_{2-4}$  olefins; selectivity among those may be controlled by speciation preferences in the hydrocarbon pool (which in turn is presumably governed by the catalyst's shape selectivity).<sup>11</sup> It seems most unlikely that any analogous mechanism could explain the  $ZnI_2$  catalyzed conversion.

Initial studies implicated a carbocation-based mechanism, involving homologation via successive olefin methylation and deprotonation (Scheme 4.2).<sup>12</sup> Formation of the first reactive  $C=C$  bonded species is catalyzed heterogeneously: the reaction does not take place if the  $ZnI_2$  is fully dissolved in methanol prior to heating. (The growth stage, in contrast, is homogeneous, proceeding equally well whether or not any solid is present.) This initiation can be completely bypassed by the addition of a suitable promoter, either an unsaturated compound (olefin or arene) or a higher alcohol; the latter presumably functions as a facile precursor to an olefin.<sup>12</sup> Since homologation products are obtained in large (molar) excess over the amount of promoter, there must be a "feedback" mechanism that regenerates light olefin building blocks; possible candidates will be discussed later.



**Scheme 4.2**

Although stoichiometrically the dehydrative condensation of methanol would lead to alkenes,  $\text{C}_n\text{H}_{2n}$ , the actual product distribution consists primarily of alkanes and arenes, with only a small amount of alkenes. Alkane formation is accomplished via hydride transfer from an unsaturated hydrocarbon to a carbocation, concluding net transfer of  $\text{H}_2$  from one olefinic hydrocarbon to another. This results in an alkane and a multiply unsaturated species which eventually ends up as an arene, as illustrated in Scheme 4.3.<sup>12</sup>

**Scheme 4.3**

Because conversion is limited by water formation, reactions are carried out with relatively high catalyst loadings: methanol-to-metal iodide molar ratios are typically around

3. However, it has been shown that much higher turnover numbers, which would clearly be needed in a practical process, can be achieved by operating in batch mode with periodic removal of volatiles (including water).<sup>12</sup>

Several other factors are notable: it has been established that P-H bonded species (phosphorous or hypophosphorous acid) can serve as alternate hydride sources and thus increase triptane yields by reducing the fraction of feed sacrificed to arene formation;<sup>13</sup> that  $\text{InI}_3$  functions as a catalyst for methanol conversion;<sup>14</sup> and that  $\text{InI}_3$  is further able to catalyze the homologation of branched alkanes.<sup>15</sup> Table 4.1 shows typical product distributions for  $\text{ZnI}_2$  and  $\text{InI}_3$  catalyzed reactions (run for 2 h at 200 °C with a 3:1 ratio of methanol:catalyst), obtained from standard refinery “PIANO” analysis<sup>12, 14</sup> (these will not be precise because of the volatility of lighter hydrocarbons and incomplete identification of GC peaks for heavier ones); for the In case, the results are generally similar except for the virtual absence of any olefins, and a corresponding increase in isoparaffins and arenes.

**Table 4.1** PIANO Analysis results for the conversion of methanol over metal iodides<sup>a</sup>

Compound or Class	Yield with ZnI <sub>2</sub> <sup>b</sup>	Yield with InI <sub>3</sub> <sup>b</sup>
<b><i>n</i>-Paraffins</b>	1.3	0.6
<b>Isoparaffins</b>	45.0	58.7
<i>i</i> -Butane	2.6	2.8
2-Methylbutane	2.9	9.1
2-Methylpentane	0.4	2.3
3-Methylpentane	0.3	1.6
2,3-Dimethylbutane	1.8	5.3
Total C <sub>6</sub> isoparaffins	2.5	9.1
2,3-Dimethylpentane	0.7	2.4
2,4-Dimethylpentane	0.4	1.5
Triptane	24.9	26.6
Total C <sub>7</sub> isoparaffins	26.2	30.7
Total C <sub>8</sub> isoparaffins	3.8	4.3
<b>Olefins</b>	14.2	0.4
Triptene	5.6	-
<b>Arenes</b>	10.7	23.3
1,2,3,5-Tetramethylbenzene	0.5	1.7
1,2,4,5-Tetramethylbenzene	0.3	1.2
Pentamethylbenzene	0.6	13.1
Hexamethylbenzene	3.4	5.5
<b>Naphthenes</b>	5.2	4.6

<sup>a</sup> For reactions run for 2 hours at 200 °C<sup>b</sup> Stated as the weight percent of the corresponding compound or class of compounds in the organic layer, after separation of the aqueous layer

The strong preference for generating the most substituted carbocation possible at each methylation step in Scheme 4.2 can account for the general selectivity to branched products (with the exception of C<sub>4</sub>), and a mixture of alkanes plus arenes will be preferred over alkenes on thermodynamic grounds. Very little *n*-butane is seen in the product profiles, even though its precursor olefin is proposed to be generated along the pathway to triptane; however, a significant amount of isobutane is observed, which is *not* on this pathway. It

has been shown that the formation of this product is most likely due to cracking of larger olefins,<sup>1</sup> particularly C<sub>7</sub> other than triptene, which cannot easily undergo this cracking pathway.

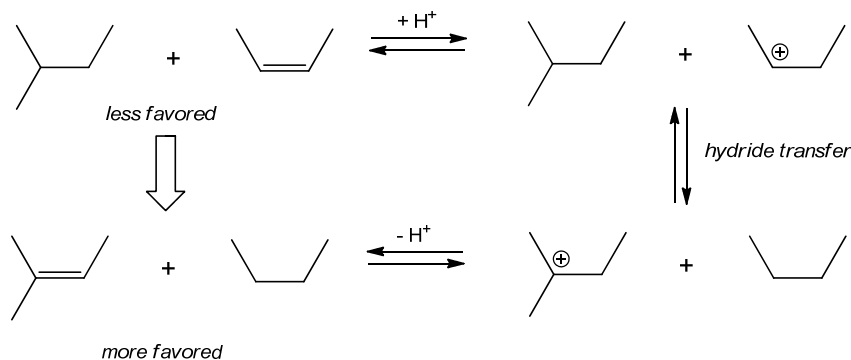
#### 4.2.3 *Relative rates of methylation versus hydride transfer and selectivity for triptane*

These points do not account for the high selectivity to triptane, which has nothing to do with thermodynamics.<sup>12</sup> In contrast, methanol condensation induced by polyphosphoric acid (reported approximately concurrently with the first ZnI<sub>2</sub> publication) takes place at similar temperatures and likewise gives primarily alkanes and arenes (in terms of both molecular weight and isomerism).<sup>8</sup>

The tentative explanation for these results centered on the fact that there will effectively be a competition between methylation and hydrogenation for each of the growing olefins in Scheme 4.2 and that the relative rates of those two processes will depend strongly on the degree of substitution of the olefin. As previously discussed,<sup>12</sup> the increased electron richness of more substituted olefins will make methylation faster, although a counterbalancing steric retardation probably sets in at some point. On the other side of the balance, hydrogenation is thermodynamically more favored for *less* substituted olefins, as exemplified in Scheme 4.4. Of course, reactions of the sort shown cannot be fully equilibrated under reaction conditions since that would lead to a thermodynamic product distribution, but the relative values of the individual rate constants for the various steps must reflect these preferences to some degree, whether or not the transformations are reversible. It was previously suggested that there *was* some degree of reversibility—i.e.,

that alkanes, once formed, could still be further transformed—but there was no definitive evidence one way or the other.<sup>12</sup>

**Scheme 4.4**



Taken together, these two trends might provide an explanation for triptane selectivity: they predict that the relative preference of hydrogenation over growth by methylation will be significantly greater for less-substituted olefins. Since triptene is a *disubstituted* olefin—the first olefin along the growth sequence that is *less* substituted than its precursor—that argument implies that growth should be increasingly efficient *up to but not beyond* C<sub>7</sub>.

In order to allow for alkanes and olefins to interconvert (but not to the point of equilibrium), alkanes must be somewhat reactive over the reaction conditions. Several thorough experiments designed to test this possibility determined that for the ZnI<sub>2</sub>-catalyzed reaction, alkanes were in fact *unreactive* and do not perturb the triptane-forming reaction.<sup>1</sup> Labeling experiments further confirmed this fact: no exchange of either methyl groups or protons from the alkane was observed. This information warranted a refinement of the proposed mechanism and can be explained by relative rates. The proposal was that the rate of methylation of triptene to generate a C<sub>8</sub> carbocation is slower than hydride

abstraction of the triptyl cation to make triptane, which is in contrast to the relative rates of methylation and hydride abstraction for the smaller olefins and carbocations along the path to making triptane (Scheme 4.2). This was confirmed by a series of methylation versus hydride abstraction competition experiments; for the lighter olefins, the rate of methylation was shown to be faster than hydride abstraction to generate the alkane. To probe the hypothesis about the relative rates of methylation for the different olefins based on the amount of substitution, a series of experiments using different C<sub>7</sub> olefins were done; these successfully demonstrated that methylation as compared to hydride abstraction for the more substituted (and more electron rich) olefins is faster than the related less substituted ones. This accounts for why the reaction is highly selective for triptane; triptene is the first *less* substituted olefin formed along the reaction pathway, and at this point hydride abstraction happens faster than the next methylation step. This mechanism is also supported by good agreement with a modeling experiment.<sup>1</sup>

Can this mechanistic framework account for the similarities and differences between ZnI<sub>2</sub>- and InI<sub>3</sub>-catalyzed reactions, as well as the non-selective polyphosphoric acid system? The following work was aimed at answering this question as well addressing the iodide content of the final reaction mixtures, which is directly correlated to its industrial applicability.

## 4.3 Results and Discussion

### 4.3.1 Investigating the differences between $\text{ZnI}_2$ and $\text{InI}_3$ catalyzed reactions

As mentioned earlier,  $\text{InI}_3$  can also catalyze the transformation of methanol to triptane;<sup>14</sup> although the general features are quite similar to the  $\text{ZnI}_2$  system and the same chain growth mechanism was postulated, there are some obvious differences between the two systems. In  $\text{InI}_3$ -catalyzed methanol conversion, no olefins are observed in the final product distribution; this is accompanied by higher quantities of aromatics, implying more efficient hydride transfer, as compared with the  $\text{ZnI}_2$  system. Methylation of arenes is also much faster with In than with Zn. Finally, at 200 °C, where alkanes appear completely inert to the  $\text{ZnI}_2$  system,  $\text{InI}_3$  is able to activate (some) alkanes: reaction of  $\text{InI}_3$  with neat alkanes results in isomerization and cracking, methanol conversion can be initiated by alkanes, and alkanes can be directly homologated with methanol (See Chapter 5).

All of these observations could be consistent with an assumption that the  $\text{InI}_3$  solution exhibits higher effective acidity (Brønsted and/or Lewis) than  $\text{ZnI}_2$ ; but is it simply a question of a quantitative factor, or is there a more fundamental qualitative difference? Are there pathways available to In but not Zn that might be responsible for some or all of the differences? For example, the activation of alkanes could conceivably involve a redox process, since reduction of In(III) to In(I) might be possible (although surely quite unfavorable) while the analogous reduction of Zn(II) to Zn(0) would not. While probing these possible mechanistic differences may be difficult, if only quantitative factors are involved, then it might be possible to “turn on” some of the typical In behavior by carrying

out Zn reactions at higher temperatures and/or for longer times. Conversely, running In reactions at lower temperatures and shorter reaction times would give results that begin to look more like Zn. On the other hand, if the reagents *are* qualitatively different, these changes would not be expected. A number of experiments have been performed to distinguish between these two alternatives.

Table 4.2 shows results for several  $\text{ZnI}_2$ -catalyzed methanol conversion experiments carried out at 230 °C. Most notably, in contrast to the behavior at 200 °C, DMB initiates the reaction, resulting in approximately the same triptane yield as a reaction initiated with  $^i\text{PrOH}$  (although this reaction was allowed to react longer, the results are comparable, because in each case MeOH/DME has been completely consumed, and it has been shown that alkanes do not significantly react further). The average yield, 45 mg, is lower than that obtained for an otherwise similar reaction at 200 °C (60 mg). The yield of aromatics appears to drop significantly, but that is probably due to the longer reaction time, leading to formation of heavier compounds not observable in the GC analysis employed. Adamantane (AdH) also initiates reaction at 230 °C, and its presence significantly improves the triptane yield (from 45 mg to 61.5 mg, initiated with  $^i\text{PrOH}$ , and to 54.6 mg, initiated by AdH). Studies on  $\text{InI}_3$ -catalyzed alkane homologation (See Chapter 5) showed that AdH decreases the rate of the reaction but increases the selectivity by inhibiting side reactions that waste methanol; slowing of the reaction would be unlikely to be noticed at the higher temperatures of these studies.

**Table 4.2** Yields of selected products from  $\text{ZnI}_2$  catalyzed reactions at 230 °C.<sup>a</sup> Unless otherwise stated, all quantities are in milligrams.

Time	Added	Added	Added	Recovered	Recovered	Isobutane	Isopentane	Triptane	PMB +
------	-------	-------	-------	-----------	-----------	-----------	------------	----------	-------



(h)	<sup>i</sup> PrOH	DMB	AdH	DMB	AdH				HMB
3	39	0	0	8	-	29	20	42	42
6	39	0	50	8	26	38	23	62	39
6	0	0	50	8	32	29	19	55	47
16	0	33	0	32	-	42	25	45	17
16	0	33	0	29	-	31	23	48	11
16	0	33	0	32	-	33	25	44	16

<sup>a</sup> All reactions contained 7.52 mmol of ZnI<sub>2</sub> and 24.7 mmol of methanol

An extensive series of reactions containing ZnI<sub>2</sub>, methanol, and <sup>i</sup>PrOH as an initiator was performed at different temperatures and reaction times; results are shown in Table 4.3. Overall, the product distributions at higher temperatures or extended times resemble those of InI<sub>3</sub> catalyzed reactions: few or no olefins simultaneously with more aromatics. Even in reactions carried out at temperatures as low as 180 °C (the lowest possible temperature at which methanol conversion will occur for ZnI<sub>2</sub>), it is possible to obtain a reaction profile with no olefins, provided the reactions are allowed to proceed for sufficient time. Time-course experiments clearly show this trend. Figure 4.1 shows the concentration of 2-methyl-2-butene (which is assumed to be representative of all olefins) over time for reactions carried out at 200 °C; complete absence of olefins is seen at longer times.

**Table 4.3** Effects of temperature and reaction time on ZnI<sub>2</sub> catalyzed methanol conversion.<sup>a</sup> Unless otherwise stated, all quantities are in milligrams.

Temperature (°C)	Time (h)	Isobutane	Isopentane	2,3-Dimethyl-2-butene	DMB	Triptane	PMB	HMB
230	3	21	nd <sup>b</sup>	0	9	42	18	26
230	3	29	20	0	8	42	19	22
215	3	36	24	0	8	55	12	4
207	3	26	19	0.6	7	60	7	5
200	16	26	21	0	6	61	7	Trace
180	16	21	17	0	6	66	6	3
180	16	23	17	0	6	67	6	3

<sup>a</sup> Reactions were carried out using 7.52 mmol of ZnI<sub>2</sub>, 24.7 mmol of Methanol, and 0.65 mmol of <sup>i</sup>PrOH

<sup>b</sup> Not determined

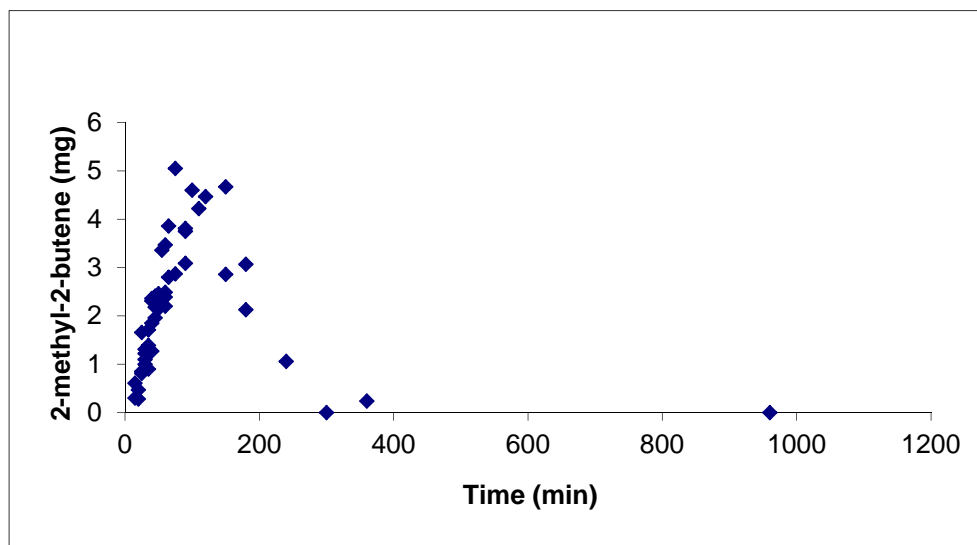


**Figure 4.1** Yield of 2-methyl-2-butene over time for  $\text{ZnI}_2$  catalyzed methanol conversion at 200 °C. Each data point represents a separate experiment.

Figure 4.2 shows the analogous behavior for aromatics: there is an initial rise in the amount of hexamethylbenzene (HMB), followed by a slow decrease as pentamethylbenzene (PMB) and tetramethylbenzene (TMB) grow in. This result indicates that HMB is not innocent under the reaction conditions; in fact, it appears to act as a methyl source once all MeOH and DME have been consumed. Consumption of HMB was further demonstrated by reaction of  $\text{ZnI}_2$  (7.52 mmol), 3 equivalents of water (22.6 mmol), and HMB (100 mg, 0.62 mmol) for 16 hours at 200 °C; from the black reaction mixture, only 42.7 mg of HMB was recovered while 22.8 mg of PMB was formed. (The poor mass balance may be accounted for by the formation of heavier aromatic species that are not detected by GC.) A related experiment using triptene in place of HMB showed slower

conversion of triptene, giving at the end a trace amount of triptane and slightly larger amounts of isobutane, isopentane, and C<sub>6</sub> and C<sub>7</sub> alkane isomers. InI<sub>3</sub> is known to carry out the same reactivity, but at lower temperatures and with much higher conversion of the olefin to other products; these results further demonstrate the apparent similarities between the two systems.

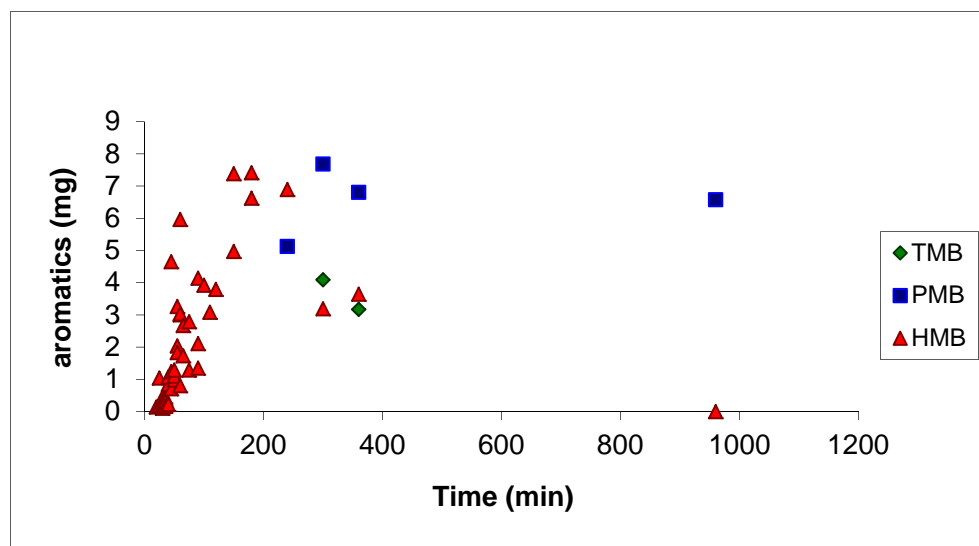


**Figure 4.2** Yield of aromatics over time for ZnI<sub>2</sub> catalyzed methanol conversion at 200 °C. Each data point represents a separate experiment.

It thus appears that the differences between ZnI<sub>2</sub>- and InI<sub>3</sub>-catalyzed reactions largely disappear when ZnI<sub>2</sub> is run at higher temperature and/or for longer times. This suggests that the converse observation—the presence of olefins in an InI<sub>3</sub> catalyzed reaction—should be possible at lower temperatures and very short reaction. Solutions containing InI<sub>3</sub> (4.13 mmol), methanol (12.4 mmol), and <sup>1</sup>PrOH (0.65 mmol) were heated at 170 °C for periods of time as short as 10 minutes; the yield of 2-methyl-2-butene (which is again taken

as representative of all olefins) as a function of time is shown in Figure 4.3. After an induction period, typical of triptane syntheses, the olefin grows quickly to low levels and then disappears; after about an hour none remains. At this low temperature, short reaction time experiments resemble the product distribution expected for a  $\text{ZnI}_2$ -catalyzed reaction; it is further confirmation that the two systems are reacting by the same mechanism and that the differences originally noted are quantitative only.

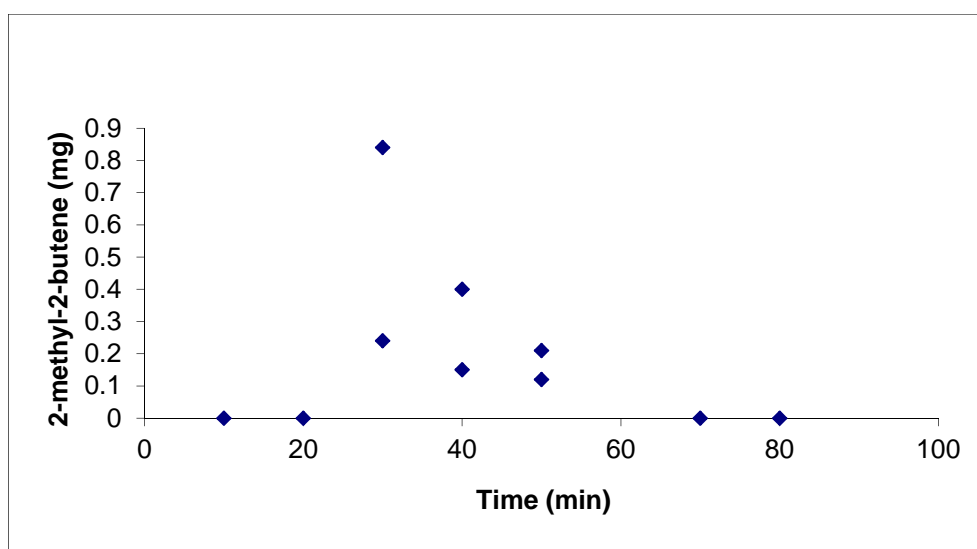


**Figure 4.3** Yield of 2-methyl-2-butene over time for  $\text{InI}_3$  catalyzed methanol conversion at 170 °C. Each point represents a separate experiment.

#### 4.3.2 Quantifying iodine-containing products

In a practical sense, one of the major downfalls of both the  $\text{ZnI}_2$ - and  $\text{InI}_3$ -catalyzed reactions is the possible iodide content of the organic product mixture. Iodide-containing products generate highly toxic and corrosive hydroiodic acid when burned, so are unfavorable for commercial processes in even parts per billion concentrations. Thus,

information on the concentrations of these products generated in the various methanol conversion reactions (including alkane homologation, discussed in Chapter 5) is highly valuable. Methyl iodide is always observed as a product by GC, but other organic iodides have yet to be identified amidst the hundreds of products.

Initial experiments for quantifying methyl iodide were attempted by employing gas chromatography (GC) and elemental analysis. First, calibration curves of methyl iodide versus cyclohexane (the internal standard used for quantification in all previously described experiments) were generated. Then, reactions were run in triplicate so that the average amount of methyl iodide as determined by GC could be obtained. The amount of iodide in heavier organic products should be obtainable, in theory, by obtaining iodine content from elemental analysis of an analogous reaction mixture, with a correction for the amount of MeI (as determined by GC). Samples were sent to Desert Analytics for elemental analysis so that an approximate amount of iodide-containing products could be calculated (Equation 1). Unfortunately, this method did not give good quantification; the elemental analysis did not account for even the amount of methyl iodide as determined by GC in the sample, likely due to the volatility of the compound, despite precautions taken to avoid its loss.

$$(M_{\text{MeI}} / M_{\text{org}}) \times (MW_{\text{I}} / MW_{\text{MeI}}) = (\% \text{ MeI in org. layer}) \times (\% \text{ I in MeI}) = \% \text{ I in org. from MeI}$$

$$(\% \text{ MeI in org. layer}) - (\% \text{ I in org. from MeI}) = \% \text{ iodide-containing products in org. layer}$$

#### **Equation 1**

Alternatively, an analysis of the product distribution using a GC equipped with split flame ionization and electron capture detectors (FID and ECD) was attempted; while FID

detection is useful for hydrocarbon analysis, ECD spectra display no response to hydrocarbons but are highly sensitive to halogenated compounds. Cyclohexane and *para*-iodotoluene were used as internal standards for quantification of the products in the FID and ECD spectra, respectively. A sample spectrum of a reaction of  $\text{ZnI}_2$  (7.52 mmol), MeOH (24.7 mmol), and *i*PrOH (0.65 mmol) at 200 °C for 3 hours is shown in Figure 4.4. Although multiple products other than MeI can be seen in the ECD signal, quantification was not reproducible for any of the systems examined. While a precise amount of iodide-containing organics could not be obtained, the amount of these species is certainly above the threshold desired for commercial production; without a doubt, this is the Achilles heel of these systems.

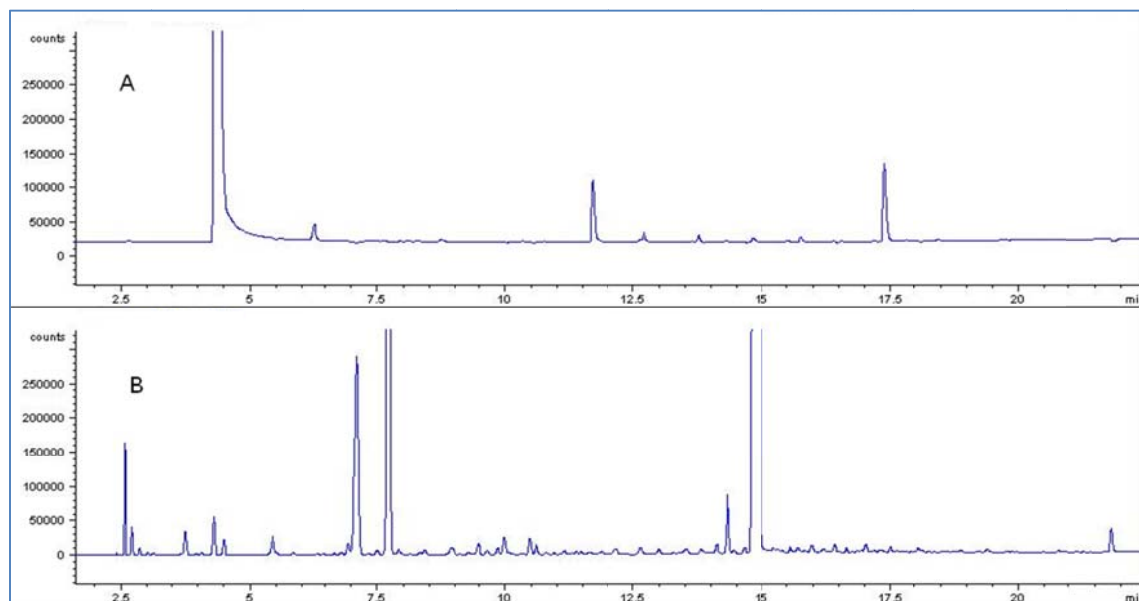


**Figure 4.4** GC trace of a reaction of  $\text{ZnI}_2$  (7.52 mmol), MeOH (24.7 mmol), and *i*PrOH (0.65 mmol) at 200 °C for 3 hours. A. ECD signal. B. FID signal.

#### 4.4 Conclusions

This work demonstrates that the differences between  $\text{ZnI}_2$ - and  $\text{InI}_3$ -catalyzed methanol are quantitative only and that the mechanisms for the two systems are in fact the same; the unusual selectivity of the product distributions observed for both can be explained by the formation of the most stable carbocations and the most highly substituted olefins and by competing methylation versus hydride abstraction rates, leading to a kinetically controlled product distribution.  $\text{InI}_3$  is somewhat more acidic and so can activate *some* alkanes at 200 °C, which is observed for  $\text{ZnI}_2$  at even higher temperatures. It is notable that the product distributions within each alkane fraction is not very different between Zn and In, even though In yields more alkanes, arenes, and fewer olefins (suggesting that hydride transfer is faster). As compared with the Pearson system, which likewise gives a mixture of alkanes and arenes, this highly acidic reaction mixture yields a product distribution that appears to be closer to thermodynamic control; this would imply that at higher temperatures, both In- and Zn-catalyzed reactions would begin to look more like thermodynamic control, and at low temperatures the Pearson reaction would begin to look like kinetic control. Getting the acidity right, so that the reaction occurs at a reasonable rate and temperature but so that the product distribution is closer to that under kinetic control, is key to designing the perfect system. Also necessary is the removal of iodide—current systems yield product mixtures with iodide content above what would be acceptable for a commercial process; the discovery of a similar system without iodide would be extremely valuable but has not yet occurred.

## 4.5 Experimental

**General considerations.**  $\text{InI}_3$  (purchased from Alfa Aesar),  $\text{ZnI}_2$  (purchased from Sigma-Aldrich), MeOH, and other organic compounds were reagent-grade commercial samples used without further purification. GC analyses were performed on an HP model 6890N chromatograph equipped with a 10 m x 0.10 mm x 0.40  $\mu\text{m}$  DB-1 column. GC experiments with split FID/ECD detection were carried out on an HP model 6890N chromatograph equipped with a 30 m x 0.320 mm x 0.25  $\mu\text{m}$  HP-5 column. GC/MS analyses were performed on an HP model 6890N chromatograph equipped with a 30 m x 25 mm x 0.40  $\mu\text{m}$  HP5-1 column and equipped with an HP 5973 mass selective EI detector.

**Standard reaction protocols.** All reactions were performed in thick-walled pressure tubes equipped with Teflon stopcocks (Kontes valves), rated up to 10 bar. The procedure for standard reactions is based on the procedure reported earlier for MeOH-to-hydrocarbon conversions using  $\text{ZnI}_2$  and  $\text{InI}_3$ . In a typical experiment, the tube was equipped with a stir bar and charged with  $\text{ZnI}_2$  (2.4 g, 7.52 mmol), MeOH (1.0 mL, 24.8 mmol), and isopropanol (0.050 mL, 0.65 mmol), if an initiator was required. (If  $\text{InI}_3$  was used as the catalyst it was weighed out in a glove box due to its hygroscopic nature; however the reactions were carried out under an atmosphere of air). If another organic compound was utilized as an additive, it was added at this stage. The pressure tube was then placed in a pre-heated oil bath behind a blast shield and stirred at the appropriate temperature for the desired period of time. After heating, the tube was removed from the bath and allowed to



cool to room temperature and then placed in an ice bath. The stopcock was removed and chloroform (1.0 mL), containing a known amount of cyclohexane as an internal standard, was pipetted into the reaction mixture followed by water (0.5 mL). The stopcock was replaced, the mixture was shaken vigorously and the organic layer separated. A small aliquot was diluted with acetone or tetradecane for GC analysis.

#### 4.6 References

1. Hazari, N.; Labinger, J. A.; Scott, V. J., *J. Catal.*, **2009**, 263, 266-276.
2. Dresselhaus, M. S.; Thomas, I. L., *Nature*, **2001**, 414, 332-337.
3. Olah, G. A., *Angew. Chem. Int. Ed.*, **2005**, 44, 2636-2639.
4. Olah, G. A.; Molnár, Á., *Hydrocarbon Chemistry*, 2nd ed. John Wiley & Sons: Hoboken, NJ, 2003.
5. Chang, C. D., *Catal. Today*, **1992**, 13, 103-111.
6. Haw, J. F.; Song, W. G.; Marcus, D. M.; Nicholas, J. B., *Acc. Chem. Res.*, **2003**, 36, 317-326.
7. Olsbye, U.; Bjorgen, M.; Svelle, S.; Lillerud, K. P.; Kolboe, S., *Catal. Today*, **2005**, 106, 108-111.
8. Pearson, D. E., *J. Chem. Soc. Chem. Commun.*, **1974**, 397-397.
9. Kim, L.; Wald, M. M.; Brandenberger, S. G., *J. Org. Chem.*, **1978**, 43, 3432-3433.
10. Chang, C. D., Shape-Selective Catalysis. In *ACS Symposium Series*, **2000**, 738, 96-114.

11. McCann, D. M.; Lesthaeghe, D.; Kletnieks, P. W.; Guenther, D. R.; Hayman, M. J.; Van Speybroeck, V.; Waroquier, M.; Haw, J. F., *Angew. Chem. Int. Ed.*, **2008**, *47*, 5179-5182.
12. Bercaw, J. E.; Diaconescu, P. L.; Grubbs, R. H.; Kay, R. D.; Kitching, S.; Labinger, J. A.; Li, X. W.; Mehrkhodavandi, P.; Morris, G. E.; Sunley, G. J.; Vagner, P., *J. Org. Chem.*, **2006**, *71*, 8907-8917.
13. Bercaw, J. E.; Grubbs, R. H.; Hazari, N.; Labinger, J. A.; Li, X. W., *Chem. Commun.*, **2007**, 2974-2976.
14. Bercaw, J. E.; Diaconescu, P. L.; Grubbs, R. H.; Hazari, N.; Kay, R. D.; Labinger, J. A.; Mehrkhodavandi, P.; Morris, G. E.; Sunley, G. J.; Vagner, P., *Inorganic Chemistry*, **2007**, *46*, 11371-11380.
15. Bercaw, J. E.; Hazari, N.; Labinger, J. A.; Scott, V. J.; Sunley, G. J., *J. Am. Chem. Soc.*, **2008**, *130*, 11988-11995.

## CHAPTER 5

### Alkane homologation with methanol catalyzed by $\text{InI}_3$ and $\text{ZnI}_2$

#### 5.1 Abstract

The ability of  $\text{InI}_3$  and  $\text{ZnI}_2$  to catalytically upgrade alkanes by homologation with methanol has been investigated. This work represents efforts to understand the mechanism and limits of this potentially valuable reactivity and is compared to the direct conversion of methanol to hydrocarbons. The work presented here was done as a collaborative effort with Nilay Hazari.<sup>1</sup>

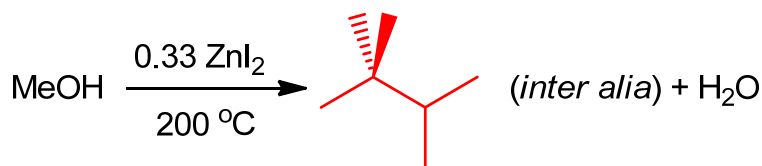
#### 5.2 Introduction

The catalytic conversion of abundant but relatively inert alkanes into higher value chemicals has been a longstanding challenge for chemists and the petrochemical industry. While there have been significant advances in our understanding of C-H activation reactions over the last three decades, they have not yet led to practical methods for alkane functionalization because of limitations imposed by unfavorable thermodynamics, low selectivity, and/or economic factors.<sup>2-5</sup> In principle one could avoid these difficult functionalization problems by simply converting a given alkane into another alkane of higher value. Well-known examples, which are extensively utilized by the petrochemical industry, include isomerization of linear to branched alkanes<sup>6</sup> and the alkylation of isobutane with olefins.<sup>7</sup> On a research scale, alkanes may be coupled by mercury-photosensitized dehydrodimerization, although selectivity is limited by the radical mechanism involved.<sup>8</sup> More recently the so-called alkane metathesis reaction has been

proposed as a potential method for upgrading light hydrocarbons such as *n*-hexane to diesel-range linear alkanes.<sup>9-11</sup>

The dehydrative condensation of methanol to hydrocarbons has attracted a good deal of interest over the years. Most often this involves reaction over shape-selective solid acids, as in the MTG (methanol-to-gasoline) and MTO (methanol-to-olefins) processes.<sup>12-15</sup> In contrast, Kim et al. reported that the reaction of MeOH with zinc iodide at 200 °C led to formation of an alkane-rich hydrocarbon mixture, with surprising selectivity to one particular alkane, 2,2,3-trimethylbutane (triptane) in overall yields of up to 20% (based on moles of carbon), corresponding to as much as half of the gasoline-range fraction (Scheme 5.1).<sup>16, 17</sup> An efficient synthetic route to triptane (research octane number = 112) would provide access to a valuable fuel component and gasoline additive.

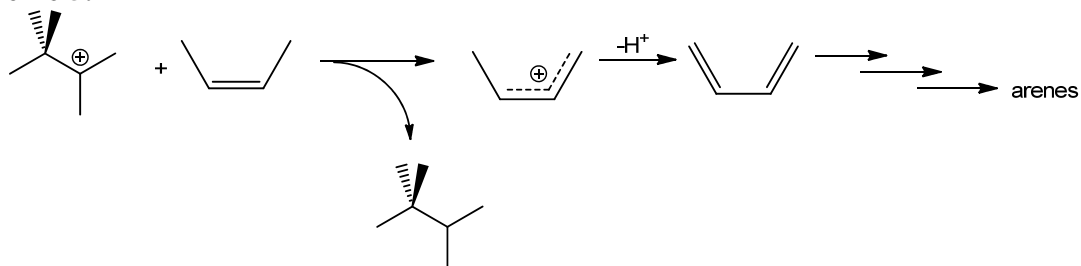
**Scheme 5.1**



Mechanistic studies on this complex reaction<sup>18, 19</sup> implicate a carbocation-based route, wherein hydrocarbon growth proceeds by successive olefin methylation and deprotonation, always favoring the most highly substituted carbocations and olefins, respectively (see Chapter 4, Introduction, for more detail). Direct C-C bond formation from methanol (and/or dimethyl ether; partial dehydration of MeOH to DME is rapid under reaction conditions) apparently takes place only when solids are present; for a completely homogeneous reaction mixture an initiator is required, typically an olefin or a higher

alcohol. Alkanes are generated via hydride transfer from an unsaturated hydrocarbon to a carbocation, with the resulting multiply-unsaturated intermediates eventually resulting in the formation of arenes, as illustrated in Scheme 5.2.

**Scheme 5.2**



According to this scheme, triptane yields are limited by two constraints. First, the aliphatic pool contains both lighter and heavier highly branched alkanes (and some olefins), along with smaller amounts of less-branched isomers; the selectivity for triptane within that pool appears to be governed by the relative rates of methylation and hydride transfer at the various stages of product growth. Second, some fraction of the methanol feed must be diverted to the aromatic pool to satisfy the stoichiometry in hydrogen. The latter factor accounts for the observation that the triptane yield is enhanced by the addition of species containing P-H bonds (phosphorous or hypophosphorous acid), which serve as alternate hydride sources.<sup>20</sup>

$\text{InI}_3$  also functions as a catalyst for this transformation.<sup>21, 22</sup> Many of the features (including reaction conditions and typical triptane yields) are quite similar for  $\text{ZnI}_2$  and  $\text{InI}_3$ , suggesting that the mechanism for the conversion of MeOH to triptane is basically the same for the two systems. However, there are some significant differences, especially in the detailed product distributions. Much of the difference in behavior can be accounted for

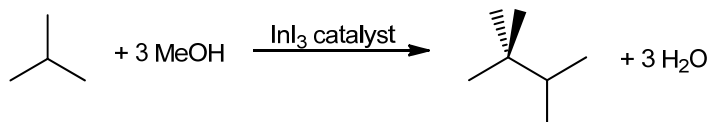
by the fact that  $\text{InI}_3$ —unlike  $\text{ZnI}_2$ —is able to activate (some) alkanes easily at 200 °C. In particular, alkanes that contain at least one tertiary center are readily isomerized by the  $\text{InI}_3$  system, and are also able to function as initiators for triptane synthesis. In contrast, olefins (or olefin precursors such as higher alcohols) are required to initiate  $\text{ZnI}_2$ -catalyzed reactions at 200 °C.<sup>18</sup> As discussed in Chapter 4, these differences are quantitative only; the same reaction pathway is being followed for both systems, resulting in similar product distributions in the two systems.

Both the isomerization of and initiation by alkanes implies that they react with  $\text{InI}_3$  and thus enter the carbocation/olefin pool, even if only in very low concentrations. This conclusion was supported by an isotopic labeling study. Analysis of the products from a reaction of  $^{13}\text{C}$ -MeOH, unlabeled 2,3-dimethylbutane (as an initiator), and  $\text{InI}_3$  by GC/MS showed that the two major triptane isotopologs were singly labeled and fully labeled (with much more of the latter). Fully labeled triptane presumably arose via *de novo* synthesis from MeOH, but a singly labeled triptane molecule must have come from the addition of a single methanol-derived  $\text{CH}_2$  group to the  $\text{C}_6$  olefin generated by the activation of unlabeled 2,3-dimethylbutane.<sup>21</sup>

It should be noted that this methylative homologation does *not* suffer from the hydrogen deficiency of the original methanol-to-triptane conversion; there is no requirement for the formation of arenes or any unsaturated hydrocarbons, removing one major limitation on selectivity. If it were possible to convert large quantities of light alkanes in this manner, using MeOH as a methylating agent, it would constitute a route for the selective conversion

of relatively low value and abundant alkanes to more valuable fuels by reactions such as Scheme 5.3. Isobutane and 2-methylbutane (isopentane) are produced on a large scale in refinery operations;<sup>23, 24</sup> they are also significant byproducts from methanol transformations such as MTG.<sup>12</sup> While the latter compound is used directly as a gasoline component, its homologation to a higher octane, less volatile C<sub>6</sub> or C<sub>7</sub> branched alkane would represent a significant upgrading of value. The following work is aimed at exploring this unprecedented and potentially useful approach.

**Scheme 5.3**



## 5.3 Results and Discussion

### 5.3.1 Homologation of 2,3-dimethylbutane

The first series of experiments were performed using reaction mixtures of InI<sub>3</sub> (4.13 mmol), MeOH (12.4 mmol), and varying amounts of 2,3-dimethylbutane (DMB), which were heated at 200 °C for two hours. A control experiment (with no DMB present) contained isopropanol as an initiator (i.e., a standard In catalyzed direct methanol conversion reaction). The results of analysis by gas chromatography (GC) are shown in Table 5.1. In all experiments conversion of DMB was between 20 and 35%, while all the MeOH/DME was consumed. Both the the yield of triptane (stated as moles of carbon in triptane per mole of converted carbon) and the selectivity to triptane (stated as the moles of carbon in triptane per mole of total converted carbon) increase with the amount of DMB

added (more than three-fold by the addition of one molar equivalent of DMB) (Table 5.1, Figure 5.1).

**Table 5.1** Yields of Triptane and polymethylbenzenes as a function of 2,3-dimethylbutane added<sup>a</sup>

InI <sub>3</sub> (mmol)	MeOH (mmol)	DMB (mmol)	DMB recovered (%)	Triptane yield (mg)	Triptane selectivity (%) <sup>c</sup>	PMB (mg)	HMB (mg)	Triptane:(PMB + HMB)
4.13	12.4	0 <sup>b</sup>	-	23	12	12	7	1.2
4.13	12.4	0.76	80	32	14	1	17	1.8
4.13	12.4	1.52	65	33	15	4	9	2.5
4.13	12.4	3.04	71	40	16	4	15	2.1
4.13	12.4	6.2	68	60	17	6	14	3.0
4.13	12.4	12.4	79	75	19	14	9	3.3
4.13	12.4							

<sup>a</sup> All reactions were heated for two hours at 200 °C.

<sup>b</sup> Isopropanol (50  $\mu$ L, 39 mg, 0.65 mmol) was added as an initiator.

<sup>c</sup> Based on total converted carbon

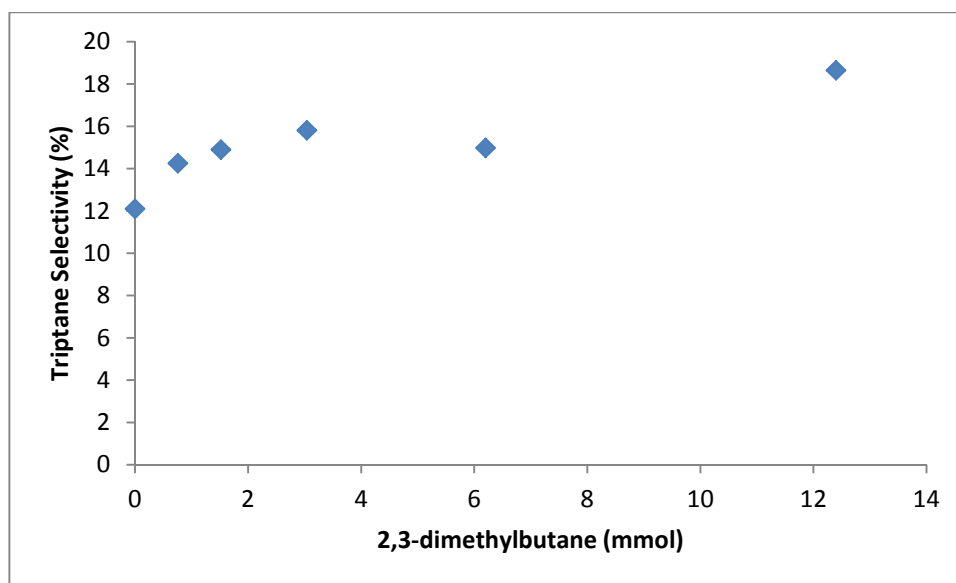


**Figure 5.1** Triptane selectivity against number of mmol of 2,3-dimethylbutane. Each point represents a separate experiment.



Because it is conceivable that addition of DMB might increase the efficiency of the direct conversion of MeOH to triptane without any direct incorporation of the added DMB, this trend does not by itself conclusively establish homologation of DMB to triptane. Two additional lines of evidence do provide support for homologation. First, a labeling experiment analogous to that reported previously<sup>21</sup> but with substantially more added DMB was performed. A reaction mixture containing DMB (1.52 mmol), InI<sub>3</sub> (4.13 mmol), and <sup>13</sup>C-labeled MeOH (12.4 mmol) was heated at 200 °C for two hours, and products were analyzed by GC/MS. Figures 5.2 and 5.3 show the MS patterns for the GC fractions of DMB and triptane, respectively. For the former, the major set of peaks from  $m/z = 71$ -76 correspond to the (P-Me)<sup>+</sup> fragment ions (where P = parent fragment ion). Of these, by far the largest is at 71 (<sup>12</sup>C<sub>5</sub>H<sub>11</sub>) and the next-largest at 72 (<sup>12</sup>C<sub>4</sub><sup>13</sup>CH<sub>11</sub>), with weaker peaks resulting from mixed isotopologs and the fully labeled isotopolog 76 (<sup>13</sup>C<sub>5</sub>H<sub>11</sub>). There is also a P<sup>+</sup> peak at 86  $m/z$  for unlabeled DMB, while the parent ions for other isotopologs are much weaker or not observed. The observed isotopolog distribution clearly demonstrates that activation of DMB has taken place, leading to exchange of carbons with the methanol-derived methylating species, as previously documented.<sup>18,21</sup>

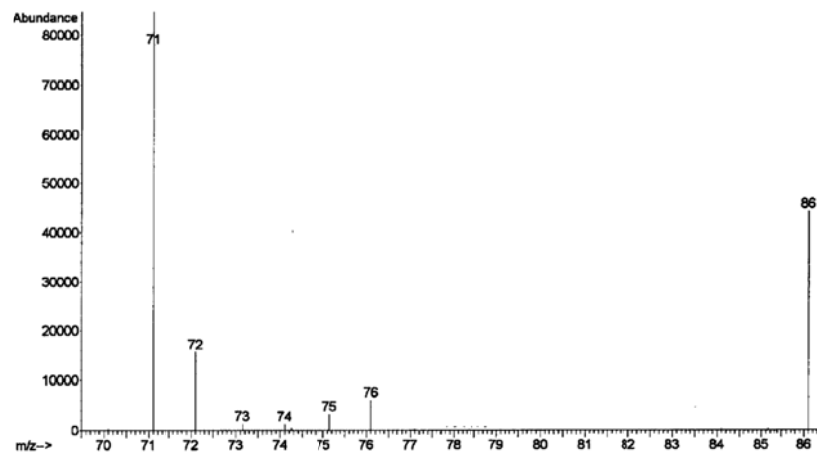


**Figure 5.2** MS of DMB fraction from reaction between  $\text{InI}_3$ ,  $^{13}\text{C}$ -labeled MeOH and DMB; 71  $((\text{P-Me})^+, ^{12}\text{C}_3\text{H}_{11})$ , 72  $((\text{P-Me})^+, ^{12}\text{C}_4^{13}\text{CH}_{11})$ , 76  $((\text{P-Me})^+, ^{13}\text{C}_5\text{H}_{11})$ , 86  $(\text{P}^+, ^{12}\text{C}_6\text{H}_{13})$

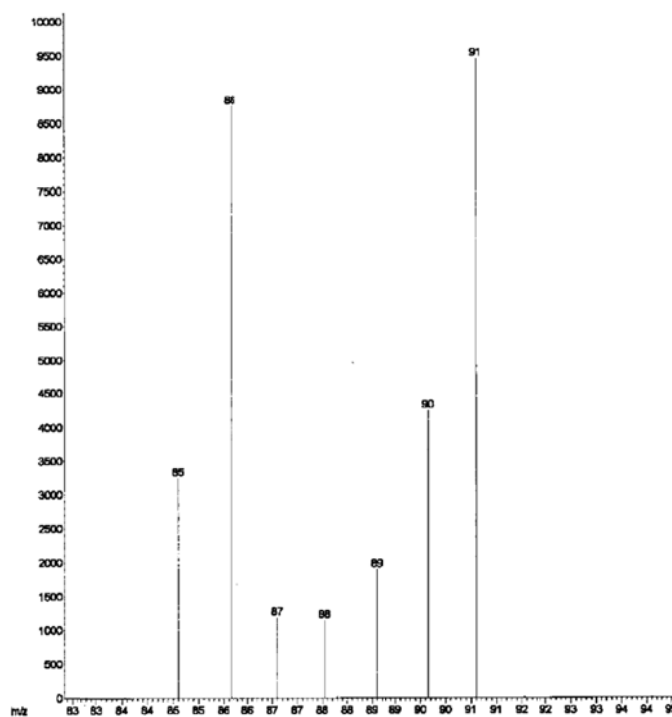


**Figure 5.3** MS of the triptane fraction from a reaction between  $\text{InI}_3$ ,  $^{13}\text{C}$ -labeled MeOH and DMB; 91  $((\text{P-Me})^+, ^{13}\text{C}_6\text{H}_{13})$ , 86  $(\text{P}^+, ^{12}\text{C}_6\text{H}_{13})$

For the triptane fraction, the main signals again correspond to (P-Me)<sup>+</sup> ions; there is barely any detectable signal in the P<sup>+</sup> region. The largest signal at 91 *m/z* is due to fully labeled <sup>13</sup>C<sub>6</sub>H<sub>13</sub>, while the next largest, at 86 *m/z*, is due to singly labeled <sup>12</sup>C<sub>5</sub><sup>13</sup>C<sub>1</sub>H<sub>13</sub>; weaker peaks are observed at intermediate values. Table 5.2 shows the relative percentage of the different isotopologs, as well as the values that would be expected for complete statistical scrambling of carbon atoms in the reaction mixture (in which 59.5% of the carbon atoms in the mixture are unlabeled and 40.5% are labeled). It is clear that the fraction of singly-labeled triptane, which would result from homologation of DMB, is far in excess of the statistical value and conversion of DMB to triptane is occurring, however the intensity of the <sup>12</sup>C<sub>1</sub><sup>13</sup>C<sub>5</sub> signal shows that some scrambling has occurred as well.

**Table 5.2** Relative statistical and observed percentages of isotopologues of (P-Me)<sup>+</sup> for triptane

Molecular Formula	Statistical Distribution (%)	Observed Distribution (%)
<sup>12</sup> C <sub>6</sub> H <sub>13</sub>	4.43	9.5
<sup>12</sup> C <sub>5</sub> <sup>13</sup> C <sub>1</sub> H <sub>13</sub>	18.12	31.6
<sup>12</sup> C <sub>4</sub> <sup>13</sup> C <sub>2</sub> H <sub>13</sub>	30.84	2.6
<sup>12</sup> C <sub>3</sub> <sup>13</sup> C <sub>3</sub> H <sub>13</sub>	27.98	3.5
<sup>12</sup> C <sub>2</sub> <sup>13</sup> C <sub>4</sub> H <sub>13</sub>	14.28	5.2
<sup>12</sup> C <sub>1</sub> <sup>13</sup> C <sub>5</sub> H <sub>13</sub>	3.89	15.5
<sup>13</sup> C <sub>6</sub> H <sub>13</sub>	0.44	32.5

The quantity of aromatic products generated (Table 5.1) provides further evidence for conversion of DMB into triptane. Stoichiometrically, when DMB and MeOH react to form triptane, the only by-product is water. In contrast, direct conversion of MeOH into triptane requires the equivalent of one molecule of H<sub>2</sub> (presumably delivered stepwise, as H<sup>+</sup> and H<sup>-</sup>), which is provided by olefins that eventually generate hydrogen-deficient arenes.<sup>18</sup> Thus, if some of the triptane being formed comes from the homologation of MeOH with DMB, a

reduction in the amount of aromatics relative to triptane would be expected, compared with a reaction in which there is only direct conversion of MeOH into triptane. In nearly all reactions the major aromatic compounds observed are pentamethylbenzene (PMB) and hexamethylbenzene (HMB), so these two species are used as the indicator for the total amount of aromatics present; as discussed in Chapter 4, tetramethylbenzenes only become more important arene products at very long reaction times and higher temperatures.

The yields of triptane, PMB and HMB and the ratio of triptane to PMB + HMB for a series of experiments with varying amounts of DMB are shown in Table 5.1. Clearly the ratio of triptane to aromatics increases as the amount of DMB present increases, supporting the conclusion that triptane arises from two competitive processes: direct conversion of MeOH to triptane (which results in aromatic byproducts) and the homologation of DMB (which does not). The reduction of arene yield is observed even at the lowest DMB concentrations, indicating that there is some homologation of the alkane to triptane even at these low concentrations.

Increasing the  $\text{InI}_3$  loading appears to reduce the contribution of direct conversion of MeOH to triptane still further. A reaction with equimolar MeOH and DMB but with twice as much In ( $\text{InI}_3\text{:MeOH:DMB} = 1\text{:}1.5\text{:}1.5$ ) gives the same overall triptane yield, but the ratio of triptane to aromatic products (which in this experiment include some tetramethylbenzenes) is 12.8, compared to the value of 3.26 for the experiment shown as the last entry in Table 5.1 ( $\text{InI}_3\text{:MeOH:DMB} = 1\text{:}3\text{:}3$ ). The analogous experiment using  $^{13}\text{C}$ -labeled MeOH in the same proportions showed much more singly labeled than fully

labeled product: the triptane (P-Me)<sup>+</sup> signals at 91 and 86 *m/z* accounted for 3% and 50% of the total, respectively, indicating that under these conditions homologation of DMB is the predominant route to triptane. The cause of this effect is unclear; it may be significant that at the higher indium loading some InI<sub>3</sub> remains undissolved at the reaction temperature, whereas solutions are completely homogeneous at the lower indium loading.

### 5.3.2 Variation of reaction conditions

The effects of changing reaction time and temperature have been investigated using the standard mixture of InI<sub>3</sub> (4.13 mmol), DMB (6.2 mmol), and MeOH (6.2 mmol). The triptane selectivities for reaction times ranging from fifteen minutes to two hours at 200 °C are shown graphically in Figure 5.4. For this (and all future) tables selectivity has been redefined as moles of triptane formed per mole of DMB charged—i.e., the putative selectivity of the homologation of DMB assuming it to be the only triptane-producing process—which is a more useful figure of merit. The high triptane-to-aromatic ratios observed in these reactions indicates that this is a reasonable assumption. Reaction times less than fifteen minutes gave yields and selectivities similar to those at fifteen minutes, but the DMB conversion was lower, as shown in Table 5.3. Even after only five minutes no unreacted MeOH/DME was detected (although it should be noted that is difficult to detect very small quantities of the highly volatile DME).

**Table 5.3** Triptane yields, selectivities, and ratio to aromatic products over time<sup>a</sup>

Time (min)	DMB recovered (%)	Triptane yield (mmol)	Triptane Selectivity (%) <sup>b</sup>	Triptane: (PMB + HMB)
5	73	0.51	30	>100
10	70	0.56	31	40
15	67	0.62	31	28
30	66	0.64	30	28
60	58	0.62	24	29 <sup>c</sup>
120	56	0.59	23	19 <sup>c</sup>

<sup>a</sup> Reactions were performed at 200 °C and used InI<sub>3</sub> (4.13 mmol), MeOH (6.2 mmol), and DMB (6.2 mmol).

<sup>b</sup> Percentage of converted DMB which becomes triptane

<sup>c</sup> Some tetramethylbenzene (TMB) was observed in this reaction and has been included, so the quoted figure is the ratio of triptane to (TMB + PMB + HMB).

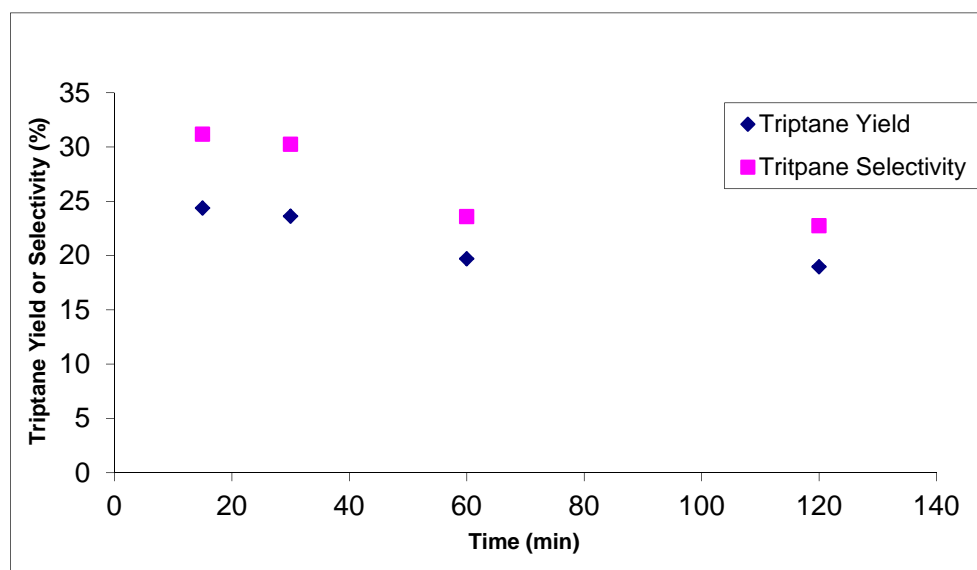


**Figure 5.4** Triptane yield and selectivity over time for a reaction containing 1:1 DMB:MeOH catalyzed by InI<sub>3</sub>. Each data point represents a different experiment.

The decrease in triptane selectivity beyond fifteen minutes corresponds to a decrease in the recovered DMB at longer reaction times, along with a much smaller decrease in the total quantity of triptane produced. This is a consequence of side reactions of DMB. It has

been previously demonstrated that both isomerization into other C<sub>6</sub> alkanes and cracking into lighter alkanes such as isobutane and isopentane are catalyzed by InI<sub>3</sub>, and further that the presence of MeOH slows down InI<sub>3</sub>-catalyzed alkane isomerization and cracking.<sup>21</sup> Because MeOH undergoes processes other than providing methylating equivalents for DMB conversion (i.e., direct conversion of MeOH to triptane and the methylation of aromatic species), MeOH/DME is completely consumed long before DMB (as noted above), so that no further homologation can occur, but the isomerization and cracking processes continue. (Triptane isomerization and cracking also take place, but at a slower rate.<sup>21</sup>) The combined yield of 2-methylpentane and 3-methylpentane, two of the major isomerization byproducts, as a function of time is shown graphically in Figure 5.5.

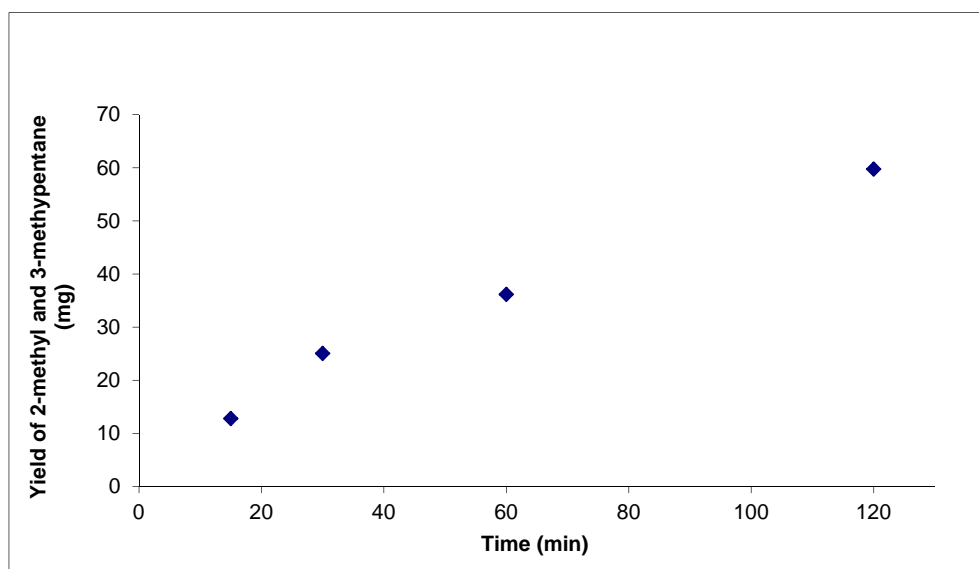


**Figure 5.5** Combined yield of 2-methyl and 3-methylpentane over time for a reaction containing 1:1 DMB:MeOH catalyzed by InI<sub>3</sub>. Each data point represents a different experiment.

The effect of temperature on the homologation of MeOH with DMB is shown in Table 5.4. As the temperature is decreased from 200 °C, the extent of isomerization and cracking of DMB and triptane decreases, which results in an increase in the triptane yield and selectivity. At these temperatures the rate of activation of the alkane and methylation of the olefin is sufficiently fast to allow significant amounts of conversion (approximately 40% conversion of DMB), but below 170 °C, conversion slows dramatically and eventually stops altogether. Furthermore, at and below 180 °C, almost all of the triptane is formed by homologation of DMB with little or no direct conversion of MeOH to triptane, as shown by the high triptane:arene ratios. The maximum selectivity for DMB homologation to triptane, 38%, was achieved at 180 °C.

**Table 5.4** Effect of temperature on triptane yield, selectivity, and ratio to (PMB + HMB)<sup>a</sup>

Temp (°C)	DMB recovered (%)	Triptane yield (mmol)	Triptane selectivity (%) <sup>b</sup>	Triptane: (PMB + HMB)
200	66	0.64	30	13
190	60	0.79	32	26
180	63	0.90	38	48
170	61	0.80	33	>100
160	78	0.18	13	nr <sup>d</sup>
150	>90	0.01	1	nr <sup>d</sup>
140	>90	0	0	nr <sup>d</sup>

<sup>a</sup> Reactions were performed for 30 minutes and used InI<sub>3</sub> (4.13 mmol), MeOH (6.2 mmol), and DMB (6.2 mmol).

<sup>b</sup> Percentage of converted DMB which becomes triptane

<sup>c</sup> Some tetramethylbenzene (TMB) was observed in this reaction and has been included so the quoted figure is the ratio of triptane to (TMB + PMB + HMB).

<sup>d</sup> Not recorded

In an effort to further suppress the direct conversion of MeOH to triptane, several experiments were performed using higher ratios of DMB to MeOH. The results (Table 5.5)



show that this does not significantly affect the triptane:aromatic ratio, but does decrease the triptane yield; thus, the optimum ratio of MeOH:DMB appears to be 1:1.

**Table 5.5** Effect of DMB concentration on triptane yield, selectivity, and ratio to (PMB + HMB)<sup>a</sup>

InI <sub>3</sub> (mmol)	MeOH (mmol)	DMB (mmol)	DMB recovered (%)	Triptane selectivity (%) <sup>b</sup>	Triptane: (PMB + HMB)
4.13	6.2	6.2	63	38	48
4.13	6.2	9.3	61	29	35
4.13	6.2	12.4	75	27	25
2.07	3.1	7.75	70	25	42
2.07	3.1	9.3	74	25	- <sup>c</sup>

<sup>a</sup> Reactions performed for 30 minutes at 180 °C

<sup>b</sup> Based on total converted carbon

<sup>c</sup> No PMB or HMB was detected.

The catalyst loading cannot be lowered substantially: for starting ratios of MeOH:InI<sub>3</sub> above 4:1 the yield of triptane drops off sharply, regardless of the amount of DMB. This inhibition is most probably a water effect (since partial dehydration of MeOH to DME is rapid at any concentration); in the direct conversion of MeOH to triptane it was observed that high effective turnover numbers were achieved in cyclic “batch” mode by removing water (use of DME instead of MeOH as feedstock for methylative homologation gives essentially identical results).<sup>18, 21</sup> The same approach works for homologation: at the end of a reaction all volatiles (including water) were removed and the remaining InI<sub>3</sub> dried under vacuum at 60 °C; a fresh charge of DMB and MeOH was added to reaction mixture and the reaction performed again, with no decrease in the triptane yield or selectivity. It appears that the reaction can be continued indefinitely if the volatiles are periodically removed in this manner.

### 5.3.3 Effect of added adamantane on homologation

Adamantane has been shown to suppress cracking and thus enhance alkane isomerization reactions that proceed through a mechanism involving carbocations, presumably by acting as a hydride transfer catalyst.<sup>25</sup> Because cracking represents a major side reaction in the alkane homologation reactions described above, the effect of adding a small amount of adamantane to a reaction between DMB and MeOH catalyzed by  $\text{InI}_3$  was examined. Table 5.6 compares the triptane yield and selectivity in the presence and absence of adamantane; there is a dramatic beneficial effect on both, along with a significant increase in the amount of DMB converted. This increase occurs because adamantane suppresses the isomerization of both DMB and triptane and also greatly reduces cracking side reactions. Table 5.7 shows that adamantane suppresses isomerization (of both  $\text{C}_6$  and  $\text{C}_7$  alkanes) as well as cracking (which leads to isobutane and isopentane, among other products) which compete with DMB homologation. The effect involves a catalytic action of adamantane, as the recovered yield of adamantane (by GC) is 90–100% of that added in all cases. Varying the loading of adamantane between 1–12 mol% (relative to DMB) had almost no effect on triptane yield or selectivity.

**Table 5.6** Comparison of triptane yield and selectivity for homologation<sup>a</sup> in the presence and absence of adamantane

Adamantane <sup>b</sup> (mg)	DMB recovered (%)	Triptane yield (mmol)	Triptane selectivity (%) <sup>c</sup>
0	63	0.90	39
10 (1.2)	30	2.32	55
50 (5.9)	51	2.10	65
100 (12)	44	2.05	59

<sup>a</sup> Reactions were performed at 180 °C for 30 minutes and used 4.13 mmol of  $\text{InI}_3$ , 6.2 mmol of DMB, and 6.2 mmol of MeOH.

<sup>b</sup> Number in parentheses is mol % of adamantane relative to DMB.

<sup>c</sup> Percentage of converted DMB which becomes triptane

**Table 5.7** Comparison of ratios of side products to starting material and triptane for homologation in the presence and absence of adamantane<sup>a</sup>

Ratio of hydrocarbons	No adamantane	With adamantane <sup>b</sup>
DMB: other C <sub>6</sub> alkanes	40:1	56:1
Triptane: other C <sub>7</sub> alkanes	10:1	17:1
(DMB + triptane): (isobutane + isopentane)	7:1	35:1

<sup>a</sup> Reactions were performed at 180 °C for 30 minutes and used 4.13 mmol of InI<sub>3</sub>, 6.2 mmol of DMB, and 6.2 mmol of MeOH.

<sup>b</sup> 50 mg of adamantane added

The increased DMB conversion does not appear to be a consequence of adamantane increasing the rate of homologation; rather it suppresses side reactions that use up the methylating agent. As noted earlier, although the synthesis of triptane requires only one equivalent of MeOH per DMB, in nearly all experiments (with or without adamantane) using either a 1:1 or 1:2 ratio of DMB to MeOH, the MeOH is completely consumed while only a fraction of the DMB has been converted. At very short times, reactions can be stopped and analyzed before all the MeOH was consumed; the results demonstrate that MeOH consumption is *slowed* by the addition of adamantane. This suggests that the increased conversion in the presence of adamantane is achieved by reducing the quantity of MeOH “wasted” by side reactions, such as the homologation of alkanes which are not on the pathway to triptane, and thus allowing the MeOH to be utilized more efficiently for homologating DMB. Furthermore, it has been demonstrated that addition of adamantane greatly suppresses the direct conversion of MeOH to triptane, so under these conditions methylative homologation becomes even more favored.

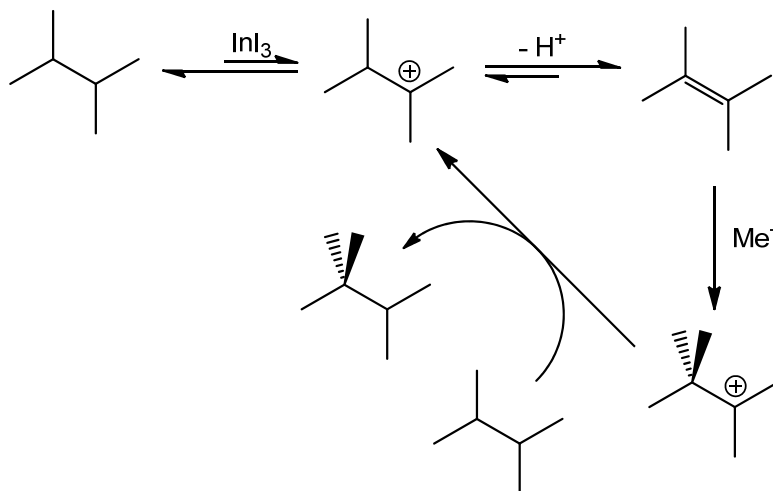
This alkane upgrading technique is not specific to DMB alone; it can be extrapolated to lighter alkanes (such as isobutane and isopentane) and less branched alkanes (such as 2-

methylpentane).<sup>1</sup> Attempts to homologate hexane resulted in only small quantities of C<sub>7</sub> products; even that required extremely long reaction times. It is believed that this is because there are only *primary* and *secondary* C-H bonds in hexane, which are more difficult to activate than *tertiary* C-H bonds; also, even if hexane is activated it will only form a disubstituted olefin, so the rate of methylation is expected to be slow. While yields and selectivities are significantly lower for these cases, it is noteworthy that this chemistry can be applied to these other alkanes.

#### 5.3.4 Mechanism

The mechanism proposed for the homologation of DMB with MeOH begins with the activation of DMB by InI<sub>3</sub> to give the 2,3-dimethylbutyl carbocation, the same as the first step in alkane isomerization catalyzed by InI<sub>3</sub>;<sup>26</sup> it should be noted that the nature of the In species in the reaction mixture is not known, just as with metal-iodide-catalyzed methanol conversion.<sup>18</sup> The 2,3-dimethylbutyl carbocation will be in equilibrium with 2,3-dimethyl-2-butene which is methylated, yielding the triptyl carbocation. The latter presumably obtains a hydride from another alkane to give triptane; most often this hydride will come from DMB, which is in the greatest abundance, resulting in the chain process shown in Scheme 5.4. The carbocation intermediates will undergo competitive skeletal rearrangements (which lead to isomerization) and scissions (which lead to cracking); the resulting side products and the carbocations and olefins derived therefrom will participate in similar chemistry, using up the MeOH that does not participate in the direct homologation route.

Scheme 5.4



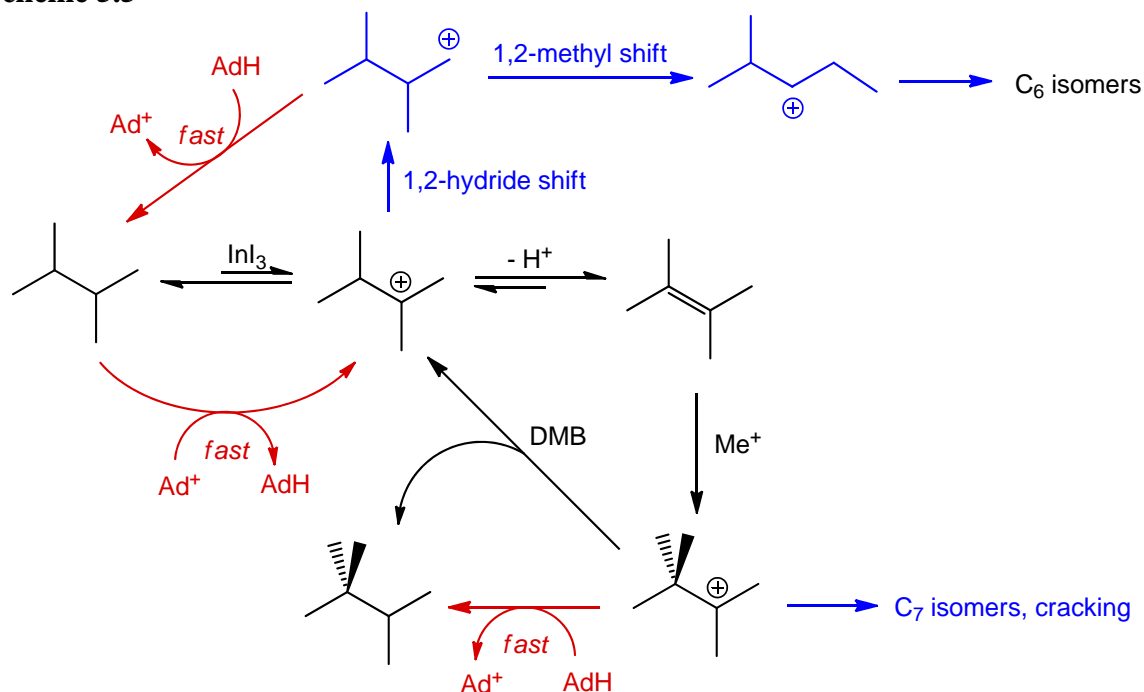
The facile transfer of  $\text{H}^-$  between alkanes and carbocations is a key feature of this chain mechanism; this must be operating (or something very similar) to permit homologation to proceed efficiently, even though the steady-state concentration of olefins which is produced via alkane activation by  $\text{InI}_3$  followed by deprotonation must be very low. It is notable that  $\text{ZnI}_2$  does *not* catalyze alkane homologation at these temperatures; however, carbocations are formed as intermediates in the  $\text{ZnI}_2$ -catalyzed conversion of  $\text{MeOH}$  to triptane,<sup>18</sup> so a chain process would seem possible in principle once reaction has been initiated. Nonetheless, reactions in which a small amount of an olefin (2,3-dimethyl-2-butene) as initiator was added to a solution containing DMB,  $\text{MeOH}$ , and  $\text{ZnI}_2$  showed no conversion of DMB to triptane at all. The proposed explanation for this observation is related to the presence or absence of olefins. Transfer of  $\text{H}^-$  from an olefin to a carbocation is particularly favorable as it generates an allylic carbocation (which ultimately leads to arenes).<sup>18</sup> In  $\text{ZnI}_2$ -catalyzed reactions, a macroscopic amount of olefin is required to generate the initial carbocation at 200 °C, and olefin concentrations remain significant until

extremely long reaction times (at which point all of the methylating equivalents have been consumed), so that transfer of  $\text{H}^-$  from alkane never competes effectively and no chain process can take place. In contrast, with  $\text{InI}_3$ -catalyzed homologation olefin concentrations are always extremely low; thus, when there is a large excess of DMB, hydride transfer from this species dominates and the chain process can proceed efficiently.

The beneficial effect of adamantane is attributed to its ability to act as an efficient hydride transfer agent, analogous to the interpretation of previous observations.<sup>25</sup> Reactions shown in Scheme 5.5 effectively catalyze the transfer of hydride between the triptyl carbocation and DMB, thus improving the efficiency of the chain process that is central to homologation, while suppressing side reactions by partially quenching the carbocations that lead to them. The primary carbocation derived from DMB, which leads to isomerization via methyl shifts, is rapidly trapped by adamantane (AdH) to reform DMB and generate the adamantyl cation ( $\text{Ad}^+$ ). Of course, AdH can also transfer hydride to the tertiary DMB-derived cation, which at first would seem to be chain-inhibitory, but is reversible: the predominant fate of the resulting  $\text{Ad}^+$  (which does not appear to undergo any side reactions of its own, under these conditions) will be to take  $\text{H}^-$  back from another molecule of DMB and start a new chain. Also, of course, the driving force for transfer of  $\text{H}^-$  from AdH to a (less stable) primary carbocation is greater than that for transfer to the tertiary carbocation; the latter process is approximately thermoneutral (in the gas phase).<sup>27-29</sup> The function of adamantane is basically a "repair" mechanism, capturing the isomeric carbocation before it can undergo skeletal rearrangement and returning it to the parent DMB pool. Furthermore,

by decreasing the lifetime of the triptyl carbocation (and others) adamantane will lower the rate of cracking. On both counts, then, the addition of adamantane inhibits the rates of side reactions relative to methylative homologation.

**Scheme 5.5**



The mechanism for the homologations of isopentane and isobutane would look much the same, starting from an earlier point in the growth sequence (for other alkanes not directly on the path to triptane, it would follow the same rules but not result in triptane). In each case, methylation of the olefin derived from the starting alkane takes place so as to generate the most substituted carbocation; thus DMB is a significant product, along with triptane, from the homologation of isopentane, and likewise isopentane is one of the products from isobutane.

### 5.3.5 $\text{ZnI}_2$ -catalyzed alkane homologation

As mentioned earlier,  $\text{ZnI}_2$  is incapable of activating alkanes at 200 °C. However, experiments described in Chapter 4 demonstrated that  $\text{ZnI}_2$  catalyzed methanol conversion reactions run at high temperature and longer reaction times yield product distributions that resemble  $\text{InI}_3$ -catalyzed reactions. At 230 °C, 2,3-dimethylbutane is capable of initiating a  $\text{ZnI}_2$ -catalyzed reaction and results in the same triptane yield as a reaction initiated with isopropanol (approximately 45 mg for 1 mL of MeOH, see Table 4.2, Chapter 4, compared with the expected 60 mg at 200 °C). The apparent drop in aromatics in this case (as compared with reactions using other initiators and  $\text{InI}_3$ -catalyzed homologation) is likely due to the longer length of reaction time and the likely generation of heavy aromatics that cannot be accounted for by the GC analysis used, rather than high amounts of homologation. Unlike with  $\text{InI}_3$ , reaction of neat 2,3-dimethylbutane (2,3-DMB) and  $\text{ZnI}_2$  only shows trace amounts of cracking and isomerization products, even at 230 °C.

Since  $\text{ZnI}_2$  can apparently activate alkanes to initiate triptane synthesis at 230 °C, can it also effect alkane homologation with methanol? The optimum conditions for  $\text{InI}_3$ -catalyzed homologation involve a 1:1 methanol:DMB ratio, but  $\text{ZnI}_2$  is considerably less soluble in that composition; most remains undissolved, and the product distribution of such a reaction (Table 5.5, Entry 1) resembles that expected for direct conversion of methanol with no participation of DMB; because solid  $\text{ZnI}_2$  is known to initiate direct methanol conversion and the lack of isomerization and cracking catalyzed by  $\text{ZnI}_2$  makes this result unsurprising. However, at a ratio of approximately 3:1 Methanol:DMB, the  $\text{ZnI}_2$  catalyst



can be completely dissolved and (in the presence of AdH, which as noted above substantially improves yield and selectivity in the  $\text{InI}_3$ -system) gives triptane yields much higher than can be accounted for by methanol conversion alone: the average yield (Entries 2–4 of Table 5.5) is about 68 mg, versus 54 mg obtained for a comparable reaction using twice as much methanol and no DMB, but with AdH (Table 4.2, Chapter 4). The following labeling study was performed to demonstrate the incorporation of DMB into triptane:  $\text{ZnI}_2$  (4.13 mmol) was predissolved in  $^{13}\text{C}$ -labeled methanol (12.4 mmol). Unlabeled DMB (3.84 mmol) and adamantane (0.367 mmol) were added and the reaction heated to 230 °C for 6 hours. The largest triptane signal in the GC/MS spectrum appears at 86  $m/z$ , corresponding to  $(\text{P-Me})^+$  for singly labeled triptane. In this case, there is also a strong signal at 91  $m/z$  corresponding to fully-labeled triptane resulting from direct methanol conversion; however some formation of fully-labeled triptane would be expected given the necessary excess of methanol over DMB to fully dissolve the  $\text{ZnI}_2$ . Thus, this finding is identical to that obtained for the analogous reaction over  $\text{InI}_3$  at 200 °C, and confirms that DMB is homologated to triptane here as well.

**Table 5.8**  $\text{ZnI}_2$  catalyzed homologation of DMB at 230 °C.<sup>a</sup> Unless otherwise stated all quantities are in milligrams.

Time (h)	Added MeOH (mg)	Added DMB (mg)	Recovered DMB (mg)	Recovered AdH (mg)	Isobutane (mg)	Isopentane (mg)	Triptyl Yield (mg)	PMB + HMB
3	199 (6.2) <sup>b</sup>	533 (6.2) <sup>b</sup>	404.5	38.9	7.8	3.4	15.6	4.2
6	398 (12.4) <sup>b</sup>	330 (3.8) <sup>b</sup>	198.4	40.9	28.1	17.4	66.3	22.5
6	398 (12.4) <sup>b</sup>	330 (3.8) <sup>b</sup>	182.9	38.8	26.8	15.6	68.6	23.5
6	398 (12.4) <sup>b</sup>	330 (3.8) <sup>b</sup>	203.6	37.2	28.1	15.5	68.1	25.0

<sup>a</sup> All reactions contained 4.13 mmol of  $\text{ZnI}_2$  and 0.367 mmol (49.9 mg) of AdH and were heated at 230 °C for 3 hours.

<sup>b</sup> Number in parenthesis is the quantity in mmol

## 5.4 Conclusions

The results presented above demonstrate that lighter branched alkanes can be converted to more valuable products through a novel process involving methylative homologation. Product distributions, as well as the observation that homologation yields are substantially improved by the addition of adamantane as hydride transfer agent, are consistent with a mechanism in which  $\text{InI}_3$  activates branched alkanes to produce tertiary carbocations. The latter are in equilibrium with olefins which undergo chain growth by reacting with methylating species generated from methanol and  $\text{InI}_3$ , as previously shown for the direct conversion of methanol to triptane.<sup>21</sup> Although carbocationic mechanisms are not usually associated with highly selective transformations, selectivities as high as 65% based on converted alkane were achieved for the homologation of DMB to triptane. Selectivities in homologations of the abundant branched alkanes isopentane and isobutane are not quite so high, but even for the most difficult case, the combined selectivity to higher branched alkanes from homologation of isobutane exceeds 40%; a process involving separation and recycling of the intermediate products might be effectively applied. Methylative homologation also affords product mixtures with much lower aromatic content than most processes for direct conversion of methanol to hydrocarbons over zeolites or other catalysts, another highly desirable feature. This route thus offers considerable promise for upgrading relatively low-value, lighter branched alkanes to species that are both less volatile and higher octane, and hence significantly more valuable fuels.

## 5.5 Experimental

**General considerations.**  $\text{InI}_3$  (purchased from Alfa Aesar),  $\text{ZnI}_2$  (purchased from Sigma-Aldrich), MeOH, and other organic compounds were reagent-grade commercial samples used without further purification. GC analyses were performed on an HP model 6890N chromatograph equipped with a 10 m x 0.10 mm x 0.40  $\mu\text{m}$  DB-1 column. GC/MS analyses were performed on an HP model 6890N chromatograph equipped with a 30 m x 25  $\mu\text{m}$  x 0.40  $\mu\text{m}$  HP5-1 column and equipped with an HP 5973 mass selective EI detector.

**Standard reaction protocols.** All reactions were performed in thick-walled pressure tubes equipped with Teflon stopcocks (Kontes valves), rated up to 10 bar. The procedure for alkane homologation reactions is based on the procedure reported earlier (Chapter 4) for MeOH-to-hydrocarbon conversions using  $\text{ZnI}_2$  and  $\text{InI}_3$ .<sup>18, 19, 21</sup> In a typical experiment, the tube was equipped with a stir bar and charged with  $\text{InI}_3$  (2.05 g, 4.1 mmol), MeOH (0.25 mL, 6.2 mmol), and DMB (0.807 mL, 6.2 mmol). (The  $\text{InI}_3$  was weighed out in a glove box due to its hygroscopic nature; however the reactions were carried out under an atmosphere of air). If adamantane was utilized, it was added at this stage. The pressure tube was then placed in a pre-heated oil bath behind a blast shield and stirred at the appropriate temperature for the desired period of time. After heating, the tube was removed from the bath and allowed to cool to room temperature and then placed in an ice bath. The stopcock was removed, and chloroform (1.0 mL), containing a known amount of cyclohexane as an internal standard, was pipetted into the reaction mixture, followed by

water (0.5 mL). The stopcock was replaced, the mixture was shaken vigorously and the organic layer separated. A small aliquot was diluted with acetone or tetradecane for GC analysis.

## 5.6 References

1. Bercaw, J. E.; Hazari, N.; Labinger, J. A.; Scott, V. J.; Sunley, G. J., *J. Am. Chem. Soc.*, **2008**, *130*, 11988-11995.
2. Crabtree, R. H., *J. Chem. Soc. Dalt. Trans.*, **2001**, 2437-2450.
3. Labinger, J. A.; Bercaw, J. E., *Nature*, **2002**, *417*, 507-514.
4. Fekl, U.; Goldberg, K. I., Homogeneous hydrocarbon C-H bond activation and functionalization with platinum. In *Advances in Inorganic Chemistry: Including Bioinorganic Studies*, Academic Press Inc: San Diego, **2003**, *54*, 259-320.
5. Goldberg, K. I., *Activation and Functionalization of C-H Bonds*. American Chemical Society: Washington, DC, 2004.
6. Ono, Y., *Catal. Today*, **2003**, *81*, 3-16.
7. Hommeltoft, S. I., *Appl. Catal. A-Gen.*, **2001**, *221*, 421-428.
8. Brown, S. H.; Crabtree, R. H., *J. Am. Chem. Soc.*, **1989**, *111*, 2935-2946.
9. Basset, J. M.; Coperet, C.; Soulivong, D.; Taoufik, M.; Thivolle-Cazat, J., *Angew. Chem. Int. Ed.*, **2006**, *45*, 6082-6085.
10. Goldman, A. S.; Roy, A. H.; Huang, Z.; Ahuja, R.; Schinski, W.; Brookhart, M., *Science*, **2006**, *312*, 257-261.
11. Vidal, V.; Theolier, A.; ThivolleCazat, J.; Basset, J. M., *Science*, **1997**, *276*, 99-102.

12. Chang, C. D., *Catal. Rev.Sci. Eng.*, **1983**, 25, 1-118.
13. Haw, J. F.; Song, W. G.; Marcus, D. M.; Nicholas, J. B., *Acc. Chem. Res.*, **2003**, 36, 317-326.
14. Olah, G. A.; Molnár, Á., *Hydrocarbon Chemistry, 2nd ed.* John Wiley & Sons: Hoboken, NJ, 2003.
15. Olsbye, U.; Bjorgen, M.; Svelle, S.; Lillerud, K. P.; Kolboe, S., *Catal. Today*, **2005**, 106, 108-111.
16. Kim, L.; Wald, M. M.; Brandenberger, S. G., *J. Org. Chem.*, **1978**, 43, 3432-3433.
17. Walspurger, S.; Prakash, G. K. S.; Olah, G. A., *Appl. Catal. A-Gen.*, **2008**, 336, 48-53.
18. Bercaw, J. E.; Diaconescu, P. L.; Grubbs, R. H.; Kay, R. D.; Kitching, S.; Labinger, J. A.; Li, X. W.; Mehrkhodavandi, P.; Morris, G. E.; Sunley, G. J.; Vagner, P., *J. Org. Chem.*, **2006**, 71, 8907-8917.
19. Hazari, N.; Labinger, J. A.; Scott, V. J., *J. Catal.*, **2009**, 263, 266-276.
20. Bercaw, J. E.; Grubbs, R. H.; Hazari, N.; Labinger, J. A.; Li, X. W., *Chem. Commun.*, **2007**, 2974-2976.
21. Bercaw, J. E.; Diaconescu, P. L.; Grubbs, R. H.; Hazari, N.; Kay, R. D.; Labinger, J. A.; Mehrkhodavandi, P.; Morris, G. E.; Sunley, G. J.; Vagner, P., *Inorganic Chemistry*, **2007**, 46, 11371-11380.
22. Kay, R. D.; Morris, G. E.; Sunley, G. J. 2005.
23. Alt, H. G.; Bohmer, I. K., *Angew. Chem. Int. Ed.*, **2008**, 47, 2619-2621.

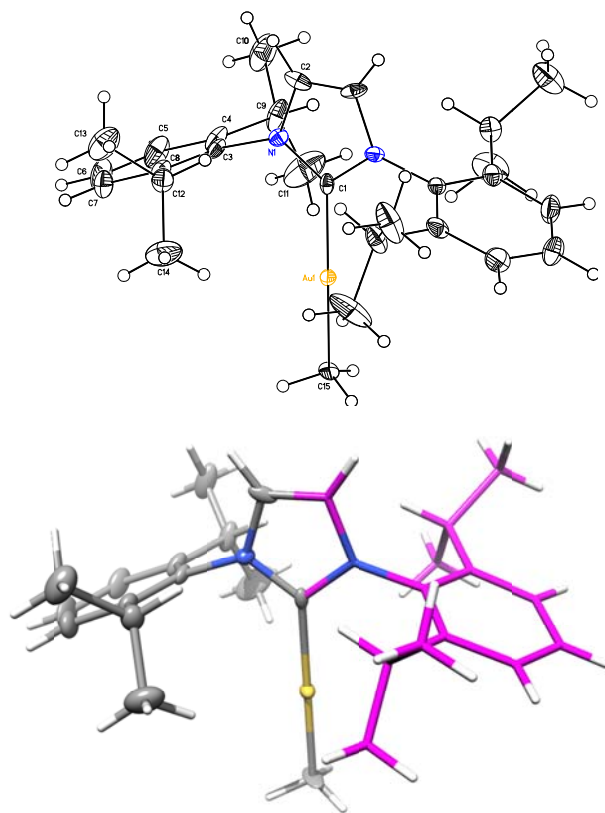
24. Grayson, M.; Eckroth, D.; Eds., *Kirk-Othmer Encyclopedia of Chemical Technology*, 3rd ed. John Wiley & Sons: New York, 1980.
25. Iglesia, E.; Soled, S. L.; Kramer, G. M., *J. Catal.*, **1993**, *144*, 238-253.
26. Mayr, H.; Schneider, R.; Irrgang, B.; Schade, C., *J. Am. Chem. Soc.*, **1990**, *112*, 4454-4459.
27. Kruppa, G. H.; Beauchamp, J. L., *J. Am. Chem. Soc.*, **1986**, *108*, 2162-2169.
28. Meotner, M.; Solomon, J. J.; Field, F. H., *J. Am. Chem. Soc.*, **1976**, *98*, 1025-1026.
29. Solomon, J. J.; Field, F. H., *J. Am. Chem. Soc.*, **1975**, *97*, 2625-2628.

## Appendices

## APPENDIX A

### Crystallographic data

#### A.1 (Idipp)AuMe (A)



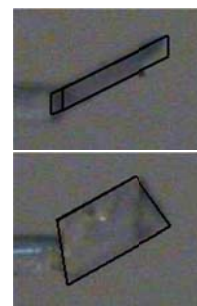
(Idipp)AuMe

**Note:** The crystallographic data have been deposited in the Cambridge Database (CCDC) and has been placed on hold pending further instructions from me. The deposition number is 775773. Ideally the CCDC would like the publication to contain a footnote of the type: "Crystallographic data have been deposited at the CCDC, 12 Union Road, Cambridge CB2 1EZ, UK and copies can be obtained on request, free of charge, by quoting the publication citation and the deposition number 775773.



**Table 1. Crystal data and structure refinement for (Idipp)AuMe (CCDC 775773)**

Empirical formula	$\text{C}_{28}\text{H}_{39}\text{N}_2\text{Au} \cdot \text{C}_6\text{H}_6$
Formula weight	678.69
Crystallization Solvent	Benzene
Crystal Habit	Plate
Crystal size	0.22 x 0.14 x 0.06 mm <sup>3</sup>
Crystal color	Colorless



### Data Collection

Type of diffractometer	Bruker KAPPA APEX II
Wavelength	0.71073 Å MoK $\alpha$
Data Collection Temperature	100(2) K
$\theta$ range for 9778 reflections used in lattice determination	2.33 to 30.25°
Unit cell dimensions	$a = 21.9555(13)$ Å $b = 9.6998(6)$ Å $c = 16.6728(10)$ Å
	$\alpha = 90^\circ$ $\beta = 113.999(2)^\circ$ $\gamma = 90^\circ$
Volume	3243.8(3) Å <sup>3</sup>
Z	4
Crystal system	Monoclinic
Space group	C 2/c
Density (calculated)	1.390 Mg/m <sup>3</sup>
F(000)	1368
$\theta$ range for data collection	2.03 to 28.70°
Completeness to $\theta = 28.70^\circ$	98.2 %
Index ranges	$-29 \leq h \leq 29, -13 \leq k \leq 12, -21 \leq l \leq 21$
Data collection scan type	$\omega$ scans; 21 settings
Reflections collected	47630
Independent reflections	4122 [ $R_{\text{int}} = 0.0374$ ]
Absorption coefficient	4.557 mm <sup>-1</sup>
Absorption correction	Semi-empirical from equivalents
Max. and min. transmission	0.7458 and 0.4946

### Structure Solution and Refinement

Structure solution program	SHELXS-97 (Sheldrick, 2008)
----------------------------	-----------------------------

Primary solution method	Patterson method
Secondary solution method	Difference Fourier map
Hydrogen placement	Geometric positions
Structure refinement program	SHELXL-97 (Sheldrick, 2008)
Refinement method	Full matrix least-squares on $F^2$
Data / restraints / parameters	4122 / 0 / 159
Treatment of hydrogen atoms	Riding
Goodness-of-fit on $F^2$	4.824
Final R indices [ $I > 2\sigma(I)$ , 3977 reflections]	$R1 = 0.0338$ , $wR2 = 0.0784$
R indices (all data)	$R1 = 0.0355$ , $wR2 = 0.0785$
Type of weighting scheme used	Sigma
Weighting scheme used	$w = 1/\sigma^2(F_o^2)$
Max shift/error	0.001
Average shift/error	0.000
Largest diff. peak and hole	4.637 and -1.116 e.Å <sup>-3</sup>

### Special Refinement Details

Crystals were mounted on a glass fiber using Paratone oil then placed on the diffractometer under a nitrogen stream at 100K.

The Au molecule sits on a 2-fold axis through C1, Au1 and C15 at  $\frac{1}{2}$ ,  $y$ ,  $\frac{3}{4}$ . The solvent benzene sits near a center of symmetry at  $\frac{1}{4}$ ,  $\frac{1}{4}$ ,  $\frac{1}{2}$  requiring half-occupancy, was refined isotropically and was restrained to be a regular hexagon.

Refinement of  $F^2$  against ALL reflections. The weighted R-factor ( $wR$ ) and goodness of fit ( $S$ ) are based on  $F^2$ , conventional R-factors ( $R$ ) are based on  $F$ , with  $F$  set to zero for negative  $F^2$ . The threshold expression of  $F^2 > 2\sigma(F^2)$  is used only for calculating R-factors(gt) etc. and is not relevant to the choice of reflections for refinement. R-factors based on  $F^2$  are statistically about twice as large as those based on  $F$ , and R-factors based on ALL data will be even larger.

All esds (except the esd in the dihedral angle between two l.s. planes) are estimated using the full covariance matrix. The cell esds are taken into account individually in the estimation of esds in distances, angles and torsion angles; correlations between esds in cell parameters are only used when they are defined by crystal symmetry. An approximate (isotropic) treatment of cell esds is used for estimating esds involving l.s. planes.

**Table 2.** Atomic coordinates ( $\times 10^4$ ) and equivalent isotropic displacement parameters ( $\text{\AA}^2 \times 10^3$ ) for (Idipp)AuMe (CCDC 775773).  $U(\text{eq})$  is defined as the trace of the orthogonalized  $U^{ij}$  tensor.

	x	y	z	$U_{\text{eq}}$	Occ
Au(1)	5000	5326(1)	7500	14(1)	1
N(1)	4854(2)	8280(3)	8037(2)	13(1)	1
C(1)	5000	7427(6)	7500	12(1)	1
C(2)	4911(2)	9629(4)	7812(3)	17(1)	1
C(3)	4678(2)	7798(4)	8734(3)	15(1)	1
C(4)	4013(2)	7440(4)	8521(3)	21(1)	1
C(5)	3858(2)	6929(5)	9198(3)	30(1)	1
C(6)	4350(3)	6768(5)	10036(3)	34(1)	1
C(7)	5002(2)	7138(4)	10222(3)	28(1)	1
C(8)	5178(2)	7676(4)	9576(3)	18(1)	1
C(9)	3476(2)	7571(5)	7599(3)	26(1)	1
C(10)	2903(2)	8464(6)	7578(4)	45(2)	1
C(11)	3220(3)	6168(6)	7192(4)	55(2)	1
C(12)	5893(2)	8077(4)	9793(3)	22(1)	1
C(13)	6163(2)	9063(6)	10590(4)	40(1)	1
C(14)	6340(2)	6826(5)	9933(4)	40(1)	1
C(15)	5000	3224(5)	7500	31(2)	1
C(21)	2245(3)	1493(6)	4610(4)	23(6)	0.50
C(22)	2699(3)	714(5)	5290(4)	41(3)	0.50
C(23)	3169(3)	1366(5)	6024(4)	10(2)	0.50
C(24)	3184(3)	2796(5)	6077(4)	42(3)	0.50
C(25)	2730(4)	3575(5)	5396(5)	45(9)	0.50
C(26)	2261(4)	2924(6)	4663(5)	31(2)	0.50

**Table 3.** Selected bond lengths [ $\text{\AA}$ ] and angles [ $^\circ$ ] for (Idipp)AuMe (CCDC 775773).

Au(1)-C(1)	2.038(5)	C(1)-Au(1)-C(15)	180.000(2)
Au(1)-C(15)	2.039(5)		

**Table 4. Bond lengths [Å] and angles [°] for (Idipp)AuMe (CCDC 775773).**

Au(1)-C(1)	2.038(5)	C(14)-C(12)-C(13)	111.4(4)
Au(1)-C(15)	2.039(5)	C(22)-C(21)-C(26)	120.0
N(1)-C(1)	1.350(4)	C(23)-C(22)-C(21)	120.0
N(1)-C(2)	1.382(4)	C(24)-C(23)-C(22)	120.0
N(1)-C(3)	1.444(5)	C(25)-C(24)-C(23)	120.0
C(1)-N(1)#1	1.350(4)	C(24)-C(25)-C(26)	120.0
C(2)-C(2)#1	1.249(10)	C(25)-C(26)-C(21)	120.0
C(3)-C(8)	1.392(6)		
C(3)-C(4)	1.398(6)		
C(4)-C(5)	1.396(7)		
C(4)-C(9)	1.514(6)		
C(5)-C(6)	1.384(7)		
C(6)-C(7)	1.383(7)		
C(7)-C(8)	1.385(7)		
C(8)-C(12)	1.512(6)		
C(9)-C(10)	1.517(7)		
C(9)-C(11)	1.522(6)		
C(12)-C(14)	1.518(6)		
C(12)-C(13)	1.547(6)		
C(21)-C(22)	1.3900		
C(21)-C(26)	1.3900		
C(22)-C(23)	1.3900		
C(23)-C(24)	1.3900		
C(24)-C(25)	1.3900		
C(25)-C(26)	1.3900		
C(1)-Au(1)-C(15)	180.000(2)		
C(1)-N(1)-C(2)	109.1(4)		
C(1)-N(1)-C(3)	123.3(3)		
C(2)-N(1)-C(3)	127.6(3)		
N(1)-C(1)-N(1)#1	104.4(5)		
N(1)-C(1)-Au(1)	127.8(2)		
N(1)#1-C(1)-Au(1)	127.8(2)		
C(2)#1-C(2)-N(1)	108.7(2)		
C(8)-C(3)-C(4)	123.3(4)		
C(8)-C(3)-N(1)	118.7(4)		
C(4)-C(3)-N(1)	118.0(4)		
C(5)-C(4)-C(3)	117.1(4)		
C(5)-C(4)-C(9)	120.3(4)		
C(3)-C(4)-C(9)	122.6(4)		
C(6)-C(5)-C(4)	120.6(4)		
C(7)-C(6)-C(5)	120.6(5)		
C(6)-C(7)-C(8)	120.9(5)		
C(7)-C(8)-C(3)	117.5(4)		
C(7)-C(8)-C(12)	120.1(4)		
C(3)-C(8)-C(12)	122.4(4)		
C(4)-C(9)-C(10)	111.5(4)		
C(4)-C(9)-C(11)	111.8(4)		
C(10)-C(9)-C(11)	110.4(4)		
C(8)-C(12)-C(14)	112.1(4)		
C(8)-C(12)-C(13)	111.3(4)		

---

Symmetry transformations used to generate equivalent atoms:

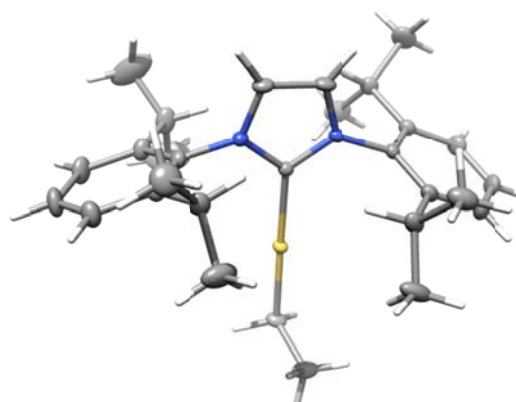
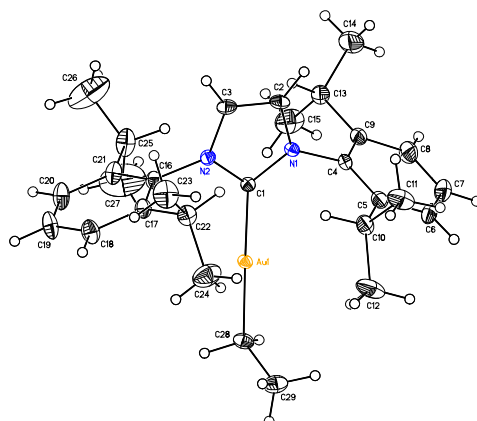
#1 -x+1,y,-z+3/2

**Table 5.** Anisotropic displacement parameters ( $\text{\AA}^2 \times 10^4$ ) for (Idipp)AuMe (CCDC 775773). The anisotropic displacement factor exponent takes the form:  $-2\pi^2 [h^2 a^{*2} U^{11} + \dots + 2 h k a^* b^* U^{12}]$

	$U^{11}$	$U^{22}$	$U^{33}$	$U^{23}$	$U^{13}$	$U^{12}$
Au(1)	238(1)	90(1)	117(1)	0	83(1)	0
N(1)	137(15)	109(15)	160(20)	-18(14)	64(14)	-26(13)
C(1)	90(20)	200(30)	80(30)	0	40(20)	0
C(2)	79(17)	129(18)	250(30)	62(17)	-5(16)	-32(15)
C(3)	199(19)	132(18)	170(20)	-47(16)	135(18)	-34(15)
C(4)	230(20)	220(20)	240(30)	-108(19)	170(20)	-64(17)
C(5)	320(20)	350(30)	340(30)	-110(20)	250(20)	-140(20)
C(6)	470(30)	410(30)	300(30)	-30(20)	310(30)	-80(20)
C(7)	380(30)	330(30)	190(30)	10(20)	160(20)	10(20)
C(8)	210(20)	190(20)	190(30)	-32(17)	120(19)	4(16)
C(9)	180(20)	420(30)	210(30)	-140(20)	100(20)	-101(19)
C(10)	290(30)	710(40)	280(30)	-200(30)	50(20)	50(30)
C(11)	330(30)	550(40)	660(50)	-400(30)	80(30)	-120(30)
C(12)	180(20)	270(20)	190(30)	-5(18)	75(19)	17(17)
C(13)	300(30)	470(30)	400(40)	-190(30)	120(20)	-70(20)
C(14)	290(30)	330(30)	520(40)	-70(30)	110(30)	80(20)
C(15)	700(50)	30(20)	170(40)	0	140(30)	0

---

## A.2 (Idipp)AuEt (E)

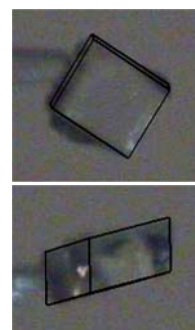


(Idipp)AuEt

**Note:** The crystallographic data have been deposited in the Cambridge Database (CCDC) and has been placed on hold pending further instructions from me. The deposition number is 775774. Ideally the CCDC would like the publication to contain a footnote of the type: "Crystallographic data have been deposited at the CCDC, 12 Union Road, Cambridge CB2 1EZ, UK and copies can be obtained on request, free of charge, by quoting the publication citation and the deposition number 775774."

**Table 1. Crystal data and structure refinement for (Idipp)AuEt (CCDC 775774).**

Empirical formula	$C_{29}H_{41}N_2Au \cdot \frac{1}{2} (C_6H_6)$
Formula weight	653.66
Crystallization Solvent	Benzene
Crystal Habit	Block
Crystal size	0.23 x 0.21 x 0.14 mm <sup>3</sup>
Crystal color	Colorless



### Data Collection

Type of diffractometer	Bruker KAPPA APEX II
Wavelength	0.71073 Å MoK $\alpha$
Data Collection Temperature	100(2) K
$\theta$ range for 9213 reflections used in lattice determination	2.45 to 36.77°
Unit cell dimensions	$a = 38.7430(18)$ Å $b = 9.6329(4)$ Å $c = 16.7611(7)$ Å
	$\alpha = 90^\circ$ $\beta = 101.923(2)^\circ$ $\gamma = 90^\circ$

Volume	6120.4(5) Å <sup>3</sup>
Z	8
Crystal system	Monoclinic
Space group	C 2/c
Density (calculated)	1.419 Mg/m <sup>3</sup>
F(000)	2632
θ range for data collection	2.15 to 36.80°
Completeness to θ = 36.80°	95.7 %
Index ranges	-56 ≤ h ≤ 65, -15 ≤ k ≤ 12, -28 ≤ l ≤ 24
Data collection scan type	ω scans; 18 settings
Reflections collected	102693
Independent reflections	14690 [R <sub>int</sub> = 0.0337]
Absorption coefficient	4.828 mm <sup>-1</sup>
Absorption correction	Semi-empirical from equivalents
Max. and min. transmission	0.7472 and 0.5782

### Structure Solution and Refinement

Structure solution program	SHELXS-97 (Sheldrick, 2008)
Primary solution method	Patterson method
Secondary solution method	Difference Fourier map
Hydrogen placement	Geometric positions
Structure refinement program	SHELXL-97 (Sheldrick, 2008)
Refinement method	Full matrix least-squares on F <sup>2</sup>
Data / restraints / parameters	14690 / 0 / 310
Treatment of hydrogen atoms	Riding
Goodness-of-fit on F <sup>2</sup>	2.449
Final R indices [I > 2σ(I), 13155 reflections]	R1 = 0.0228, wR2 = 0.0538
R indices (all data)	R1 = 0.0280, wR2 = 0.0542
Type of weighting scheme used	Sigma
Weighting scheme used	w = 1/σ <sup>2</sup> (F <sub>o</sub> <sup>2</sup> )
Max shift/error	0.006
Average shift/error	0.000
Largest diff. peak and hole	2.763 and -1.121 e.Å <sup>-3</sup>

### Special Refinement Details

Crystals were mounted on a glass fiber using Paratone oil then placed on the diffractometer under a

nitrogen stream at 100K.

The solvent benzene was restrained to a regular hexagon (with isotropic temperature factors) during least-squares refinement and sits at a center of symmetry at  $\frac{3}{4}, \frac{3}{4}, \frac{1}{2}$  which requires an occupancy of half.

Refinement of  $F^2$  against ALL reflections. The weighted R-factor ( $wR$ ) and goodness of fit ( $S$ ) are based on  $F^2$ , conventional R-factors ( $R$ ) are based on  $F$ , with  $F$  set to zero for negative  $F^2$ . The threshold expression of  $F^2 > 2\sigma(F^2)$  is used only for calculating R-factors(gt) etc. and is not relevant to the choice of reflections for refinement. R-factors based on  $F^2$  are statistically about twice as large as those based on  $F$ , and R-factors based on ALL data will be even larger.

All esds (except the esd in the dihedral angle between two l.s. planes) are estimated using the full covariance matrix. The cell esds are taken into account individually in the estimation of esds in distances, angles and torsion angles; correlations between esds in cell parameters are only used when they are defined by crystal symmetry. An approximate (isotropic) treatment of cell esds is used for estimating esds involving l.s. planes.

**Table 2. Atomic coordinates ( $\times 10^4$ ) and equivalent isotropic displacement parameters ( $\text{\AA}^2 \times 10^3$ ) for (Idipp)AuEt (CCDC 775774).  $U_{eq}$  is defined as the trace of the orthogonalized  $U^{ij}$  tensor.**

	x	y	z	$U_{eq}$	Occ
Au(1)	8863(1)	4841(1)	4566(1)	12(1)	1
N(1)	8861(1)	1831(1)	5141(1)	13(1)	1
N(2)	8736(1)	1924(1)	3839(1)	14(1)	1
C(1)	8809(1)	2743(2)	4510(1)	12(1)	1
C(2)	8824(1)	475(2)	4868(1)	18(1)	1
C(3)	8745(1)	531(2)	4050(1)	18(1)	1
C(4)	8953(1)	2254(2)	5985(1)	14(1)	1
C(5)	9299(1)	2673(2)	6295(1)	20(1)	1
C(6)	9374(1)	3157(2)	7101(1)	26(1)	1
C(7)	9116(1)	3210(2)	7557(1)	29(1)	1
C(8)	8778(1)	2759(2)	7235(1)	26(1)	1
C(9)	8690(1)	2249(2)	6436(1)	17(1)	1
C(10)	9586(1)	2601(2)	5801(1)	23(1)	1
C(11)	9841(1)	1412(2)	6099(1)	32(1)	1
C(12)	9787(1)	3981(2)	5817(2)	37(1)	1
C(13)	8317(1)	1763(2)	6081(1)	20(1)	1
C(14)	8181(1)	743(3)	6644(2)	43(1)	1
C(15)	8067(1)	3003(2)	5866(2)	44(1)	1



C(16)	8668(1)	2454(2)	3018(1)	16(1)	1
C(17)	8948(1)	2526(2)	2613(1)	18(1)	1
C(18)	8878(1)	3095(2)	1831(1)	26(1)	1
C(19)	8541(1)	3537(2)	1475(1)	29(1)	1
C(20)	8270(1)	3432(2)	1885(1)	27(1)	1
C(21)	8327(1)	2894(2)	2677(1)	21(1)	1
C(22)	9317(1)	2032(2)	2997(1)	22(1)	1
C(23)	9450(1)	967(2)	2451(1)	36(1)	1
C(24)	9572(1)	3254(2)	3199(2)	41(1)	1
C(25)	8028(1)	2826(2)	3132(1)	28(1)	1
C(26)	7727(1)	1932(4)	2708(2)	70(1)	1
C(27)	7898(1)	4235(3)	3289(2)	71(1)	1
C(28)	8937(1)	6960(2)	4629(1)	19(1)	1
C(29)	9320(1)	7426(2)	4869(1)	25(1)	1
<hr/>					
C(41)	7919(1)	8523(3)	4515(2)	22(1)	0.50
C(42)	7915(1)	7092(3)	4619(2)	60(2)	0.50
C(43)	7641(1)	6468(2)	4906(2)	34(1)	0.50
C(44)	7370(1)	7276(3)	5090(2)	37(1)	0.50
C(45)	7374(1)	8707(3)	4986(2)	48(2)	0.50
C(46)	7648(1)	9331(2)	4698(2)	52(1)	0.50

**Table 3.** Selected bond lengths [Å] and angles [°] for (Idipp)AuEt (CCDC 775774).

Au(1)-C(1)	2.0322(16)	C(1)-Au(1)-C(28)	177.86(7)
Au(1)-C(28)	2.0605(17)		

**Table 4.** Bond lengths [Å] and angles [°] for (Idipp)AuEt (CCDC 775774).

Au(1)-C(1)	2.0322(16)	C(17)-C(18)	1.394(2)
Au(1)-C(28)	2.0605(17)	C(17)-C(22)	1.519(3)
N(1)-C(1)	1.3570(19)	C(18)-C(19)	1.383(3)
N(1)-C(2)	1.382(2)	C(19)-C(20)	1.375(3)
N(1)-C(4)	1.444(2)	C(20)-C(21)	1.399(3)
N(2)-C(1)	1.356(2)	C(21)-C(25)	1.514(3)
N(2)-C(3)	1.386(2)	C(22)-C(24)	1.530(3)
N(2)-C(16)	1.441(2)	C(22)-C(23)	1.533(3)
C(2)-C(3)	1.343(3)	C(25)-C(27)	1.490(3)
C(4)-C(9)	1.391(2)	C(25)-C(26)	1.505(3)
C(4)-C(5)	1.391(2)	C(28)-C(29)	1.523(3)
C(5)-C(6)	1.402(3)	C(41)-C(42)	1.3900
C(5)-C(10)	1.519(3)	C(41)-C(46)	1.3900
C(6)-C(7)	1.378(3)	C(42)-C(43)	1.3900
C(7)-C(8)	1.379(3)	C(43)-C(44)	1.3900
C(8)-C(9)	1.400(2)	C(44)-C(45)	1.3900
C(9)-C(13)	1.518(3)	C(45)-C(46)	1.3900
C(10)-C(11)	1.527(3)		
C(10)-C(12)	1.538(3)	C(1)-Au(1)-C(28)	177.86(7)
C(13)-C(14)	1.530(3)	C(1)-N(1)-C(2)	111.44(13)
C(13)-C(15)	1.532(3)	C(1)-N(1)-C(4)	123.18(13)
C(16)-C(17)	1.393(2)	C(2)-N(1)-C(4)	125.36(13)
C(16)-C(21)	1.391(2)	C(1)-N(2)-C(3)	111.22(13)

C(1)-N(2)-C(16)	123.54(13)
C(3)-N(2)-C(16)	125.23(13)
N(2)-C(1)-N(1)	104.00(13)
N(2)-C(1)-Au(1)	128.24(11)
N(1)-C(1)-Au(1)	127.65(11)
C(3)-C(2)-N(1)	106.63(14)
C(2)-C(3)-N(2)	106.71(14)
C(9)-C(4)-C(5)	123.78(16)
C(9)-C(4)-N(1)	118.04(15)
C(5)-C(4)-N(1)	118.16(15)
C(4)-C(5)-C(6)	116.57(17)
C(4)-C(5)-C(10)	122.67(16)
C(6)-C(5)-C(10)	120.76(17)
C(7)-C(6)-C(5)	121.15(19)
C(6)-C(7)-C(8)	120.67(18)
C(7)-C(8)-C(9)	120.56(18)
C(4)-C(9)-C(8)	117.21(17)
C(4)-C(9)-C(13)	122.27(15)
C(8)-C(9)-C(13)	120.49(16)
C(11)-C(10)-C(5)	110.62(15)
C(11)-C(10)-C(12)	110.58(17)
C(5)-C(10)-C(12)	112.16(17)
C(9)-C(13)-C(14)	112.14(16)
C(9)-C(13)-C(15)	110.80(16)
C(14)-C(13)-C(15)	111.36(19)
C(17)-C(16)-C(21)	123.53(15)
C(17)-C(16)-N(2)	118.35(15)
C(21)-C(16)-N(2)	118.11(15)
C(18)-C(17)-C(16)	117.22(17)
C(18)-C(17)-C(22)	120.30(17)
C(16)-C(17)-C(22)	122.48(15)
C(19)-C(18)-C(17)	120.61(18)
C(20)-C(19)-C(18)	120.78(18)
C(19)-C(20)-C(21)	120.85(19)
C(16)-C(21)-C(20)	116.99(17)
C(16)-C(21)-C(25)	122.71(16)
C(20)-C(21)-C(25)	120.29(17)
C(17)-C(22)-C(24)	111.18(16)
C(17)-C(22)-C(23)	111.10(16)
C(24)-C(22)-C(23)	111.44(18)
C(27)-C(25)-C(26)	110.3(2)
C(27)-C(25)-C(21)	111.8(2)
C(26)-C(25)-C(21)	112.72(17)
C(29)-C(28)-Au(1)	115.07(12)
C(42)-C(41)-C(46)	120.0
C(43)-C(42)-C(41)	120.0
C(44)-C(43)-C(42)	120.0
C(43)-C(44)-C(45)	120.0
C(44)-C(45)-C(46)	120.0
C(45)-C(46)-C(41)	120.0

**Table 5. Anisotropic displacement parameters ( $\text{\AA}^2 \times 10^4$ ) for (Idipp)AuEt (CCDC 775774). The anisotropic displacement factor exponent takes the form:  $-2\pi^2 [h^2 a^{*2} U^{11} + \dots + 2 h k a^* b^* U^{12}]$**

	$U^{11}$	$U^{22}$	$U^{33}$	$U^{23}$	$U^{13}$	$U^{12}$
Au(1)	156(1)	95(1)	121(1)	1(1)	40(1)	7(1)
N(1)	141(7)	110(6)	136(6)	8(4)	32(5)	1(5)
N(2)	156(7)	123(6)	131(6)	-11(5)	27(5)	5(5)
C(1)	130(8)	115(7)	127(7)	-3(5)	32(6)	9(5)
C(2)	201(9)	99(7)	247(9)	10(6)	60(7)	1(6)
C(3)	222(9)	106(7)	229(8)	-32(6)	60(7)	-10(6)
C(4)	161(8)	144(7)	121(7)	26(5)	12(6)	0(6)
C(5)	177(9)	223(9)	190(8)	63(6)	12(7)	-26(6)
C(6)	236(10)	334(10)	179(9)	23(7)	-42(8)	-79(8)
C(7)	356(13)	349(11)	157(9)	-15(7)	6(9)	-67(9)
C(8)	305(11)	324(10)	159(8)	-1(7)	83(8)	-23(8)
C(9)	184(9)	187(8)	155(8)	19(6)	48(7)	-10(6)
C(10)	142(9)	315(10)	224(9)	87(7)	18(7)	-18(7)
C(11)	273(11)	255(10)	449(13)	74(9)	144(10)	28(8)
C(12)	224(11)	295(11)	592(15)	205(10)	115(11)	5(8)
C(13)	159(9)	259(9)	196(8)	18(6)	55(7)	-14(6)
C(14)	333(14)	529(15)	422(14)	156(11)	58(11)	-183(11)
C(15)	233(12)	358(13)	676(18)	56(12)	-32(12)	28(9)
C(16)	177(8)	166(8)	123(7)	-24(6)	27(6)	14(6)
C(17)	189(9)	210(8)	153(8)	-2(6)	39(7)	24(6)
C(18)	278(11)	340(11)	176(9)	30(7)	78(8)	43(8)
C(19)	346(12)	392(12)	133(8)	43(7)	39(8)	104(9)
C(20)	230(10)	378(11)	184(9)	-1(7)	-6(8)	117(8)
C(21)	176(9)	277(9)	161(8)	-32(6)	29(7)	58(7)
C(22)	160(9)	267(9)	227(9)	15(7)	54(7)	17(7)
C(23)	333(13)	359(12)	395(13)	-22(9)	97(10)	141(9)
C(24)	242(12)	355(12)	600(16)	-35(11)	-3(11)	-36(9)
C(25)	187(10)	453(12)	218(9)	-32(8)	49(8)	91(8)
C(26)	507(19)	930(20)	810(20)	-517(18)	433(18)	-338(17)
C(27)	570(20)	556(18)	1160(30)	-280(18)	550(20)	75(15)
C(28)	224(9)	116(7)	237(9)	2(6)	90(8)	15(6)
C(29)	218(10)	176(8)	381(11)	-28(7)	88(9)	-4(7)



Z	4
Crystal system	Triclinic
Space group	P-1
Density (calculated)	1.455 Mg/m <sup>3</sup>
F(000)	1372
Data collection program	Bruker APEX2 v2009.7-0
$\theta$ range for data collection	1.60 to 40.98°
Completeness to $\theta = 40.98^\circ$	95.8 %
Index ranges	$-17 \leq h \leq 19, -23 \leq k \leq 23, -42 \leq l \leq 42$
Data collection scan type	$\omega$ scans; 22 settings
Data reduction program	Bruker SAINT-Plus v7.66A
Reflections collected	160907
Independent reflections	39266 [ $R_{\text{int}} = 0.0533$ ]
Absorption coefficient	4.742 mm <sup>-1</sup>
Absorption correction	None
Max. and min. transmission	0.5365 and 0.4661

### Structure Solution and Refinement

Structure solution program	SHELXS-97 (Sheldrick, 2008)
Primary solution method	Patterson method
Secondary solution method	Difference Fourier map
Hydrogen placement	Geometric positions
Structure refinement program	SHELXL-97 (Sheldrick, 2008)
Refinement method	Full matrix least-squares on $F^2$
Data / restraints / parameters	39266 / 0 / 693
Treatment of hydrogen atoms	Riding
Goodness-of-fit on $F^2$	1.086
Final R indices [ $I > 2\sigma(I)$ , 28921 reflections]	$R1 = 0.0251, wR2 = 0.0434$
R indices (all data)	$R1 = 0.0425, wR2 = 0.0443$
Type of weighting scheme used	Sigma
Weighting scheme used	$w = 1/\sigma^2(F_o^2)$
Max shift/error	0.013
Average shift/error	0.000
Largest diff. peak and hole	3.960 and -2.261 e.Å <sup>-3</sup>

### Special Refinement Details

Crystals were mounted on a glass fiber using Paratone oil then placed on the diffractometer under a nitrogen stream at 100K.

Refinement of  $F^2$  against ALL reflections. The weighted R-factor ( $wR$ ) and goodness of fit ( $S$ ) are based on  $F^2$ , conventional R-factors ( $R$ ) are based on  $F$ , with  $F$  set to zero for negative  $F^2$ . The threshold expression of  $F^2 > 2\sigma(F^2)$  is used only for calculating R-factors(gt) etc. and is not relevant to the choice of reflections for refinement. R-factors based on  $F^2$  are statistically about twice as large as those based on  $F$ , and R-factors based on ALL data will be even larger.

All esds (except the esd in the dihedral angle between two l.s. planes) are estimated using the full covariance matrix. The cell esds are taken into account individually in the estimation of esds in distances, angles and torsion angles; correlations between esds in cell parameters are only used when they are defined by crystal symmetry. An approximate (isotropic) treatment of cell esds is used for estimating esds involving l.s. planes.

**Table 2. Atomic coordinates ( $\times 10^4$ ) and equivalent isotropic displacement parameters ( $\text{\AA}^2 \times 10^3$ ) for (Idipp)AuPh (CCDC 775775).  $U_{eq}$  is defined as the trace of the orthogonalized  $U^{ij}$  tensor.**

	x	y	z	$U_{eq}$
Au(1)	8875(1)	3737(1)	6617(1)	13(1)
N(1A)	6217(1)	5164(1)	6862(1)	13(1)
N(2A)	6094(1)	3729(1)	6521(1)	13(1)
C(1A)	6945(1)	4253(1)	6677(1)	14(1)
C(2A)	4924(1)	5209(1)	6818(1)	15(1)
C(3A)	4843(1)	4307(1)	6605(1)	15(1)
C(4A)	6728(1)	5953(1)	7092(1)	16(1)
C(5A)	6886(1)	5829(1)	7685(1)	18(1)
C(6A)	7385(1)	6611(1)	7892(1)	26(1)
C(7A)	7714(2)	7452(1)	7527(1)	31(1)
C(8A)	7558(2)	7544(1)	6942(1)	28(1)
C(9A)	7054(1)	6796(1)	6710(1)	20(1)
C(10A)	6578(1)	4887(1)	8084(1)	22(1)
C(11A)	5686(2)	5199(1)	8646(1)	28(1)
C(12A)	7819(2)	4165(2)	8233(1)	34(1)
C(13A)	6951(2)	6857(1)	6062(1)	25(1)
C(14A)	6459(2)	7969(1)	5816(1)	34(1)
C(15A)	8270(2)	6422(1)	5722(1)	33(1)
C(16A)	6447(1)	2719(1)	6284(1)	15(1)
C(17A)	6563(1)	1815(1)	6671(1)	21(1)
C(18A)	6881(2)	850(1)	6419(1)	29(1)
C(19A)	7065(2)	805(1)	5822(1)	31(1)

C(20A)	6955(1)	1708(1)	5452(1)	25(1)
C(21A)	6655(1)	2699(1)	5673(1)	17(1)
C(22A)	6381(2)	1852(1)	7331(1)	28(1)
C(23A)	5363(2)	1239(2)	7647(1)	54(1)
C(24A)	7653(2)	1461(2)	7571(1)	40(1)
C(25A)	6658(1)	3688(1)	5264(1)	22(1)
C(26A)	5961(2)	3699(2)	4740(1)	33(1)
C(27A)	8040(2)	3841(1)	5052(1)	28(1)
C(28A)	10790(1)	3106(1)	6511(1)	16(1)
C(29A)	11286(1)	2253(1)	6869(1)	23(1)
C(30A)	12550(2)	1703(1)	6748(1)	30(1)
C(31A)	13352(1)	2015(1)	6266(1)	32(1)
C(32A)	12902(1)	2872(1)	5908(1)	28(1)
C(33A)	11641(1)	3417(1)	6030(1)	21(1)
Au(2)	10274(1)	2037(1)	1275(1)	14(1)
N(1B)	7601(1)	2579(1)	2023(1)	12(1)
N(2B)	7520(1)	1793(1)	1270(1)	12(1)
C(1B)	8355(1)	2140(1)	1551(1)	14(1)
C(2B)	6324(1)	2500(1)	2036(1)	15(1)
C(3B)	6265(1)	2010(1)	1559(1)	14(1)
C(4B)	8073(1)	3097(1)	2438(1)	13(1)
C(5B)	8382(1)	2515(1)	2956(1)	16(1)
C(6B)	8856(1)	3026(1)	3348(1)	22(1)
C(7B)	9005(2)	4066(1)	3229(1)	23(1)
C(8B)	8678(1)	4622(1)	2718(1)	20(1)
C(9B)	8199(1)	4150(1)	2306(1)	15(1)
C(10B)	8278(1)	1367(1)	3074(1)	18(1)
C(11B)	7578(2)	1130(1)	3689(1)	25(1)
C(12B)	9621(2)	675(1)	2981(1)	25(1)
C(13B)	7870(1)	4770(1)	1737(1)	18(1)
C(14B)	6938(2)	5806(1)	1846(1)	26(1)
C(15B)	9090(2)	4969(1)	1333(1)	30(1)
C(16B)	7876(1)	1348(1)	708(1)	13(1)
C(17B)	7921(1)	271(1)	686(1)	15(1)
C(18B)	8220(1)	-121(1)	135(1)	18(1)
C(19B)	8466(1)	535(1)	-364(1)	20(1)
C(20B)	8418(1)	1596(1)	-326(1)	19(1)
C(21B)	8120(1)	2035(1)	213(1)	15(1)
C(22B)	7681(1)	-443(1)	1239(1)	20(1)
C(23B)	7380(2)	-1493(1)	1123(1)	31(1)
C(24B)	8824(2)	-641(1)	1588(1)	28(1)
C(25B)	8012(1)	3206(1)	242(1)	18(1)
C(26B)	6728(2)	3802(1)	68(1)	30(1)
C(27B)	9145(2)	3621(1)	-134(1)	29(1)
C(28B)	12164(1)	1910(1)	920(1)	20(1)
C(29B)	13089(1)	1027(1)	1028(1)	25(1)
C(30B)	14328(1)	872(2)	710(1)	32(1)
C(31B)	14690(2)	1621(2)	282(1)	34(1)
C(32B)	13807(2)	2523(2)	180(1)	34(1)
C(33B)	12565(1)	2666(1)	494(1)	26(1)
N(3)	235(1)	1225(1)	4518(1)	28(1)
C(41)	262(1)	1246(1)	5006(1)	22(1)

---

C(42)	297(2)	1279(1)	5633(1)	29(1)
-------	--------	---------	---------	-------

---

**Table 3.** Selected bond lengths [Å] and angles [°] for (Idipp)AuPh (CCDC 775775).

Au(1)-C(1A)	2.0284(12)	C(1A)-Au(1)-C(28A)	174.45(5)
Au(1)-C(28A)	2.0363(13)	C(1B)-Au(2)-C(28B)	174.44(5)
Au(2)-C(1B)	2.0334(13)		
Au(2)-C(28B)	2.0396(13)		



**Table 4. Bond lengths [ $\text{\AA}$ ] and angles [ $^\circ$ ] for (Idipp)AuPh (CCDC 775775).**


---

Au(1)-C(1A)	2.0284(12)
Au(1)-C(28A)	2.0363(13)
N(1A)-C(1A)	1.3542(16)
N(1A)-C(2A)	1.3927(17)
N(1A)-C(4A)	1.4393(18)
N(2A)-C(1A)	1.3527(18)
N(2A)-C(3A)	1.3948(15)
N(2A)-C(16A)	1.4377(16)
C(2A)-C(3A)	1.3442(19)
C(4A)-C(9A)	1.400(2)
C(4A)-C(5A)	1.4004(19)
C(5A)-C(6A)	1.398(2)
C(5A)-C(10A)	1.513(2)
C(6A)-C(7A)	1.377(3)
C(7A)-C(8A)	1.384(2)
C(8A)-C(9A)	1.395(2)
C(9A)-C(13A)	1.518(2)
C(10A)-C(11A)	1.532(2)
C(10A)-C(12A)	1.533(2)
C(13A)-C(14A)	1.521(2)
C(13A)-C(15A)	1.535(2)
C(16A)-C(17A)	1.398(2)
C(16A)-C(21A)	1.4019(19)
C(17A)-C(18A)	1.399(2)
C(17A)-C(22A)	1.519(2)
C(18A)-C(19A)	1.376(3)
C(19A)-C(20A)	1.376(2)
C(20A)-C(21A)	1.3979(19)
C(21A)-C(25A)	1.515(2)
C(22A)-C(23A)	1.524(3)
C(22A)-C(24A)	1.527(2)
C(25A)-C(26A)	1.521(2)
C(25A)-C(27A)	1.527(2)
C(28A)-C(29A)	1.382(2)
C(28A)-C(33A)	1.403(2)
C(29A)-C(30A)	1.399(2)
C(30A)-C(31A)	1.374(3)
C(31A)-C(32A)	1.373(3)
C(32A)-C(33A)	1.396(2)
Au(2)-C(1B)	2.0334(13)
Au(2)-C(28B)	2.0396(13)
N(1B)-C(1B)	1.3577(14)
N(1B)-C(2B)	1.3860(17)
N(1B)-C(4B)	1.4389(17)
N(2B)-C(1B)	1.3559(17)
N(2B)-C(3B)	1.3912(15)
N(2B)-C(16B)	1.4486(15)
C(2B)-C(3B)	1.3516(18)

---

C(4B)-C(9B)	1.399(2)
C(4B)-C(5B)	1.3995(19)
C(5B)-C(6B)	1.393(2)
C(5B)-C(10B)	1.512(2)
C(6B)-C(7B)	1.387(2)
C(7B)-C(8B)	1.379(2)
C(8B)-C(9B)	1.400(2)
C(9B)-C(13B)	1.5255(19)
C(10B)-C(11B)	1.532(2)
C(10B)-C(12B)	1.5342(19)
C(13B)-C(14B)	1.529(2)
C(13B)-C(15B)	1.530(2)
C(16B)-C(17B)	1.3997(19)
C(16B)-C(21B)	1.4015(19)
C(17B)-C(18B)	1.3962(18)
C(17B)-C(22B)	1.518(2)
C(18B)-C(19B)	1.384(2)
C(19B)-C(20B)	1.382(2)
C(20B)-C(21B)	1.3965(18)
C(21B)-C(25B)	1.513(2)
C(22B)-C(23B)	1.524(2)
C(22B)-C(24B)	1.538(2)
C(25B)-C(26B)	1.529(2)
C(25B)-C(27B)	1.530(2)
C(28B)-C(29B)	1.389(2)
C(28B)-C(33B)	1.398(2)
C(29B)-C(30B)	1.398(2)
C(30B)-C(31B)	1.380(3)
C(31B)-C(32B)	1.378(3)
C(32B)-C(33B)	1.398(2)
N(3)-C(41)	1.143(2)
C(41)-C(42)	1.466(2)

C(1A)-Au(1)-C(28A)	174.45(5)
C(1A)-N(1A)-C(2A)	111.00(11)
C(1A)-N(1A)-C(4A)	123.55(11)
C(2A)-N(1A)-C(4A)	125.41(10)
C(1A)-N(2A)-C(3A)	111.34(11)
C(1A)-N(2A)-C(16A)	124.03(10)
C(3A)-N(2A)-C(16A)	124.60(12)
N(2A)-C(1A)-N(1A)	104.48(10)
N(2A)-C(1A)-Au(1)	125.48(9)
N(1A)-C(1A)-Au(1)	130.04(10)
C(3A)-C(2A)-N(1A)	106.91(11)
C(2A)-C(3A)-N(2A)	106.27(12)
C(9A)-C(4A)-C(5A)	123.60(13)
C(9A)-C(4A)-N(1A)	118.08(12)
C(5A)-C(4A)-N(1A)	118.31(13)
C(6A)-C(5A)-C(4A)	116.64(15)
C(6A)-C(5A)-C(10A)	120.75(13)
C(4A)-C(5A)-C(10A)	122.58(13)
C(7A)-C(6A)-C(5A)	121.26(15)
C(6A)-C(7A)-C(8A)	120.58(16)
C(7A)-C(8A)-C(9A)	121.01(16)

C(8A)-C(9A)-C(4A)	116.90(14)
C(8A)-C(9A)-C(13A)	121.33(15)
C(4A)-C(9A)-C(13A)	121.64(13)
C(5A)-C(10A)-C(11A)	112.59(13)
C(5A)-C(10A)-C(12A)	110.50(14)
C(11A)-C(10A)-C(12A)	110.04(12)
C(9A)-C(13A)-C(14A)	112.62(13)
C(9A)-C(13A)-C(15A)	109.55(13)
C(14A)-C(13A)-C(15A)	110.07(13)
C(17A)-C(16A)-C(21A)	123.67(13)
C(17A)-C(16A)-N(2A)	118.58(12)
C(21A)-C(16A)-N(2A)	117.75(12)
C(16A)-C(17A)-C(18A)	116.54(14)
C(16A)-C(17A)-C(22A)	122.99(13)
C(18A)-C(17A)-C(22A)	120.46(15)
C(19A)-C(18A)-C(17A)	121.12(16)
C(18A)-C(19A)-C(20A)	121.01(14)
C(19A)-C(20A)-C(21A)	120.88(15)
C(20A)-C(21A)-C(16A)	116.75(14)
C(20A)-C(21A)-C(25A)	120.55(13)
C(16A)-C(21A)-C(25A)	122.55(12)
C(17A)-C(22A)-C(23A)	112.94(16)
C(17A)-C(22A)-C(24A)	111.08(13)
C(23A)-C(22A)-C(24A)	110.01(15)
C(21A)-C(25A)-C(26A)	113.67(14)
C(21A)-C(25A)-C(27A)	109.97(12)
C(26A)-C(25A)-C(27A)	109.71(12)
C(29A)-C(28A)-C(33A)	116.17(12)
C(29A)-C(28A)-Au(1)	121.42(10)
C(33A)-C(28A)-Au(1)	121.89(11)
C(28A)-C(29A)-C(30A)	122.32(15)
C(31A)-C(30A)-C(29A)	120.07(17)
C(32A)-C(31A)-C(30A)	119.34(13)
C(31A)-C(32A)-C(33A)	120.30(15)
C(32A)-C(33A)-C(28A)	121.76(15)
C(1B)-Au(2)-C(28B)	174.44(5)
C(1B)-N(1B)-C(2B)	111.38(11)
C(1B)-N(1B)-C(4B)	123.77(11)
C(2B)-N(1B)-C(4B)	124.80(9)
C(1B)-N(2B)-C(3B)	111.66(10)
C(1B)-N(2B)-C(16B)	123.76(10)
C(3B)-N(2B)-C(16B)	124.31(11)
N(2B)-C(1B)-N(1B)	104.02(10)
N(2B)-C(1B)-Au(2)	125.43(8)
N(1B)-C(1B)-Au(2)	130.51(10)
C(3B)-C(2B)-N(1B)	106.85(10)
C(2B)-C(3B)-N(2B)	106.08(12)
C(9B)-C(4B)-C(5B)	123.47(12)
C(9B)-C(4B)-N(1B)	118.66(12)
C(5B)-C(4B)-N(1B)	117.87(12)
C(6B)-C(5B)-C(4B)	116.96(14)
C(6B)-C(5B)-C(10B)	120.95(13)
C(4B)-C(5B)-C(10B)	122.01(12)
C(7B)-C(6B)-C(5B)	121.12(14)

C(8B)-C(7B)-C(6B)	120.50(14)
C(7B)-C(8B)-C(9B)	120.96(14)
C(4B)-C(9B)-C(8B)	116.97(13)
C(4B)-C(9B)-C(13B)	122.80(12)
C(8B)-C(9B)-C(13B)	120.21(13)
C(5B)-C(10B)-C(11B)	112.04(11)
C(5B)-C(10B)-C(12B)	110.06(12)
C(11B)-C(10B)-C(12B)	110.92(12)
C(9B)-C(13B)-C(14B)	112.10(11)
C(9B)-C(13B)-C(15B)	111.02(12)
C(14B)-C(13B)-C(15B)	110.50(13)
C(17B)-C(16B)-C(21B)	123.67(11)
C(17B)-C(16B)-N(2B)	118.62(11)
C(21B)-C(16B)-N(2B)	117.68(12)
C(18B)-C(17B)-C(16B)	116.94(13)
C(18B)-C(17B)-C(22B)	121.55(13)
C(16B)-C(17B)-C(22B)	121.51(11)
C(19B)-C(18B)-C(17B)	120.86(14)
C(20B)-C(19B)-C(18B)	120.73(12)
C(19B)-C(20B)-C(21B)	121.08(13)
C(20B)-C(21B)-C(16B)	116.72(13)
C(20B)-C(21B)-C(25B)	120.25(13)
C(16B)-C(21B)-C(25B)	122.97(11)
C(17B)-C(22B)-C(23B)	113.38(13)
C(17B)-C(22B)-C(24B)	111.43(13)
C(23B)-C(22B)-C(24B)	109.45(13)
C(21B)-C(25B)-C(26B)	110.57(13)
C(21B)-C(25B)-C(27B)	111.99(11)
C(26B)-C(25B)-C(27B)	110.97(13)
C(29B)-C(28B)-C(33B)	115.90(13)
C(29B)-C(28B)-Au(2)	122.99(12)
C(33B)-C(28B)-Au(2)	120.65(11)
C(28B)-C(29B)-C(30B)	122.40(17)
C(31B)-C(30B)-C(29B)	120.46(16)
C(32B)-C(31B)-C(30B)	118.45(14)
C(31B)-C(32B)-C(33B)	120.78(18)
C(32B)-C(33B)-C(28B)	121.93(16)
N(3)-C(41)-C(42)	179.62(18)

**Table 5.** Anisotropic displacement parameters ( $\text{\AA}^2 \times 10^4$ ) for (Idipp)AuPh (CCDC 775775). The anisotropic displacement factor exponent takes the form:  $-2\pi^2 [h^2 a^{*2} U^{11} + \dots + 2 h k a^* b^* U^{12}]$

	$U^{11}$	$U^{22}$	$U^{33}$	$U^{23}$	$U^{13}$	$U^{12}$
Au(1)	120(1)	134(1)	131(1)	-18(1)	-17(1)	-21(1)
N(1A)	134(5)	138(5)	123(4)	-26(4)	-15(4)	-23(4)
N(2A)	125(5)	131(5)	143(5)	-30(4)	-11(4)	-17(4)
C(1A)	146(5)	159(6)	115(5)	-18(4)	-17(4)	-18(5)
C(2A)	126(5)	173(6)	142(5)	-30(4)	-19(4)	-13(5)
C(3A)	126(5)	174(6)	150(5)	-37(5)	-3(4)	-18(5)

C(4A)	144(6)	181(7)	170(6)	-65(5)	-27(4)	-32(5)
C(5A)	163(6)	241(7)	160(6)	-65(5)	-32(5)	-42(5)
C(6A)	258(7)	363(9)	207(7)	-125(6)	-46(6)	-97(7)
C(7A)	338(8)	348(10)	304(8)	-153(7)	-53(7)	-155(7)
C(8A)	349(8)	240(8)	296(8)	-58(6)	-36(7)	-156(7)
C(9A)	225(7)	201(7)	196(6)	-41(5)	-38(5)	-73(5)
C(10A)	240(7)	282(8)	152(6)	-5(5)	-70(5)	-45(6)
C(11A)	237(7)	392(10)	189(7)	23(6)	-33(6)	-8(7)
C(12A)	333(9)	400(11)	228(8)	-22(7)	-59(6)	53(8)
C(13A)	366(8)	220(8)	195(7)	27(5)	-72(6)	-157(6)
C(14A)	355(9)	312(10)	343(9)	61(7)	-79(7)	-71(7)
C(15A)	553(11)	226(8)	181(7)	-6(6)	-21(7)	-39(8)
C(16A)	131(5)	128(6)	196(6)	-33(5)	-1(4)	-26(4)
C(17A)	162(6)	168(7)	262(7)	22(5)	23(5)	-14(5)
C(18A)	246(7)	139(7)	428(10)	29(6)	70(7)	-26(6)
C(19A)	303(8)	144(7)	461(10)	-106(7)	91(7)	-47(6)
C(20A)	258(7)	212(8)	290(8)	-129(6)	40(6)	-49(6)
C(21A)	155(6)	160(7)	194(6)	-57(5)	17(5)	-34(5)
C(22A)	272(8)	263(9)	240(7)	82(6)	12(6)	2(6)
C(23A)	306(9)	990(20)	298(10)	154(11)	16(8)	-233(11)
C(24A)	314(9)	490(13)	366(10)	135(9)	-49(7)	-115(8)
C(25A)	291(7)	176(7)	149(6)	-32(5)	-6(5)	16(6)
C(26A)	285(8)	479(12)	219(7)	-7(7)	-53(6)	-36(8)
C(27A)	375(9)	241(8)	245(7)	56(6)	-64(6)	-139(7)
C(28A)	168(6)	164(6)	156(6)	-40(5)	-25(5)	-55(5)
C(29A)	164(6)	286(8)	258(7)	-13(6)	-54(5)	-41(6)
C(30A)	205(7)	259(9)	449(10)	-1(7)	-133(7)	3(6)
C(31A)	138(6)	349(10)	504(11)	-195(8)	-44(7)	-9(6)
C(32A)	172(7)	393(10)	303(8)	-136(7)	72(6)	-123(6)
C(33A)	208(7)	233(8)	211(7)	-38(5)	-3(5)	-73(6)
Au(2)	121(1)	198(1)	123(1)	-56(1)	-7(1)	-41(1)
N(1B)	131(5)	138(5)	99(4)	-22(4)	-5(3)	-30(4)
N(2B)	124(4)	151(5)	94(4)	-24(4)	-2(3)	-48(4)
C(1B)	167(6)	140(6)	97(5)	-18(4)	-1(4)	-23(5)
C(2B)	134(5)	170(6)	147(5)	-31(5)	-3(4)	-34(5)
C(3B)	126(5)	175(6)	137(5)	-29(4)	-4(4)	-40(5)
C(4B)	132(5)	144(6)	117(5)	-38(4)	-10(4)	-27(4)
C(5B)	195(6)	149(6)	137(5)	-32(4)	-33(5)	-10(5)
C(6B)	305(7)	199(7)	169(6)	-35(5)	-107(5)	-25(6)
C(7B)	314(8)	203(7)	214(7)	-73(5)	-120(6)	-39(6)
C(8B)	231(7)	155(7)	226(7)	-44(5)	-55(5)	-52(5)
C(9B)	146(6)	148(6)	157(6)	-26(5)	-18(4)	-36(5)
C(10B)	252(7)	153(7)	151(6)	-14(5)	-53(5)	-35(5)
C(11B)	281(8)	240(8)	219(7)	-4(6)	-11(6)	-58(6)
C(12B)	301(8)	169(7)	249(7)	-19(5)	20(6)	1(6)
C(13B)	223(6)	196(7)	139(6)	2(5)	-26(5)	-76(5)
C(14B)	308(8)	211(8)	261(7)	28(6)	-51(6)	-29(6)
C(15B)	291(8)	342(10)	243(8)	26(6)	31(6)	-106(7)
C(16B)	133(5)	171(6)	100(5)	-30(4)	-18(4)	-43(4)
C(17B)	147(6)	184(7)	131(5)	-38(5)	-5(4)	-46(5)
C(18B)	192(6)	199(7)	177(6)	-77(5)	-8(5)	-59(5)
C(19B)	207(6)	273(8)	131(6)	-68(5)	-9(5)	-68(6)
C(20B)	206(6)	270(8)	105(5)	-15(5)	-17(5)	-65(5)

C(21B)	144(5)	193(7)	124(5)	-22(4)	-28(4)	-50(5)
C(22B)	248(7)	154(7)	177(6)	-25(5)	38(5)	-44(5)
C(23B)	398(9)	197(8)	314(8)	-35(6)	52(7)	-112(7)
C(24B)	371(9)	252(8)	185(7)	42(6)	-44(6)	-32(7)
C(25B)	245(7)	184(7)	125(5)	7(5)	-30(5)	-75(5)
C(26B)	291(8)	244(9)	358(9)	8(7)	-55(7)	-13(7)
C(27B)	323(8)	287(9)	283(8)	-6(6)	-8(6)	-161(7)
C(28B)	175(6)	294(8)	166(6)	-124(5)	1(5)	-74(5)
C(29B)	179(6)	301(9)	293(8)	-66(6)	-67(6)	-77(6)
C(30B)	165(7)	396(10)	412(10)	-196(8)	-64(6)	-14(6)
C(31B)	148(7)	599(13)	306(8)	-200(8)	12(6)	-97(7)
C(32B)	227(7)	583(13)	241(8)	-41(8)	4(6)	-182(8)
C(33B)	164(6)	370(10)	257(7)	-68(6)	-28(5)	-85(6)
<hr/>						
N(3)	343(7)	229(7)	273(7)	8(5)	-67(6)	-60(6)
C(41)	234(7)	144(7)	289(8)	-1(5)	-70(6)	-49(5)
C(42)	393(9)	245(9)	287(8)	-43(6)	-162(7)	-57(7)

#### A.4 (Idipp)AuI<sub>2</sub>Me (B)

## Data Collection

Type of diffractometer	Bruker KAPPA APEX II	
Wavelength	0.71073 Å MoK $\alpha$	
Data Collection Temperature	100(2) K	
$\theta$ range for 9847 reflections used in lattice determination	2.44 to 29.12°	
Unit cell dimensions	a = 19.8666(13) Å b = 15.6120(10) Å c = 20.3678(13) Å	$\alpha = 90^\circ$ $\beta = 103.519(3)^\circ$ $\gamma = 90^\circ$
Volume	6142.2(7) Å <sup>3</sup>	
Z	8	
Crystal system	Monoclinic	
Space group	P 2 <sub>1</sub> /n	
Density (calculated)	1.956 Mg/m <sup>3</sup>	
F(000)	3414	
$\theta$ range for data collection	1.83 to 25.00°	
Completeness to $\theta = 25.00^\circ$	100.0 %	
Index ranges	-23 $\leq$ h $\leq$ 21, -18 $\leq$ k $\leq$ 18, -23 $\leq$ l $\leq$ 24	
Data collection scan type	$\omega$ scans; 12 settings	
Reflections collected	107698	
Independent reflections	10815 [ $R_{\text{int}} = 0.0757$ ]	
Absorption coefficient	7.213 mm <sup>-1</sup>	
Absorption correction	Semi-empirical from equivalents	
Max. and min. transmission	0.4370 and 0.2977	

## Structure Solution and Refinement

Structure solution program	SHELXS-97 (Sheldrick, 2008)
Primary solution method	Patterson method
Secondary solution method	Difference Fourier map
Hydrogen placement	Geometric positions
Structure refinement program	SHELXL-97 (Sheldrick, 2008)
Refinement method	Full matrix least-squares on F <sup>2</sup>
Data / restraints / parameters	10815 / 103 / 699
Treatment of hydrogen atoms	Riding
Goodness-of-fit on F <sup>2</sup>	3.050
Final R indices [ $I > 2\sigma(I)$ , 9164 reflections]	R1 = 0.0642, wR2 = 0.1381



R indices (all data)	R1 = 0.0767, wR2 = 0.1398
Type of weighting scheme used	Sigma
Weighting scheme used	$w=1/\sigma^2(F_o^2)$
Max shift/error	0.006
Average shift/error	0.000
Largest diff. peak and hole	5.152 and -1.911 e.Å <sup>-3</sup>

### Special Refinement Details

Crystals were mounted on a glass fiber using Paratone oil then placed on the diffractometer under a nitrogen stream at 100K.

One of the molecules in the asymmetric unit shares the site with a molecule without iodine as a ligand. The ratio is 89:11. The minor species was refined with one overall temperature factor and the geometry was restrained to be similar to the major species using the SAME command in SHELX.

Refinement of  $F^2$  against ALL reflections. The weighted R-factor ( $wR$ ) and goodness of fit ( $S$ ) are based on  $F^2$ , conventional R-factors ( $R$ ) are based on  $F$ , with  $F$  set to zero for negative  $F^2$ . The threshold expression of  $F^2 > 2\sigma(F^2)$  is used only for calculating R-factors(gt) etc. and is not relevant to the choice of reflections for refinement. R-factors based on  $F^2$  are statistically about twice as large as those based on  $F$ , and R-factors based on ALL data will be even larger.

All esds (except the esd in the dihedral angle between two l.s. planes) are estimated using the full covariance matrix. The cell esds are taken into account individually in the estimation of esds in distances, angles and torsion angles; correlations between esds in cell parameters are only used when they are defined by crystal symmetry. An approximate (isotropic) treatment of cell esds is used for estimating esds involving l.s. planes.

**Table 2. Atomic coordinates (  $\times 10^4$ ) and equivalent isotropic displacement parameters (Å<sup>2</sup> $\times 10^3$ ) for (Idipp)AuI<sub>2</sub>Me (CCDC 775776).  $U_{eq}$  is defined as the trace of the orthogonalized  $U_{ij}$  tensor.**

	x	y	z	$U_{eq}$	Occ
I(66)	9529(1)	4812(1)	9421(1)	40(1)	1
Au(1)	7885(1)	4226(1)	6736(1)	19(1)	1
I(1A)	8236(1)	4259(1)	8052(1)	37(1)	1
I(2A)	7643(1)	4332(1)	5432(1)	42(1)	1

N(1A)	6699(4)	2909(5)	6795(4)	13(2)	1
N(2A)	7655(4)	2245(5)	6812(4)	12(2)	1
C(1A)	7364(5)	3049(7)	6763(5)	17(2)	1
C(2A)	6574(5)	2054(7)	6869(5)	18(2)	1
C(3A)	7180(5)	1627(7)	6880(5)	20(3)	1
C(4A)	6145(5)	3534(7)	6730(5)	15(2)	1
C(5A)	5966(5)	3817(7)	7318(6)	23(3)	1
C(6A)	5353(6)	4312(7)	7229(7)	30(3)	1
C(7A)	4955(6)	4511(8)	6596(7)	33(3)	1
C(8A)	5156(6)	4209(7)	6037(6)	28(3)	1
C(9A)	5741(6)	3700(7)	6083(6)	22(3)	1
C(10A)	6384(6)	3607(7)	8022(6)	27(3)	1
C(11A)	6041(8)	2902(10)	8364(7)	52(4)	1
C(12A)	6493(7)	4387(8)	8495(6)	40(3)	1
C(13A)	5902(6)	3295(7)	5457(5)	24(3)	1
C(14A)	5525(6)	2464(7)	5279(6)	25(3)	1
C(15A)	5747(7)	3931(8)	4862(6)	36(3)	1
C(16A)	8350(5)	2015(7)	6772(5)	15(2)	1
C(17A)	8848(5)	1879(7)	7378(5)	17(2)	1
C(18A)	9514(5)	1642(7)	7316(6)	21(3)	1
C(19A)	9648(6)	1525(8)	6703(6)	29(3)	1
C(20A)	9146(6)	1633(8)	6118(6)	28(3)	1
C(21A)	8477(5)	1876(7)	6136(5)	18(2)	1
C(22A)	8670(6)	1924(7)	8057(5)	19(2)	1
C(23A)	8501(6)	1024(8)	8291(6)	29(3)	1
C(24A)	9271(6)	2319(9)	8594(6)	35(3)	1
C(25A)	7904(6)	1913(8)	5492(5)	24(3)	1
C(26A)	7541(7)	1017(8)	5368(6)	34(3)	1
C(27A)	8155(7)	2145(9)	4879(6)	41(3)	1
C(28A)	8387(5)	5464(7)	6695(5)	19(2)	1
Au(2)	1685(1)	1191(1)	6808(1)	19(1)	0.893(2)
I(1B)	1521(1)	1015(1)	5514(1)	38(1)	0.893(2)
I(2B)	1773(1)	1131(1)	8110(1)	29(1)	0.893(2)
N(1B)	1868(4)	3181(6)	6856(4)	13(2)	0.893(2)
N(2B)	2838(4)	2600(6)	6825(5)	13(2)	0.893(2)
C(1B)	2169(5)	2422(7)	6840(5)	11(2)	0.893(2)
C(2B)	2345(6)	3827(8)	6866(6)	23(3)	0.893(2)
C(3B)	2941(6)	3447(8)	6847(6)	20(3)	0.893(2)
C(4B)	1139(5)	3382(7)	6837(5)	14(3)	0.893(2)
C(5B)	675(6)	3455(7)	6230(6)	19(3)	0.893(2)
C(6B)	-5(6)	3689(9)	6239(6)	27(4)	0.893(2)
C(7B)	-171(5)	3852(9)	6835(7)	23(4)	0.893(2)
C(8B)	303(6)	3801(8)	7439(6)	20(3)	0.893(2)
C(9B)	980(5)	3565(7)	7468(5)	14(3)	0.893(2)
C(10B)	883(6)	3329(9)	5558(6)	27(3)	0.893(2)
C(11B)	1059(10)	4199(10)	5287(8)	55(5)	0.893(2)
C(12B)	327(8)	2911(11)	5042(7)	43(4)	0.893(2)
C(13B)	1514(6)	3536(8)	8136(6)	19(3)	0.893(2)
C(14B)	1825(6)	4423(8)	8341(6)	20(3)	0.893(2)
C(15B)	1194(7)	3191(8)	8708(6)	27(3)	0.893(2)
C(16B)	3398(5)	2026(7)	6796(5)	14(3)	0.893(2)
C(17B)	3563(6)	1897(8)	6175(6)	22(3)	0.893(2)
C(18B)	4162(6)	1442(10)	6168(6)	25(4)	0.893(2)

C(19B)	4581(6)	1110(9)	6748(7)	23(4)	0.893(2)
C(20B)	4399(7)	1217(11)	7346(7)	27(3)	0.893(2)
C(21B)	3812(6)	1690(7)	7409(6)	19(3)	0.893(2)
C(22B)	3126(7)	2302(9)	5524(6)	25(3)	0.893(2)
C(23B)	3431(8)	3184(12)	5380(9)	39(5)	0.893(2)
C(24B)	3080(13)	1724(14)	4911(8)	44(5)	0.893(2)
C(25B)	3646(6)	1854(8)	8074(6)	24(3)	0.893(2)
C(26B)	4087(9)	2617(10)	8413(7)	36(4)	0.893(2)
C(27B)	3804(8)	1039(9)	8555(7)	34(4)	0.893(2)
C(28B)	1213(6)	-26(8)	6781(6)	21(3)	0.893(2)
Au(3)	1837(3)	1629(4)	7107(3)	32(2)	0.107(2)
N(1C)	1962(15)	3556(9)	6737(19)	32(2)	0.107(2)
N(2C)	2923(13)	2926(17)	6740(20)	32(2)	0.107(2)
C(1C)	2276(10)	2800(10)	6848(15)	32(2)	0.107(2)
C(2C)	2410(20)	4156(14)	6580(30)	32(2)	0.107(2)
C(3C)	3001(18)	3746(19)	6590(30)	32(2)	0.107(2)
C(4C)	1236(16)	3781(11)	6715(18)	32(2)	0.107(2)
C(5C)	763(18)	3790(40)	6110(19)	32(2)	0.107(2)
C(6C)	68(19)	3930(70)	6120(20)	32(2)	0.107(2)
C(7C)	-110(18)	4020(90)	6720(30)	32(2)	0.107(2)
C(8C)	360(20)	3980(70)	7320(20)	32(2)	0.107(2)
C(9C)	1062(18)	3890(40)	7349(19)	32(2)	0.107(2)
C(10C)	960(20)	3610(40)	5441(18)	32(2)	0.107(2)
C(11C)	560(50)	4210(50)	4890(30)	32(2)	0.107(2)
C(12C)	820(60)	2700(40)	5220(40)	32(2)	0.107(2)
C(13C)	1600(20)	3960(40)	8012(19)	32(2)	0.107(2)
C(14C)	1420(50)	4670(50)	8460(30)	32(2)	0.107(2)
C(15C)	1670(50)	3110(50)	8410(30)	32(2)	0.107(2)
C(16C)	3460(12)	2310(20)	6730(20)	32(2)	0.107(2)
C(17C)	3530(30)	2020(40)	6100(30)	32(2)	0.107(2)
C(18C)	4010(60)	1370(70)	6090(40)	32(2)	0.107(2)
C(19C)	4430(60)	1050(70)	6680(40)	32(2)	0.107(2)
C(20C)	4340(50)	1330(70)	7280(40)	32(2)	0.107(2)
C(21C)	3840(30)	1950(40)	7340(30)	32(2)	0.107(2)
C(22C)	3160(50)	2470(60)	5440(20)	32(2)	0.107(2)
C(23C)	3580(80)	3240(80)	5280(70)	32(2)	0.107(2)
C(24C)	3020(100)	1850(90)	4840(30)	32(2)	0.107(2)
C(25C)	3700(30)	2190(50)	8010(20)	32(2)	0.107(2)
C(26C)	4270(70)	2810(70)	8370(50)	32(2)	0.107(2)
C(27C)	3690(70)	1370(60)	8470(40)	32(2)	0.107(2)
C(28C)	1360(40)	520(20)	7390(30)	32(2)	0.107(2)

**Table 3.** Selected bond lengths [Å] and angles [°] for (Idipp)AuI<sub>2</sub>Me (CCDC 775776).

Au(1)-C(1A)	2.116(11)	Au(2)-C(28B)	2.114(12)
Au(1)-C(28A)	2.185(11)	Au(2)-C(1B)	2.143(11)
Au(1)-I(2A)	2.5917(10)	Au(2)-I(1B)	2.5934(11)
Au(1)-I(1A)	2.6092(10)	Au(2)-I(2B)	2.6194(10)

Au(3)-C(28C)	2.114(12)		
Au(3)-C(1C)	2.143(11)		
C(1A)-Au(1)-C(28A)	177.9(4)	C(28B)-Au(2)-C(1B)	179.7(5)
C(1A)-Au(1)-I(2A)	96.2(3)	C(28B)-Au(2)-I(1B)	85.9(3)
C(28A)-Au(1)-I(2A)	83.2(3)	C(1B)-Au(2)-I(1B)	94.3(3)
C(1A)-Au(1)-I(1A)	90.3(3)	C(28B)-Au(2)-I(2B)	85.3(3)
C(28A)-Au(1)-I(1A)	90.4(3)	C(1B)-Au(2)-I(2B)	94.5(3)
I(2A)-Au(1)-I(1A)	173.30(3)	I(1B)-Au(2)-I(2B)	171.20(4)
C(28C)-Au(3)-C(1C)	176.3(17)		

**Table 4. Bond lengths [Å] and angles [°] for (Idipp)AuI<sub>2</sub>Me (CCDC 775776).**

I(66)-I(66)#1	2.7084(18)	I(2B)-Au(2)	2.6194(10)
Au(1)-C(1A)	2.116(11)	Au(2)-C(28B)	2.114(12)
Au(1)-C(28A)	2.185(11)	Au(2)-C(1B)	2.143(11)
Au(1)-I(2A)	2.5917(10)	N(1B)-C(1B)	1.330(13)
Au(1)-I(1A)	2.6092(10)	N(1B)-C(2B)	1.382(15)
N(1A)-C(1A)	1.356(13)	N(1B)-C(4B)	1.474(12)
N(1A)-C(2A)	1.372(13)	N(2B)-C(3B)	1.338(14)
N(1A)-C(4A)	1.454(12)	N(2B)-C(1B)	1.365(12)
N(2A)-C(1A)	1.376(13)	N(2B)-C(16B)	1.439(13)
N(2A)-C(3A)	1.377(13)	C(2B)-C(3B)	1.333(16)
N(2A)-C(16A)	1.448(12)	C(4B)-C(5B)	1.363(15)
C(2A)-C(3A)	1.372(15)	C(4B)-C(9B)	1.422(15)
C(4A)-C(9A)	1.398(15)	C(5B)-C(6B)	1.405(16)
C(4A)-C(5A)	1.399(15)	C(5B)-C(10B)	1.533(16)
C(5A)-C(6A)	1.417(16)	C(6B)-C(7B)	1.354(17)
C(5A)-C(10A)	1.515(16)	C(7B)-C(8B)	1.366(16)
C(6A)-C(7A)	1.381(17)	C(8B)-C(9B)	1.383(15)
C(7A)-C(8A)	1.375(17)	C(9B)-C(13B)	1.518(15)
C(8A)-C(9A)	1.393(15)	C(10B)-C(12B)	1.485(17)
C(9A)-C(13A)	1.522(15)	C(10B)-C(11B)	1.537(19)
C(10A)-C(12A)	1.537(16)	C(13B)-C(14B)	1.533(16)
C(10A)-C(11A)	1.543(17)	C(13B)-C(15B)	1.549(17)
C(13A)-C(14A)	1.500(16)	C(16B)-C(17B)	1.395(15)
C(13A)-C(15A)	1.540(15)	C(16B)-C(21B)	1.425(15)
C(16A)-C(21A)	1.393(14)	C(17B)-C(18B)	1.390(16)
C(16A)-C(17A)	1.405(14)	C(17B)-C(22B)	1.540(15)
C(17A)-C(18A)	1.408(14)	C(18B)-C(19B)	1.377(17)
C(17A)-C(22A)	1.508(15)	C(19B)-C(20B)	1.359(16)
C(18A)-C(19A)	1.348(16)	C(20B)-C(21B)	1.411(16)
C(19A)-C(20A)	1.372(17)	C(21B)-C(25B)	1.489(16)
C(20A)-C(21A)	1.392(15)	C(22B)-C(24B)	1.527(17)
C(21A)-C(25A)	1.525(14)	C(22B)-C(23B)	1.559(19)
C(22A)-C(23A)	1.545(16)	C(25B)-C(26B)	1.542(18)
C(22A)-C(24A)	1.547(15)	C(25B)-C(27B)	1.591(18)
C(25A)-C(27A)	1.493(16)	Au(3)-C(28C)	2.114(12)
C(25A)-C(26A)	1.567(17)	Au(3)-C(1C)	2.143(11)
I(1B)-Au(2)	2.5934(11)	N(1C)-C(1C)	1.330(14)

N(1C)-C(2C)	1.382(15)	C(7A)-C(6A)-C(5A)	121.9(11)
N(1C)-C(4C)	1.474(12)	C(8A)-C(7A)-C(6A)	118.9(11)
N(2C)-C(3C)	1.338(15)	C(7A)-C(8A)-C(9A)	122.6(11)
N(2C)-C(1C)	1.365(12)	C(8A)-C(9A)-C(4A)	117.1(10)
N(2C)-C(16C)	1.440(13)	C(8A)-C(9A)-C(13A)	121.1(10)
C(2C)-C(3C)	1.333(16)	C(4A)-C(9A)-C(13A)	121.7(9)
C(4C)-C(5C)	1.363(15)	C(5A)-C(10A)-C(12A)	112.8(10)
C(4C)-C(9C)	1.422(15)	C(5A)-C(10A)-C(11A)	112.3(11)
C(5C)-C(6C)	1.405(16)	C(12A)-C(10A)-C(11A)	107.2(11)
C(5C)-C(10C)	1.533(16)	C(14A)-C(13A)-C(9A)	111.8(9)
C(6C)-C(7C)	1.354(17)	C(14A)-C(13A)-C(15A)	111.7(10)
C(7C)-C(8C)	1.366(16)	C(9A)-C(13A)-C(15A)	110.4(10)
C(8C)-C(9C)	1.383(15)	C(21A)-C(16A)-C(17A)	123.3(9)
C(9C)-C(13C)	1.518(15)	C(21A)-C(16A)-N(2A)	118.3(9)
C(10C)-C(12C)	1.485(17)	C(17A)-C(16A)-N(2A)	118.2(9)
C(10C)-C(11C)	1.537(19)	C(16A)-C(17A)-C(18A)	116.4(9)
C(13C)-C(14C)	1.533(16)	C(16A)-C(17A)-C(22A)	122.1(9)
C(13C)-C(15C)	1.549(17)	C(18A)-C(17A)-C(22A)	121.4(10)
C(16C)-C(17C)	1.395(15)	C(19A)-C(18A)-C(17A)	120.8(10)
C(16C)-C(21C)	1.425(15)	C(18A)-C(19A)-C(20A)	121.8(11)
C(17C)-C(18C)	1.390(16)	C(19A)-C(20A)-C(21A)	121.0(11)
C(17C)-C(22C)	1.540(15)	C(20A)-C(21A)-C(16A)	116.6(10)
C(18C)-C(19C)	1.378(17)	C(20A)-C(21A)-C(25A)	120.9(10)
C(19C)-C(20C)	1.359(16)	C(16A)-C(21A)-C(25A)	122.2(9)
C(20C)-C(21C)	1.411(16)	C(17A)-C(22A)-C(23A)	110.8(9)
C(21C)-C(25C)	1.489(16)	C(17A)-C(22A)-C(24A)	111.1(9)
C(22C)-C(24C)	1.527(17)	C(23A)-C(22A)-C(24A)	109.3(9)
C(22C)-C(23C)	1.559(19)	C(27A)-C(25A)-C(21A)	113.6(10)
C(25C)-C(26C)	1.542(18)	C(27A)-C(25A)-C(26A)	108.3(10)
C(25C)-C(27C)	1.591(18)	C(21A)-C(25A)-C(26A)	109.1(9)
		C(28B)-Au(2)-C(1B)	179.7(5)
C(1A)-Au(1)-C(28A)	177.9(4)	C(28B)-Au(2)-I(1B)	85.9(3)
C(1A)-Au(1)-I(2A)	96.2(3)	C(1B)-Au(2)-I(1B)	94.3(3)
C(28A)-Au(1)-I(2A)	83.2(3)	C(28B)-Au(2)-I(2B)	85.3(3)
C(1A)-Au(1)-I(1A)	90.3(3)	C(1B)-Au(2)-I(2B)	94.5(3)
C(28A)-Au(1)-I(1A)	90.4(3)	I(1B)-Au(2)-I(2B)	171.20(4)
I(2A)-Au(1)-I(1A)	173.30(3)	C(1B)-N(1B)-C(2B)	109.8(9)
C(1A)-N(1A)-C(2A)	111.4(8)	C(1B)-N(1B)-C(4B)	129.4(9)
C(1A)-N(1A)-C(4A)	127.8(9)	C(2B)-N(1B)-C(4B)	120.8(9)
C(2A)-N(1A)-C(4A)	120.7(8)	C(3B)-N(2B)-C(1B)	110.0(9)
C(1A)-N(2A)-C(3A)	111.1(9)	C(3B)-N(2B)-C(16B)	120.2(9)
C(1A)-N(2A)-C(16A)	127.7(9)	C(1B)-N(2B)-C(16B)	129.8(9)
C(3A)-N(2A)-C(16A)	121.1(9)	N(1B)-C(1B)-N(2B)	105.4(9)
N(1A)-C(1A)-N(2A)	104.3(9)	N(1B)-C(1B)-Au(2)	126.7(7)
N(1A)-C(1A)-Au(1)	129.0(8)	N(2B)-C(1B)-Au(2)	127.8(8)
N(2A)-C(1A)-Au(1)	126.5(7)	C(3B)-C(2B)-N(1B)	106.6(11)
C(3A)-C(2A)-N(1A)	107.1(9)	C(2B)-C(3B)-N(2B)	108.2(11)
C(2A)-C(3A)-N(2A)	106.1(10)	C(5B)-C(4B)-C(9B)	123.9(10)
C(9A)-C(4A)-C(5A)	123.0(10)	C(5B)-C(4B)-N(1B)	119.5(9)
C(9A)-C(4A)-N(1A)	117.8(9)	C(9B)-C(4B)-N(1B)	116.4(9)
C(5A)-C(4A)-N(1A)	118.2(9)	C(4B)-C(5B)-C(6B)	117.2(10)
C(4A)-C(5A)-C(6A)	116.4(10)	C(4B)-C(5B)-C(10B)	122.3(10)
C(4A)-C(5A)-C(10A)	123.3(10)	C(6B)-C(5B)-C(10B)	120.4(10)
C(6A)-C(5A)-C(10A)	120.3(10)	C(7B)-C(6B)-C(5B)	119.9(10)

C(6B)-C(7B)-C(8B)	122.4(10)	C(12C)-C(10C)-C(11C)	109.2(13)
C(7B)-C(8B)-C(9B)	120.8(11)	C(5C)-C(10C)-C(11C)	109.7(11)
C(8B)-C(9B)-C(4B)	115.7(9)	C(9C)-C(13C)-C(14C)	111.7(10)
C(8B)-C(9B)-C(13B)	121.1(10)	C(9C)-C(13C)-C(15C)	111.1(10)
C(4B)-C(9B)-C(13B)	123.2(9)	C(14C)-C(13C)-C(15C)	108.6(10)
C(12B)-C(10B)-C(5B)	112.2(10)	C(17C)-C(16C)-C(21C)	122.1(10)
C(12B)-C(10B)-C(11B)	109.2(12)	C(17C)-C(16C)-N(2C)	118.3(9)
C(5B)-C(10B)-C(11B)	109.7(11)	C(21C)-C(16C)-N(2C)	119.1(9)
C(9B)-C(13B)-C(14B)	111.7(10)	C(18C)-C(17C)-C(16C)	117.7(10)
C(9B)-C(13B)-C(15B)	111.1(10)	C(18C)-C(17C)-C(22C)	120.9(10)
C(14B)-C(13B)-C(15B)	108.6(10)	C(16C)-C(17C)-C(22C)	121.1(10)
C(17B)-C(16B)-C(21B)	122.1(10)	C(19C)-C(18C)-C(17C)	122.0(11)
C(17B)-C(16B)-N(2B)	118.3(9)	C(20C)-C(19C)-C(18C)	119.2(11)
C(21B)-C(16B)-N(2B)	119.1(9)	C(19C)-C(20C)-C(21C)	123.0(11)
C(18B)-C(17B)-C(16B)	117.8(10)	C(20C)-C(21C)-C(16C)	115.7(10)
C(18B)-C(17B)-C(22B)	120.9(10)	C(20C)-C(21C)-C(25C)	122.4(10)
C(16B)-C(17B)-C(22B)	121.1(10)	C(16C)-C(21C)-C(25C)	121.9(10)
C(19B)-C(18B)-C(17B)	122.1(11)	C(24C)-C(22C)-C(17C)	112.0(11)
C(20B)-C(19B)-C(18B)	119.2(11)	C(24C)-C(22C)-C(23C)	108.7(11)
C(19B)-C(20B)-C(21B)	123.0(11)	C(17C)-C(22C)-C(23C)	111.0(10)
C(20B)-C(21B)-C(16B)	115.7(10)	C(21C)-C(25C)-C(26C)	108.5(10)
C(20B)-C(21B)-C(25B)	122.4(10)	C(21C)-C(25C)-C(27C)	111.6(10)
C(16B)-C(21B)-C(25B)	121.9(10)	C(26C)-C(25C)-C(27C)	109.4(10)
C(24B)-C(22B)-C(17B)	112.0(10)		
C(24B)-C(22B)-C(23B)	108.7(11)		
C(17B)-C(22B)-C(23B)	111.0(10)		
C(21B)-C(25B)-C(26B)	108.5(10)		
C(21B)-C(25B)-C(27B)	111.6(10)		
C(26B)-C(25B)-C(27B)	109.4(10)		
C(28C)-Au(3)-C(1C)	176.3(17)		
C(1C)-N(1C)-C(2C)	109.8(9)		
C(1C)-N(1C)-C(4C)	129.3(9)		
C(2C)-N(1C)-C(4C)	120.7(9)		
C(3C)-N(2C)-C(1C)	109.9(9)		
C(3C)-N(2C)-C(16C)	120.1(9)		
C(1C)-N(2C)-C(16C)	129.7(9)		
N(1C)-C(1C)-N(2C)	105.5(9)		
N(1C)-C(1C)-Au(3)	126.7(7)		
N(2C)-C(1C)-Au(3)	127.8(8)		
C(3C)-C(2C)-N(1C)	106.6(11)		
C(2C)-C(3C)-N(2C)	108.2(11)		
C(5C)-C(4C)-C(9C)	123.9(10)		
C(5C)-C(4C)-N(1C)	119.4(9)		
C(9C)-C(4C)-N(1C)	116.3(9)		
C(4C)-C(5C)-C(6C)	117.2(10)		
C(4C)-C(5C)-C(10C)	122.3(10)		
C(6C)-C(5C)-C(10C)	120.4(10)		
C(7C)-C(6C)-C(5C)	119.8(10)		
C(6C)-C(7C)-C(8C)	122.3(10)		
C(7C)-C(8C)-C(9C)	120.8(11)		
C(8C)-C(9C)-C(4C)	115.7(10)		
C(8C)-C(9C)-C(13C)	121.0(10)		
C(4C)-C(9C)-C(13C)	123.1(10)		
C(12C)-C(10C)-C(5C)	112.2(11)		

---

Symmetry transformations used to generate equivalent atoms:

#1 -x+2,-y+1,-z+2

**Table 5. Anisotropic displacement parameters ( $\text{\AA}^2 \times 10^4$ ) for (Idipp)AuI<sub>2</sub>Me (CCDC 775776). The anisotropic displacement factor exponent takes the form:  $-2\pi^2 [h^2 a^{*2} U^{11} + \dots + 2 h k a^* b^* U^{12}]$**

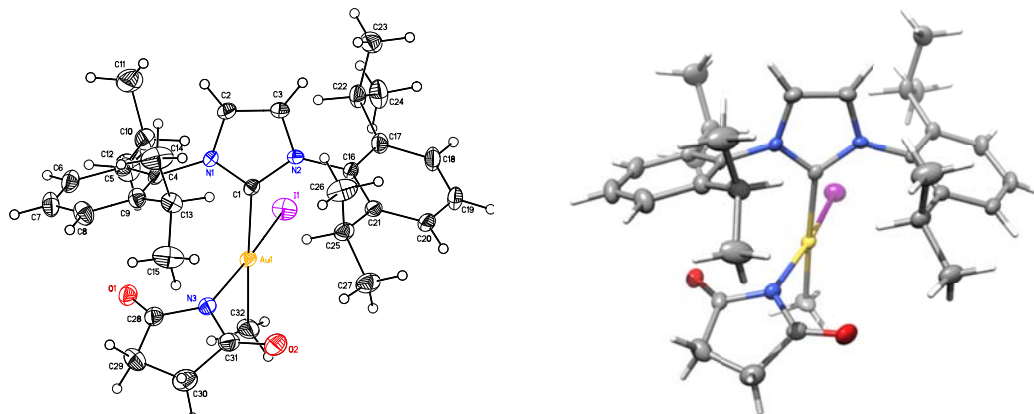
	U <sup>11</sup>	U <sup>22</sup>	U <sup>33</sup>	U <sup>23</sup>	U <sup>13</sup>	U <sup>12</sup>
I(66)	448(5)	334(5)	420(5)	5(4)	135(4)	-134(4)
Au(1)	140(2)	140(2)	318(3)	-10(2)	87(2)	-1(2)
I(1A)	397(5)	254(5)	386(5)	-86(4)	-51(4)	57(4)
I(2A)	522(6)	360(6)	405(6)	109(4)	142(4)	-78(4)
N(1A)	80(40)	130(50)	150(50)	20(40)	-20(30)	20(30)
N(2A)	90(40)	180(50)	100(40)	10(40)	0(30)	10(40)
C(1A)	160(50)	260(70)	100(60)	-10(50)	50(40)	50(50)
C(2A)	110(50)	120(60)	310(70)	0(50)	40(50)	-70(40)
C(3A)	210(60)	160(60)	230(60)	10(50)	60(50)	-50(50)
C(4A)	110(50)	120(60)	220(60)	10(50)	10(40)	20(40)
C(5A)	160(60)	170(60)	360(70)	-100(50)	80(50)	-30(50)
C(6A)	280(70)	200(70)	450(80)	-120(60)	140(60)	-10(50)
C(7A)	160(60)	250(70)	550(90)	-110(60)	20(60)	30(50)
C(8A)	260(60)	170(60)	350(70)	-40(60)	-40(50)	30(50)
C(9A)	190(60)	130(60)	300(70)	-10(50)	0(50)	30(50)
C(10A)	360(70)	210(70)	250(70)	-60(50)	70(50)	60(50)
C(11A)	690(110)	530(110)	440(90)	220(80)	300(80)	-40(80)
C(12A)	600(90)	300(80)	290(70)	0(60)	80(70)	70(70)
C(13A)	280(60)	270(70)	160(60)	30(50)	30(50)	90(50)
C(14A)	340(70)	220(70)	180(60)	-40(50)	50(50)	40(50)
C(15A)	420(80)	350(80)	230(70)	90(60)	-90(60)	-40(60)
C(16A)	70(50)	150(60)	240(60)	50(50)	50(40)	20(40)
C(17A)	140(50)	120(60)	250(60)	-30(50)	80(50)	-30(40)
C(18A)	150(60)	100(60)	370(70)	10(50)	40(50)	20(40)
C(19A)	170(60)	260(70)	460(80)	40(60)	130(60)	70(50)
C(20A)	230(60)	340(80)	360(70)	70(60)	230(60)	90(50)
C(21A)	190(60)	150(60)	210(60)	20(50)	70(50)	0(50)
C(22A)	220(60)	200(60)	140(60)	-10(50)	10(50)	10(50)
C(23A)	230(60)	370(80)	300(70)	40(60)	130(50)	20(50)
C(24A)	220(60)	460(90)	300(70)	-10(60)	-70(50)	110(60)
C(25A)	210(60)	340(70)	160(60)	90(50)	50(50)	100(50)
C(26A)	480(80)	380(80)	160(70)	20(60)	70(60)	30(60)
C(27A)	460(80)	490(100)	320(80)	110(70)	160(60)	60(70)
C(28A)	190(30)	190(30)	200(30)	-14(10)	58(11)	-3(10)
Au(2)	150(2)	176(3)	258(3)	10(3)	68(2)	17(2)
I(1B)	515(6)	311(6)	324(6)	-81(4)	136(5)	-70(5)
I(2B)	277(5)	284(5)	329(5)	52(4)	123(4)	7(4)
N(1B)	30(50)	190(60)	180(50)	-20(40)	30(40)	30(40)
N(2B)	120(50)	160(60)	150(50)	0(40)	120(40)	20(40)
C(1B)	40(50)	140(60)	140(60)	-40(50)	-10(40)	-10(50)
C(2B)	170(60)	270(80)	260(80)	-50(60)	60(50)	-50(60)
C(3B)	130(60)	200(80)	310(80)	-60(60)	130(50)	-30(50)

C(4B)	70(50)	120(60)	210(70)	0(50)	20(50)	10(50)
C(5B)	200(70)	80(60)	290(80)	10(50)	50(60)	40(50)
C(6B)	170(70)	290(90)	290(80)	60(60)	-60(60)	20(60)
C(7B)	50(60)	200(90)	470(90)	30(70)	110(60)	40(50)
C(8B)	210(70)	130(80)	290(80)	0(60)	150(60)	-40(50)
C(9B)	140(30)	140(30)	140(30)	3(10)	33(11)	-1(10)
C(10B)	190(70)	390(90)	250(80)	-10(60)	80(60)	-50(60)
C(11B)	900(140)	410(110)	410(100)	-10(80)	300(100)	-240(100)
C(12B)	380(90)	570(120)	310(90)	-160(80)	30(70)	10(80)
C(13B)	250(70)	130(70)	190(70)	30(50)	60(60)	30(50)
C(14B)	200(60)	220(70)	160(70)	-10(50)	20(50)	-30(50)
C(15B)	270(70)	270(80)	300(80)	-30(60)	130(60)	50(60)
C(16B)	100(60)	130(70)	210(70)	-10(50)	90(50)	-30(50)
C(17B)	230(70)	170(70)	230(70)	40(60)	30(60)	-60(60)
C(18B)	230(80)	360(90)	210(80)	-80(60)	160(60)	40(70)
C(19B)	80(70)	290(80)	310(80)	-40(60)	50(60)	0(60)
C(20B)	110(60)	310(90)	350(80)	180(70)	-20(60)	20(60)
C(21B)	210(70)	130(70)	240(70)	20(50)	90(50)	-40(50)
C(22B)	170(60)	370(90)	230(70)	20(60)	100(60)	40(60)
C(23B)	310(100)	520(110)	440(100)	100(80)	300(70)	60(80)
C(24B)	390(100)	520(130)	370(90)	0(80)	0(80)	110(90)
C(25B)	160(60)	300(80)	240(70)	60(60)	0(50)	40(60)
C(26B)	590(120)	290(100)	270(80)	40(70)	230(80)	-30(80)
C(27B)	450(100)	340(100)	240(80)	0(70)	90(70)	-140(80)
C(28B)	200(30)	200(30)	220(30)	6(10)	50(12)	-3(10)

---



### A.5 (Idipp)AuMeI(C<sub>4</sub>H<sub>4</sub>NO<sub>2</sub>)



(Idipp)AuMeI(C<sub>4</sub>H<sub>4</sub>NO<sub>2</sub>)

**Note:** The crystallographic data have been deposited in the Cambridge Database (CCDC) and has been placed on hold pending further instructions from me. The deposition number is 775777. Ideally the CCDC would like the publication to contain a footnote of the type: "Crystallographic data have been deposited at the CCDC, 12 Union Road, Cambridge CB2 1EZ, UK and copies can be obtained on request, free of charge, by quoting the publication citation and the deposition number 775777."

**Table 1. Crystal data and structure refinement for (Idipp)AuMeI(C<sub>4</sub>H<sub>4</sub>NO<sub>2</sub>) (CCDC 775777).**

Empirical formula	C <sub>32</sub> H <sub>43</sub> N <sub>3</sub> O <sub>2</sub> IAu • 2(C <sub>2</sub> H <sub>3</sub> N)
Formula weight	907.67
Crystallization Solvent	Acetonitrile
Crystal Habit	Fragment
Crystal size	0.20 x 0.17 x 0.07 mm <sup>3</sup>
Crystal color	Pale yellow



#### Data Collection

Type of diffractometer	Bruker KAPPA APEX II
Wavelength	0.71073 Å MoKα
Data Collection Temperature	100(2) K
θ range for 9129 reflections used in lattice determination	3.16 to 34.84°
Unit cell dimensions	a = 13.7649(7) Å b = 20.2960(9) Å
	α = 90° β = 104.003(3)°

	$c = 14.0178(7) \text{ \AA}$	$\gamma = 90^\circ$
Volume	$3799.8(3) \text{ \AA}^3$	
Z	4	
Crystal system	Monoclinic	
Space group	$P 2_1/n$	
Density (calculated)	$1.587 \text{ Mg/m}^3$	
F(000)	1792	
Data collection program	Bruker APEX2 v2009.7-0	
$\theta$ range for data collection	$1.83$ to $37.91^\circ$	
Completeness to $\theta = 37.91^\circ$	95.5 %	
Index ranges	$-23 \leq h \leq 23$ , $-34 \leq k \leq 35$ , $-23 \leq l \leq 23$	
Data collection scan type	$\omega$ scans; 15 settings	
Data reduction program	Bruker SAINT-Plus v7.66A	
Reflections collected	160542	
Independent reflections	19627 [ $R_{\text{int}} = 0.0618$ ]	
Absorption coefficient	$4.720 \text{ mm}^{-1}$	
Absorption correction	Semi-empirical from equivalents	
Max. and min. transmission	0.7474 and 0.6007	

## Structure Solution and Refinement

Structure solution program	SHELXS-97 (Sheldrick, 2008)
Primary solution method	Patterson method
Secondary solution method	Difference Fourier map
Hydrogen placement	Geometric positions
Structure refinement program	SHELXL-97 (Sheldrick, 2008)
Refinement method	Full matrix least-squares on $F^2$
Data / restraints / parameters	19627 / 0 / 417
Treatment of hydrogen atoms	Riding
Goodness-of-fit on $F^2$	2.030
Final R indices [ $I > 2\sigma(I)$ , 15181 reflections]	$R1 = 0.0417$ , $wR2 = 0.0813$
R indices (all data)	$R1 = 0.0611$ , $wR2 = 0.0840$
Type of weighting scheme used	Sigma
Weighting scheme used	$w = 1/\sigma^2(F_o^2)$
Max shift/error	0.004
Average shift/error	0.000
Largest diff. peak and hole	7.927 and $-2.259 \text{ e.\AA}^{-3}$

## Special Refinement Details

Crystals were mounted on a glass fiber using Paratone oil then placed on the diffractometer under a nitrogen stream at 100K.

Refinement of  $F^2$  against ALL reflections. The weighted R-factor ( $wR$ ) and goodness of fit ( $S$ ) are based on  $F^2$ , conventional R-factors ( $R$ ) are based on  $F$ , with  $F$  set to zero for negative  $F^2$ . The threshold expression of  $F^2 > 2\sigma(F^2)$  is used only for calculating R-factors(gt) etc. and is not relevant to the choice of reflections for refinement. R-factors based on  $F^2$  are statistically about twice as large as those based on  $F$ , and R-factors based on ALL data will be even larger.

All esds (except the esd in the dihedral angle between two l.s. planes) are estimated using the full covariance matrix. The cell esds are taken into account individually in the estimation of esds in distances, angles and torsion angles; correlations between esds in cell parameters are only used when they are defined by crystal symmetry. An approximate (isotropic) treatment of cell esds is used for estimating esds involving l.s. planes.

**Table 2. Atomic coordinates ( $\times 10^4$ ) and equivalent isotropic displacement parameters ( $\text{\AA}^2 \times 10^3$ ) for (Idipp)AuMeI(C<sub>4</sub>H<sub>4</sub>NO<sub>2</sub>) (CCDC 775777).  $U_{eq}$  is defined as the trace of the orthogonalized  $U_{ij}$  tensor.**

	x	y	z	$U_{eq}$
Au(1)	2356(1)	5996(1)	6926(1)	18(1)
I(1)	2253(1)	5060(1)	8120(1)	31(1)
O(1)	4012(2)	6040(1)	5707(2)	26(1)
O(2)	1066(2)	7118(1)	5367(2)	40(1)
N(1)	3832(2)	6886(1)	8418(2)	17(1)
N(2)	2448(2)	6829(1)	8860(2)	17(1)
N(3)	2570(2)	6585(1)	5805(2)	21(1)
C(1)	2911(2)	6636(1)	8138(2)	16(1)
C(2)	3982(2)	7220(1)	9301(2)	22(1)
C(3)	3113(2)	7189(1)	9572(2)	22(1)
C(4)	4587(2)	6871(1)	7855(2)	19(1)
C(5)	5227(2)	6332(1)	7940(2)	22(1)
C(6)	5976(2)	6360(1)	7424(3)	29(1)
C(7)	6063(2)	6890(1)	6843(3)	31(1)
C(8)	5411(3)	7420(1)	6768(3)	30(1)
C(9)	4666(2)	7429(1)	7292(2)	22(1)
C(10)	5158(2)	5752(1)	8616(2)	27(1)
C(11)	5941(3)	5819(2)	9582(3)	43(1)
C(12)	5225(3)	5090(1)	8116(3)	39(1)
C(13)	4017(2)	8038(1)	7286(2)	26(1)
C(14)	4637(3)	8571(2)	7940(3)	44(1)

C(15)	3568(3)	8301(1)	6260(3)	39(1)
C(16)	1418(2)	6720(1)	8891(2)	19(1)
C(17)	1210(2)	6269(1)	9581(2)	23(1)
C(18)	202(2)	6170(2)	9563(3)	30(1)
C(19)	-546(2)	6505(2)	8916(3)	32(1)
C(20)	-319(2)	6972(1)	8287(2)	27(1)
C(21)	679(2)	7099(1)	8266(2)	22(1)
C(22)	2018(2)	5927(1)	10363(3)	27(1)
C(23)	2262(3)	6317(2)	11337(3)	34(1)
C(24)	1733(3)	5228(2)	10600(3)	37(1)
C(25)	927(2)	7655(1)	7637(2)	24(1)
C(26)	1300(3)	8254(2)	8284(3)	41(1)
C(27)	56(3)	7859(2)	6802(3)	32(1)
C(28)	3370(2)	6447(1)	5391(2)	23(1)
C(29)	3272(3)	6856(1)	4472(3)	31(1)
C(30)	2240(3)	7176(2)	4295(3)	34(1)
C(31)	1868(2)	6972(1)	5213(2)	27(1)
C(32)	1759(3)	5356(2)	5768(3)	34(1)
<hr/>				
N(41)	2052(3)	10226(1)	1549(2)	43(1)
C(42)	1618(3)	9922(1)	917(3)	33(1)
C(43)	1086(3)	9519(1)	102(3)	34(1)
<hr/>				
N(51)	1810(2)	3558(2)	4071(3)	44(1)
C(52)	1283(3)	3978(2)	3731(3)	40(1)
C(53)	634(3)	4518(2)	3246(4)	56(1)

**Table 3.** Selected bond lengths [ $\text{\AA}$ ] and angles [ $^\circ$ ] for (Idipp)AuMeI(C<sub>4</sub>H<sub>4</sub>NO<sub>2</sub>) (CCDC 775777).

Au(1)-N(3)	2.051(2)	N(3)-Au(1)-C(32)	82.51(11)
Au(1)-C(32)	2.086(3)	N(3)-Au(1)-C(1)	99.53(9)
Au(1)-C(1)	2.128(3)	C(32)-Au(1)-C(1)	177.37(10)
Au(1)-I(1)	2.5597(2)	N(3)-Au(1)-I(1)	167.03(6)
		C(32)-Au(1)-I(1)	88.41(10)
		C(1)-Au(1)-I(1)	89.84(6)

**Table 4.** Bond lengths [ $\text{\AA}$ ] and angles [ $^\circ$ ] for (Idipp)AuMeI(C<sub>4</sub>H<sub>4</sub>NO<sub>2</sub>) (CCDC 775777).

Au(1)-N(3)	2.051(2)	N(2)-C(3)	1.387(4)
Au(1)-C(32)	2.086(3)	N(2)-C(16)	1.446(3)
Au(1)-C(1)	2.128(3)	N(3)-C(31)	1.362(4)
Au(1)-I(1)	2.5597(2)	N(3)-C(28)	1.391(3)
O(1)-C(28)	1.213(4)	C(2)-C(3)	1.341(4)
O(2)-C(31)	1.213(4)	C(4)-C(5)	1.392(4)
N(1)-C(1)	1.334(3)	C(4)-C(9)	1.400(4)
N(1)-C(2)	1.383(3)	C(5)-C(6)	1.396(4)
N(1)-C(4)	1.449(3)	C(5)-C(10)	1.527(4)
N(2)-C(1)	1.376(3)	C(6)-C(7)	1.372(4)

C(7)-C(8)	1.389(4)	C(6)-C(7)-C(8)	120.3(3)
C(8)-C(9)	1.398(4)	C(7)-C(8)-C(9)	120.9(3)
C(9)-C(13)	1.525(4)	C(8)-C(9)-C(4)	116.9(2)
C(10)-C(11)	1.518(5)	C(8)-C(9)-C(13)	120.7(2)
C(10)-C(12)	1.530(4)	C(4)-C(9)-C(13)	122.3(2)
C(13)-C(15)	1.519(5)	C(11)-C(10)-C(5)	110.3(3)
C(13)-C(14)	1.536(5)	C(11)-C(10)-C(12)	112.2(3)
C(16)-C(21)	1.401(4)	C(5)-C(10)-C(12)	111.9(3)
C(16)-C(17)	1.411(4)	C(15)-C(13)-C(9)	113.2(2)
C(17)-C(18)	1.396(4)	C(15)-C(13)-C(14)	110.9(2)
C(17)-C(22)	1.527(4)	C(9)-C(13)-C(14)	109.2(3)
C(18)-C(19)	1.376(5)	C(21)-C(16)-C(17)	123.2(2)
C(19)-C(20)	1.381(4)	C(21)-C(16)-N(2)	117.8(2)
C(20)-C(21)	1.404(4)	C(17)-C(16)-N(2)	119.0(2)
C(21)-C(25)	1.522(4)	C(18)-C(17)-C(16)	116.6(3)
C(22)-C(24)	1.530(4)	C(18)-C(17)-C(22)	119.7(3)
C(22)-C(23)	1.544(5)	C(16)-C(17)-C(22)	123.6(2)
C(25)-C(27)	1.516(4)	C(19)-C(18)-C(17)	121.5(3)
C(25)-C(26)	1.529(4)	C(18)-C(19)-C(20)	120.8(3)
C(28)-C(29)	1.510(4)	C(19)-C(20)-C(21)	120.8(3)
C(29)-C(30)	1.526(5)	C(16)-C(21)-C(20)	116.9(3)
C(30)-C(31)	1.551(4)	C(16)-C(21)-C(25)	122.6(2)
N(41)-C(42)	1.125(5)	C(20)-C(21)-C(25)	120.4(3)
C(42)-C(43)	1.450(5)	C(17)-C(22)-C(24)	113.4(3)
N(51)-C(52)	1.144(5)	C(17)-C(22)-C(23)	111.5(2)
C(52)-C(53)	1.473(6)	C(24)-C(22)-C(23)	107.2(3)
		C(27)-C(25)-C(21)	113.8(3)
N(3)-Au(1)-C(32)	82.51(11)	C(27)-C(25)-C(26)	109.3(2)
N(3)-Au(1)-C(1)	99.53(9)	C(21)-C(25)-C(26)	109.6(3)
C(32)-Au(1)-C(1)	177.37(10)	O(1)-C(28)-N(3)	124.3(3)
N(3)-Au(1)-I(1)	167.03(6)	O(1)-C(28)-C(29)	126.4(3)
C(32)-Au(1)-I(1)	88.41(10)	N(3)-C(28)-C(29)	109.2(3)
C(1)-Au(1)-I(1)	89.84(6)	C(28)-C(29)-C(30)	105.1(2)
C(1)-N(1)-C(2)	112.0(2)	C(29)-C(30)-C(31)	103.5(3)
C(1)-N(1)-C(4)	126.0(2)	O(2)-C(31)-N(3)	125.1(3)
C(2)-N(1)-C(4)	121.8(2)	O(2)-C(31)-C(30)	125.5(3)
C(1)-N(2)-C(3)	109.7(2)	N(3)-C(31)-C(30)	109.4(2)
C(1)-N(2)-C(16)	127.6(2)	N(41)-C(42)-C(43)	178.3(4)
C(3)-N(2)-C(16)	122.6(2)	N(51)-C(52)-C(53)	176.6(4)
C(31)-N(3)-C(28)	112.2(2)		
C(31)-N(3)-Au(1)	126.23(19)		
C(28)-N(3)-Au(1)	118.55(18)		
N(1)-C(1)-N(2)	104.6(2)		
N(1)-C(1)-Au(1)	126.79(17)		
N(2)-C(1)-Au(1)	128.34(18)		
C(3)-C(2)-N(1)	106.3(2)		
C(2)-C(3)-N(2)	107.4(2)		
C(5)-C(4)-C(9)	123.4(2)		
C(5)-C(4)-N(1)	119.5(2)		
C(9)-C(4)-N(1)	117.0(2)		
C(4)-C(5)-C(6)	117.1(2)		
C(4)-C(5)-C(10)	121.7(2)		
C(6)-C(5)-C(10)	121.2(2)		
C(7)-C(6)-C(5)	121.4(3)		

**Table 5.** Anisotropic displacement parameters ( $\text{\AA}^2 \times 10^4$ ) for (Idipp)AuMeI(C<sub>4</sub>H<sub>4</sub>NO<sub>2</sub>) (CCDC 775777). The anisotropic displacement factor exponent takes the form:  $-2\pi^2 [h^2 a^{*2} U^{11} + \dots + 2 h k a^* b^* U^{12}]$

	U <sup>11</sup>	U <sup>22</sup>	U <sup>33</sup>	U <sup>23</sup>	U <sup>13</sup>	U <sup>12</sup>
Au(1)	157(1)	183(1)	184(1)	-24(1)	25(1)	-25(1)
I(1)	402(1)	198(1)	306(1)	14(1)	65(1)	-60(1)
O(1)	207(11)	288(9)	299(12)	-52(8)	63(9)	19(8)
O(2)	276(13)	590(14)	313(13)	50(11)	11(11)	171(11)
N(1)	123(10)	194(8)	173(10)	-6(7)	21(8)	-12(7)
N(2)	167(10)	194(8)	131(10)	-13(7)	14(8)	-1(7)
N(3)	187(11)	239(9)	196(11)	24(8)	31(9)	24(8)
C(1)	149(11)	151(9)	180(12)	25(8)	23(10)	3(8)
C(2)	190(13)	244(11)	199(13)	-33(9)	4(11)	-29(9)
C(3)	216(14)	254(11)	169(12)	-50(9)	27(11)	-20(9)
C(4)	138(12)	208(10)	212(13)	-17(9)	32(10)	-21(8)
C(5)	181(13)	223(10)	243(14)	-33(10)	22(11)	20(9)
C(6)	195(14)	301(13)	369(18)	-87(12)	79(13)	15(11)
C(7)	255(16)	332(13)	397(19)	-101(13)	168(15)	-67(12)
C(8)	353(18)	262(12)	340(17)	-26(11)	169(15)	-88(11)
C(9)	218(14)	204(10)	254(14)	-24(9)	78(12)	-26(9)
C(10)	258(15)	246(11)	299(16)	42(11)	59(13)	79(11)
C(11)	400(20)	497(18)	360(20)	38(16)	12(17)	171(16)
C(12)	460(20)	241(13)	480(20)	28(13)	146(19)	68(13)
C(13)	321(16)	204(10)	242(14)	7(10)	74(12)	23(10)
C(14)	550(20)	270(14)	410(20)	-82(13)	-55(18)	99(14)
C(15)	600(30)	216(12)	312(18)	-8(12)	23(17)	75(13)
C(16)	136(12)	232(10)	196(13)	-37(9)	33(10)	14(9)
C(17)	194(14)	265(12)	254(15)	9(10)	80(12)	32(10)
C(18)	199(15)	373(14)	356(18)	21(13)	135(14)	-2(11)
C(19)	175(15)	465(17)	354(19)	-61(14)	116(14)	-10(12)
C(20)	169(13)	387(14)	233(14)	-59(12)	20(11)	62(11)
C(21)	178(13)	286(11)	182(13)	-57(10)	23(10)	45(10)
C(22)	213(14)	293(12)	316(16)	75(11)	115(13)	71(10)
C(23)	327(18)	427(16)	261(17)	67(13)	73(14)	118(13)
C(24)	317(19)	363(15)	480(20)	133(15)	208(17)	65(13)
C(25)	221(14)	256(11)	232(14)	19(10)	7(11)	54(10)
C(26)	470(20)	281(14)	390(20)	12(13)	-59(17)	-14(13)
C(27)	308(17)	327(13)	288(17)	16(12)	-21(14)	96(12)
C(28)	218(14)	233(11)	248(14)	-57(10)	50(12)	-37(10)
C(29)	398(19)	286(13)	282(16)	-8(11)	153(15)	-44(12)
C(30)	350(19)	323(14)	314(18)	72(12)	17(15)	2(12)
C(31)	271(16)	291(12)	227(14)	-22(11)	18(12)	48(11)
C(32)	351(19)	410(15)	258(16)	-153(13)	95(15)	-155(13)
N(41)	650(20)	370(14)	263(16)	-25(12)	111(16)	-50(14)
C(42)	410(20)	284(13)	336(18)	58(12)	173(16)	26(12)
C(43)	296(18)	286(13)	430(20)	-11(13)	86(16)	-8(12)
N(51)	371(18)	413(15)	500(20)	57(14)	26(16)	-94(13)

C(52)	254(17)	477(19)	440(20)	-165(16)	4(16)	-51(14)
C(53)	400(20)	600(20)	590(30)	-160(20)	-50(20)	191(19)

---

Type of diffractometer	Bruker KAPPA APEX II		
Wavelength	0.71073 Å MoKα		
Data Collection Temperature	100(2) K		
θ range for 9715 reflections used in lattice determination	2.28 to 36.42°		
Unit cell dimensions	a = 10.2676(5) Å	α= 90°	
	b = 17.2876(8) Å	β= 94.674(3)°	
	c = 17.9053(8) Å	γ = 90°	
Volume	3167.7(3) Å³		



Z	4
Crystal system	Monoclinic
Space group	$P 2_1/n$
Density (calculated)	1.876 Mg/m <sup>3</sup>
F(000)	1736
Data collection program	Bruker APEX2 v2009.7-0
$\theta$ range for data collection	2.21 to 37.67°
Completeness to $\theta = 37.67^\circ$	99.7 %
Index ranges	$-17 \leq h \leq 17, -29 \leq k \leq 29, -30 \leq l \leq 27$
Data collection scan type	$\omega$ scans; 11 settings
Data reduction program	Bruker SAINT-Plus v7.66A
Reflections collected	125726
Independent reflections	16845 [ $R_{\text{int}} = 0.0418$ ]
Absorption coefficient	7.282 mm <sup>-1</sup>
Absorption correction	Semi-empirical from equivalents
Max. and min. transmission	0.4395 and 0.2986

## Structure Solution and Refinement

Structure solution program	SHELXS-97 (Sheldrick, 2008)
Primary solution method	Direct methods
Secondary solution method	Difference Fourier map
Hydrogen placement	Geometric positions
Structure refinement program	SHELXL-97 (Sheldrick, 2008)
Refinement method	Full matrix least-squares on $F^2$
Data / restraints / parameters	16845 / 0 / 369
Treatment of hydrogen atoms	Riding
Goodness-of-fit on $F^2$	1.783
Final R indices [ $I > 2\sigma(I)$ , 13863 reflections]	$R1 = 0.0274, wR2 = 0.0411$
R indices (all data)	$R1 = 0.0403, wR2 = 0.0418$
Type of weighting scheme used	Sigma
Weighting scheme used	$w = 1/\sigma^2(F_o^2)$
Max shift/error	0.002
Average shift/error	0.000
Largest diff. peak and hole	2.802 and -1.839 e.Å <sup>-3</sup>

## Special Refinement Details

Crystals were mounted on a glass fiber using Paratone oil then placed on the diffractometer under a nitrogen stream at 100K.

Refinement of  $F^2$  against ALL reflections. The weighted R-factor ( $wR$ ) and goodness of fit ( $S$ ) are based on  $F^2$ , conventional R-factors ( $R$ ) are based on  $F$ , with  $F$  set to zero for negative  $F^2$ . The threshold expression of  $F^2 > 2\sigma(F^2)$  is used only for calculating R-factors(gt) etc. and is not relevant to the choice of reflections for refinement. R-factors based on  $F^2$  are statistically about twice as large as those based on  $F$ , and R-factors based on ALL data will be even larger.

All esds (except the esd in the dihedral angle between two l.s. planes) are estimated using the full covariance matrix. The cell esds are taken into account individually in the estimation of esds in distances, angles and torsion angles; correlations between esds in cell parameters are only used when they are defined by crystal symmetry. An approximate (isotropic) treatment of cell esds is used for estimating esds involving l.s. planes.

**Table 2. Atomic coordinates ( $\times 10^4$ ) and equivalent isotropic displacement parameters ( $\text{\AA}^2 \times 10^3$ ) for VJS85 (CCDC 8093339).  $U(\text{eq})$  is defined as the trace of the orthogonalized  $U^{ij}$  tensor.**

	x	y	z	$U_{\text{eq}}$
Au(1)	5340(1)	128(1)	2260(1)	14(1)
Br(1)	3524(1)	877(1)	2622(1)	24(1)
Br(2)	7080(1)	-661(1)	1844(1)	24(1)
S(1)	4172(1)	-1522(1)	2475(1)	18(1)
F(1)	1641(1)	-1629(1)	2154(1)	37(1)
F(2)	2360(1)	-2209(1)	3168(1)	44(1)
F(3)	2192(1)	-973(1)	3143(1)	36(1)
O(1)	4333(1)	-2180(1)	2011(1)	26(1)
O(2)	4072(1)	-787(1)	2032(1)	21(1)
O(3)	4986(1)	-1449(1)	3160(1)	24(1)
N(1)	6891(1)	1507(1)	1888(1)	12(1)
N(2)	6767(1)	1412(1)	3089(1)	14(1)
C(1)	6442(2)	1058(1)	2427(1)	13(1)
C(2)	7488(2)	2157(1)	2214(1)	16(1)
C(3)	7423(2)	2091(1)	2959(1)	17(1)
C(4)	7028(2)	1278(1)	1112(1)	13(1)
C(5)	8238(2)	961(1)	967(1)	14(1)
C(6)	8384(2)	749(1)	225(1)	19(1)
C(7)	7377(2)	854(1)	-329(1)	20(1)
C(8)	6202(2)	1166(1)	-162(1)	18(1)
C(9)	5995(2)	1396(1)	568(1)	14(1)

C(10)	9376(2)	880(1)	1558(1)	17(1)
C(11)	10300(2)	1575(1)	1531(1)	26(1)
C(12)	10183(2)	145(1)	1482(1)	25(1)
C(13)	4705(2)	1762(1)	721(1)	20(1)
C(14)	4510(3)	2525(1)	293(1)	36(1)
C(15)	3568(2)	1213(1)	514(1)	33(1)
C(16)	6618(2)	1096(1)	3834(1)	17(1)
C(17)	7465(2)	493(1)	4079(1)	21(1)
C(18)	7322(2)	206(1)	4798(1)	29(1)
C(19)	6425(2)	519(1)	5244(1)	31(1)
C(20)	5655(2)	1131(1)	4998(1)	28(1)
C(21)	5720(2)	1438(1)	4277(1)	21(1)
C(22)	8550(2)	199(1)	3624(1)	26(1)
C(23)	9784(2)	694(1)	3775(1)	39(1)
C(24)	8861(3)	-658(1)	3754(1)	45(1)
C(25)	4875(2)	2125(1)	4029(1)	24(1)
C(26)	5505(2)	2882(1)	4334(1)	35(1)
C(27)	3485(2)	2059(1)	4268(1)	33(1)
C(28)	2504(2)	-1585(1)	2751(1)	26(1)

**Table 3. Selected bond lengths [Å] and angles [°] for VJS85 (CCDC 8093339).**

Au(1)-C(1)	1.9753(16)	C(1)-Au(1)-O(2)	175.14(6)
Au(1)-O(2)	2.0679(12)	C(1)-Au(1)-Br(1)	88.16(5)
Au(1)-Br(1)	2.4023(2)	O(2)-Au(1)-Br(1)	88.61(4)
Au(1)-Br(2)	2.4135(2)	C(1)-Au(1)-Br(2)	94.45(5)
		O(2)-Au(1)-Br(2)	88.66(4)
		Br(1)-Au(1)-Br(2)	176.752(7)

**Table 4. Bond lengths [Å] and angles [°] for VJS85 (CCDC 8093339).**

Au(1)-C(1)	1.9753(16)
Au(1)-O(2)	2.0679(12)
Au(1)-Br(1)	2.4023(2)
Au(1)-Br(2)	2.4135(2)
S(1)-O(1)	1.4261(12)
S(1)-O(3)	1.4329(12)
S(1)-O(2)	1.4974(12)
S(1)-C(28)	1.823(2)
F(1)-C(28)	1.334(2)
F(2)-C(28)	1.329(2)
F(3)-C(28)	1.323(2)
N(1)-C(1)	1.3479(19)
N(1)-C(2)	1.385(2)
N(1)-C(4)	1.4633(18)
N(2)-C(1)	1.3508(18)
N(2)-C(3)	1.383(2)
N(2)-C(16)	1.4612(19)
C(2)-C(3)	1.346(2)
C(4)-C(9)	1.396(2)
C(4)-C(5)	1.402(2)
C(5)-C(6)	1.398(2)
C(5)-C(10)	1.518(2)
C(6)-C(7)	1.385(2)
C(7)-C(8)	1.376(2)
C(8)-C(9)	1.399(2)
C(9)-C(13)	1.513(2)
C(10)-C(12)	1.529(2)
C(10)-C(11)	1.534(2)
C(13)-C(15)	1.528(3)
C(13)-C(14)	1.529(2)
C(16)-C(21)	1.396(2)
C(16)-C(17)	1.404(2)
C(17)-C(18)	1.398(2)
C(17)-C(22)	1.520(3)
C(18)-C(19)	1.378(3)
C(19)-C(20)	1.372(3)
C(20)-C(21)	1.401(2)
C(21)-C(25)	1.516(3)
C(22)-C(24)	1.529(3)
C(22)-C(23)	1.534(3)
C(25)-C(27)	1.528(3)
C(25)-C(26)	1.540(3)
C(1)-Au(1)-O(2)	175.14(6)
C(1)-Au(1)-Br(1)	88.16(5)

O(2)-Au(1)-Br(1)	88.61(4)
C(1)-Au(1)-Br(2)	94.45(5)
O(2)-Au(1)-Br(2)	88.66(4)
Br(1)-Au(1)-Br(2)	176.752(7)
O(1)-S(1)-O(3)	118.85(8)
O(1)-S(1)-O(2)	111.98(7)
O(3)-S(1)-O(2)	112.82(7)
O(1)-S(1)-C(28)	105.47(9)
O(3)-S(1)-C(28)	105.62(8)
O(2)-S(1)-C(28)	99.68(8)
S(1)-O(2)-Au(1)	122.04(7)
C(1)-N(1)-C(2)	109.35(12)
C(1)-N(1)-C(4)	126.07(12)
C(2)-N(1)-C(4)	123.05(13)
C(1)-N(2)-C(3)	109.00(12)
C(1)-N(2)-C(16)	126.52(13)
C(3)-N(2)-C(16)	124.02(12)
N(1)-C(1)-N(2)	107.02(13)
N(1)-C(1)-Au(1)	125.82(10)
N(2)-C(1)-Au(1)	126.79(11)
C(3)-C(2)-N(1)	106.98(14)
C(2)-C(3)-N(2)	107.63(13)
C(9)-C(4)-C(5)	124.21(13)
C(9)-C(4)-N(1)	119.83(14)
C(5)-C(4)-N(1)	115.94(13)
C(6)-C(5)-C(4)	116.39(14)
C(6)-C(5)-C(10)	120.13(15)
C(4)-C(5)-C(10)	123.41(13)
C(7)-C(6)-C(5)	120.93(16)
C(8)-C(7)-C(6)	120.83(15)
C(7)-C(8)-C(9)	121.13(15)
C(4)-C(9)-C(8)	116.51(15)
C(4)-C(9)-C(13)	124.13(13)
C(8)-C(9)-C(13)	119.36(14)
C(5)-C(10)-C(12)	114.02(13)
C(5)-C(10)-C(11)	110.37(13)
C(12)-C(10)-C(11)	107.88(15)
C(9)-C(13)-C(15)	111.03(15)
C(9)-C(13)-C(14)	110.53(16)
C(15)-C(13)-C(14)	110.38(16)
C(21)-C(16)-C(17)	123.85(14)
C(21)-C(16)-N(2)	118.92(14)
C(17)-C(16)-N(2)	117.08(15)
C(18)-C(17)-C(16)	116.30(17)
C(18)-C(17)-C(22)	120.74(16)
C(16)-C(17)-C(22)	122.82(15)
C(19)-C(18)-C(17)	121.24(18)
C(20)-C(19)-C(18)	120.76(16)
C(19)-C(20)-C(21)	121.24(18)

C(16)-C(21)-C(20)	116.51(16)
C(16)-C(21)-C(25)	123.64(14)
C(20)-C(21)-C(25)	119.81(16)
C(17)-C(22)-C(24)	113.25(17)
C(17)-C(22)-C(23)	110.47(15)
C(24)-C(22)-C(23)	110.71(18)
C(21)-C(25)-C(27)	112.68(16)
C(21)-C(25)-C(26)	110.42(17)
C(27)-C(25)-C(26)	109.81(16)
F(3)-C(28)-F(2)	107.91(15)
F(3)-C(28)-F(1)	107.33(16)
F(2)-C(28)-F(1)	107.84(16)
F(3)-C(28)-S(1)	111.73(13)
F(2)-C(28)-S(1)	110.51(14)
F(1)-C(28)-S(1)	111.34(13)

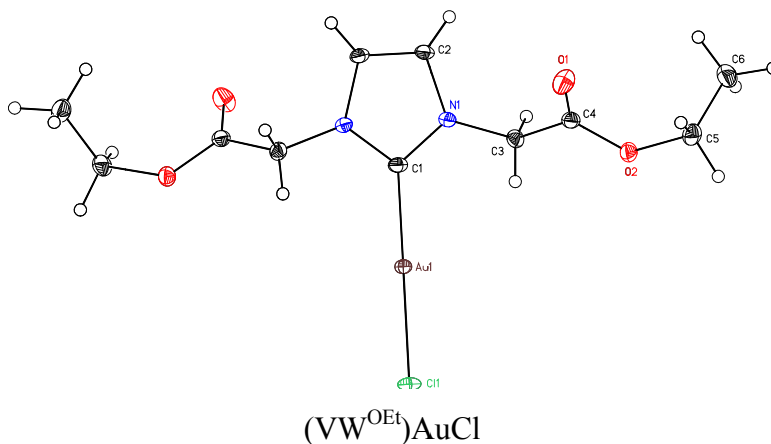
**Table 5.** Anisotropic displacement parameters ( $\text{\AA}^2 \times 10^4$ ) for VJS85 (CCDC 8093339). The anisotropic displacement factor exponent takes the form:  $-2\pi^2 [h^2 a^{*2} U^{11} + \dots + 2 h k a^* b^* U^{12}]$

	$U^{11}$	$U^{22}$	$U^{33}$	$U^{23}$	$U^{13}$	$U^{12}$
Au(1)	150(1)	146(1)	111(1)	2(1)	-3(1)	-13(1)
Br(1)	150(1)	249(1)	325(1)	-33(1)	6(1)	17(1)
Br(2)	250(1)	184(1)	295(1)	-43(1)	91(1)	-1(1)
S(1)	209(2)	174(2)	164(2)	17(1)	11(2)	-31(2)
F(1)	240(7)	457(7)	412(7)	-47(5)	-39(6)	-78(6)
F(2)	385(9)	366(7)	605(8)	226(6)	206(7)	-21(6)
F(3)	310(8)	396(7)	399(6)	-85(5)	107(6)	12(6)
O(1)	320(8)	213(6)	245(6)	-42(5)	40(6)	-15(6)
O(2)	256(7)	180(6)	188(5)	28(4)	-39(5)	-68(5)
O(3)	275(8)	260(6)	169(5)	40(5)	-19(5)	-27(5)
N(1)	131(7)	136(6)	107(5)	-13(4)	3(5)	7(5)
N(2)	149(7)	161(6)	100(5)	-23(4)	-5(5)	11(5)
C(1)	126(8)	147(7)	116(6)	-18(5)	-4(5)	24(6)
C(2)	164(8)	139(7)	179(7)	-24(5)	10(6)	-13(6)
C(3)	175(9)	168(7)	168(7)	-53(6)	-3(6)	-5(6)
C(4)	147(8)	137(7)	97(6)	-4(5)	18(5)	-12(6)
C(5)	142(8)	168(7)	124(6)	0(5)	10(6)	-7(6)
C(6)	182(9)	237(8)	159(7)	-17(6)	39(6)	32(7)
C(7)	218(9)	271(9)	115(7)	-26(6)	23(6)	-7(7)
C(8)	166(9)	246(8)	117(6)	-9(6)	-20(6)	0(6)
C(9)	140(8)	159(7)	135(6)	-3(5)	6(6)	-4(6)
C(10)	132(8)	236(8)	149(7)	-13(6)	12(6)	21(6)
C(11)	170(10)	293(10)	296(9)	-32(7)	-14(7)	-17(7)
C(12)	184(9)	265(8)	293(9)	-38(7)	-23(7)	46(8)

C(13)	170(9)	259(9)	153(7)	-14(6)	-8(6)	57(7)
C(14)	448(15)	291(10)	340(10)	11(8)	32(10)	163(10)
C(15)	170(10)	524(13)	283(10)	-46(9)	12(8)	-13(9)
C(16)	204(9)	207(8)	92(6)	-8(5)	-13(6)	5(6)
C(17)	236(10)	254(9)	145(7)	-8(6)	-35(7)	40(7)
C(18)	330(12)	351(11)	180(8)	68(7)	-42(7)	67(9)
C(19)	359(13)	450(12)	129(8)	72(7)	-6(8)	0(10)
C(20)	281(11)	408(11)	146(8)	-25(7)	43(7)	19(9)
C(21)	217(10)	267(9)	134(7)	-31(6)	20(6)	11(7)
C(22)	270(11)	308(10)	188(8)	13(7)	-29(7)	137(8)
C(23)	222(12)	630(15)	321(11)	-84(10)	-39(9)	121(10)
C(24)	610(18)	394(12)	342(11)	72(9)	42(11)	285(12)
C(25)	242(10)	272(9)	198(8)	-43(6)	53(7)	57(7)
C(26)	386(14)	311(11)	354(10)	-137(8)	60(10)	53(9)
C(27)	272(12)	417(12)	297(10)	-3(8)	82(9)	80(9)
C(28)	277(11)	217(9)	283(9)	28(7)	47(8)	-31(8)

---

### A.7 (VW<sup>OE</sup>t)AuCl



**Note:** The crystallographic data have been deposited in the Cambridge Database (CCDC) and has been placed on hold pending further instructions from me. The deposition number is 699491. Ideally the CCDC would like the publication to contain a footnote of the type: "Crystallographic data have been deposited at the CCDC, 12 Union Road, Cambridge CB2 1EZ, UK and copies can be obtained on request, free of charge, by quoting the publication citation and the deposition number 699491."

**Table 1. Crystal data and structure refinement for (VW<sup>OE</sup>t)AuCl (CCDC 699491).**

Empirical formula	C <sub>11</sub> H <sub>16</sub> N <sub>2</sub> O <sub>4</sub> AuCl
Formula weight	472.67
Crystallization Solvent	THF/hexanes
Crystal Habit	Trigonal-prism
Crystal size	0.24 x 0.22 x 0.17 mm <sup>3</sup>
Crystal color	Colorless

#### Data Collection

Type of diffractometer	Bruker KAPPA APEX II
Wavelength	0.71073 Å MoKα
Data Collection Temperature	100(2) K
θ range for 9867 reflections used in lattice determination	2.91 to 52.82°
Unit cell dimensions	a = 19.3637(8) Å b = 9.6925(4) Å c = 7.5022(3) Å





Volume	1408.03(10) Å <sup>3</sup>
Z	4
Crystal system	Orthorhombic
Space group	<i>Pbcn</i>
Density (calculated)	2.230 Mg/m <sup>3</sup>
F(000)	896
Data collection program	Bruker APEX2 v2.1-0
θ range for data collection	2.10 to 53.23°
Completeness to θ = 53.23°	97.5 %
Index ranges	-29 ≤ h ≤ 43, -21 ≤ k ≤ 20, -15 ≤ l ≤ 16
Data collection scan type	ω scans; 24 settings
Data reduction program	Bruker SAINT-Plus v7.34A
Reflections collected	112180
Independent reflections	8240 [R <sub>int</sub> = 0.0331]
Absorption coefficient	10.649 mm <sup>-1</sup>
Absorption correction	Semi-empirical from equivalents
Max. and min. transmission	0.4545 and 0.3132

### Structure Solution and Refinement

Structure solution program	SHELXS-97 (Sheldrick, 2008)
Primary solution method	Direct methods
Secondary solution method	Difference Fourier map
Hydrogen placement	Difference Fourier map
Structure refinement program	SHELXL-97 (Sheldrick, 2008)
Refinement method	Full matrix least-squares on F <sup>2</sup>
Data / restraints / parameters	8240 / 0 / 120
Treatment of hydrogen atoms	Unrestrained
Goodness-of-fit on F <sup>2</sup>	3.036
Final R indices [I > 2σ(I), 6275 reflections]	R1 = 0.0425, wR2 = 0.0495
R indices (all data)	R1 = 0.0574, wR2 = 0.0500
Type of weighting scheme used	Sigma
Weighting scheme used	w = 1/σ <sup>2</sup> (F <sub>o</sub> <sup>2</sup> )
Max shift/error	0.004
Average shift/error	0.000
Largest diff. peak and hole	6.212 and -4.877 e.Å <sup>-3</sup>

## Special Refinement Details

Crystals were mounted on a glass fiber using Paratone oil then placed on the diffractometer under a nitrogen stream at 100K.

Refinement of  $F^2$  against ALL reflections. The weighted R-factor ( $wR$ ) and goodness of fit ( $S$ ) are based on  $F^2$ , conventional R-factors ( $R$ ) are based on  $F$ , with  $F$  set to zero for negative  $F^2$ . The threshold expression of  $F^2 > 2\sigma(F^2)$  is used only for calculating R-factors(gt) etc. and is not relevant to the choice of reflections for refinement. R-factors based on  $F^2$  are statistically about twice as large as those based on  $F$ , and R-factors based on ALL data will be even larger.

All esds (except the esd in the dihedral angle between two l.s. planes) are estimated using the full covariance matrix. The cell esds are taken into account individually in the estimation of esds in distances, angles and torsion angles; correlations between esds in cell parameters are only used when they are defined by crystal symmetry. An approximate (isotropic) treatment of cell esds is used for estimating esds involving l.s. planes.

**Table 2. Atomic coordinates ( $\times 10^4$ ) and equivalent isotropic displacement parameters ( $\text{\AA}^2 \times 10^3$ ) for VJS43 (CCDC 699491).  $U_{eq}$  is defined as the trace of the orthogonalized  $U^{ij}$  tensor.**

	x	y	z	$U_{eq}$
Au(1)	0	763(1)	7500	11(1)
Cl(1)	0	-1596(1)	7500	15(1)
O(1)	1796(1)	4289(1)	7944(2)	21(1)
O(2)	2240(1)	2815(1)	5909(2)	15(1)
N(1)	464(1)	3658(1)	6718(2)	11(1)
C(1)	0	2801(2)	7500	12(1)
C(2)	291(1)	5029(1)	7006(2)	12(1)
C(3)	1064(1)	3204(2)	5730(2)	13(1)
C(4)	1734(1)	3518(1)	6700(2)	12(1)
C(5)	2952(1)	3102(2)	6450(2)	16(1)
C(6)	3240(1)	4239(2)	5304(3)	20(1)

**Table 3. Selected bond lengths [ $\text{\AA}$ ] and angles [ $^\circ$ ] for VJS43 (CCDC 699491).**

Au(1)-C(1)	1.9753(17)	C(1)-Au(1)-Cl(1)	180.0
Au(1)-Cl(1)	2.2863(4)		

**Table 4. Bond lengths [Å] and angles [°] for VJS43 (CCDC 699491).**


---

Au(1)-C(1)	1.9753(17)
Au(1)-Cl(1)	2.2863(4)
O(1)-C(4)	1.2018(19)
O(2)-C(4)	1.3327(16)
O(2)-C(5)	1.4641(15)
N(1)-C(1)	1.3573(15)
N(1)-C(2)	1.3871(18)
N(1)-C(3)	1.4464(16)
C(1)-N(1)#1	1.3573(15)
C(2)-C(2)#1	1.349(3)
C(2)-H(2)	0.88(2)
C(3)-C(4)	1.5184(17)
C(3)-H(3A)	0.96(2)
C(3)-H(3B)	0.85(2)
C(5)-C(6)	1.505(2)
C(5)-H(5A)	0.92(2)
C(5)-H(5B)	0.96(2)
C(6)-H(6A)	0.95(3)
C(6)-H(6B)	0.94(2)
C(6)-H(6C)	0.97(3)

C(1)-Au(1)-Cl(1)	180.0
C(4)-O(2)-C(5)	118.14(11)
C(1)-N(1)-C(2)	111.05(11)
C(1)-N(1)-C(3)	124.53(11)
C(2)-N(1)-C(3)	124.41(11)
N(1)-C(1)-N(1)#1	104.50(15)
N(1)-C(1)-Au(1)	127.75(7)
N(1)#1-C(1)-Au(1)	127.75(7)
C(2)#1-C(2)-N(1)	106.70(7)
C(2)#1-C(2)-H(2)	130.4(15)
N(1)-C(2)-H(2)	122.8(15)
N(1)-C(3)-C(4)	112.34(11)
N(1)-C(3)-H(3A)	111.0(12)
C(4)-C(3)-H(3A)	107.9(12)
N(1)-C(3)-H(3B)	108.5(12)
C(4)-C(3)-H(3B)	112.4(12)
H(3A)-C(3)-H(3B)	104.4(18)
O(1)-C(4)-O(2)	126.22(12)
O(1)-C(4)-C(3)	125.57(12)
O(2)-C(4)-C(3)	108.19(11)
O(2)-C(5)-C(6)	109.23(12)
O(2)-C(5)-H(5A)	108.4(14)
C(6)-C(5)-H(5A)	111.0(17)
O(2)-C(5)-H(5B)	102.0(12)
C(6)-C(5)-H(5B)	111.0(13)
H(5A)-C(5)-H(5B)	115(2)

C(5)-C(6)-H(6A)	111.4(14)
C(5)-C(6)-H(6B)	109.7(15)
H(6A)-C(6)-H(6B)	106(2)
C(5)-C(6)-H(6C)	111(2)
H(6A)-C(6)-H(6C)	103(2)
H(6B)-C(6)-H(6C)	115(2)

---

Symmetry transformations used to generate equivalent atoms:

#1 -x,y,-z+3/2

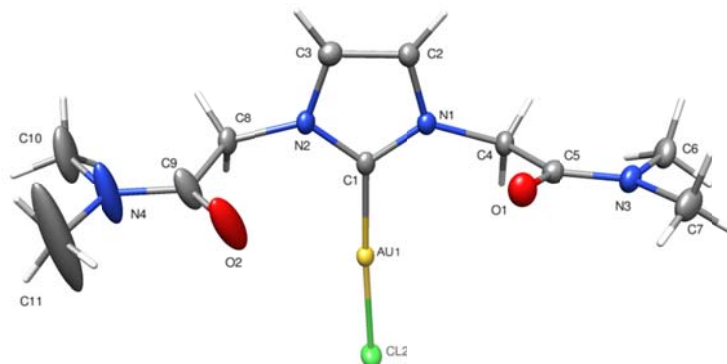
**Table 5.** Anisotropic displacement parameters ( $\text{\AA}^2 \times 10^4$ ) for VJS43 (CCDC 699491). The anisotropic displacement factor exponent takes the form:  $-2\pi^2 [h^2 a^{*2} U^{11} + \dots + 2 h k a^* b^* U^{12}]$

	$U^{11}$	$U^{22}$	$U^{33}$	$U^{23}$	$U^{13}$	$U^{12}$
Au(1)	109(1)	78(1)	137(1)	0	-10(1)	0
Cl(1)	209(1)	67(1)	177(2)	0	-22(2)	0
O(1)	170(4)	237(6)	210(5)	-115(4)	-48(3)	31(3)
O(2)	112(3)	152(4)	175(4)	-33(4)	3(3)	-5(3)
N(1)	116(3)	85(4)	142(4)	-3(3)	-3(3)	-9(3)
C(1)	131(4)	84(5)	159(6)	0	-45(7)	0
C(2)	142(4)	79(5)	150(5)	9(4)	-17(4)	-12(3)
C(3)	113(4)	131(5)	136(5)	-23(4)	-1(3)	-17(3)
C(4)	128(4)	103(5)	141(5)	-3(4)	-10(4)	-5(3)
C(5)	124(4)	179(6)	190(6)	6(5)	-36(4)	24(4)
C(6)	147(5)	211(7)	253(8)	14(6)	-9(5)	-31(4)

**Table 6.** Hydrogen coordinates ( $\times 10^4$ ) and isotropic displacement parameters ( $\text{\AA}^2 \times 10^3$ ) for VJS43 (CCDC 699491).

	x	y	z	$U_{\text{iso}}$
H(2)	523(10)	5720(20)	6540(30)	11(5)
H(3A)	1084(9)	3640(20)	4580(30)	9(4)
H(3B)	1018(9)	2350(20)	5500(30)	7(4)
H(5A)	2951(12)	3350(30)	7630(30)	12(5)
H(5B)	3178(9)	2240(30)	6200(30)	13(5)
H(6A)	3206(11)	4020(30)	4080(40)	16(5)
H(6B)	2979(12)	5040(20)	5460(40)	16(5)
H(6C)	3734(14)	4350(30)	5480(40)	42(8)

## A.8 (VW<sup>NMe<sub>2</sub></sup>)AuCl



VJS48

**Note:** The crystallographic data have been deposited in the Cambridge Database (CCDC) and has been placed on hold pending further instructions from me. The deposition number is 809337. Ideally the CCDC would like the publication to contain a footnote of the type: "Crystallographic data have been deposited at the CCDC, 12 Union Road, Cambridge CB2 1EZ, UK and copies can be obtained on request, free of charge, by quoting the publication citation and the deposition number 809337."

**Table 1. Crystal data and structure refinement for VJS48 (CCDC 809337).**

Empirical formula	C <sub>11</sub> H <sub>18</sub> N <sub>4</sub> O <sub>2</sub> ClAu • H <sub>2</sub> O
Formula weight	488.73
Crystallization Solvent	Not given
Crystal Habit	Fragment
Crystal size	0.22 x 0.22 x 0.10 mm <sup>3</sup>
Crystal color	Colorless



### Data Collection

Type of diffractometer	Bruker KAPPA APEX II
Wavelength	0.71073 Å MoKα
Data Collection Temperature	100(2) K
θ range for 9029 reflections used in lattice determination	2.60 to 41.88°
Unit cell dimensions	a = 13.4844(6) Å b = 10.7178(5) Å c = 12.4577(6) Å
	α = 90° β = 113.353(2)° γ = 90°
Volume	1652.93(13) Å <sup>3</sup>

Z	4
Crystal system	Monoclinic
Space group	$P 2_1/c$
Density (calculated)	1.964 Mg/m <sup>3</sup>
F(000)	936
Data collection program	Bruker APEX2 v2009.7-0
$\theta$ range for data collection	2.51 to 42.17°
Completeness to $\theta = 42.17^\circ$	97.3 %
Index ranges	$-24 \leq h \leq 25, -17 \leq k \leq 20, -20 \leq l \leq 23$
Data collection scan type	$\omega$ scans; 17 settings
Data reduction program	Bruker SAINT-Plus v7.66A
Reflections collected	98097
Independent reflections	11359 [ $R_{\text{int}} = 0.0310$ ]
Absorption coefficient	9.073 mm <sup>-1</sup>
Absorption correction	Semi-empirical from equivalents
Max. and min. transmission	0.4439 and 0.2459

## Structure Solution and Refinement

Structure solution program	SHELXS-97 (Sheldrick, 2008)
Primary solution method	Direct methods
Secondary solution method	Difference Fourier map
Hydrogen placement	Geometric positions
Structure refinement program	SHELXL-97 (Sheldrick, 2008)
Refinement method	Full matrix least-squares on $F^2$
Data / restraints / parameters	11359 / 0 / 186
Treatment of hydrogen atoms	Riding
Goodness-of-fit on $F^2$	2.324
Final R indices [ $I > 2\sigma(I)$ , 9607 reflections]	$R1 = 0.0237, wR2 = 0.0432$
R indices (all data)	$R1 = 0.0311, wR2 = 0.0436$
Type of weighting scheme used	Sigma
Weighting scheme used	$w = 1/\sigma^2(F_o^2)$
Max shift/error	0.006
Average shift/error	0.000
Largest diff. peak and hole	4.550 and -2.121 e.Å <sup>-3</sup>

## Special Refinement Details

Crystals were mounted on a glass fiber using Paratone oil then placed on the diffractometer under a nitrogen stream at 100K.

There is a disordered solvent in the crystal that could not be identified or modeled satisfactorily. The model was adjusted by solvent flattening through the implementation SQUEEZE where two voids of  $82\text{\AA}^3$  were assigned  $28e^-$  each and the observed intensities were adjusted accordingly.

Refinement of  $F^2$  against ALL reflections. The weighted R-factor ( $wR$ ) and goodness of fit ( $S$ ) are based on  $F^2$ , conventional R-factors ( $R$ ) are based on  $F$ , with  $F$  set to zero for negative  $F^2$ . The threshold expression of  $F^2 > 2\sigma(F^2)$  is used only for calculating R-factors(gt) etc. and is not relevant to the choice of reflections for refinement. R-factors based on  $F^2$  are statistically about twice as large as those based on  $F$ , and R-factors based on ALL data will be even larger.

All esds (except the esd in the dihedral angle between two l.s. planes) are estimated using the full covariance matrix. The cell esds are taken into account individually in the estimation of esds in distances, angles and torsion angles; correlations between esds in cell parameters are only used when they are defined by crystal symmetry. An approximate (isotropic) treatment of cell esds is used for estimating esds involving l.s. planes.

**Table 2. Atomic coordinates ( $\times 10^4$ ) and equivalent isotropic displacement parameters ( $\text{\AA}^2 \times 10^3$ ) for VJS48 (CCDC 809337).  $U_{eq}$  is defined as the trace of the orthogonalized  $U^{ij}$  tensor.**

	x	y	z	$U_{eq}$
Au(1)	7979(1)	6594(1)	2008(1)	15(1)
Cl(2)	7164(1)	8239(1)	811(1)	23(1)
O(1)	9939(1)	3665(1)	1362(1)	28(1)
O(2)	6627(1)	3287(2)	2017(2)	57(1)
N(1)	9758(1)	4794(1)	3214(1)	16(1)
N(2)	8408(1)	4400(1)	3656(1)	17(1)
N(3)	11358(1)	4828(1)	1421(1)	23(1)
N(4)	5632(2)	3493(2)	3105(2)	65(1)
C(1)	8747(1)	5177(1)	3017(1)	16(1)
C(2)	10054(1)	3792(2)	3972(1)	19(1)
C(3)	9203(1)	3542(1)	4253(1)	20(1)
C(4)	10476(1)	5361(2)	2736(1)	18(1)
C(5)	10572(1)	4536(2)	1782(1)	20(1)
C(6)	12185(1)	5763(2)	1966(2)	28(1)
C(7)	11516(2)	4026(2)	553(2)	32(1)

C(8)	7377(1)	4480(2)	3771(1)	20(1)
C(9)	6514(1)	3699(2)	2882(2)	36(1)
C(10)	5486(2)	3985(3)	4125(2)	59(1)
C(11)	4771(3)	2683(8)	2325(5)	193(4)
O(3)	7880(1)	2754(1)	746(1)	34(1)

**Table 3. Selected bond lengths [Å] and angles [°] for VJS48 (CCDC 809337).**

Au(1)-C(1)	1.9816(14)	C(1)-Au(1)-Cl(2)	176.97(4)
Au(1)-Cl(2)	2.2888(4)		



**Table 4. Bond lengths [ $\text{\AA}$ ] and angles [ $^\circ$ ] for VJS48 (CCDC 809337).**


---

Au(1)-C(1)	1.9816(14)
Au(1)-Cl(2)	2.2888(4)
O(1)-C(5)	1.233(2)
O(2)-C(9)	1.229(2)
N(1)-C(1)	1.3496(17)
N(1)-C(2)	1.3794(19)
N(1)-C(4)	1.4555(18)
N(2)-C(1)	1.3510(18)
N(2)-C(3)	1.3840(19)
N(2)-C(8)	1.4561(18)
N(3)-C(5)	1.3417(19)
N(3)-C(6)	1.452(2)
N(3)-C(7)	1.462(2)
N(4)-C(9)	1.343(3)
N(4)-C(10)	1.460(3)
N(4)-C(11)	1.466(3)
C(2)-C(3)	1.353(2)
C(4)-C(5)	1.528(2)
C(8)-C(9)	1.503(2)
C(1)-Au(1)-Cl(2)	176.97(4)
C(1)-N(1)-C(2)	111.02(12)
C(1)-N(1)-C(4)	125.88(12)
C(2)-N(1)-C(4)	123.08(12)
C(1)-N(2)-C(3)	110.83(12)
C(1)-N(2)-C(8)	125.54(12)
C(3)-N(2)-C(8)	123.54(12)
C(5)-N(3)-C(6)	124.50(13)
C(5)-N(3)-C(7)	118.47(15)
C(6)-N(3)-C(7)	116.20(13)
C(9)-N(4)-C(10)	123.81(17)
C(9)-N(4)-C(11)	119.6(2)
C(10)-N(4)-C(11)	116.5(2)
N(1)-C(1)-N(2)	104.96(12)
N(1)-C(1)-Au(1)	125.84(10)
N(2)-C(1)-Au(1)	129.20(10)
C(3)-C(2)-N(1)	106.67(13)
C(2)-C(3)-N(2)	106.52(13)
N(1)-C(4)-C(5)	110.62(12)
O(1)-C(5)-N(3)	122.71(14)
O(1)-C(5)-C(4)	120.70(13)
N(3)-C(5)-C(4)	116.57(14)
N(2)-C(8)-C(9)	112.65(12)
O(2)-C(9)-N(4)	123.33(17)
O(2)-C(9)-C(8)	121.20(16)
N(4)-C(9)-C(8)	115.47(15)

---

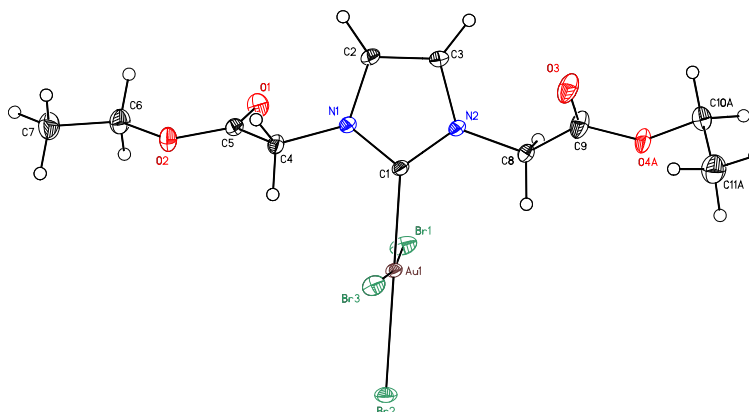
**Table 5.** Anisotropic displacement parameters ( $\text{\AA}^2 \times 10^4$ ) for VJS48 (CCDC 809337). The anisotropic displacement factor exponent takes the form:  $-2\pi^2 [h^2 a^{*2} U^{11} + \dots + 2 h k a^* b^* U^{12}]$

	$U^{11}$	$U^{22}$	$U^{33}$	$U^{23}$	$U^{13}$	$U^{12}$
Au(1)	140(1)	176(1)	168(1)	-2(1)	82(1)	2(1)
Cl(2)	191(1)	243(2)	280(2)	66(1)	114(1)	43(1)
O(1)	278(6)	306(7)	269(5)	-81(5)	139(5)	-19(5)
O(2)	238(6)	964(15)	527(9)	-501(9)	166(6)	-78(7)
N(1)	153(4)	190(6)	172(4)	-5(4)	91(4)	2(4)
N(2)	158(5)	198(6)	185(5)	-5(4)	103(4)	-5(4)
N(3)	244(6)	289(7)	212(5)	16(5)	149(4)	43(5)
N(4)	290(8)	1040(20)	751(14)	-629(13)	336(9)	-332(10)
C(1)	150(5)	185(6)	153(5)	-33(5)	81(4)	-22(5)
C(2)	187(6)	208(7)	198(6)	17(5)	90(5)	23(5)
C(3)	208(6)	211(7)	199(6)	23(5)	94(5)	10(5)
C(4)	168(5)	222(7)	200(6)	2(5)	109(4)	-10(5)
C(5)	199(6)	251(8)	172(5)	21(5)	88(5)	47(5)
C(6)	286(8)	302(9)	329(8)	56(7)	209(6)	12(6)
C(7)	405(9)	369(10)	283(7)	21(7)	240(7)	114(8)
C(8)	176(5)	227(7)	231(6)	-28(5)	130(5)	-18(5)
C(9)	180(7)	516(12)	405(9)	-247(9)	140(6)	-53(7)
C(10)	358(11)	830(20)	774(16)	-441(15)	417(11)	-251(12)
C(11)	600(20)	3560(90)	1960(50)	-2250(60)	850(30)	-1190(40)
O(3)	308(6)	403(8)	375(6)	-135(6)	210(5)	-23(5)

**Table 6.** Hydrogen bonds for VJS48 (CCDC 809337) [ $\text{\AA}$  and  $^\circ$ ].

D-H...A	d(D-H)	d(H...A)	d(D...A)	$\angle(\text{DHA})$
O(3)-H(3B)...O(2)	0.69	2.11	2.7947(19)	170.3
O(3)-H(3A)...O(1)	0.70	2.09	2.7505(18)	158.3

## A.9 (VW<sup>OE<sub>t</sub></sup>)AuBr<sub>3</sub>



(VW<sup>OE<sub>t</sub></sup>)AuBr<sub>3</sub>

**Note:** The crystallographic data have been deposited in the Cambridge Database (CCDC) and has been placed on hold pending further instructions from me. The deposition number is 703018. Ideally the CCDC would like the publication to contain a footnote of the type: "Crystallographic data have been deposited at the CCDC, 12 Union Road, Cambridge CB2 1EZ, UK and copies can be obtained on request, free of charge, by quoting the publication citation and the deposition number 703018."

**Table 1. Crystal data and structure refinement for (VW<sup>OE<sub>t</sub></sup>)AuBr<sub>3</sub> (CCDC 703018).**

Empirical formula	C <sub>11</sub> H <sub>16</sub> N <sub>2</sub> O <sub>4</sub> Br <sub>3</sub> Au
Formula weight	676.95
Crystallization Solvent	THF/hexane
Crystal Habit	Blade
Crystal size	0.26 x 0.11 x 0.05 mm <sup>3</sup>
Crystal color	Dichroic - orange/yellow



### Data Collection

Type of diffractometer	Bruker KAPPA APEX II
Wavelength	0.71073 Å MoKα
Data Collection Temperature	100(2) K
θ range for 9928 reflections used in lattice determination	2.49 to 44.53°
Unit cell dimensions	a = 9.2780(3) Å b = 8.1873(3) Å β = 90.257(2)°

	$c = 22.3335(8) \text{ \AA}$
Volume	$1696.48(10) \text{ \AA}^3$
Z	4
Crystal system	Monoclinic
Space group	$P2_1/c$
Density (calculated)	$2.650 \text{ Mg/m}^3$
F(000)	1248
$\theta$ range for data collection	$1.82$ to $44.60^\circ$
Completeness to $\theta = 44.60^\circ$	81.1 %
Index ranges	$-17 \leq h \leq 18$ , $-15 \leq k \leq 9$ , $-40 \leq l \leq 39$
Data collection scan type	$\omega$ scans; 14 settings
Reflections collected	54388
Independent reflections	11112 [ $R_{\text{int}} = 0.0316$ ]
Absorption coefficient	$15.752 \text{ mm}^{-1}$
Absorption correction	Semi-empirical from equivalents
Max. and min. transmission	0.4463 and 0.1885

## Structure Solution and Refinement

Structure solution program	SHELXS-97 (Sheldrick, 2008)
Primary solution method	Direct methods
Secondary solution method	Difference Fourier map
Hydrogen placement	Geometric positions
Structure refinement program	SHELXL-97 (Sheldrick, 2008)
Refinement method	Full matrix least-squares on $F^2$
Data / restraints / parameters	11112 / 0 / 221
Treatment of hydrogen atoms	Riding
Goodness-of-fit on $F^2$	1.675
Final R indices [ $I > 2\sigma(I)$ , 9400 reflections]	$R1 = 0.0302$ , $wR2 = 0.0447$
R indices (all data)	$R1 = 0.0410$ , $wR2 = 0.0455$
Type of weighting scheme used	Sigma
Weighting scheme used	$w = 1/\sigma^2(F_o^2)$
Max shift/error	0.003
Average shift/error	0.000
Largest diff. peak and hole	3.881 and $-2.923 \text{ e.\AA}^{-3}$

## Special Refinement Details

Crystals were mounted on a glass fiber using Paratone oil then placed on the diffractometer under a nitrogen stream at 100K.

Refinement of  $F^2$  against ALL reflections. The weighted R-factor ( $wR$ ) and goodness of fit ( $S$ ) are based on  $F^2$ , conventional R-factors ( $R$ ) are based on  $F$ , with  $F$  set to zero for negative  $F^2$ . The threshold expression of  $F^2 > 2\sigma(F^2)$  is used only for calculating R-factors(gt) etc. and is not relevant to the choice of reflections for refinement. R-factors based on  $F^2$  are statistically about twice as large as those based on  $F$ , and R-factors based on ALL data will be even larger.

All esds (except the esd in the dihedral angle between two l.s. planes) are estimated using the full covariance matrix. The cell esds are taken into account individually in the estimation of esds in distances, angles and torsion angles; correlations between esds in cell parameters are only used when they are defined by crystal symmetry. An approximate (isotropic) treatment of cell esds is used for estimating esds involving l.s. planes.

**Table 2. Atomic coordinates ( $\times 10^4$ ) and equivalent isotropic displacement parameters ( $\text{\AA}^2 \times 10^3$ ) for VJS45 (CCDC 703018).  $U(\text{eq})$  is defined as the trace of the orthogonalized  $U^{ij}$  tensor.**

	x	y	z	$U_{\text{eq}}$	Occ
Au(1)	3815(1)	2755(1)	5651(1)	10(1)	1
Br(1)	3595(1)	-187(1)	5720(1)	18(1)	1
Br(2)	6162(1)	2773(1)	6153(1)	16(1)	1
Br(3)	3766(1)	5719(1)	5636(1)	16(1)	1
O(1)	-339(2)	799(2)	6335(1)	18(1)	1
O(2)	-512(2)	2781(2)	7031(1)	17(1)	1
O(3)	1623(2)	3459(2)	3536(1)	24(1)	1
O(4A)	3342(3)	1679(3)	3251(1)	18(1)	0.731(6)
O(4B)	3783(7)	2180(10)	3366(3)	17(1)	0.269(6)
N(1)	612(2)	3030(2)	5495(1)	12(1)	1
N(2)	1595(2)	2149(2)	4684(1)	13(1)	1
C(1)	1886(2)	2689(2)	5243(1)	11(1)	1
C(2)	-504(2)	2686(2)	5099(1)	15(1)	1
C(3)	112(2)	2135(2)	4590(1)	15(1)	1
C(4)	386(2)	3568(2)	6107(1)	14(1)	1
C(5)	-191(2)	2194(2)	6494(1)	13(1)	1
C(6)	-1170(2)	1639(2)	7452(1)	20(1)	1
C(7)	-1707(3)	2655(3)	7965(1)	24(1)	1
C(8)	2663(2)	1588(2)	4254(1)	14(1)	1
C(9)	2483(2)	2411(2)	3652(1)	20(1)	1
C(10A)	3339(3)	2346(3)	2640(1)	20(1)	0.731(6)

C(11A)	4319(4)	3800(4)	2605(2)	27(1)	0.731(6)
C(10B)	3970(9)	3134(10)	2820(3)	20(2)	0.269(6)
C(11B)	3034(9)	2526(11)	2323(4)	26(2)	0.269(6)

**Table 3. Selected bond lengths [Å] and angles [°] for VJS45 (CCDC 703018).**

Au(1)-C(1)	2.0053(16)	C(1)-Au(1)-Br(1)	85.81(5)
Au(1)-Br(1)	2.4218(2)	C(1)-Au(1)-Br(3)	90.22(5)
Au(1)-Br(3)	2.4276(2)	Br(1)-Au(1)-Br(3)	173.434(7)
Au(1)-Br(2)	2.44475(19)	C(1)-Au(1)-Br(2)	178.77(5)
		Br(1)-Au(1)-Br(2)	92.975(6)
		Br(3)-Au(1)-Br(2)	90.976(6)

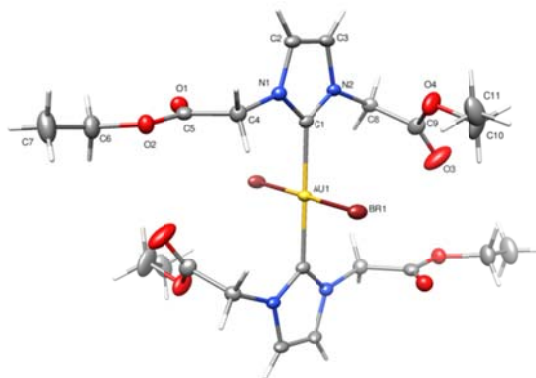
**Table 4. Bond lengths [Å] and angles [°] for VJS45 (CCDC 703018).**

Au(1)-C(1)	2.0053(16)	C(1)-N(1)-C(2)	110.34(14)
Au(1)-Br(1)	2.4218(2)	C(1)-N(1)-C(4)	126.09(14)
Au(1)-Br(3)	2.4276(2)	C(2)-N(1)-C(4)	123.42(15)
Au(1)-Br(2)	2.44475(19)	C(1)-N(2)-C(3)	109.65(14)
O(1)-C(5)	1.204(2)	C(1)-N(2)-C(8)	125.36(14)
O(2)-C(5)	1.328(2)	C(3)-N(2)-C(8)	124.92(14)
O(2)-C(6)	1.461(2)	N(1)-C(1)-N(2)	106.44(14)
O(3)-C(9)	1.199(2)	N(1)-C(1)-Au(1)	126.20(12)
O(4A)-C(9)	1.342(3)	N(2)-C(1)-Au(1)	127.09(12)
O(4A)-C(10A)	1.469(4)	C(3)-C(2)-N(1)	106.65(15)
O(4B)-C(9)	1.380(6)	C(2)-C(3)-N(2)	106.91(15)
O(4B)-C(10B)	1.459(10)	N(1)-C(4)-C(5)	111.32(14)
N(1)-C(1)	1.340(2)	O(1)-C(5)-O(2)	125.73(17)
N(1)-C(2)	1.387(2)	O(1)-C(5)-C(4)	125.18(16)
N(1)-C(4)	1.453(2)	O(2)-C(5)-C(4)	109.09(15)
N(2)-C(1)	1.350(2)	O(2)-C(6)-C(7)	106.04(16)
N(2)-C(3)	1.391(2)	N(2)-C(8)-C(9)	111.88(15)
N(2)-C(8)	1.457(2)	O(3)-C(9)-O(4A)	124.9(2)
C(2)-C(3)	1.353(3)	O(3)-C(9)-O(4B)	125.5(3)
C(4)-C(5)	1.518(3)	O(4A)-C(9)-O(4B)	26.9(3)
C(6)-C(7)	1.503(3)	O(3)-C(9)-C(8)	125.48(18)
C(8)-C(9)	1.514(3)	O(4)-C(9)-C(8)	109.31(17)
C(10A)-C(11A)	1.500(4)	O(4B)-C(9)-C(8)	104.8(3)
C(10B)-C(11B)	1.491(11)	O(4A)-C(10A)-C(11A)	110.2(3)
		O(4B)-C(10B)-C(11B)	111.9(7)
C(1)-Au(1)-Br(1)	85.81(5)		
C(1)-Au(1)-Br(3)	90.22(5)		
Br(1)-Au(1)-Br(3)	173.434(7)		
C(1)-Au(1)-Br(2)	178.77(5)		
Br(1)-Au(1)-Br(2)	92.975(6)		
Br(3)-Au(1)-Br(2)	90.976(6)		
C(5)-O(2)-C(6)	116.46(14)		
C(9)-O(4A)-C(10A)	117.0(2)		
C(9)-O(4B)-C(10B)	114.8(5)		

**Table 5.** Anisotropic displacement parameters ( $\text{\AA}^2 \times 10^4$ ) for VJS45 (CCDC 703018). The anisotropic displacement factor exponent takes the form:  $-2\pi^2 [h^2 a^{*2} U^{11} + \dots + 2 h k a^* b^* U^{12}]$

	$U^{11}$	$U^{22}$	$U^{33}$	$U^{23}$	$U^{13}$	$U^{12}$
Au(1)	71(1)	102(1)	115(1)	-8(1)	-4(1)	10(1)
Br(1)	122(1)	108(1)	307(1)	17(1)	-14(1)	8(1)
Br(2)	98(1)	200(1)	189(1)	-17(1)	-41(1)	14(1)
Br(3)	139(1)	105(1)	225(1)	-10(1)	6(1)	8(1)
O(1)	217(7)	140(6)	185(6)	-16(5)	6(5)	12(5)
O(2)	219(7)	160(6)	135(5)	-15(4)	48(5)	-29(5)
O(3)	238(7)	249(7)	235(7)	68(5)	91(6)	126(6)
O(4A)	186(11)	201(11)	141(9)	-7(7)	61(8)	51(9)
O(4B)	90(20)	290(30)	130(20)	-10(20)	19(18)	0(20)
N(1)	90(5)	141(7)	126(6)	-19(5)	0(5)	16(5)
N(2)	81(5)	164(7)	135(6)	-28(5)	6(5)	17(5)
C(1)	79(6)	120(7)	123(6)	-5(5)	5(5)	5(5)
C(2)	86(6)	225(9)	152(7)	4(6)	-1(6)	28(6)
C(3)	94(6)	214(9)	148(7)	-17(6)	-12(6)	9(6)
C(4)	128(7)	153(8)	129(7)	-24(5)	27(6)	5(6)
C(5)	105(6)	165(8)	130(6)	-4(6)	2(5)	22(6)
C(6)	225(9)	196(9)	167(8)	29(7)	39(7)	-22(7)
C(7)	269(10)	262(10)	175(8)	32(7)	37(8)	28(8)
C(8)	105(7)	184(8)	134(7)	-30(6)	17(6)	27(6)
C(9)	218(9)	193(9)	200(8)	26(6)	83(7)	72(7)
C(10A)	223(13)	244(14)	141(12)	-4(9)	16(10)	1(11)
C(11A)	299(16)	260(16)	254(15)	13(12)	48(13)	-17(13)
C(10B)	190(30)	200(40)	210(30)	60(30)	70(30)	-60(30)
C(11B)	210(30)	410(50)	160(40)	20(30)	-10(30)	0(30)

### A.10 [(VW<sup>OEt</sup>)<sub>2</sub>AuBr<sub>2</sub>][PF<sub>6</sub>]



VJS50

**Note:** The crystallographic data have been deposited in the Cambridge Database (CCDC) and has been placed on hold pending further instructions from me. The deposition number is 809338. Ideally the CCDC would like the publication to contain a footnote of the type: "Crystallographic data have been deposited at the CCDC, 12 Union Road, Cambridge CB2 1EZ, UK and copies can be obtained on request, free of charge, by quoting the publication citation and the deposition number 809338."

**Table 1. Crystal data and structure refinement for VJS50\_809338.**

Empirical formula	[C <sub>22</sub> H <sub>32</sub> N <sub>4</sub> O <sub>8</sub> Br <sub>2</sub> Au] <sup>+</sup> [F <sub>6</sub> P] <sup>−</sup>
Formula weight	982.27
Crystallization Solvent	Dichloromethane/petroleum ether
Crystal Habit	Needle
Crystal size	0.19 x 0.07 x 0.04 mm <sup>3</sup>
Crystal color	Colorless



#### Data Collection

Type of diffractometer	Bruker KAPPA APEX II
Wavelength	0.71073 Å MoKα
Data Collection Temperature	100(2) K
θ range for 9986 reflections used in lattice determination	2.23 to 34.66°
Unit cell dimensions	a = 8.3552(4) Å b = 10.4228(4) Å c = 10.8746(8) Å
	α = 111.780(3)° β = 105.647(3)° γ = 101.200(2)°
Volume	799.64(8) Å <sup>3</sup>



Z	1
Crystal system	Triclinic
Space group	P-1
Density (calculated)	2.040 Mg/m <sup>3</sup>
F(000)	474
Data collection program	Bruker APEX2 v2009.7-0
$\theta$ range for data collection	2.18 to 35.04°
Completeness to $\theta = 35.04^\circ$	92.5 %
Index ranges	$-13 \leq h \leq 13$ , $-16 \leq k \leq 16$ , $-17 \leq l \leq 17$
Data collection scan type	$\omega$ scans; 27 settings
Data reduction program	Bruker SAINT-Plus v7.66A
Reflections collected	45623
Independent reflections	6542 [ $R_{\text{int}} = 0.0268$ ]
Absorption coefficient	7.232 mm <sup>-1</sup>
Absorption correction	Semi-empirical from equivalents
Max. and min. transmission	0.4370 and 0.2693

## Structure Solution and Refinement

Structure solution program	SHELXS-97 (Sheldrick, 2008)
Primary solution method	Direct methods
Secondary solution method	Difference Fourier map
Hydrogen placement	Geometric positions
Structure refinement program	SHELXL-97 (Sheldrick, 2008)
Refinement method	Full matrix least-squares on $F^2$
Data / restraints / parameters	6542 / 0 / 204
Treatment of hydrogen atoms	Riding
Goodness-of-fit on $F^2$	1.990
Final R indices [ $I > 2\sigma(I)$ , 6342 reflections]	$R1 = 0.0195$ , $wR2 = 0.0329$
R indices (all data)	$R1 = 0.0211$ , $wR2 = 0.0330$
Type of weighting scheme used	Sigma
Weighting scheme used	$w = 1/\sigma^2(F_o^2)$
Max shift/error	0.002
Average shift/error	0.000
Largest diff. peak and hole	1.469 and -1.105 e.Å <sup>-3</sup>

## Special Refinement Details

Crystals were mounted on a glass fiber using Paratone oil then placed on the diffractometer under a nitrogen stream at 100K.

Refinement of  $F^2$  against ALL reflections. The weighted R-factor ( $wR$ ) and goodness of fit ( $S$ ) are based on  $F^2$ , conventional R-factors ( $R$ ) are based on  $F$ , with  $F$  set to zero for negative  $F^2$ . The threshold expression of  $F^2 > 2\sigma(F^2)$  is used only for calculating R-factors(gt) etc. and is not relevant to the choice of reflections for refinement. R-factors based on  $F^2$  are statistically about twice as large as those based on  $F$ , and R-factors based on ALL data will be even larger.

All esds (except the esd in the dihedral angle between two l.s. planes) are estimated using the full covariance matrix. The cell esds are taken into account individually in the estimation of esds in distances, angles and torsion angles; correlations between esds in cell parameters are only used when they are defined by crystal symmetry. An approximate (isotropic) treatment of cell esds is used for estimating esds involving l.s. planes.

**Table 2. Atomic coordinates ( $\times 10^4$ ) and equivalent isotropic displacement parameters ( $\text{\AA}^2 \times 10^3$ ) for VJS50\_809338.  $U(\text{eq})$  is defined as the trace of the orthogonalized  $U^{ij}$  tensor.**

	x	y	z	$U_{\text{eq}}$
Au(1)	0	0	10000	14(1)
Br(1)	-665(1)	2117(1)	9892(1)	22(1)
O(1)	1528(1)	-2388(1)	6831(1)	23(1)
O(2)	-204(1)	-2201(1)	4960(1)	24(1)
O(3)	3007(2)	3347(2)	13810(2)	49(1)
O(4)	3976(2)	4087(1)	12387(1)	34(1)
N(1)	2493(2)	599(1)	8522(1)	17(1)
N(2)	3855(2)	1391(1)	10774(1)	15(1)
C(1)	2266(2)	698(2)	9727(2)	16(1)
C(2)	4260(2)	1220(2)	8820(2)	20(1)
C(3)	5114(2)	1730(2)	10234(2)	19(1)
C(4)	1114(2)	-86(2)	7102(2)	21(1)
C(5)	863(2)	-1695(2)	6310(2)	20(1)
C(6)	-624(3)	-3748(2)	4049(2)	32(1)
C(7)	-1450(3)	-3997(2)	2535(2)	47(1)
C(8)	4175(2)	1847(2)	12281(2)	18(1)
C(9)	3639(2)	3166(2)	12928(2)	23(1)
C(10)	3436(3)	5379(2)	12847(2)	49(1)
C(11)	3076(3)	5801(2)	11653(2)	42(1)
P(1)	5000	0	5000	23(1)

F(1)	4043(2)	1077(1)	5730(1)	36(1)
F(2)	6510(1)	554(1)	6527(1)	32(1)
F(3)	3879(1)	-1265(1)	5234(1)	32(1)

---

**Table 3.** Selected bond lengths [Å] and angles [°] for VJS50\_809338.

---

Au(1)-C(1)#1	2.0320(14)
Au(1)-C(1)	2.0320(14)
Au(1)-Br(1)#1	2.41299(16)
Au(1)-Br(1)	2.41303(16)

C(1)#1-Au(1)-C(1)	180.000(1)
C(1)#1-Au(1)-Br(1)#1	88.28(4)
C(1)-Au(1)-Br(1)#1	91.72(4)
C(1)#1-Au(1)-Br(1)	91.72(4)
C(1)-Au(1)-Br(1)	88.28(4)
Br(1)#1-Au(1)-Br(1)	180.0

---

Symmetry transformations used to generate equivalent atoms:

#1 -x,-y,-z+2

**Table 4. Bond lengths [Å] and angles [°] for VJS50\_809338.**

---

Au(1)-C(1)#1	2.0320(14)
Au(1)-C(1)	2.0320(14)
Au(1)-Br(1)#1	2.41299(16)
Au(1)-Br(1)	2.41303(16)
O(1)-C(5)	1.2012(17)
O(2)-C(5)	1.3285(18)
O(2)-C(6)	1.454(2)
O(3)-C(9)	1.1891(19)
O(4)-C(9)	1.3218(18)
O(4)-C(10)	1.458(2)
N(1)-C(1)	1.3436(17)
N(1)-C(2)	1.3847(18)
N(1)-C(4)	1.4576(19)
N(2)-C(1)	1.3350(19)
N(2)-C(3)	1.3851(17)
N(2)-C(8)	1.4557(18)
C(2)-C(3)	1.346(2)
C(4)-C(5)	1.514(2)
C(6)-C(7)	1.502(2)
C(8)-C(9)	1.509(2)
C(10)-C(11)	1.494(3)
P(1)-F(2)#2	1.5996(9)
P(1)-F(2)	1.5996(9)
P(1)-F(1)#2	1.6003(10)
P(1)-F(1)	1.6003(10)
P(1)-F(3)	1.6053(9)
P(1)-F(3)#2	1.6053(9)
C(1)#1-Au(1)-C(1)	180.000(1)
C(1)#1-Au(1)-Br(1)#1	88.28(4)
C(1)-Au(1)-Br(1)#1	91.72(4)
C(1)#1-Au(1)-Br(1)	91.72(4)
C(1)-Au(1)-Br(1)	88.28(4)
Br(1)#1-Au(1)-Br(1)	180.0

C(5)-O(2)-C(6)	116.20(12)
C(9)-O(4)-C(10)	117.45(14)
C(1)-N(1)-C(2)	109.71(13)
C(1)-N(1)-C(4)	125.84(13)
C(2)-N(1)-C(4)	124.44(12)
C(1)-N(2)-C(3)	110.24(12)
C(1)-N(2)-C(8)	124.30(12)
C(3)-N(2)-C(8)	125.19(13)
N(2)-C(1)-N(1)	106.46(12)
N(2)-C(1)-Au(1)	124.72(10)
N(1)-C(1)-Au(1)	128.81(11)
C(3)-C(2)-N(1)	107.02(12)
C(2)-C(3)-N(2)	106.57(13)
N(1)-C(4)-C(5)	111.86(12)
O(1)-C(5)-O(2)	126.16(15)
O(1)-C(5)-C(4)	124.92(14)
O(2)-C(5)-C(4)	108.92(12)
O(2)-C(6)-C(7)	106.94(14)
N(2)-C(8)-C(9)	112.57(11)
O(3)-C(9)-O(4)	124.98(16)
O(3)-C(9)-C(8)	124.06(14)
O(4)-C(9)-C(8)	110.95(13)
O(4)-C(10)-C(11)	107.27(16)
F(2)#2-P(1)-F(2)	180.0
F(2)#2-P(1)-F(1)#2	90.02(5)
F(2)-P(1)-F(1)#2	89.98(5)
F(2)#2-P(1)-F(1)	89.98(5)
F(2)-P(1)-F(1)	90.02(5)
F(1)#2-P(1)-F(1)	180.0
F(2)#2-P(1)-F(3)	89.97(5)
F(2)-P(1)-F(3)	90.03(5)
F(1)#2-P(1)-F(3)	90.19(5)
F(1)-P(1)-F(3)	89.81(5)
F(2)#2-P(1)-F(3)#2	90.03(5)
F(2)-P(1)-F(3)#2	89.97(5)
F(1)#2-P(1)-F(3)#2	89.81(5)
F(1)-P(1)-F(3)#2	90.19(5)
F(3)-P(1)-F(3)#2	180.0

---

Symmetry transformations used to generate equivalent atoms:

#1 -x,-y,-z+2

#2 -x+1,-y,-z+1

**Table 5.** Anisotropic displacement parameters ( $\text{\AA}^2 \times 10^4$ ) for VJS50\_809338. The anisotropic displacement factor exponent takes the form:  $-2\pi^2 [h^2 a^{*2} U^{11} + \dots + 2 h k a^* b^* U^{12}]$

	$U^{11}$	$U^{22}$	$U^{33}$	$U^{23}$	$U^{13}$	$U^{12}$
Au(1)	107(1)	153(1)	153(1)	72(1)	55(1)	36(1)
Br(1)	179(1)	204(1)	329(1)	152(1)	123(1)	83(1)
O(1)	214(6)	233(6)	236(6)	101(5)	73(5)	75(5)

O(2)	245(6)	235(6)	171(5)	56(5)	60(5)	61(5)
O(3)	708(11)	648(11)	555(10)	412(9)	504(9)	466(9)
O(4)	538(9)	233(6)	402(8)	172(6)	293(7)	193(6)
N(1)	168(6)	178(6)	173(6)	73(5)	81(5)	50(5)
N(2)	134(6)	158(6)	182(6)	75(5)	80(5)	52(5)
C(1)	150(7)	160(7)	186(7)	87(6)	85(6)	64(5)
C(2)	181(8)	189(7)	248(8)	92(6)	135(6)	42(6)
C(3)	147(7)	167(7)	257(8)	84(6)	115(6)	40(6)
C(4)	217(8)	229(8)	171(7)	87(6)	76(6)	72(6)
C(5)	161(7)	237(8)	181(7)	78(6)	89(6)	36(6)
C(6)	391(11)	247(9)	229(9)	39(7)	95(8)	58(8)
C(7)	641(15)	348(11)	217(9)	39(8)	65(10)	40(10)
C(8)	163(7)	221(7)	160(7)	104(6)	52(6)	62(6)
C(9)	241(9)	295(8)	167(7)	119(7)	68(6)	121(7)
C(10)	839(18)	264(10)	475(13)	141(9)	359(13)	316(11)
C(11)	435(12)	253(9)	448(12)	150(9)	24(10)	80(9)
P(1)	298(3)	220(3)	181(3)	105(2)	117(3)	62(2)
F(1)	457(7)	350(6)	344(6)	146(5)	230(5)	194(5)
F(2)	378(6)	312(6)	215(5)	140(4)	60(4)	47(5)
F(3)	371(6)	317(6)	306(6)	201(5)	134(5)	32(5)

---



	b = 10.4936(3) Å	$\beta = 107.5490(10)^\circ$
	c = 14.0657(4) Å	$\gamma = 94.2860(10)^\circ$
Volume	1415.63(7) Å <sup>3</sup>	
Z	2	
Crystal system	Triclinic	
Space group	P-1	
Density (calculated)	2.047 Mg/m <sup>3</sup>	
F(000)	826	
Data collection program	Bruker APEX2 v2.1-0	
$\theta$ range for data collection	1.95 to 49.96°	
Completeness to $\theta = 49.96^\circ$	82.3 %	
Index ranges	$-20 \leq h \leq 20, -16 \leq k \leq 21, -29 \leq l \leq 26$	
Data collection scan type	$\omega$ scans; 30 settings	
Data reduction program	Bruker SAINT-Plus v7.34A	
Reflections collected	128447	
Independent reflections	24422 [ $R_{\text{int}} = 0.0395$ ]	
Absorption coefficient	7.181 mm <sup>-1</sup>	
Absorption correction	Semi-empirical from equivalents	
Max. and min. transmission	0.7498 and 0.4225	

## Structure Solution and Refinement

Structure solution program	SHELXS-97 (Sheldrick, 2008)
Primary solution method	Direct methods
Secondary solution method	Difference Fourier map
Hydrogen placement	Geometric positions
Structure refinement program	SHELXL-97 (Sheldrick, 2008)
Refinement method	Full matrix least-squares on $F^2$
Data / restraints / parameters	24422 / 0 / 326
Treatment of hydrogen atoms	Riding
Goodness-of-fit on $F^2$	1.404
Final R indices [ $I > 2\sigma(I)$ , 19699 reflections]	$R1 = 0.0277, wR2 = 0.0408$
R indices (all data)	$R1 = 0.0448, wR2 = 0.0426$
Type of weighting scheme used	Sigma
Weighting scheme used	$w = 1/\sigma^2(F_o^2)$
Max shift/error	0.003



Average shift/error	0.000
Largest diff. peak and hole	2.670 and -1.967 e.Å <sup>-3</sup>

### Special Refinement Details

Crystals were mounted on a glass fiber using Paratone oil then placed on the diffractometer under a nitrogen stream at 100K.

Refinement of  $F^2$  against ALL reflections. The weighted R-factor ( $wR$ ) and goodness of fit ( $S$ ) are based on  $F^2$ , conventional R-factors ( $R$ ) are based on  $F$ , with  $F$  set to zero for negative  $F^2$ . The threshold expression of  $F^2 > 2\sigma(F^2)$  is used only for calculating R-factors(gt) etc. and is not relevant to the choice of reflections for refinement. R-factors based on  $F^2$  are statistically about twice as large as those based on  $F$ , and R-factors based on ALL data will be even larger.

All esds (except the esd in the dihedral angle between two l.s. planes) are estimated using the full covariance matrix. The cell esds are taken into account individually in the estimation of esds in distances, angles and torsion angles; correlations between esds in cell parameters are only used when they are defined by crystal symmetry. An approximate (isotropic) treatment of cell esds is used for estimating esds involving l.s. planes.

**Table 2. Atomic coordinates (  $\times 10^4$ ) and equivalent isotropic displacement parameters ( $\text{\AA}^2 \times 10^3$ ) for VJS31 (CCDC 679443).  $U_{eq}$  is defined as the trace of the orthogonalized  $U^{ij}$  tensor.**

	x	y	z	$U_{eq}$
Ir(1)	6868(1)	3473(1)	3365(1)	11(1)
I(1)	6594(1)	3995(1)	1390(1)	19(1)
Cl(1)	8963(1)	2491(1)	3569(1)	15(1)
Cl(2)	4906(1)	4580(1)	3328(1)	17(1)
O(1)	5130(1)	1013(1)	2868(1)	24(1)
O(2)	8079(1)	5197(1)	3801(1)	16(1)
N(1)	8127(1)	4497(1)	5334(1)	15(1)
C(1)	5808(1)	1960(1)	3049(1)	16(1)
C(2)	8464(1)	5344(1)	4744(1)	16(1)
C(3)	7224(1)	3343(1)	4885(1)	15(1)
C(4)	8580(2)	4679(1)	6416(1)	21(1)
As(1)	957(1)	336(1)	2287(1)	12(1)
C(5)	1915(1)	-1066(1)	2029(1)	15(1)
C(6)	1483(2)	-1643(1)	1082(1)	19(1)
C(7)	2180(2)	-2654(1)	888(1)	19(1)
C(8)	3270(2)	-3110(1)	1641(1)	17(1)

C(9)	3678(1)	-2542(1)	2585(1)	17(1)
C(10)	3020(1)	-1504(1)	2786(1)	15(1)
C(11)	-970(1)	-272(1)	1928(1)	16(1)
C(12)	-1314(2)	-1535(1)	2146(1)	20(1)
C(13)	-2694(2)	-1998(1)	1884(1)	25(1)
C(14)	-3737(2)	-1220(1)	1395(1)	27(1)
C(15)	-3392(2)	32(1)	1182(1)	24(1)
C(16)	-2010(2)	514(1)	1448(1)	18(1)
C(17)	1735(1)	836(1)	3659(1)	13(1)
C(18)	1410(1)	92(1)	4394(1)	15(1)
C(19)	2026(2)	455(1)	5387(1)	19(1)
C(20)	2937(2)	1546(1)	5640(1)	21(1)
C(21)	3260(2)	2278(1)	4904(1)	18(1)
C(22)	2660(1)	1926(1)	3905(1)	14(1)
C(23)	1276(1)	1761(1)	1517(1)	14(1)
C(24)	2236(2)	1698(1)	995(1)	17(1)
C(25)	2542(2)	2771(1)	490(1)	21(1)
C(26)	1868(2)	3876(1)	511(1)	21(1)
C(27)	926(2)	3934(1)	1040(1)	19(1)
C(28)	619(1)	2878(1)	1559(1)	15(1)

**Table 3. Selected bond lengths [Å] and angles [°] for VJS31 (CCDC 679443).**

Ir(1)-C(1)	1.8221(12)	C(1)-Ir(1)-C(3)	95.23(5)
Ir(1)-C(3)	2.0651(11)	C(1)-Ir(1)-O(2)	177.07(4)
Ir(1)-O(2)	2.0875(9)	C(3)-Ir(1)-O(2)	81.88(4)
Ir(1)-Cl(2)	2.3565(3)	C(1)-Ir(1)-Cl(2)	91.68(4)
Ir(1)-Cl(1)	2.3610(3)	C(3)-Ir(1)-Cl(2)	87.10(4)
Ir(1)-I(1)	2.76746(12)	O(2)-Ir(1)-Cl(2)	87.69(3)
		C(1)-Ir(1)-Cl(1)	92.81(4)
		C(3)-Ir(1)-Cl(1)	88.00(4)
		O(2)-Ir(1)-Cl(1)	87.60(3)
		Cl(2)-Ir(1)-Cl(1)	173.633(10)
		C(1)-Ir(1)-I(1)	93.06(4)
		C(3)-Ir(1)-I(1)	171.68(3)
		O(2)-Ir(1)-I(1)	89.83(2)
		Cl(2)-Ir(1)-I(1)	91.961(8)
		Cl(1)-Ir(1)-I(1)	92.306(7)

**Table 4. Bond lengths [Å] and angles [°] for VJS31 (CCDC 679443).**

Ir(1)-C(1)	1.8221(12)	As(1)-C(17)	1.9075(11)
Ir(1)-C(3)	2.0651(11)	As(1)-C(5)	1.9107(12)
Ir(1)-O(2)	2.0875(9)	As(1)-C(23)	1.9114(11)
Ir(1)-Cl(2)	2.3565(3)	As(1)-C(11)	1.9147(14)
Ir(1)-Cl(1)	2.3610(3)	C(5)-C(6)	1.3922(16)
Ir(1)-I(1)	2.76746(12)	C(5)-C(10)	1.3964(16)
O(1)-C(1)	1.1455(15)	C(6)-C(7)	1.3867(18)
O(2)-C(2)	1.2704(15)	C(7)-C(8)	1.3927(17)
N(1)-C(2)	1.3112(16)	C(8)-C(9)	1.3857(17)
N(1)-C(4)	1.4590(16)	C(9)-C(10)	1.3885(17)
N(1)-C(3)	1.4766(16)	C(11)-C(16)	1.3931(17)

C(11)-C(12)	1.4025(16)	C(16)-C(11)-C(12)	120.58(13)
C(12)-C(13)	1.378(2)	C(16)-C(11)-As(1)	120.91(9)
C(13)-C(14)	1.393(2)	C(12)-C(11)-As(1)	118.51(10)
C(14)-C(15)	1.391(2)	C(13)-C(12)-C(11)	119.52(13)
C(15)-C(16)	1.385(2)	C(12)-C(13)-C(14)	120.14(12)
C(17)-C(22)	1.3936(17)	C(15)-C(14)-C(13)	120.15(14)
C(17)-C(18)	1.3987(16)	C(16)-C(15)-C(14)	120.32(13)
C(18)-C(19)	1.3860(17)	C(15)-C(16)-C(11)	119.29(12)
C(19)-C(20)	1.3879(19)	C(22)-C(17)-C(18)	121.42(10)
C(20)-C(21)	1.3917(18)	C(22)-C(17)-As(1)	118.50(8)
C(21)-C(22)	1.3889(16)	C(18)-C(17)-As(1)	120.05(9)
C(23)-C(24)	1.3858(19)	C(19)-C(18)-C(17)	118.85(12)
C(23)-C(28)	1.3993(16)	C(18)-C(19)-C(20)	120.21(11)
C(24)-C(25)	1.3967(17)	C(19)-C(20)-C(21)	120.58(11)
C(25)-C(26)	1.392(2)	C(22)-C(21)-C(20)	120.08(12)
C(26)-C(27)	1.377(2)	C(21)-C(22)-C(17)	118.86(11)
C(27)-C(28)	1.3947(16)	C(24)-C(23)-C(28)	121.52(11)
		C(24)-C(23)-As(1)	119.17(8)
C(1)-Ir(1)-C(3)	95.23(5)	C(28)-C(23)-As(1)	119.11(9)
C(1)-Ir(1)-O(2)	177.07(4)	C(23)-C(24)-C(25)	119.21(11)
C(3)-Ir(1)-O(2)	81.88(4)	C(26)-C(25)-C(24)	119.51(13)
C(1)-Ir(1)-Cl(2)	91.68(4)	C(27)-C(26)-C(25)	120.89(11)
C(3)-Ir(1)-Cl(2)	87.10(4)	C(26)-C(27)-C(28)	120.46(11)
O(2)-Ir(1)-Cl(2)	87.69(3)	C(27)-C(28)-C(23)	118.38(12)
C(1)-Ir(1)-Cl(1)	92.81(4)		
C(3)-Ir(1)-Cl(1)	88.00(4)		
O(2)-Ir(1)-Cl(1)	87.60(3)		
Cl(2)-Ir(1)-Cl(1)	173.633(10)		
C(1)-Ir(1)-I(1)	93.06(4)		
C(3)-Ir(1)-I(1)	171.68(3)		
O(2)-Ir(1)-I(1)	89.83(2)		
Cl(2)-Ir(1)-I(1)	91.961(8)		
Cl(1)-Ir(1)-I(1)	92.306(7)		
C(2)-O(2)-Ir(1)	110.68(7)		
C(2)-N(1)-C(4)	122.05(11)		
C(2)-N(1)-C(3)	118.88(10)		
C(4)-N(1)-C(3)	119.04(10)		
O(1)-C(1)-Ir(1)	178.53(12)		
O(2)-C(2)-N(1)	122.74(11)		
N(1)-C(3)-Ir(1)	105.77(7)		
C(17)-As(1)-C(5)	108.17(5)		
C(17)-As(1)-C(23)	107.33(5)		
C(5)-As(1)-C(23)	109.52(5)		
C(17)-As(1)-C(11)	113.69(5)		
C(5)-As(1)-C(11)	105.77(5)		
C(23)-As(1)-C(11)	112.25(5)		
C(6)-C(5)-C(10)	121.05(11)		
C(6)-C(5)-As(1)	118.86(9)		
C(10)-C(5)-As(1)	120.09(9)		
C(7)-C(6)-C(5)	119.21(11)		
C(6)-C(7)-C(8)	120.19(11)		
C(9)-C(8)-C(7)	120.12(11)		
C(8)-C(9)-C(10)	120.50(11)		
C(9)-C(10)-C(5)	118.89(11)		

**Table 5.** Anisotropic displacement parameters ( $\text{\AA}^2 \times 10^4$ ) for VJS31 (CCDC 679443). The anisotropic displacement factor exponent takes the form:  $-2\pi^2 [h^2 a^{*2} U^{11} + \dots + 2 h k a^* b^* U^{12}]$

	$U^{11}$	$U^{22}$	$U^{33}$	$U^{23}$	$U^{13}$	$U^{12}$
Ir(1)	110(1)	105(1)	132(1)	12(1)	42(1)	1(1)
I(1)	231(1)	209(1)	152(1)	44(1)	72(1)	15(1)
Cl(1)	121(1)	153(1)	188(1)	-10(1)	49(1)	10(1)
Cl(2)	144(1)	156(1)	236(1)	27(1)	70(1)	51(1)
O(1)	212(5)	186(4)	295(5)	-26(3)	72(4)	-53(4)
O(2)	162(4)	139(3)	177(4)	1(3)	66(3)	-22(3)
N(1)	137(5)	161(4)	153(4)	-22(3)	54(3)	-3(3)
C(1)	137(5)	164(4)	172(5)	15(4)	50(4)	24(4)
C(2)	135(6)	141(4)	207(5)	-13(4)	67(4)	3(4)
C(3)	170(6)	138(4)	149(4)	10(3)	57(4)	-18(4)
C(4)	203(7)	254(5)	166(5)	-31(4)	67(4)	-21(5)
As(1)	139(1)	115(1)	103(1)	6(1)	23(1)	7(1)
C(5)	165(6)	125(4)	140(4)	6(3)	32(4)	14(4)
C(6)	222(7)	187(5)	137(4)	-11(4)	7(4)	45(4)
C(7)	228(7)	184(5)	157(5)	-33(4)	38(4)	15(4)
C(8)	175(6)	141(4)	206(5)	-10(4)	58(4)	9(4)
C(9)	159(6)	153(4)	185(5)	9(4)	19(4)	12(4)
C(10)	163(6)	147(4)	131(4)	-4(3)	19(4)	-3(4)
C(11)	164(6)	165(4)	131(4)	-20(3)	42(4)	-25(4)
C(12)	269(7)	164(4)	172(5)	-7(4)	77(5)	-34(5)
C(13)	309(8)	231(5)	233(6)	-51(5)	136(6)	-103(5)
C(14)	202(7)	370(7)	239(6)	-99(5)	107(5)	-112(6)
C(15)	174(7)	302(6)	222(6)	-40(5)	46(5)	-3(5)
C(16)	164(6)	190(5)	166(5)	-19(4)	33(4)	-3(4)
C(17)	142(5)	134(4)	111(4)	3(3)	36(4)	22(4)
C(18)	152(6)	162(4)	152(4)	31(4)	54(4)	22(4)
C(19)	185(6)	250(5)	133(4)	46(4)	50(4)	13(5)
C(20)	179(6)	308(6)	125(5)	-14(4)	33(4)	3(5)
C(21)	151(6)	220(5)	155(5)	-28(4)	35(4)	-24(4)
C(22)	145(5)	153(4)	134(4)	4(3)	39(4)	0(4)
C(23)	146(5)	147(4)	107(4)	6(3)	27(4)	-1(4)
C(24)	177(6)	194(5)	147(4)	-5(4)	48(4)	12(4)
C(25)	220(7)	251(5)	159(5)	-8(4)	96(5)	-44(5)
C(26)	289(8)	183(5)	152(5)	19(4)	70(5)	-45(5)
C(27)	246(7)	145(4)	167(5)	28(4)	53(4)	-2(4)
C(28)	169(6)	149(4)	135(4)	11(3)	50(4)	10(4)



Volume	5462.6(4) Å <sup>3</sup>
Z	4
Crystal system	Triclinic
Space group	P-1
Density (calculated)	2.178 Mg/m <sup>3</sup>
F(000)	3336
Data collection program	Bruker APEX2 v2.1-0
θ range for data collection	1.75 to 38.71°
Completeness to θ = 38.71°	91.9 %
Index ranges	-24 ≤ h ≤ 24, -35 ≤ k ≤ 35, -36 ≤ l ≤ 36
Data collection scan type	ω scans; 17 settings
Data reduction program	Bruker SAINT-Plus v7.34A
Reflections collected	225695
Independent reflections	57323 [R <sub>int</sub> = 0.0421]
Absorption coefficient	6.704 mm <sup>-1</sup>
Absorption correction	Semi-empirical from equivalents
Max. and min. transmission	0.7476 and 0.4619

## Structure Solution and Refinement

Structure solution program	SHELXS-97 (Sheldrick, 2008)
Primary solution method	Direct methods
Secondary solution method	Difference Fourier map
Hydrogen placement	Geometric positions
Structure refinement program	SHELXL-97 (Sheldrick, 2008)
Refinement method	Full matrix least-squares on F <sup>2</sup>
Data / restraints / parameters	57323 / 0 / 1153
Treatment of hydrogen atoms	Riding
Goodness-of-fit on F <sup>2</sup>	2.192
Final R indices [I > 2σ(I), 38228 reflections]	R1 = 0.0559, wR2 = 0.0859
R indices (all data)	R1 = 0.0964, wR2 = 0.0882
Type of weighting scheme used	Sigma
Weighting scheme used	w = 1/σ <sup>2</sup> (F <sub>o</sub> <sup>2</sup> )
Max shift/error	0.005
Average shift/error	0.000
Largest diff. peak and hole	8.991 and -6.547 e.Å <sup>-3</sup>

## Special Refinement Details

Crystals were mounted on a glass fiber using Paratone oil then placed on the diffractometer under a nitrogen stream at 100K.

Refinement of  $F^2$  against ALL reflections. The weighted R-factor ( $wR$ ) and goodness of fit ( $S$ ) are based on  $F^2$ , conventional R-factors ( $R$ ) are based on  $F$ , with  $F$  set to zero for negative  $F^2$ . The threshold expression of  $F^2 > 2\sigma(F^2)$  is used only for calculating R-factors(gt) etc. and is not relevant to the choice of reflections for refinement. R-factors based on  $F^2$  are statistically about twice as large as those based on  $F$ , and R-factors based on ALL data will be even larger.

All esds (except the esd in the dihedral angle between two l.s. planes) are estimated using the full covariance matrix. The cell esds are taken into account individually in the estimation of esds in distances, angles and torsion angles; correlations between esds in cell parameters are only used when they are defined by crystal symmetry. An approximate (isotropic) treatment of cell esds is used for estimating esds involving l.s. planes.

**Table 2. Atomic coordinates ( $\times 10^4$ ) and equivalent isotropic displacement parameters ( $\text{\AA}^2 \times 10^3$ ) for VJS30 (CCDC 680342).  $U_{eq}$  is defined as the trace of the orthogonalized  $U^{ij}$  tensor.**

	x	y	z	$U_{eq}$
Ir(1)	6581(1)	5717(1)	3266(1)	16(1)
I(1A)	5461(1)	6676(1)	2969(1)	29(1)
I(2A)	8197(1)	6291(1)	3115(1)	34(1)
I(3A)	7630(1)	4769(1)	3653(1)	27(1)
I(4A)	4982(1)	5146(1)	3427(1)	19(1)
I(5A)	6129(1)	4868(1)	1865(1)	29(1)
O(1A)	7235(2)	6682(2)	4776(2)	34(1)
C(1A)	6983(3)	6317(2)	4208(2)	21(1)
Ir(2)	8813(1)	9279(1)	6831(1)	14(1)
I(1B)	10396(1)	9914(1)	6718(1)	21(1)
I(2B)	7693(1)	10136(1)	6340(1)	30(1)
I(3B)	7211(1)	8616(1)	6911(1)	32(1)
I(4B)	10005(1)	8405(1)	7252(1)	26(1)
I(5B)	9145(1)	10204(1)	8194(1)	29(1)
O(1B)	8307(3)	8261(2)	5345(2)	38(1)
C(1B)	8519(3)	8641(2)	5899(2)	24(1)
As(1)	4992(1)	2020(1)	124(1)	19(1)
C(11A)	4783(3)	2415(2)	1035(2)	21(1)
C(12A)	3941(3)	2156(2)	1139(2)	26(1)

C(13A)	3785(3)	2470(2)	1807(2)	26(1)
C(14A)	4433(4)	3029(2)	2323(2)	29(1)
C(15A)	5281(3)	3283(2)	2219(2)	25(1)
C(16A)	5459(3)	2972(2)	1568(2)	22(1)
C(17A)	6294(3)	1718(2)	215(2)	23(1)
C(18A)	6697(3)	1578(3)	-341(2)	33(1)
C(19A)	7640(4)	1358(3)	-282(3)	39(1)
C(20A)	8183(4)	1285(3)	332(3)	38(1)
C(21A)	7794(4)	1453(3)	897(3)	40(1)
C(22A)	6857(4)	1657(3)	836(2)	38(1)
C(23A)	3990(3)	1256(2)	-502(2)	20(1)
C(24A)	4213(4)	584(3)	-647(2)	33(1)
C(25A)	3469(4)	38(3)	-1125(3)	44(1)
C(26A)	2526(4)	170(3)	-1422(2)	38(1)
C(27A)	2314(3)	835(3)	-1280(2)	29(1)
C(28A)	3034(3)	1385(2)	-825(2)	28(1)
C(29A)	4859(3)	2696(2)	-293(2)	23(1)
C(30A)	4753(3)	2469(3)	-1020(2)	29(1)
C(31A)	4669(4)	2951(3)	-1333(2)	36(1)
C(32A)	4675(4)	3650(3)	-943(3)	36(1)
C(33A)	4793(3)	3880(3)	-216(2)	32(1)
C(34A)	4879(3)	3397(2)	105(2)	27(1)
As(2)	618(1)	2916(1)	-4(1)	21(1)
C(11B)	786(3)	2602(2)	-927(2)	20(1)
C(12B)	1616(3)	2880(2)	-1024(2)	23(1)
C(13B)	1700(3)	2637(2)	-1716(2)	29(1)
C(14B)	996(3)	2129(2)	-2262(2)	28(1)
C(15B)	171(3)	1851(2)	-2155(2)	27(1)
C(16B)	63(3)	2096(2)	-1482(2)	23(1)
C(17B)	-705(3)	3164(2)	-77(2)	25(1)
C(18B)	-1114(4)	3491(3)	-528(3)	38(1)
C(19B)	-2063(4)	3689(3)	-563(3)	44(1)
C(20B)	-2577(4)	3579(3)	-135(3)	45(1)
C(21B)	-2164(4)	3260(3)	318(3)	41(1)
C(22B)	-1214(3)	3046(3)	356(2)	32(1)
C(23B)	1560(3)	3712(2)	639(2)	22(1)
C(24B)	2574(3)	3633(2)	881(2)	25(1)
C(25B)	3241(3)	4211(2)	1347(2)	27(1)
C(26B)	2930(3)	4853(3)	1580(2)	28(1)
C(27B)	1925(3)	4929(2)	1353(2)	31(1)
C(28B)	1233(3)	4356(2)	873(2)	28(1)
C(29B)	819(3)	2192(2)	357(2)	24(1)
C(30B)	846(3)	1524(3)	-74(2)	30(1)
C(31B)	979(4)	1008(3)	206(3)	43(1)
C(32B)	1086(4)	1177(3)	914(3)	43(1)
C(33B)	1056(4)	1835(3)	1335(3)	42(1)
C(34B)	925(3)	2362(3)	1081(2)	36(1)
As(3)	2410(1)	5905(1)	4279(1)	15(1)
C(11C)	2252(3)	4911(2)	3816(2)	16(1)
C(12C)	2357(3)	4618(2)	3140(2)	19(1)
C(13C)	2265(3)	3894(2)	2810(2)	24(1)
C(14C)	2055(3)	3475(2)	3145(2)	23(1)



C(15C)	1957(3)	3775(2)	3826(2)	24(1)
C(16C)	2059(3)	4492(2)	4168(2)	19(1)
C(17C)	2041(3)	6312(2)	3583(2)	18(1)
C(18C)	2708(3)	6354(2)	3212(2)	20(1)
C(19C)	2433(3)	6657(2)	2709(2)	22(1)
C(20C)	1524(3)	6918(2)	2592(2)	27(1)
C(21C)	865(3)	6868(3)	2959(2)	33(1)
C(22C)	1124(3)	6562(2)	3455(2)	25(1)
C(23C)	3765(3)	6262(2)	4840(2)	15(1)
C(24C)	4306(3)	5905(2)	5234(2)	18(1)
C(25C)	5279(3)	6175(2)	5649(2)	21(1)
C(26C)	5696(3)	6799(2)	5678(2)	21(1)
C(27C)	5160(3)	7154(2)	5295(2)	21(1)
C(28C)	4168(3)	6886(2)	4865(2)	19(1)
C(29C)	1584(3)	6155(2)	4888(2)	16(1)
C(30C)	580(3)	5869(2)	4642(2)	23(1)
C(31C)	-9(3)	6068(2)	5093(2)	28(1)
C(32C)	408(3)	6537(2)	5784(2)	29(1)
C(33C)	1394(3)	6821(2)	6029(2)	24(1)
C(34C)	1997(3)	6628(2)	5583(2)	18(1)
As(4)	2747(1)	9193(1)	5727(1)	14(1)
C(11D)	3570(3)	8975(2)	5114(2)	17(1)
C(12D)	3187(3)	8476(2)	4433(2)	21(1)
C(13D)	3816(3)	8278(2)	4006(2)	28(1)
C(14D)	4792(3)	8572(3)	4260(2)	31(1)
C(15D)	5172(3)	9064(3)	4935(2)	32(1)
C(16D)	4558(3)	9281(2)	5368(2)	27(1)
C(17D)	1405(3)	8792(2)	5167(2)	17(1)
C(18D)	1063(3)	8149(2)	5136(2)	20(1)
C(19D)	109(3)	7834(2)	4691(2)	21(1)
C(20D)	-480(3)	8166(2)	4295(2)	20(1)
C(21D)	-134(3)	8806(2)	4329(2)	22(1)
C(22D)	818(3)	9125(2)	4765(2)	20(1)
C(23D)	2843(3)	10180(2)	6193(2)	15(1)
C(24D)	2818(3)	10598(2)	5802(2)	17(1)
C(25D)	2859(3)	11314(2)	6127(2)	19(1)
C(26D)	2927(3)	11612(2)	6843(2)	22(1)
C(27D)	2942(3)	11199(2)	7228(2)	21(1)
C(28D)	2907(3)	10478(2)	6908(2)	19(1)
C(29D)	3200(3)	8774(2)	6407(2)	17(1)
C(30D)	4110(3)	8502(2)	6466(2)	24(1)
C(31D)	4427(3)	8196(3)	6954(2)	29(1)
C(32D)	3848(3)	8163(2)	7383(2)	25(1)
C(33D)	2942(3)	8432(2)	7315(2)	21(1)
C(34D)	2608(3)	8738(2)	6826(2)	19(1)
C(41)	3491(5)	436(4)	1469(4)	69(2)
Cl(1)	3548(1)	337(1)	642(1)	57(1)
Cl(2)	4412(1)	4(1)	1900(1)	67(1)
C(42)	9192(9)	4120(5)	2459(5)	153(6)
Cl(3)	9866(1)	4426(1)	2066(1)	63(1)
Cl(4)	8925(2)	3218(1)	2182(1)	78(1)

C(43)	6646(4)	1318(3)	7641(4)	60(2)
Cl(5)	5344(1)	1243(1)	7380(1)	58(1)
Cl(6)	7213(1)	2108(1)	8286(1)	52(1)
C(44)	1805(4)	4677(3)	8916(3)	44(1)
Cl(7)	600(1)	4430(1)	8911(1)	72(1)
Cl(8)	2716(1)	4663(1)	9653(1)	50(1)

**Table 3.** Selected bond lengths [Å] and angles [°] for VJS30 (CCDC 680342).

Ir(1)-C(1A)	1.847(4)	Ir(2)-C(1B)	1.862(4)
Ir(1)-I(4A)	2.6808(3)	Ir(2)-I(1B)	2.6762(3)
Ir(1)-I(1A)	2.6872(4)	Ir(2)-I(2B)	2.6836(4)
Ir(1)-I(2A)	2.6927(3)	Ir(2)-I(3B)	2.6927(3)
Ir(1)-I(3A)	2.6928(3)	Ir(2)-I(4B)	2.6949(3)
Ir(1)-I(5A)	2.7326(3)	Ir(2)-I(5B)	2.7304(3)
O(1A)-C(1A)	1.116(5)	O(1B)-C(1B)	1.105(5)
C(1A)-Ir(1)-I(4A)	91.38(12)		
C(1A)-Ir(1)-I(1A)	88.32(13)		
I(4A)-Ir(1)-I(1A)	88.437(10)		
C(1A)-Ir(1)-I(2A)	88.21(12)		
I(4A)-Ir(1)-I(2A)	179.467(11)		
I(1A)-Ir(1)-I(2A)	91.892(11)		
C(1A)-Ir(1)-I(3A)	88.49(13)		
I(4A)-Ir(1)-I(3A)	87.846(10)		
I(1A)-Ir(1)-I(3A)	175.046(10)		
I(2A)-Ir(1)-I(3A)	91.801(11)		
C(1A)-Ir(1)-I(5A)	175.39(12)		
I(4A)-Ir(1)-I(5A)	93.191(10)		
I(1A)-Ir(1)-I(5A)	92.390(11)		
I(2A)-Ir(1)-I(5A)	87.215(10)		
I(3A)-Ir(1)-I(5A)	91.087(10)		
O(1A)-C(1A)-Ir(1)	179.2(4)		
C(1B)-Ir(2)-I(1B)	91.46(12)		
C(1B)-Ir(2)-I(2B)	88.34(14)		
I(1B)-Ir(2)-I(2B)	87.586(10)		
C(1B)-Ir(2)-I(3B)	87.09(12)		
I(1B)-Ir(2)-I(3B)	178.550(11)		
I(2B)-Ir(2)-I(3B)	92.361(11)		
C(1B)-Ir(2)-I(4B)	88.87(14)		
I(1B)-Ir(2)-I(4B)	89.352(10)		
I(2B)-Ir(2)-I(4B)	175.802(10)		
I(3B)-Ir(2)-I(4B)	90.626(11)		
C(1B)-Ir(2)-I(5B)	177.11(12)		
I(1B)-Ir(2)-I(5B)	91.131(10)		
I(2B)-Ir(2)-I(5B)	90.484(11)		
I(3B)-Ir(2)-I(5B)	90.319(10)		
I(4B)-Ir(2)-I(5B)	92.448(11)		
O(1B)-C(1B)-Ir(2)	177.3(4)		

**Table 4. Bond lengths [Å] and angles [°] for VJS30 (CCDC 680342).**


---

Ir(1)-C(1A)	1.847(4)
Ir(1)-I(4A)	2.6808(3)
Ir(1)-I(1A)	2.6872(4)
Ir(1)-I(2A)	2.6927(3)
Ir(1)-I(3A)	2.6928(3)
Ir(1)-I(5A)	2.7326(3)
O(1A)-C(1A)	1.116(5)
Ir(2)-C(1B)	1.862(4)
Ir(2)-I(1B)	2.6762(3)
Ir(2)-I(2B)	2.6836(4)
Ir(2)-I(3B)	2.6927(3)
Ir(2)-I(4B)	2.6949(3)
Ir(2)-I(5B)	2.7304(3)
O(1B)-C(1B)	1.105(5)
As(1)-C(29A)	1.897(4)
As(1)-C(23A)	1.905(4)
As(1)-C(11A)	1.913(4)
As(1)-C(17A)	1.913(4)
C(11A)-C(12A)	1.392(6)
C(11A)-C(16A)	1.393(6)
C(12A)-C(13A)	1.408(5)
C(13A)-C(14A)	1.368(6)
C(14A)-C(15A)	1.395(6)
C(15A)-C(16A)	1.390(5)
C(17A)-C(18A)	1.384(5)
C(17A)-C(22A)	1.385(6)
C(18A)-C(19A)	1.386(7)
C(19A)-C(20A)	1.376(7)
C(20A)-C(21A)	1.384(6)
C(21A)-C(22A)	1.368(7)
C(23A)-C(24A)	1.372(6)
C(23A)-C(28A)	1.401(6)
C(24A)-C(25A)	1.396(7)
C(25A)-C(26A)	1.372(7)
C(26A)-C(27A)	1.355(7)
C(27A)-C(28A)	1.373(6)
C(29A)-C(34A)	1.386(6)
C(29A)-C(30A)	1.402(5)
C(30A)-C(31A)	1.378(7)
C(31A)-C(32A)	1.381(7)
C(32A)-C(33A)	1.400(6)
C(33A)-C(34A)	1.390(6)
As(2)-C(17B)	1.905(4)
As(2)-C(11B)	1.908(4)
As(2)-C(29B)	1.909(4)

---

As(2)-C(23B)	1.910(4)
C(11B)-C(12B)	1.389(5)
C(11B)-C(16B)	1.389(6)
C(12B)-C(13B)	1.409(5)
C(13B)-C(14B)	1.371(6)
C(14B)-C(15B)	1.394(6)
C(15B)-C(16B)	1.382(5)
C(17B)-C(18B)	1.370(7)
C(17B)-C(22B)	1.391(6)
C(18B)-C(19B)	1.384(7)
C(19B)-C(20B)	1.379(7)
C(20B)-C(21B)	1.362(8)
C(21B)-C(22B)	1.395(7)
C(23B)-C(28B)	1.375(6)
C(23B)-C(24B)	1.402(6)
C(24B)-C(25B)	1.375(6)
C(25B)-C(26B)	1.361(6)
C(26B)-C(27B)	1.385(6)
C(27B)-C(28B)	1.392(6)
C(29B)-C(30B)	1.363(6)
C(29B)-C(34B)	1.407(6)
C(30B)-C(31B)	1.390(7)
C(31B)-C(32B)	1.376(7)
C(32B)-C(33B)	1.341(8)
C(33B)-C(34B)	1.377(7)
As(3)-C(29C)	1.904(3)
As(3)-C(23C)	1.908(4)
As(3)-C(17C)	1.910(4)
As(3)-C(11C)	1.913(4)
C(11C)-C(12C)	1.390(5)
C(11C)-C(16C)	1.400(5)
C(12C)-C(13C)	1.393(6)
C(13C)-C(14C)	1.380(6)
C(14C)-C(15C)	1.396(5)
C(15C)-C(16C)	1.382(6)
C(17C)-C(22C)	1.382(5)
C(17C)-C(18C)	1.397(5)
C(18C)-C(19C)	1.395(6)
C(19C)-C(20C)	1.379(6)
C(20C)-C(21C)	1.386(6)
C(21C)-C(22C)	1.386(6)
C(23C)-C(28C)	1.385(5)
C(23C)-C(24C)	1.388(5)
C(24C)-C(25C)	1.380(5)
C(25C)-C(26C)	1.386(6)
C(26C)-C(27C)	1.368(6)
C(27C)-C(28C)	1.407(5)
C(29C)-C(34C)	1.392(5)
C(29C)-C(30C)	1.395(5)

C(30C)-C(31C)	1.385(5)
C(31C)-C(32C)	1.383(6)
C(32C)-C(33C)	1.372(6)
C(33C)-C(34C)	1.392(5)
As(4)-C(11D)	1.905(3)
As(4)-C(23D)	1.905(4)
As(4)-C(17D)	1.907(4)
As(4)-C(29D)	1.911(4)
C(11D)-C(12D)	1.385(5)
C(11D)-C(16D)	1.387(5)
C(12D)-C(13D)	1.394(5)
C(13D)-C(14D)	1.365(6)
C(14D)-C(15D)	1.370(6)
C(15D)-C(16D)	1.389(5)
C(17D)-C(18D)	1.385(5)
C(17D)-C(22D)	1.390(5)
C(18D)-C(19D)	1.392(5)
C(19D)-C(20D)	1.380(6)
C(20D)-C(21D)	1.377(6)
C(21D)-C(22D)	1.386(6)
C(23D)-C(28D)	1.390(5)
C(23D)-C(24D)	1.397(5)
C(24D)-C(25D)	1.384(5)
C(25D)-C(26D)	1.393(5)
C(26D)-C(27D)	1.377(6)
C(27D)-C(28D)	1.393(6)
C(29D)-C(30D)	1.389(5)
C(29D)-C(34D)	1.391(5)
C(30D)-C(31D)	1.379(6)
C(31D)-C(32D)	1.394(5)
C(32D)-C(33D)	1.382(6)
C(33D)-C(34D)	1.383(5)
C(41)-Cl(1)	1.716(7)
C(41)-Cl(2)	1.806(7)
C(42)-Cl(3)	1.672(8)
C(42)-Cl(4)	1.746(9)
C(43)-Cl(6)	1.712(6)
C(43)-Cl(5)	1.736(6)
C(44)-Cl(8)	1.733(5)
C(44)-Cl(7)	1.752(5)
C(1A)-Ir(1)-I(4A)	91.38(12)
C(1A)-Ir(1)-I(1A)	88.32(13)
I(4A)-Ir(1)-I(1A)	88.437(10)
C(1A)-Ir(1)-I(2A)	88.21(12)
I(4A)-Ir(1)-I(2A)	179.467(11)
I(1A)-Ir(1)-I(2A)	91.892(11)
C(1A)-Ir(1)-I(3A)	88.49(13)
I(4A)-Ir(1)-I(3A)	87.846(10)

I(1A)-Ir(1)-I(3A)	175.046(10)
I(2A)-Ir(1)-I(3A)	91.801(11)
C(1A)-Ir(1)-I(5A)	175.39(12)
I(4A)-Ir(1)-I(5A)	93.191(10)
I(1A)-Ir(1)-I(5A)	92.390(11)
I(2A)-Ir(1)-I(5A)	87.215(10)
I(3A)-Ir(1)-I(5A)	91.087(10)
O(1A)-C(1A)-Ir(1)	179.2(4)
C(1B)-Ir(2)-I(1B)	91.46(12)
C(1B)-Ir(2)-I(2B)	88.34(14)
I(1B)-Ir(2)-I(2B)	87.586(10)
C(1B)-Ir(2)-I(3B)	87.09(12)
I(1B)-Ir(2)-I(3B)	178.550(11)
I(2B)-Ir(2)-I(3B)	92.361(11)
C(1B)-Ir(2)-I(4B)	88.87(14)
I(1B)-Ir(2)-I(4B)	89.352(10)
I(2B)-Ir(2)-I(4B)	175.802(10)
I(3B)-Ir(2)-I(4B)	90.626(11)
C(1B)-Ir(2)-I(5B)	177.11(12)
I(1B)-Ir(2)-I(5B)	91.131(10)
I(2B)-Ir(2)-I(5B)	90.484(11)
I(3B)-Ir(2)-I(5B)	90.319(10)
I(4B)-Ir(2)-I(5B)	92.448(11)
O(1B)-C(1B)-Ir(2)	177.3(4)
C(29A)-As(1)-C(23A)	106.32(17)
C(29A)-As(1)-C(11A)	109.24(17)
C(23A)-As(1)-C(11A)	110.82(16)
C(29A)-As(1)-C(17A)	110.26(17)
C(23A)-As(1)-C(17A)	109.92(18)
C(11A)-As(1)-C(17A)	110.21(17)
C(12A)-C(11A)-C(16A)	121.9(3)
C(12A)-C(11A)-As(1)	119.1(3)
C(16A)-C(11A)-As(1)	118.9(3)
C(11A)-C(12A)-C(13A)	118.2(4)
C(14A)-C(13A)-C(12A)	119.8(4)
C(13A)-C(14A)-C(15A)	121.8(4)
C(16A)-C(15A)-C(14A)	119.2(4)
C(15A)-C(16A)-C(11A)	119.0(4)
C(18A)-C(17A)-C(22A)	119.2(4)
C(18A)-C(17A)-As(1)	119.5(3)
C(22A)-C(17A)-As(1)	121.2(3)
C(17A)-C(18A)-C(19A)	120.0(4)
C(20A)-C(19A)-C(18A)	120.3(4)
C(19A)-C(20A)-C(21A)	119.5(4)
C(22A)-C(21A)-C(20A)	120.4(5)
C(21A)-C(22A)-C(17A)	120.5(4)
C(24A)-C(23A)-C(28A)	120.3(4)
C(24A)-C(23A)-As(1)	120.1(3)
C(28A)-C(23A)-As(1)	119.6(3)

C(23A)-C(24A)-C(25A)	118.4(4)
C(26A)-C(25A)-C(24A)	120.8(5)
C(27A)-C(26A)-C(25A)	120.4(5)
C(26A)-C(27A)-C(28A)	120.3(4)
C(27A)-C(28A)-C(23A)	119.6(4)
C(34A)-C(29A)-C(30A)	120.4(4)
C(34A)-C(29A)-As(1)	121.5(3)
C(30A)-C(29A)-As(1)	118.1(3)
C(31A)-C(30A)-C(29A)	119.2(4)
C(30A)-C(31A)-C(32A)	120.9(4)
C(31A)-C(32A)-C(33A)	120.1(5)
C(34A)-C(33A)-C(32A)	119.4(5)
C(29A)-C(34A)-C(33A)	120.0(4)
C(17B)-As(2)-C(11B)	108.32(17)
C(17B)-As(2)-C(29B)	110.35(18)
C(11B)-As(2)-C(29B)	109.87(18)
C(17B)-As(2)-C(23B)	108.96(18)
C(11B)-As(2)-C(23B)	111.01(16)
C(29B)-As(2)-C(23B)	108.33(18)
C(12B)-C(11B)-C(16B)	122.2(3)
C(12B)-C(11B)-As(2)	119.7(3)
C(16B)-C(11B)-As(2)	118.2(3)
C(11B)-C(12B)-C(13B)	117.5(4)
C(14B)-C(13B)-C(12B)	120.3(4)
C(13B)-C(14B)-C(15B)	121.5(4)
C(16B)-C(15B)-C(14B)	119.0(4)
C(15B)-C(16B)-C(11B)	119.5(4)
C(18B)-C(17B)-C(22B)	121.3(4)
C(18B)-C(17B)-As(2)	119.2(3)
C(22B)-C(17B)-As(2)	119.4(4)
C(17B)-C(18B)-C(19B)	118.9(5)
C(20B)-C(19B)-C(18B)	120.5(5)
C(21B)-C(20B)-C(19B)	120.4(5)
C(20B)-C(21B)-C(22B)	120.2(5)
C(17B)-C(22B)-C(21B)	118.6(5)
C(28B)-C(23B)-C(24B)	120.6(4)
C(28B)-C(23B)-As(2)	119.6(3)
C(24B)-C(23B)-As(2)	119.7(3)
C(25B)-C(24B)-C(23B)	118.9(4)
C(26B)-C(25B)-C(24B)	121.2(4)
C(25B)-C(26B)-C(27B)	119.9(4)
C(26B)-C(27B)-C(28B)	120.3(4)
C(23B)-C(28B)-C(27B)	119.0(4)
C(30B)-C(29B)-C(34B)	120.5(4)
C(30B)-C(29B)-As(2)	121.1(3)
C(34B)-C(29B)-As(2)	118.4(4)
C(29B)-C(30B)-C(31B)	119.6(4)
C(32B)-C(31B)-C(30B)	119.8(5)
C(33B)-C(32B)-C(31B)	120.3(5)

C(32B)-C(33B)-C(34B)	121.8(5)
C(33B)-C(34B)-C(29B)	118.1(5)
C(29C)-As(3)-C(23C)	108.23(15)
C(29C)-As(3)-C(17C)	110.43(16)
C(23C)-As(3)-C(17C)	108.38(16)
C(29C)-As(3)-C(11C)	108.98(16)
C(23C)-As(3)-C(11C)	111.29(16)
C(17C)-As(3)-C(11C)	109.53(16)
C(12C)-C(11C)-C(16C)	121.2(4)
C(12C)-C(11C)-As(3)	119.0(3)
C(16C)-C(11C)-As(3)	119.8(3)
C(11C)-C(12C)-C(13C)	118.9(4)
C(14C)-C(13C)-C(12C)	120.4(4)
C(13C)-C(14C)-C(15C)	120.1(4)
C(16C)-C(15C)-C(14C)	120.5(4)
C(15C)-C(16C)-C(11C)	118.8(3)
C(22C)-C(17C)-C(18C)	121.0(4)
C(22C)-C(17C)-As(3)	119.8(3)
C(18C)-C(17C)-As(3)	119.2(3)
C(19C)-C(18C)-C(17C)	118.6(4)
C(20C)-C(19C)-C(18C)	120.2(4)
C(19C)-C(20C)-C(21C)	120.6(4)
C(20C)-C(21C)-C(22C)	119.8(4)
C(17C)-C(22C)-C(21C)	119.7(4)
C(28C)-C(23C)-C(24C)	121.9(4)
C(28C)-C(23C)-As(3)	118.7(3)
C(24C)-C(23C)-As(3)	119.4(3)
C(25C)-C(24C)-C(23C)	118.8(4)
C(24C)-C(25C)-C(26C)	120.2(4)
C(27C)-C(26C)-C(25C)	121.0(4)
C(26C)-C(27C)-C(28C)	119.9(4)
C(23C)-C(28C)-C(27C)	118.3(4)
C(34C)-C(29C)-C(30C)	120.4(3)
C(34C)-C(29C)-As(3)	118.9(3)
C(30C)-C(29C)-As(3)	120.6(3)
C(31C)-C(30C)-C(29C)	119.5(4)
C(32C)-C(31C)-C(30C)	119.7(4)
C(33C)-C(32C)-C(31C)	121.1(4)
C(32C)-C(33C)-C(34C)	120.0(4)
C(29C)-C(34C)-C(33C)	119.3(4)
C(11D)-As(4)-C(23D)	109.56(16)
C(11D)-As(4)-C(17D)	107.98(15)
C(23D)-As(4)-C(17D)	111.79(16)
C(11D)-As(4)-C(29D)	108.33(16)
C(23D)-As(4)-C(29D)	110.29(16)
C(17D)-As(4)-C(29D)	108.79(16)
C(12D)-C(11D)-C(16D)	120.9(3)
C(12D)-C(11D)-As(4)	119.0(3)
C(16D)-C(11D)-As(4)	119.9(3)



C(11D)-C(12D)-C(13D)	118.9(4)
C(14D)-C(13D)-C(12D)	120.1(4)
C(13D)-C(14D)-C(15D)	121.1(4)
C(14D)-C(15D)-C(16D)	120.1(4)
C(11D)-C(16D)-C(15D)	118.9(4)
C(18D)-C(17D)-C(22D)	121.5(4)
C(18D)-C(17D)-As(4)	118.7(3)
C(22D)-C(17D)-As(4)	119.7(3)
C(17D)-C(18D)-C(19D)	118.8(4)
C(20D)-C(19D)-C(18D)	119.9(4)
C(21D)-C(20D)-C(19D)	121.0(4)
C(20D)-C(21D)-C(22D)	120.0(4)
C(21D)-C(22D)-C(17D)	118.9(4)
C(28D)-C(23D)-C(24D)	120.4(4)
C(28D)-C(23D)-As(4)	120.5(3)
C(24D)-C(23D)-As(4)	119.1(3)
C(25D)-C(24D)-C(23D)	120.0(3)
C(24D)-C(25D)-C(26D)	119.5(4)
C(27D)-C(26D)-C(25D)	120.6(4)
C(26D)-C(27D)-C(28D)	120.5(4)
C(23D)-C(28D)-C(27D)	119.0(4)
C(30D)-C(29D)-C(34D)	121.2(4)
C(30D)-C(29D)-As(4)	119.3(3)
C(34D)-C(29D)-As(4)	119.5(3)
C(31D)-C(30D)-C(29D)	118.8(3)
C(30D)-C(31D)-C(32D)	120.6(4)
C(33D)-C(32D)-C(31D)	119.8(4)
C(32D)-C(33D)-C(34D)	120.4(3)
C(33D)-C(34D)-C(29D)	119.1(4)
Cl(1)-C(41)-Cl(2)	113.1(4)
Cl(3)-C(42)-Cl(4)	118.5(4)
Cl(6)-C(43)-Cl(5)	113.9(3)
Cl(8)-C(44)-Cl(7)	111.6(3)

**Table 5.** Anisotropic displacement parameters ( $\text{\AA}^2 \times 10^4$ ) for VJS30 (CCDC 680342). The anisotropic displacement factor exponent takes the form:  $-2\pi^2 [h^2 a^{*2} U^{11} + \dots + 2 h k a^* b^* U^{12}]$

	$U^{11}$	$U^{22}$	$U^{33}$	$U^{23}$	$U^{13}$	$U^{12}$
Ir(1)	197(1)	153(1)	132(1)	40(1)	62(1)	-7(1)
I(1A)	392(2)	229(1)	324(2)	180(1)	130(1)	72(1)
I(2A)	332(2)	343(2)	315(2)	43(1)	164(1)	-119(1)
I(3A)	237(1)	257(2)	268(1)	80(1)	51(1)	75(1)
I(4A)	201(1)	191(1)	233(1)	106(1)	97(1)	29(1)
I(5A)	361(2)	267(2)	218(1)	68(1)	74(1)	-37(1)
O(1A)	450(20)	305(19)	172(14)	14(13)	79(14)	-16(15)

C(1A)	210(20)	210(20)	240(20)	107(17)	57(17)	10(17)
Ir(2)	142(1)	162(1)	125(1)	45(1)	47(1)	14(1)
I(1B)	200(1)	219(1)	265(1)	126(1)	116(1)	37(1)
I(2B)	278(2)	350(2)	250(1)	130(1)	47(1)	138(1)
I(3B)	220(2)	379(2)	317(2)	82(1)	104(1)	-91(1)
I(4B)	291(2)	266(2)	341(2)	196(1)	146(1)	109(1)
I(5B)	394(2)	256(2)	208(1)	60(1)	100(1)	-23(1)
O(1B)	510(20)	390(20)	171(15)	32(14)	111(15)	-28(17)
C(1B)	270(20)	240(20)	240(20)	102(18)	102(18)	31(18)
As(1)	226(2)	212(2)	148(2)	67(2)	61(2)	36(2)
C(11A)	290(20)	220(20)	167(18)	101(16)	100(16)	67(17)
C(12A)	320(20)	250(20)	210(20)	88(18)	91(18)	59(19)
C(13A)	280(20)	340(30)	240(20)	158(19)	121(18)	110(20)
C(14A)	470(30)	260(20)	210(20)	112(18)	160(20)	200(20)
C(15A)	390(30)	180(20)	201(19)	80(17)	93(18)	90(19)
C(16A)	290(20)	190(20)	158(18)	79(16)	38(16)	28(17)
C(17A)	250(20)	220(20)	217(19)	70(17)	61(17)	31(17)
C(18A)	300(30)	400(30)	310(20)	130(20)	120(20)	60(20)
C(19A)	300(30)	490(30)	440(30)	180(30)	190(20)	90(20)
C(20A)	220(20)	330(30)	490(30)	60(20)	80(20)	50(20)
C(21A)	340(30)	550(40)	330(30)	230(30)	50(20)	160(20)
C(22A)	420(30)	510(30)	240(20)	170(20)	130(20)	190(30)
C(23A)	250(20)	210(20)	135(17)	48(15)	57(16)	32(17)
C(24A)	280(20)	300(30)	300(20)	40(20)	0(20)	50(20)
C(25A)	400(30)	170(20)	530(30)	-30(20)	30(30)	40(20)
C(26A)	400(30)	310(30)	280(20)	20(20)	30(20)	-60(20)
C(27A)	230(20)	410(30)	220(20)	120(20)	29(17)	30(20)
C(28A)	350(30)	280(20)	240(20)	118(19)	93(19)	100(20)
C(29A)	210(20)	290(20)	202(19)	127(18)	49(16)	26(18)
C(30A)	290(20)	360(30)	220(20)	130(20)	54(18)	-10(20)
C(31A)	400(30)	450(30)	230(20)	170(20)	40(20)	-10(20)
C(32A)	360(30)	450(30)	360(30)	280(20)	90(20)	110(20)
C(33A)	310(30)	340(30)	400(30)	230(20)	140(20)	140(20)
C(34A)	310(20)	290(20)	250(20)	126(19)	110(19)	86(19)
As(2)	200(2)	259(2)	158(2)	71(2)	56(2)	5(2)
C(11B)	220(20)	250(20)	171(18)	106(16)	80(16)	63(17)
C(12B)	230(20)	260(20)	206(19)	110(17)	60(16)	49(17)
C(13B)	350(30)	330(30)	300(20)	160(20)	210(20)	140(20)
C(14B)	320(20)	360(30)	210(20)	128(19)	110(19)	190(20)
C(15B)	350(30)	220(20)	200(20)	57(17)	34(18)	122(19)
C(16B)	260(20)	240(20)	216(19)	114(17)	68(17)	50(18)
C(17B)	190(20)	250(20)	240(20)	51(18)	46(17)	-5(17)
C(18B)	310(30)	460(30)	370(30)	150(20)	120(20)	100(20)
C(19B)	260(30)	590(40)	480(30)	230(30)	80(20)	130(30)
C(20B)	210(30)	400(30)	630(40)	70(30)	130(30)	20(20)
C(21B)	300(30)	410(30)	540(30)	140(30)	200(30)	0(20)

C(22B)	260(20)	370(30)	310(20)	80(20)	120(20)	-30(20)
C(23B)	200(20)	280(20)	173(18)	65(17)	63(16)	24(17)
C(24B)	260(20)	290(20)	210(20)	103(18)	74(17)	49(19)
C(25B)	180(20)	380(30)	240(20)	140(20)	36(17)	11(19)
C(26B)	260(20)	330(30)	193(19)	64(19)	25(17)	-40(20)
C(27B)	330(30)	260(20)	250(20)	10(19)	80(20)	30(20)
C(28B)	210(20)	330(30)	230(20)	41(19)	62(17)	34(19)
C(29B)	200(20)	340(20)	220(20)	163(19)	50(17)	-17(18)
C(30B)	330(30)	340(30)	290(20)	190(20)	80(20)	40(20)
C(31B)	440(30)	400(30)	500(30)	260(30)	100(30)	100(20)
C(32B)	340(30)	560(40)	540(30)	440(30)	20(20)	-30(30)
C(33B)	350(30)	640(40)	300(30)	290(30)	0(20)	-140(30)
C(34B)	330(30)	500(30)	210(20)	140(20)	24(19)	-130(20)

As(3)	137(2)	169(2)	133(2)	61(2)	35(1)	34(2)
C(11C)	135(18)	147(18)	188(17)	50(15)	41(15)	4(14)
C(12C)	168(19)	210(20)	180(18)	73(16)	38(15)	13(16)
C(13C)	230(20)	260(20)	179(19)	48(17)	26(16)	49(18)
C(14C)	170(20)	170(20)	270(20)	32(17)	26(17)	12(16)
C(15C)	180(20)	250(20)	310(20)	149(19)	57(17)	4(17)
C(16C)	172(19)	230(20)	168(17)	67(16)	49(15)	1(16)
C(17C)	200(20)	158(18)	175(17)	76(15)	50(15)	39(15)
C(18C)	200(20)	180(20)	225(19)	76(16)	90(16)	44(16)
C(19C)	270(20)	210(20)	176(18)	80(16)	67(16)	39(17)
C(20C)	300(20)	330(30)	200(20)	157(19)	45(18)	60(20)
C(21C)	230(20)	430(30)	420(30)	270(20)	90(20)	160(20)
C(22C)	170(20)	340(20)	300(20)	180(20)	52(17)	88(18)
C(23C)	134(18)	162(18)	147(16)	41(14)	47(14)	37(14)
C(24C)	166(19)	220(20)	178(17)	100(16)	47(15)	35(16)
C(25C)	190(20)	250(20)	188(18)	128(17)	16(15)	58(17)
C(26C)	170(20)	220(20)	179(18)	48(16)	22(15)	1(16)
C(27C)	220(20)	190(20)	207(19)	71(16)	26(16)	9(17)
C(28C)	173(19)	200(20)	198(18)	91(16)	33(15)	41(16)
C(29C)	161(18)	172(18)	184(17)	92(15)	66(15)	63(15)
C(30C)	170(20)	260(20)	221(19)	46(17)	47(16)	17(17)
C(31C)	170(20)	350(30)	280(20)	80(20)	88(18)	-41(19)
C(32C)	260(20)	350(30)	300(20)	100(20)	180(20)	50(20)
C(33C)	290(20)	210(20)	198(19)	28(17)	108(17)	40(18)
C(34C)	163(19)	170(19)	182(17)	48(15)	55(15)	9(15)

As(4)	129(2)	173(2)	132(2)	63(2)	36(1)	22(2)
C(11D)	157(18)	178(19)	187(18)	85(15)	55(15)	33(15)
C(12D)	180(20)	220(20)	211(19)	58(16)	74(16)	-8(16)
C(13D)	310(20)	260(20)	230(20)	4(18)	145(19)	-6(19)
C(14D)	280(20)	360(30)	340(20)	100(20)	210(20)	10(20)
C(15D)	200(20)	430(30)	310(20)	100(20)	107(19)	-50(20)
C(16D)	170(20)	350(30)	240(20)	66(19)	54(17)	-48(18)
C(17D)	160(18)	210(20)	143(16)	71(15)	51(14)	22(15)
C(18D)	155(19)	190(20)	227(19)	87(16)	21(15)	31(16)

C(19D)	200(20)	164(19)	232(19)	64(16)	26(16)	-3(16)
C(20D)	137(19)	240(20)	180(18)	49(16)	14(15)	13(16)
C(21D)	190(20)	290(20)	191(18)	129(17)	30(16)	42(17)
C(22D)	190(20)	240(20)	218(19)	139(17)	77(16)	45(16)
C(23D)	117(17)	161(18)	166(17)	56(15)	24(14)	-5(14)
C(24D)	129(18)	230(20)	157(17)	86(16)	26(14)	-8(15)
C(25D)	120(18)	230(20)	245(19)	118(17)	52(15)	14(15)
C(26D)	170(20)	180(20)	250(20)	30(17)	60(16)	-4(16)
C(27D)	200(20)	210(20)	161(17)	26(16)	36(15)	-15(16)
C(28D)	143(18)	250(20)	190(18)	116(16)	44(15)	0(16)
C(29D)	191(19)	160(18)	143(16)	65(15)	33(14)	34(15)
C(30D)	170(20)	330(20)	290(20)	171(19)	104(17)	97(18)
C(31D)	190(20)	450(30)	310(20)	200(20)	110(18)	150(20)
C(32D)	280(20)	300(20)	210(20)	160(18)	61(17)	82(19)
C(33D)	190(20)	270(20)	166(18)	84(17)	77(15)	42(17)
C(34D)	172(19)	220(20)	187(18)	99(16)	45(15)	45(16)
C(41)	870(50)	500(40)	790(50)	270(40)	340(40)	220(40)
CI(1)	827(11)	386(8)	627(9)	207(7)	414(9)	199(8)
CI(2)	877(12)	584(11)	482(9)	92(8)	250(9)	35(9)
C(42)	2610(130)	800(70)	1230(80)	-230(60)	1510(90)	-360(80)
CI(3)	425(8)	747(12)	658(10)	273(9)	69(7)	91(8)
CI(4)	1432(17)	569(11)	588(10)	272(8)	634(11)	207(11)
C(43)	400(30)	610(40)	770(40)	230(40)	180(30)	110(30)
CI(5)	373(8)	816(12)	438(8)	161(8)	59(6)	69(8)
CI(6)	484(8)	634(10)	463(8)	212(7)	148(7)	-30(7)
C(44)	440(30)	490(40)	340(30)	120(30)	120(20)	90(30)
CI(7)	323(8)	594(11)	1311(16)	479(11)	197(9)	149(7)
CI(8)	428(8)	442(8)	596(9)	229(7)	77(7)	67(6)

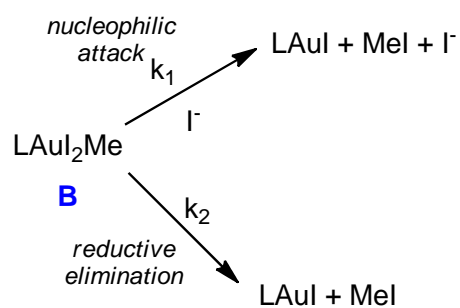
---

## APPENDIX B

### Rate law derivations for kinetic studies on (Idipp)AuI<sub>2</sub>Me

**For pathways from 4-coordinate Au**

*For the case without excess I<sub>2</sub>:*



For nucleophilic attack at 4-coordinate Au:

$$\text{rate}_{\text{Nu}} = k_1[\text{B}][\text{I}^-]$$

-predicts a first-order dependence of the rate on  $[\text{I}^-]$

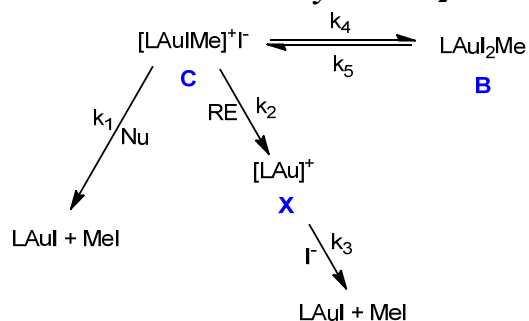
For reductive elimination:

$$\text{rate}_{\text{RE}} = k_2[\text{B}]$$

-predicts no dependence of the rate on  $[\text{I}^-]$

**For pathways from 3-coordinate Au:**

**For the case without any excess  $I_2$ :**



Assume  $k_3 \gg k_2$  because  $[LAu(NCMe)]^+$  is known (Nolan, 2009) and no Au(I) species other than LAuI is observed

Assume steady state in [C]

For nucleophilic attack at 3-coordinate Au:

$$\frac{d[A]}{dt} = 0 = -k_4[C][I^-] + k_5[B] - k_1[C][I^-]$$

$$[A] = \frac{k_5[B]}{[I^-](k_4 + k_1)}$$

$$\text{rate}_{\text{Nu}} = k_1[C][I^-] = \frac{k_1 k_5 [B][I^-]}{[I^-](k_4 + k_1)} = \frac{k_1 k_5 [B]}{k_4 + k_1} \text{ which simplifies to } \frac{k_1 [B]}{K_1(\text{pre-equil})} \text{ for } k_4 \gg k_1$$

-predicts no dependence of the rate on  $[I^-]$

For reductive elimination (again assumes  $k_3 \gg k_2$ ):

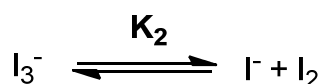
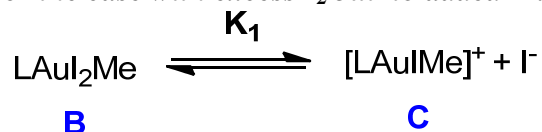
$$\frac{d[A]}{dt} = 0 = -k_4[C][I^-] + k_5[B] - k_1[C]$$

$$[C] = \frac{k_5[B]}{k_4[I^-] + k_2}$$

$$\text{rate}_{\text{RE}} = k_2[C] = \frac{k_2 k_5 [B]}{k_4[I^-] + k_2}$$

- predicts an inverse dependence on  $[I^-]$

For the case with excess  $I_2$  but no added  $I^-$  :



Assume  $K_1$  is small; since  $K_2$  is also small, the  $[I_2] \sim$  amount added in excess

1) by charge balance,  $[C] = [I^-] + [I_3^-]$

$$2) K_2 = \frac{[I^-][I_2]}{[I_3^-]} \quad \text{rearrange} \quad [I_3^-] = \frac{[I^-][I_2]}{K_2}$$

$$\text{Eq. 1 becomes: } [C] = [I^-] + \frac{[I^-][I_2]}{K_2}$$

$$\text{But } [I_2] \gg K_2, \text{ so : } [C] \sim \frac{[I^-][I_2]}{K_2} \quad \text{and rearrange: } [I^-] = \frac{[C]K_2}{[I_2]}$$

3)  $[B] = [B]_0 - [C]$  where  $[B]_0$  = concentration of B at  $t = 0$

4)  $K_1 = \frac{[C][I^-]}{[B]}$  substitute in  $[I^-]$  (from Eq. 1 and 2) and  $[B]$  (from Eq 3):

$$K_1 = \frac{K_2[C]^2}{[I_2]([B]_0 - [C])}$$

Solve for  $[C]$ :

$$[C] = \frac{(-K_1[I_2]/K_2) + \{(K_1[I_2]/K_2)^2 + 4K_1[I_2][B]_0/K_2\}^{1/2}}{2}$$

Since  $K_1$  is small:

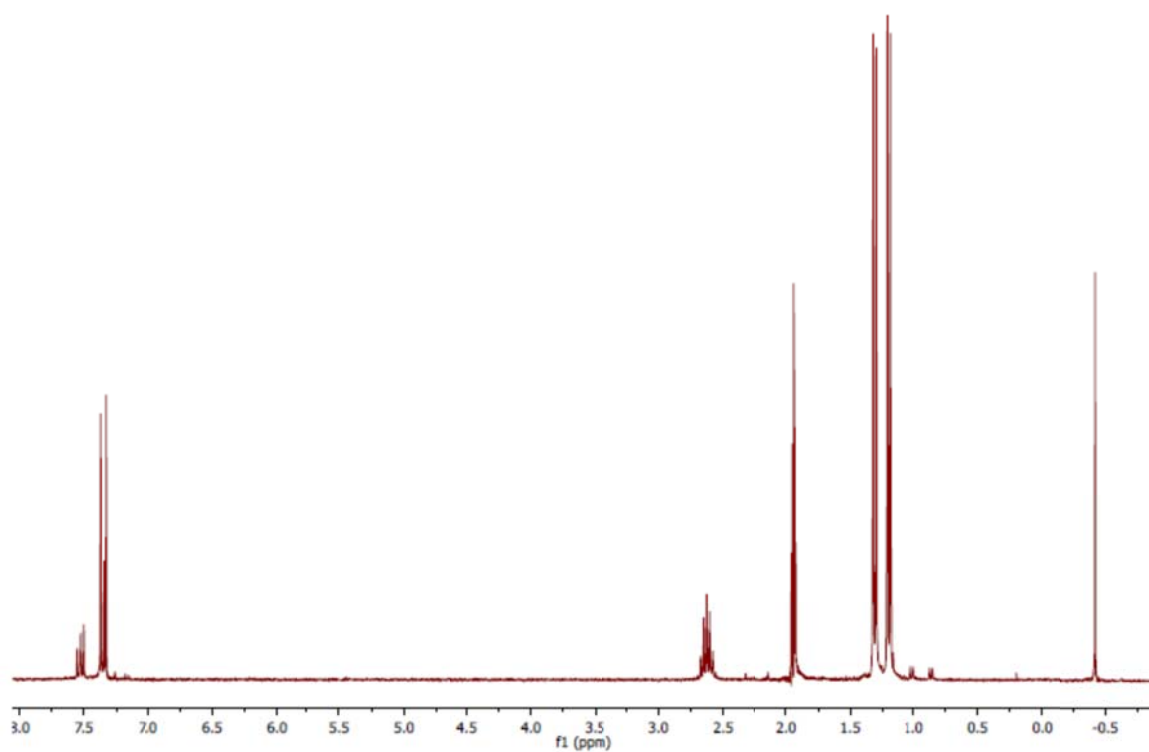
$$[C] \sim (K_1[I_2][B]_0/K_2)^{1/2}$$

- $\frac{1}{2}$  order in  $[B]_0$  initially
- initial rate should be proportional to  $[I_2]^{1/2}$

## APPENDIX C

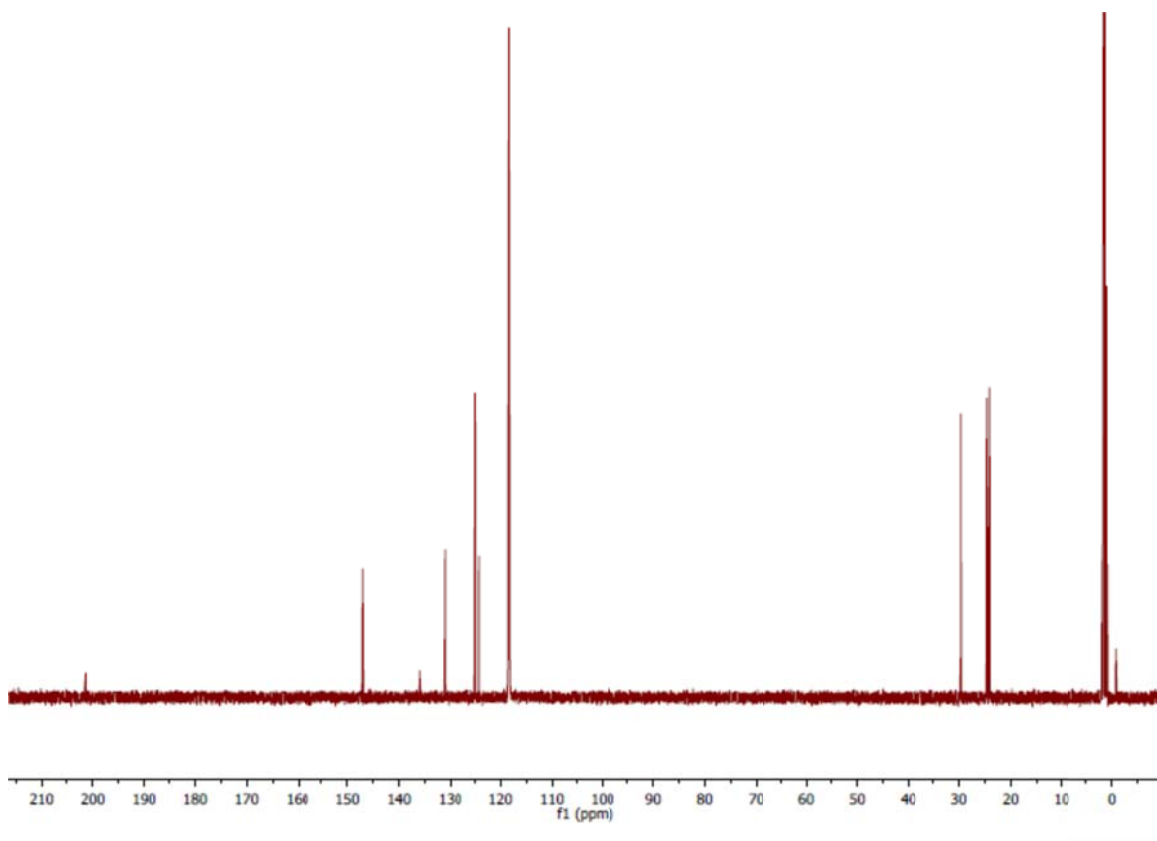
### NMR and mass spectral data for (Idipp)Au-complexes

#### C.1 (Idipp)AuMe (A) $^1\text{H}$ , $^{13}\text{C}$



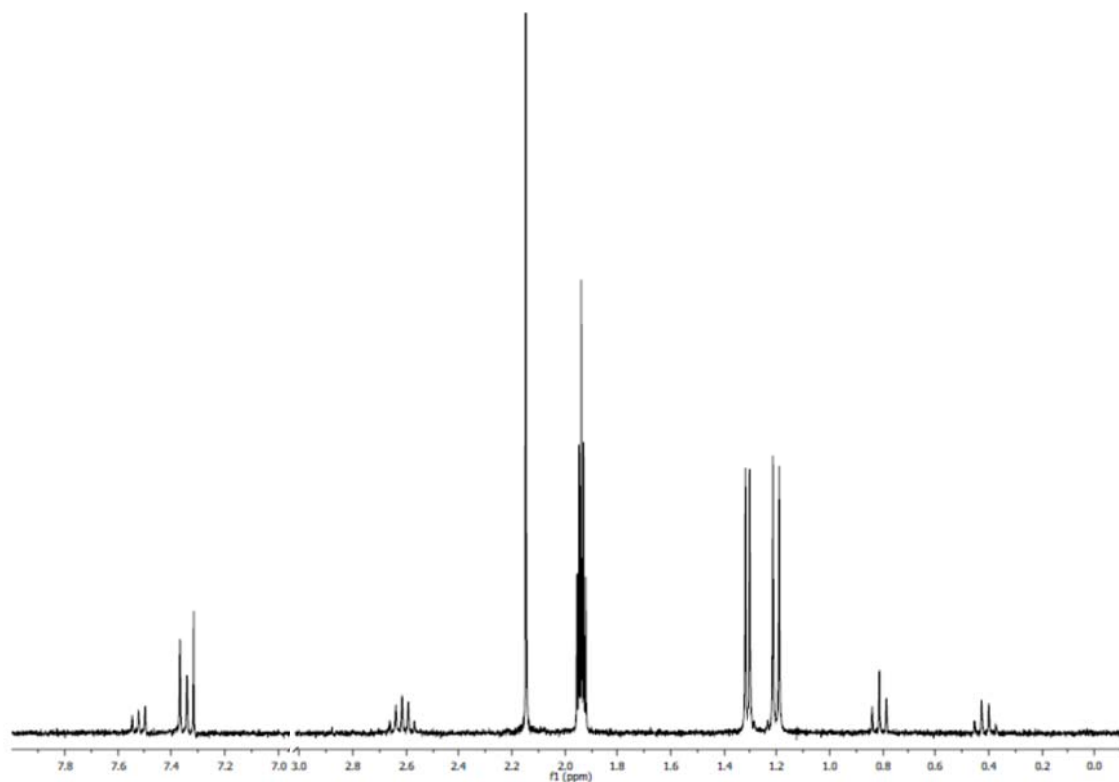
$^1\text{H}$  NMR ( $\text{CD}_3\text{CN}$ ):  $\delta$  7.53 (t,  $J = 9$  Hz, 2H,  $p$ -ArH), 7.37 (d,  $^3J_{\text{HH}} = 9$  Hz, 4 H,  $m$ -ArH), 7.34 (s, 2H, NHC backbone), 2.64 (sep,  $^3J_{\text{HH}} = 6$  Hz, 4H,  $\text{CH}(\text{CH}_3)_2$ ), 1.32 (d,  $^3J_{\text{HH}} = 3$  Hz, 6H,  $\text{CH}(\text{CH}_3)_2$ ), 1.21 (d,  $^3J_{\text{HH}} = 3$  Hz, 6H,  $\text{CH}(\text{CH}_3)_2$ ), -0.41 (d,  $^1J_{\text{CH}} = 120$  Hz, 3H,  $\text{CH}_3$ ).



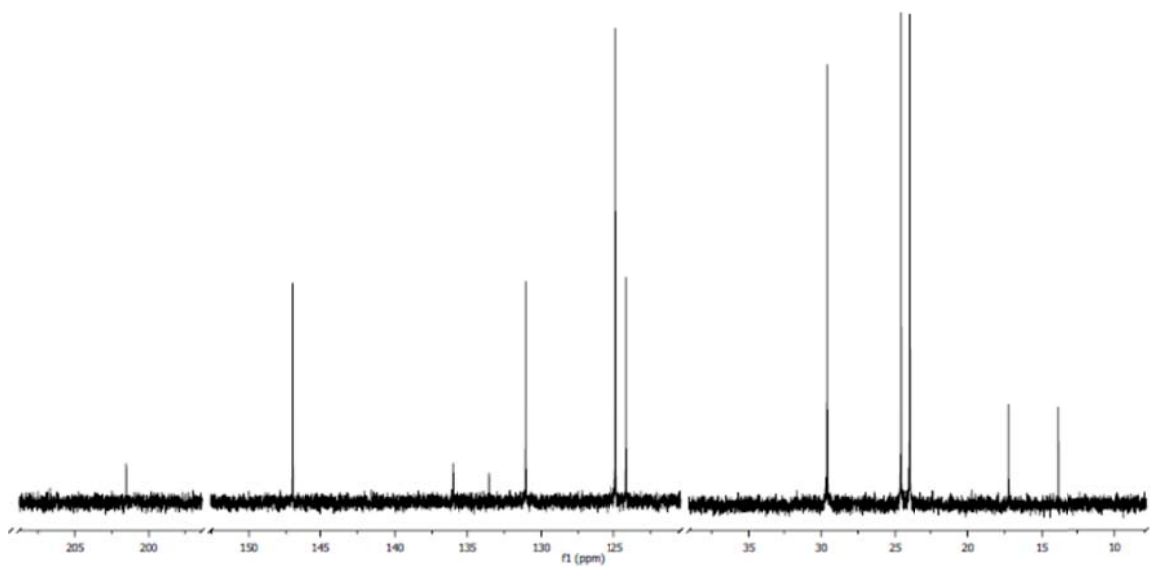


$^{13}\text{C}$  NMR ( $\text{CD}_3\text{CN}$ ):  $\delta$  201.4 ( $^2J_{\text{CC}} = 32.5$  Hz, carbene), 147.1 (Ar), 136.1 (Ar), 131.1 (Ar), 124.9 (NHC backbone), 124.2 (Ar), 29.5 ( $i\text{Pr}$ ), 24.5 ( $i\text{Pr}$ ), 23.9 ( $i\text{Pr}$ ), -0.8 (Me).

**C.2 (Idipp)AuEt (E)  $^1\text{H}$ ,  $^{13}\text{C}$**

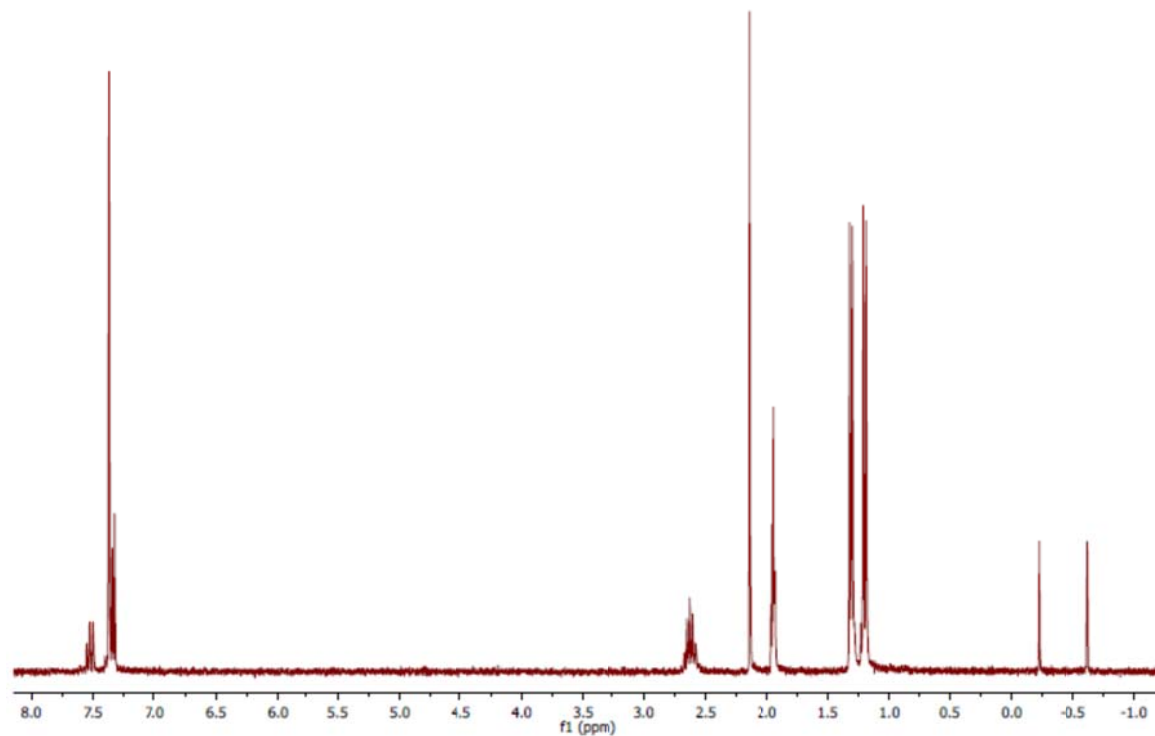


$^1\text{H}$  NMR ( $\text{CD}_3\text{CN}$ ):  $\delta$  7.52 (t,  $J = 9$  Hz, 2H,  $p$ -ArH), 7.35 (d,  $J = 9$  Hz, 4 H,  $m$ -ArH), 7.32 (s, 2H, NHC backbone), 2.62 (sep,  $J = 6$  Hz, 4H,  $\text{CH}(\text{CH}_3)_2$ ), 1.31 (d,  $J = 3$  Hz, 6H,  $\text{CH}(\text{CH}_3)_2$ ), 1.20 (d,  $J = 3$  Hz, 6H,  $\text{CH}(\text{CH}_3)_2$ ), 0.82 (t,  $J = 8$  Hz, 3H,  $\text{CH}_2\text{CH}_3$ ), 0.43 (q,  $J = 8$  Hz, 2H,  $\text{CH}_2\text{CH}_3$ ).

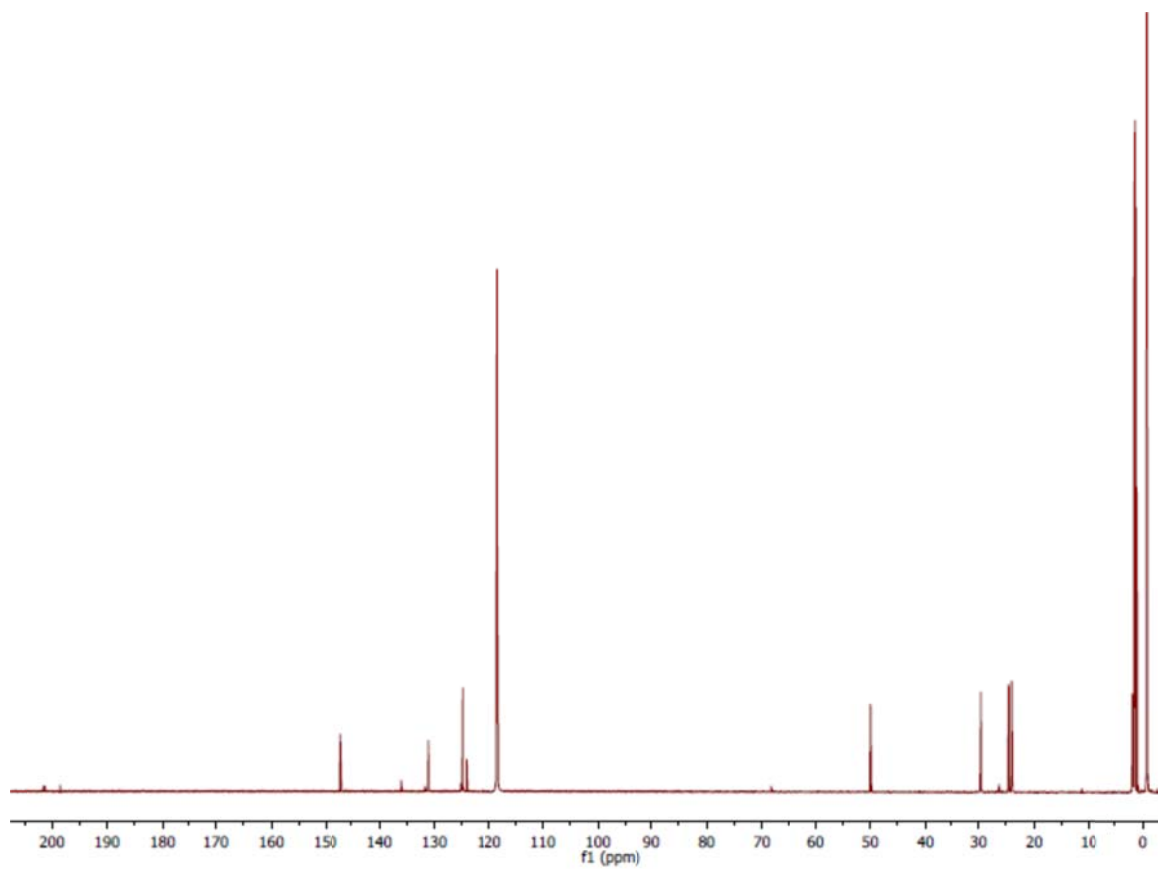


$^{13}\text{C}$  NMR ( $\text{CD}_3\text{CN}$ ):  $\delta$  201.6 (carbene), 147.1 (Ar), 136.1 (Ar), 131.1 (Ar), 124.9 (NHC backbone), 124.2 (Ar), 29.6 ( $i\text{Pr}$ ), 24.6 ( $i\text{Pr}$ ), 24.0 ( $i\text{Pr}$ ), 17.3 (Et), 13.9 (Et).

**C.3 (Idipp)Au<sup>13</sup>CH<sub>3</sub> <sup>1</sup>H, <sup>13</sup>C**

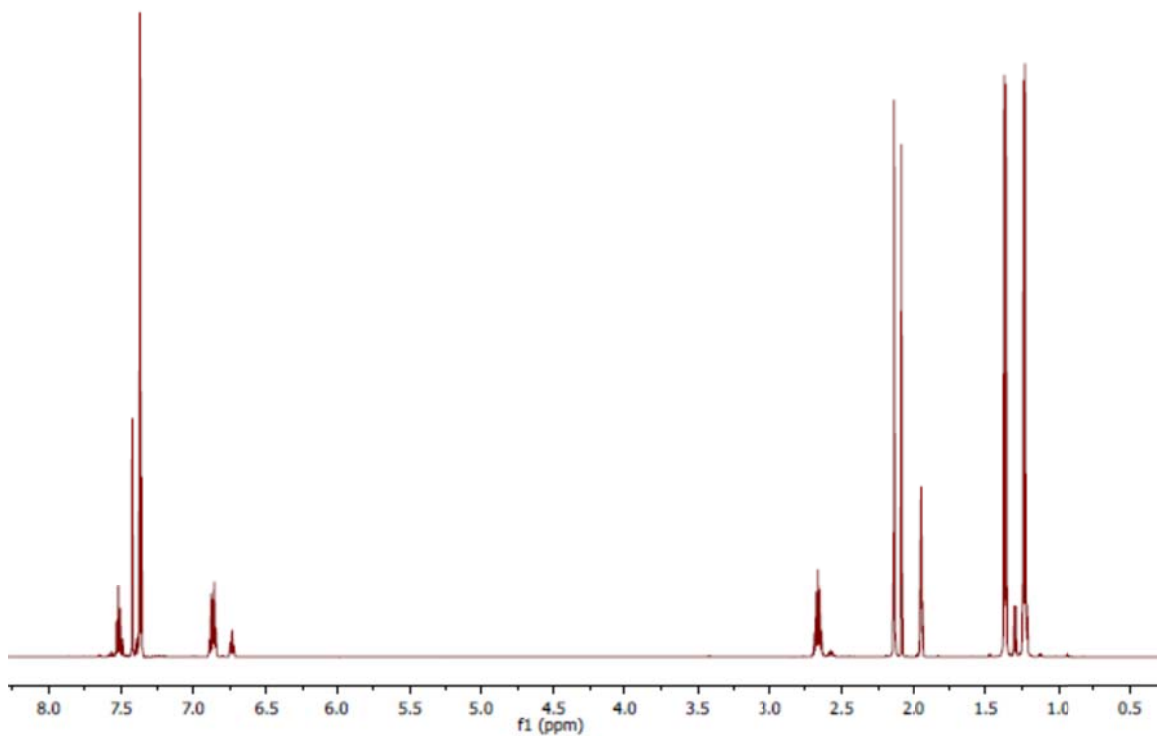


<sup>1</sup>H NMR (CD<sub>3</sub>CN): δ 7.53 (t, *J* = 9 Hz, 2H, *p*-ArH), 7.37 (d, <sup>3</sup>*J*<sub>HH</sub> = 9 Hz, 4 H, *m*-ArH), 7.34 (s, 2H, NHC backbone), 2.64 (sep, <sup>3</sup>*J*<sub>HH</sub> = 6 Hz, 4H, CH(CH<sub>3</sub>)<sub>2</sub>), 1.32 (d, <sup>3</sup>*J*<sub>HH</sub> = 3 Hz, 6H, CH(CH<sub>3</sub>)<sub>2</sub>), 1.21 (d, <sup>3</sup>*J*<sub>HH</sub> = 3 Hz, 6H, CH(CH<sub>3</sub>)<sub>2</sub>), -0.41 (d, <sup>1</sup>*J*<sub>CH</sub> = 120 Hz, 3H, CH<sub>3</sub>).

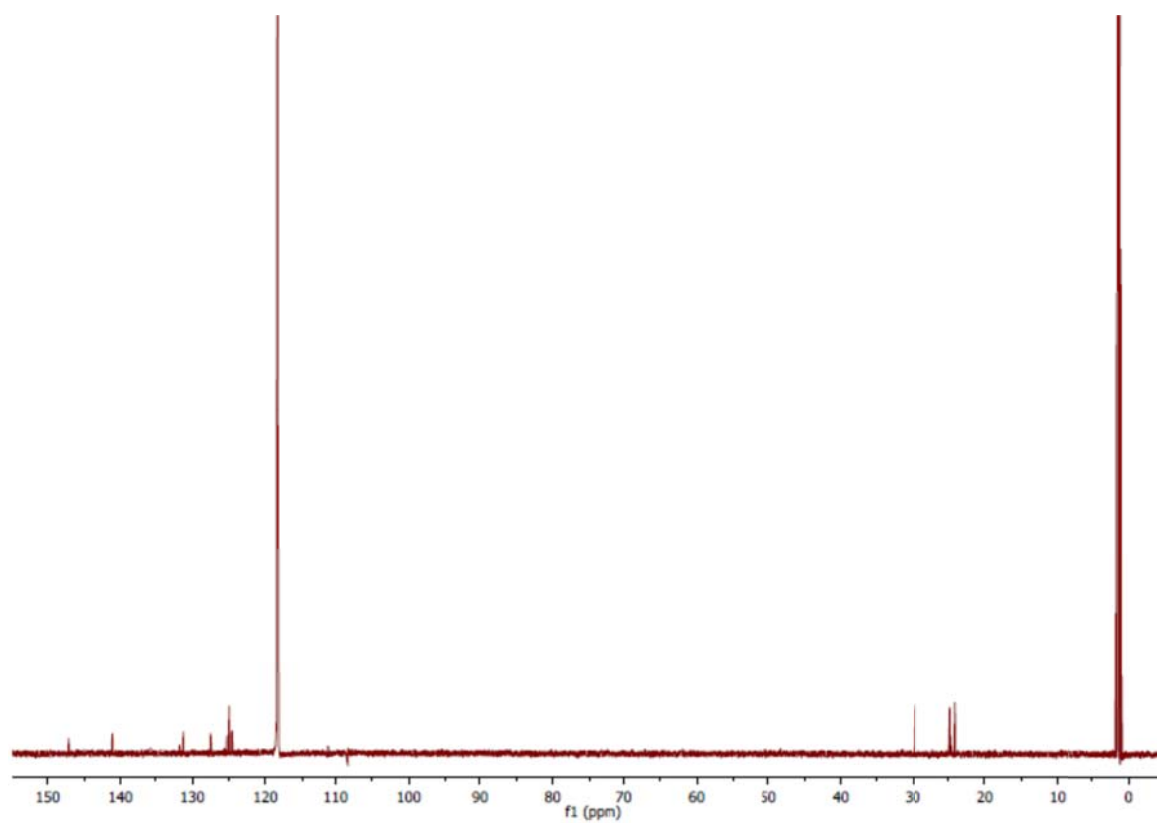


$^{13}\text{C}$  NMR ( $\text{CD}_3\text{CN}$ ):  $\delta$  201.4 ( $^2J_{\text{CC}} = 32.5$  Hz, carbene), 147.1 (Ar), 136.1 (Ar), 131.1 (Ar), 124.9 (NHC backbone), 124.2 (Ar), 29.5 ( $i\text{Pr}$ ), 24.5 ( $i\text{Pr}$ ), 23.9 ( $i\text{Pr}$ ), -0.8 (Me).

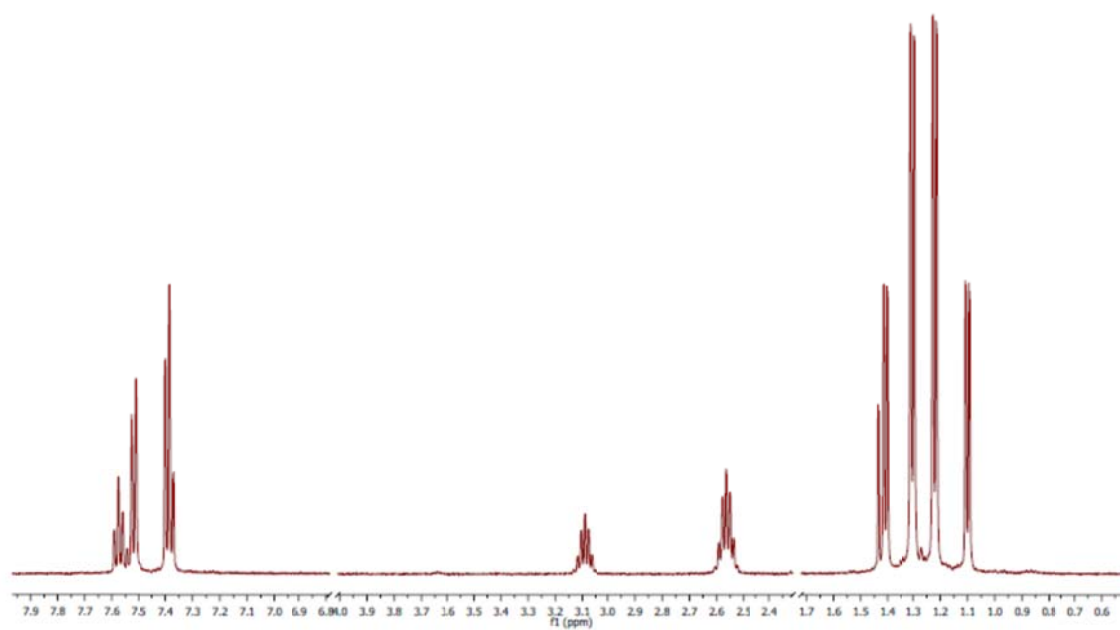
**C.4 (Idipp)AuPh (F)  $^1\text{H}$ ,  $^{13}\text{C}$**



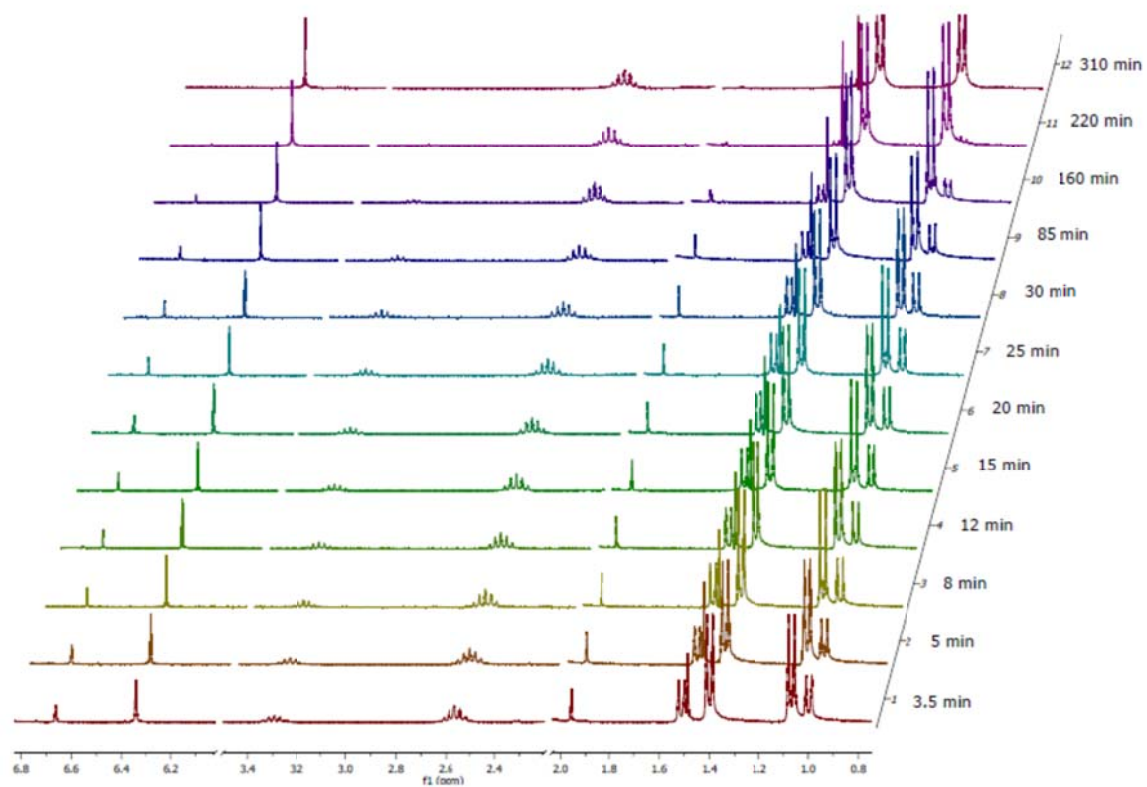
$^1\text{H}$  NMR ( $\text{CD}_3\text{CN}$ ):  $\delta$  7.52 (t,  $J = 9$  Hz, 2H,  $p$ -ArH), 7.42 (s, 2H, NHC backbone), 7.37 (d,  $^3J_{\text{HH}} = 6$  Hz, 4 H,  $m$ -ArH), 6.90-6.70 (m, Ph), 2.66 (sep,  $^3J_{\text{HH}} = 6$  Hz, 4H,  $\text{CH}(\text{CH}_3)_2$ ), 1.36 (d,  $^3J_{\text{HH}} = 6$  Hz, 6H,  $\text{CH}(\text{CH}_3)_2$ ), 1.23 (d,  $^3J_{\text{HH}} = 6$  Hz, 6H,  $\text{CH}(\text{CH}_3)_2$ ).



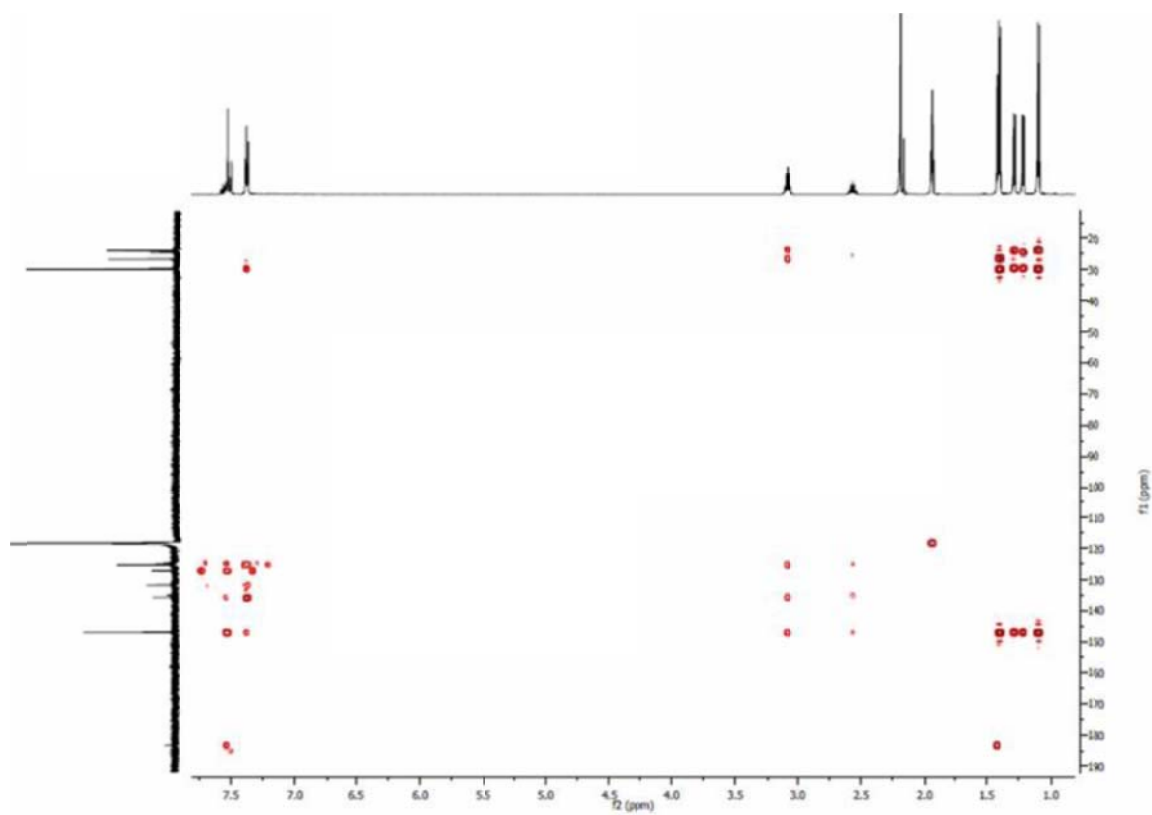
$^{13}\text{C}$  NMR ( $\text{CD}_3\text{CN}$ ):  $\delta$  carbene unresolved, 147.1, 141.0, 131.7, 131.2, 127.5, 125.3, 125.0, 124.6, 124.2, 26.7 ( $i\text{Pr}$ ), 24.8 ( $i\text{Pr}$ ), 24.0 ( $i\text{Pr}$ ).

**C.5  $^1\text{H}$  spectrum of A + I<sub>2</sub>**

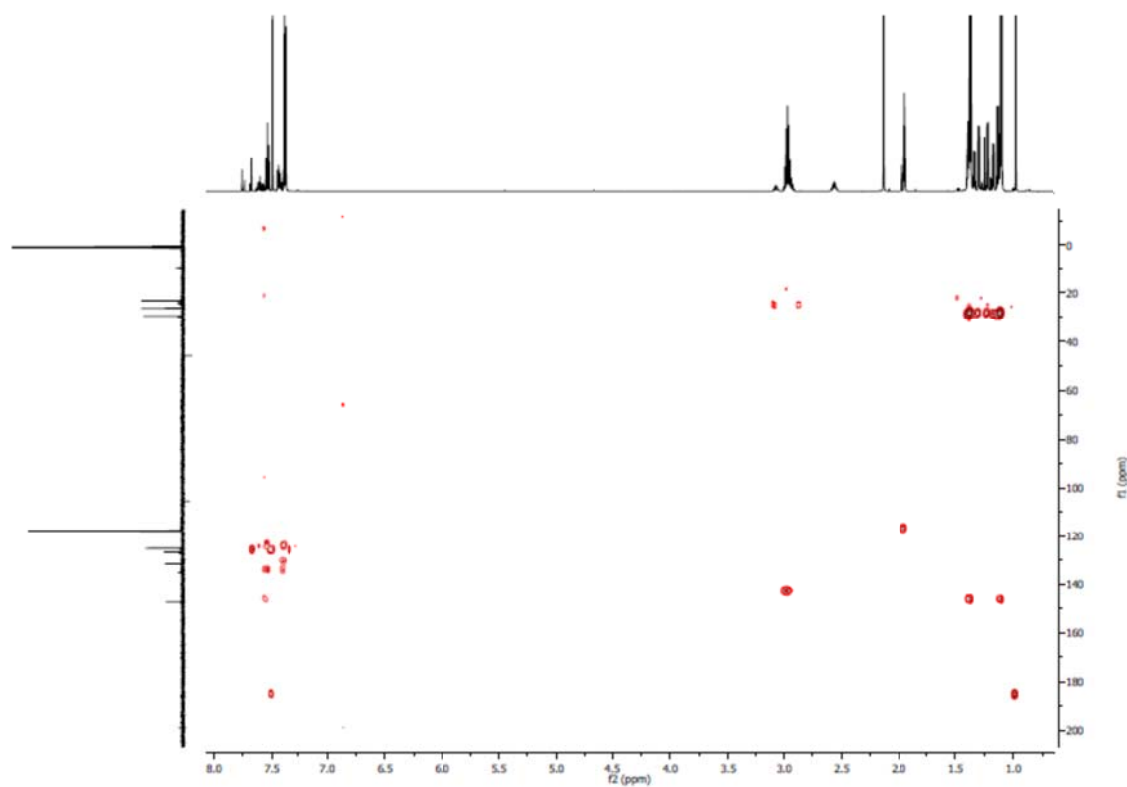




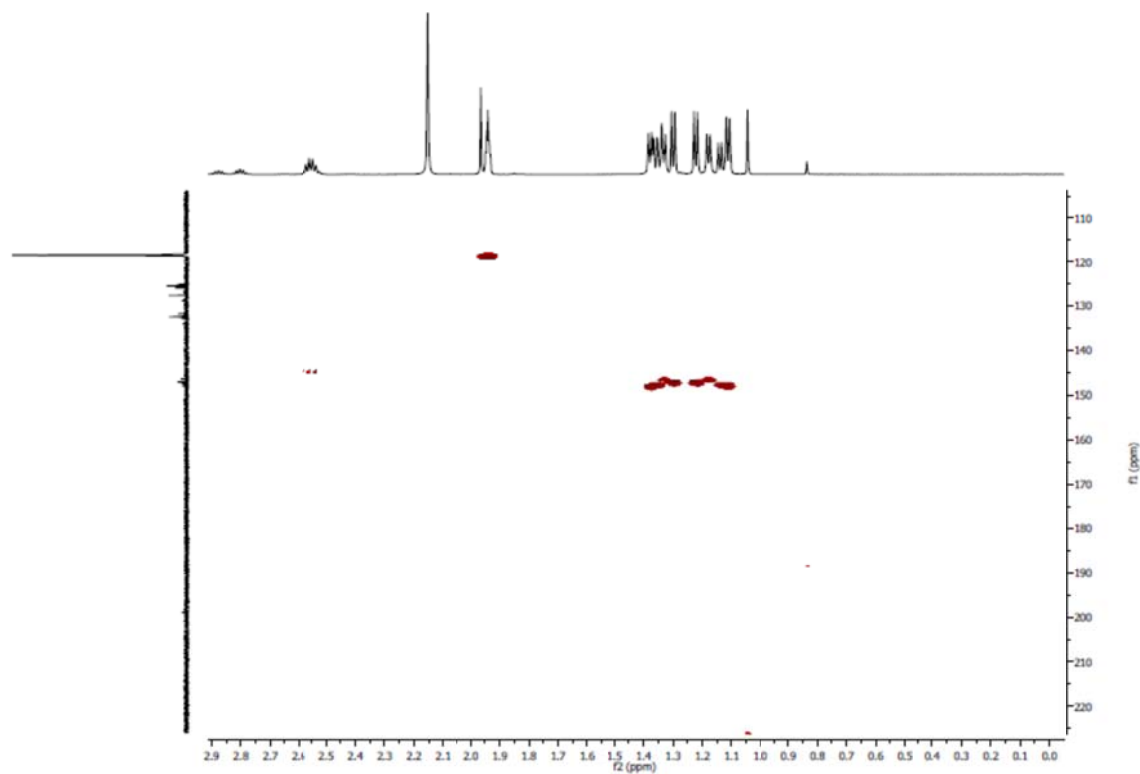
Typical reaction of 4-166 A + I<sub>2</sub> + MI monitored over time

**C.6 HMBC spectrum for A + I<sub>2</sub> + KI**

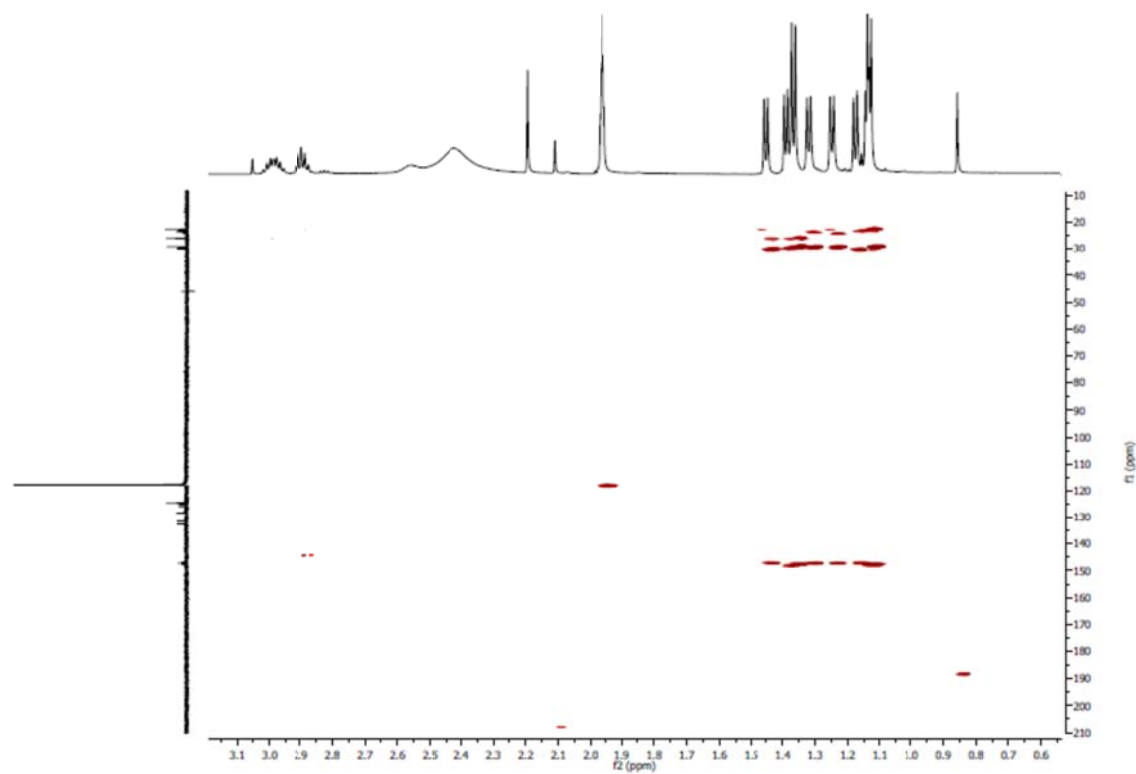
Two carbene resonances ( $\delta$  182.3 ppm (**B**) and  $\delta$  184.0 ppm (**D**)) are clearly seen; the one at 182.3 ppm displays coupling to the singlet (methyl) at  $\delta$  1.46.

**C.7 HMBC spectrum for A + Br<sub>2</sub>**

One major carbene  $^{13}\text{C}$  resonance is visible at  $\delta$  185.2 ppm which displays coupling to a singlet (methyl) at  $\delta$  0.99 ppm in the  $^1\text{H}$  NMR spectrum.

**C.8 HMBC spectrum for A + Cl<sub>2</sub>**

A carbene peak at  $\delta$  188.7 ppm couples to a singlet at  $\delta$  0.83; a second carbene peak at  $\delta$  225.8 ppm shows coupling to a singlet at  $\delta$  1.05 ppm. This suggests *cis* and *trans* isomers of (Idipp)AuCl<sub>2</sub>Me.

**C.9 HMBC spectrum for A + ICl**

A carbene peak at  $\delta$  188.7 ppm couples to a singlet at  $\delta$  0.85; a second carbene peak at  $\delta$  208.0 ppm shows coupling to a singlet at  $\delta$  2.10 ppm.

# C.10 FAB MS<sup>+</sup> spectrum of monomethyl species from A + Br<sub>2</sub>

CALTECH  
9/30/2009

Page 1

File: 093009-08

Date Run: 09-30-2009 (16:00:34)

Sample: Sample 303 m/z760 HR FAB NOE

Instrument: JEOL MSRoute

Ionization mode: FAB+

Valerie Scott

Scan: 11-16

Base: m/z 585; 17%FS

TIC: 1745554 (Max Inten : 178053)

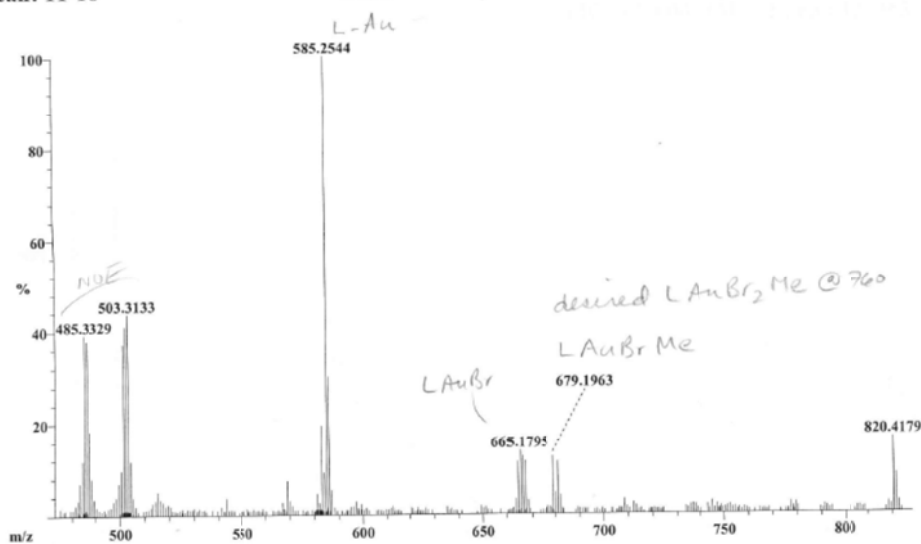
Selected Isotopes : C H N<sub>1-3</sub> Br<sub>0-2</sub> Au<sub>0-2</sub>

Error Limit : 5 ppm

<u>Measured Mass</u>	<u>% Base</u>	<u>Formula</u>	<u>Calculated Mass</u>	<u>Error</u>
679.1963	12.5%	C <sub>28</sub> H <sub>39</sub> N <sub>2</sub> Br Au	679.1963	0.1

Scan: 11-16

Base: m/z 585; 17%FS TIC: 1745554 (Max Inten : 178053)



m/z fragment of 679.20, corresponding to (Idipp)AuBrMe<sup>+</sup>, suggests the presence of

(Idipp)AuBr<sub>2</sub>Me

### C.11 FAB MS<sup>+</sup> spectrum of monomethyl species from A + Cl<sub>2</sub>

Scan: 3-9

Base: m/z 503; 11.7%FS

TIC: 1446047 (Max Inten : 122363)

Selected Isotopes : C H N<sub>1,3</sub> Au<sub>0,1</sub> Cl<sub>1,3</sub>

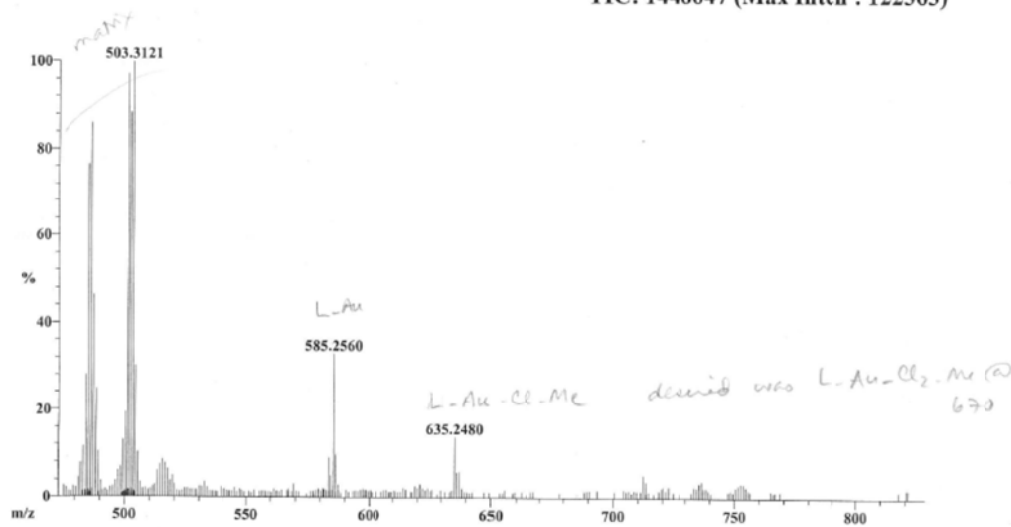
Error Limit : 5 ppm

<u>Measured</u> <u>Mass</u>	<u>% Base</u>	<u>Formula</u>	<u>Calculated</u> <u>Mass</u>	<u>Error</u>
635.2480	13.9%	C <sub>28</sub> H <sub>39</sub> N <sub>2</sub> Au Cl	635.2468	1.9

Scan: 3-9

Base: m/z 503; 11.7%FS

TIC: 1446047 (Max Inten : 122363)



m/z fragment of 635.25, corresponding to (Idipp)AuClMe<sup>+</sup>, suggests presence of

(Idipp)AuCl<sub>2</sub>Me

C.12 FAB MS<sup>+</sup> spectrum of monoalkyl species from E + Cl<sub>2</sub>

CALTECH

9/30/2009

Page 1

File: 093009-07

Date Run: 09-30-2009 (15:37:05)

Sample: Sample 301 m/z 685 HR FAB NOE

Instrument: JEOL MSRoute

Ionization mode: FAB+

Valerie Scott

Scan: 4-11

Base: m/z 585; 28.8%FS

TIC: 2219310 (Max Inten : 301842)

M theo = 649.2624

Selected Isotopes : C H N<sub>1-4</sub> Cl<sub>0-3</sub> Au<sub>0-1</sub>

Error Limit : 10 mmu

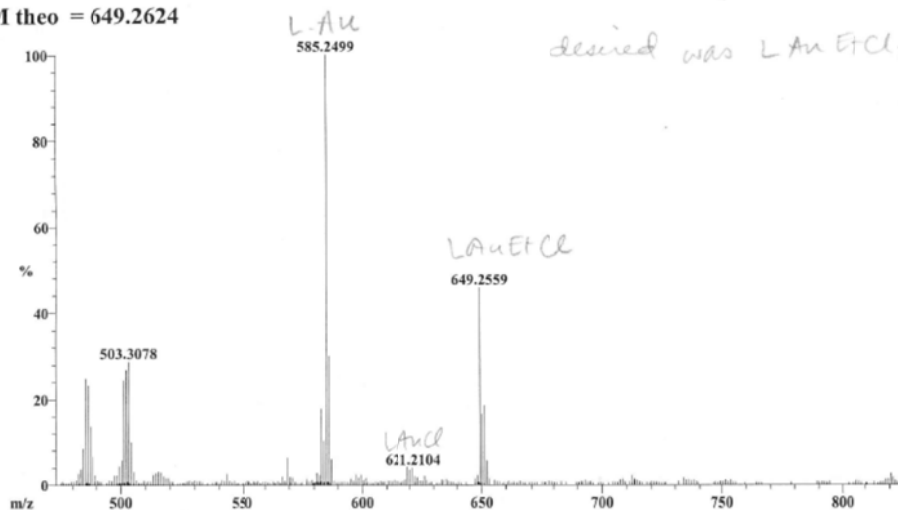
<u>Measured</u> <u>Mass</u>	<u>% Base</u>	<u>Formula</u>	<u>Calculated</u> <u>Mass</u>	<u>Error</u>
649.2559	45.7%	C <sub>29</sub> H <sub>41</sub> N <sub>2</sub> Cl Au	649.2624	-6.5

Scan: 4-11

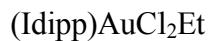
Base: m/z 585; 28.8%FS

TIC: 2219310 (Max Inten : 301842)

M theo = 649.2624



m/z fragment of 649.25, corresponding to (Idipp)AuClEt<sup>+</sup>, suggests presence of





### C.13 FAB MS<sup>+</sup> spectrum of F+ Cl<sub>2</sub>

CALTECH

9/30/2009

Page 1

File: 093009-06

Date Run: 09-30-2009 (15:27:23)

Sample: Sample 302 m/z 733 HR FAB NOE

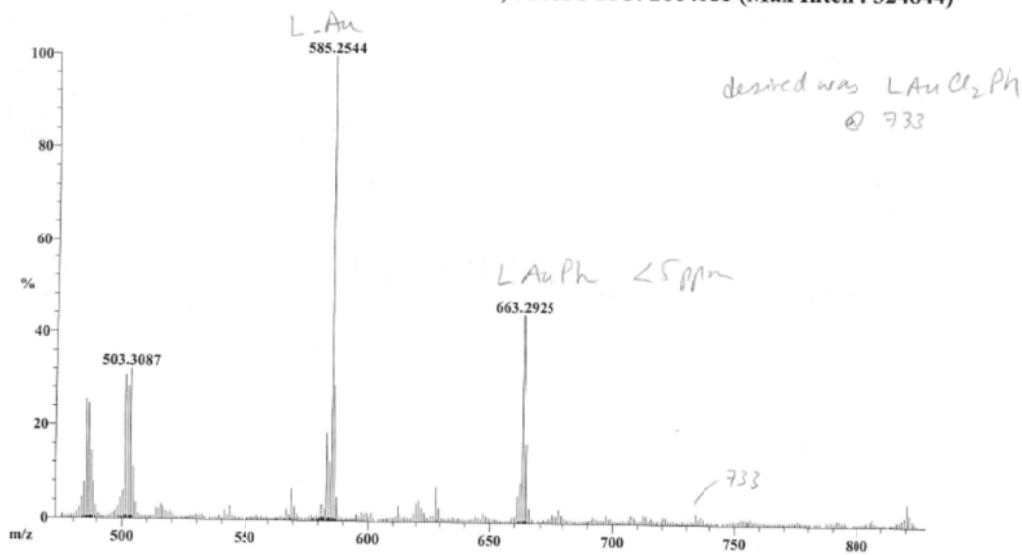
Instrument: JEOL MSRoute

Ionization mode: FAB+

Valerie Scott

Scan: 6-14

Base: m/z 585; 31% FSTIC: 2664181 (Max Inten : 324844)



m/z fragment of 663.29, corresponding to (Idipp)AuPh<sup>+</sup>, shows no indication of a

Au(III)-monoaryl species, supported by <sup>1</sup>H NMR experiments

## APPENDIX D

Table of raw kinetic isotope effect data  
and Arrhenius plots and equations

### D.1 Table of raw kinetic isotope effect data

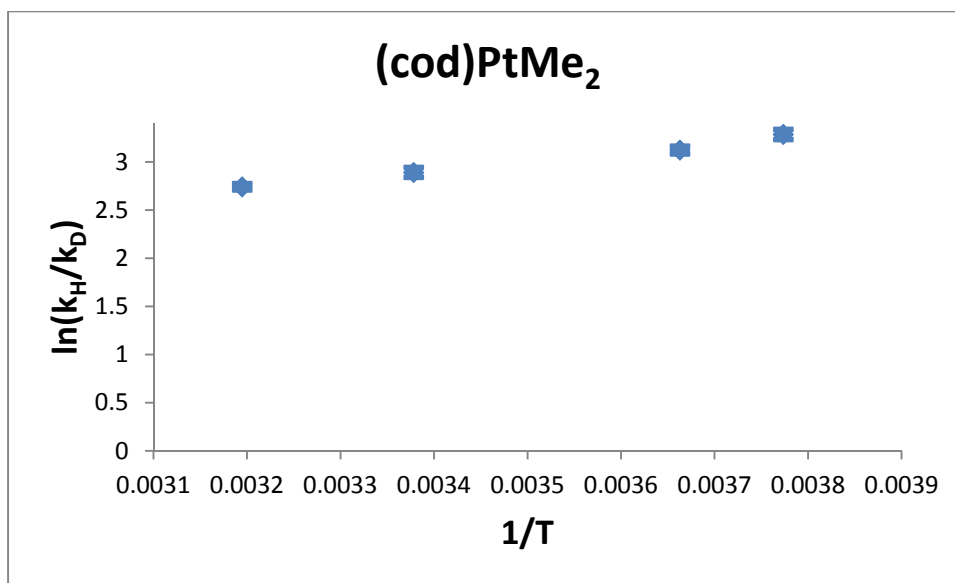
Complex	Temp (°C)	Method	Run 1	Run 2	Run 3	Run 4
(cod)PtMe <sub>2</sub>	-8	1	18.8	20.2	21.8	21.6
			20.7	21.2	20.9	
	0	2	27.9	27.3	26.6	24.8
		1	19.7	22.3	18.0	
		2	21.7	21.8	22.9	20.3
			21.7			
		3	24.3	21.0	23.4	
	23	1	17.6	17.4	19.4	17.8
	40	1	16.1	17.0	16.1	
		2	16.0	15.4	15.0	
<sup>t</sup> Bu <sub>2</sub> Cp <sub>2</sub> ZrMe <sub>2</sub>	-8	1	10.7	13.6	10.3	
		2	10.9	10.4	10.6	
	0	2	10.0	10.0	11.3	
	23	1	10.4	10.8	8.8	
		2	10.1	10.3		
	40	1	8.7	9.2	8.7	8.8
			8.6	9.0	9.9	10.3
		2	10.0	11.4	10.0	8.9
			8.9	9.0		
(Idipp)AuMe	-8	1	10.1	8.5	8.8	
		2	8.6	8.2	7.6	
	0	2	7.0	7.2	7.2	
	23	1	8.6	9.5	10.3	9.9
			8.6			
	40	2	13.4	12.5	12.5	
		1	5.6	7.3	10.5	10.6
		2	10.2	8.1	9.3	
ZnMe <sub>2</sub>	-8	2	3.2	3.2	3.7	
	0	2	2.9	3.0	3.4	
	23	1	2.3	3.4	3.7	

	40	2	3.1	2.9	2.6	
(PONOP)RhMe	-8	1	5.5	7.1	5.4	
	0	2	8.0	9.5	14.0	
	23	1	6.2	5.5	6.5	6.1
			6.4			
(PONOP)IrMe	-8	1	14.2	12.6		
	23	1	9.8	11.3	11.8	10.2
			9.9	10.2		
(dppe)PdMe <sub>2</sub> (TFA)	-8	2	9.7	9.8	8.8	10.4
	0	2	8.6	9.1	7.4	7.5
	23	2	7.0	6.7	6.9	7.1
	40	2	7.4	7.0	7.3	7.0

## D.2 General Considerations for Arrhenius plots

All equations and errors of Arrhenius plots were generated using a linear least squares regression with a 95% confidence level by Matlab.

### D.3 Arrhenius plot and equation for (cod)PtMe<sub>2</sub>



$$cf(x) = p1 \cdot x + p2$$

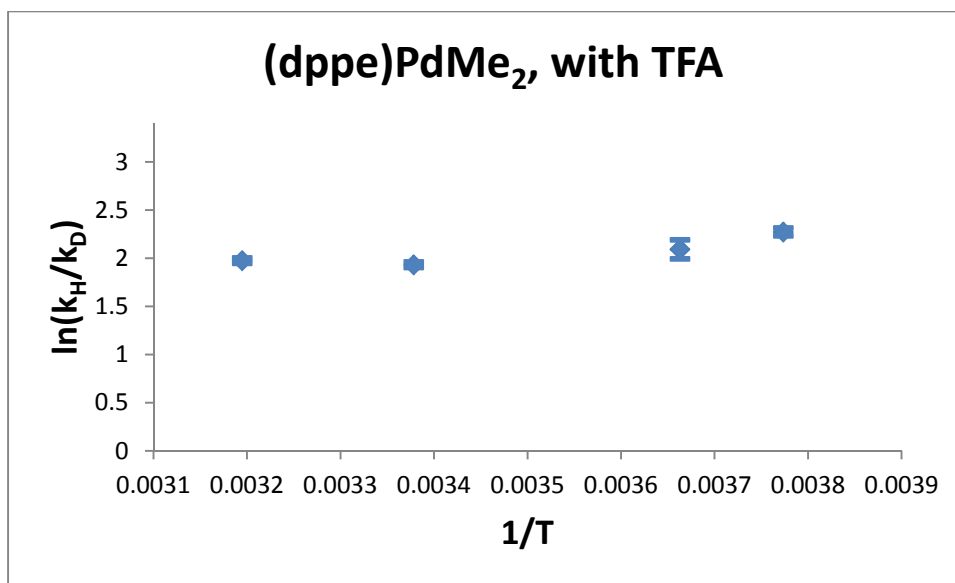
Coefficients (with 95% confidence bounds):

$$p1 = 856.5 \text{ (425.4, 1288)}$$

$$p2 = -0.006875 \text{ (-1.535, 1.521)}$$

$$\text{goodness of fit (R squared)} = 0.97337$$

#### D.4 Arrhenius plot for (dppe)PdMe<sub>2</sub> with TFA



$$cf(x) = p1 \cdot x + p2$$

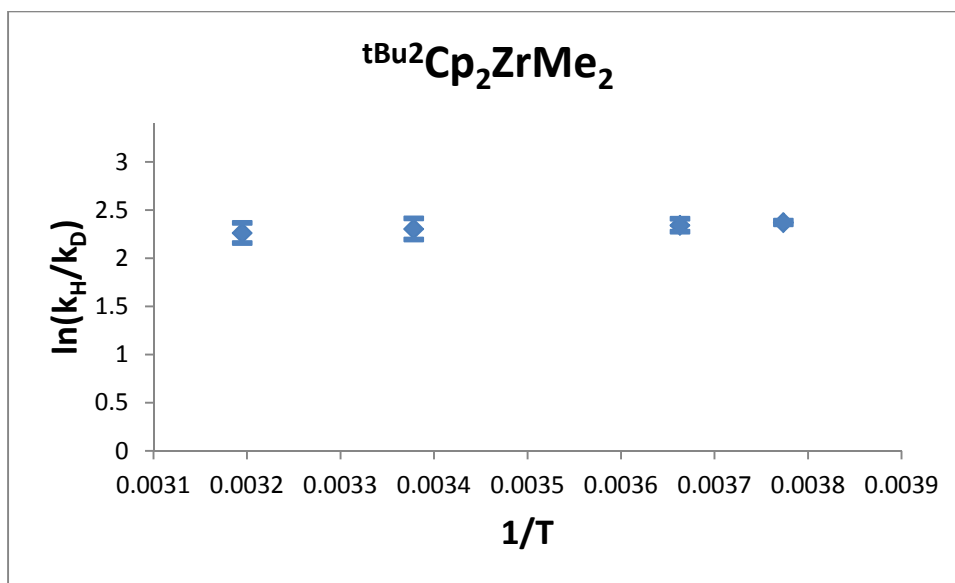
Coefficients (with 95% confidence bounds):

$$p1 = 479.8 \text{ } (-385, 1345)$$

$$p2 = 0.3765 \text{ } (-2.717, 3.47)$$

$$\text{goodness of fit (R squared)} = 0.74023$$

### D.5 Arrhenius plot for $t\text{Bu}^2\text{Cp}_2\text{ZrMe}_2$



$$cf(x) = p1 \cdot x + p2$$

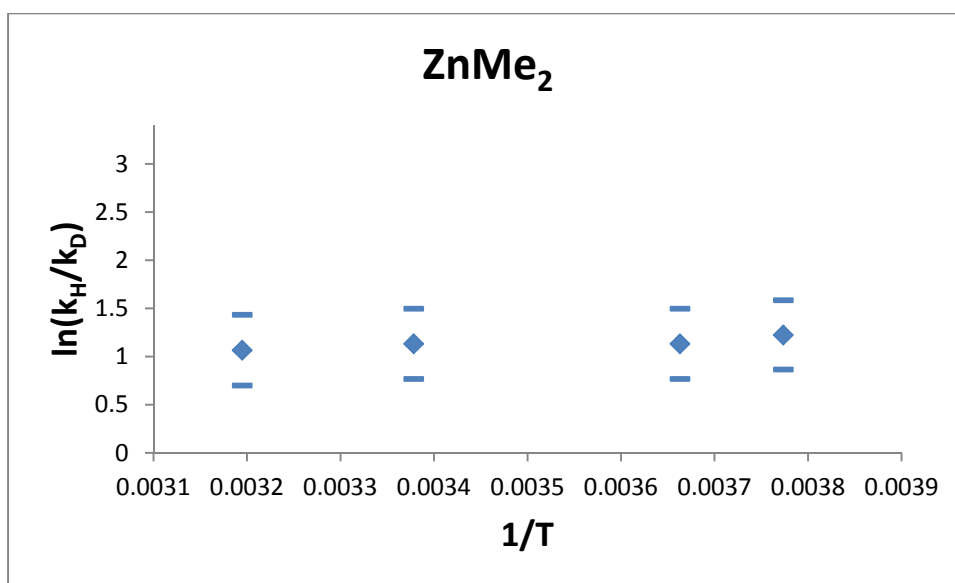
Coefficients (with 95% confidence bounds):

$$p1 = 172.6 \text{ (111.2, 234)}$$

$$p2 = 1.714 \text{ (1.494, 1.934)}$$

$$\text{goodness of fit (R squared)} = 0.98651$$

### D.6 Arrhenius plot for $\text{ZnMe}_2$



$$cf(x) = p1 \cdot x + p2$$

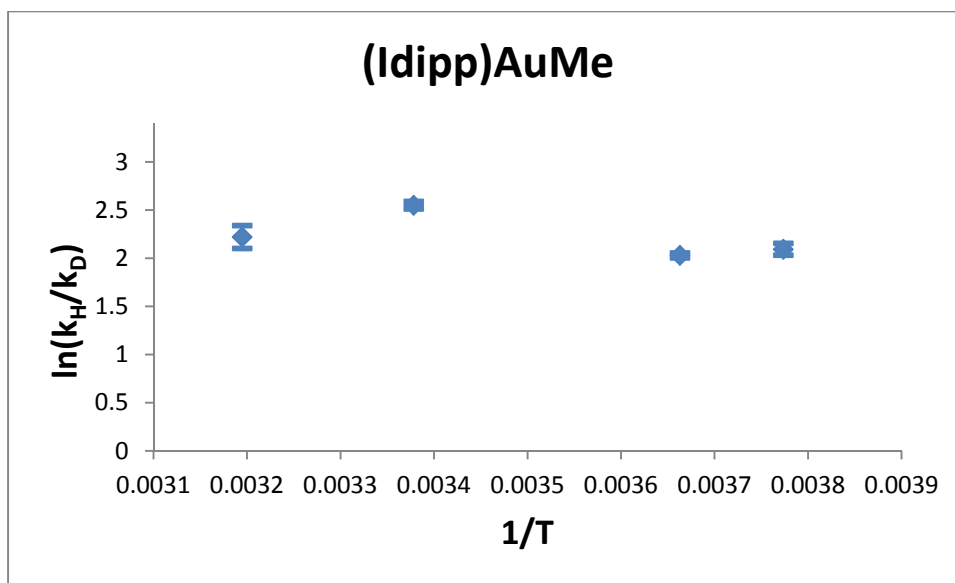
Coefficients (with 95% confidence bounds):

$$p1 = 178.5 \text{ } (-220.2, 577.1)$$

$$p2 = 0.5181 \text{ } (-0.8668, 1.903)$$

$$\text{goodness of fit (R squared)} = 0.64977$$

### D.7 Arrhenius plot for (Idipp)AuMe



$$cf(x) = p1 * x + p2$$

Coefficients (with 95% confidence bounds):

$$p1 = -294.7 \text{ } (-2008, 1419)$$

$$p2 = 3.227 \text{ } (-2.647, 9.1)$$

goodness of fit (R squared) = 0.21497



## APPENDIX E

### Attempts to observe C-H activation using NHC-supported Au-complexes

#### E.1 Abstract

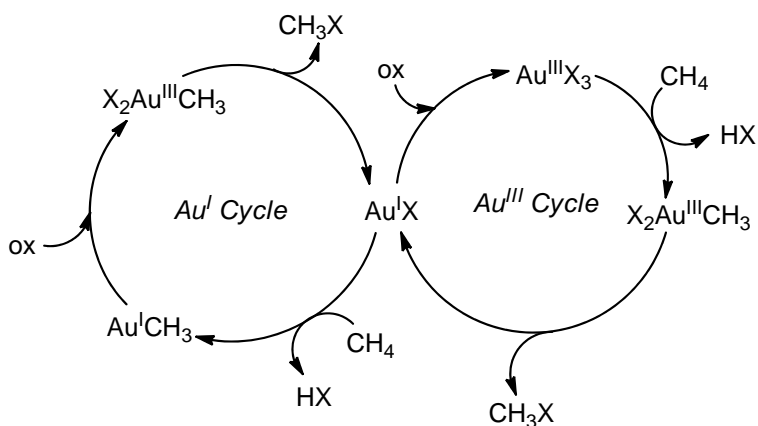
C-H activation with Au complexes has been known in the literature for some time, but understanding of the mechanisms at work is severely limited. Following the success in observing the functionalization of a (Idipp)Au-alkyl species, where Idipp = 1,3-bis(2,6-diisopropylphenyl)imidazol-2-ylidene, experiments on related complexes have been carried out to attempt to learn more about the remaining steps of possible C-H activation mechanism(s).

#### E.2 Introduction

The activation of C-H bonds remains a topic of considerable interest; the stability of these bonds typically renders them inert to chemical reactions, but advances in organometallic chemistry over the last several decades have demonstrated the ability to access these reactions.<sup>1-5</sup> This reactivity has been demonstrated with Au.<sup>6-22</sup> In one example, Au<sub>2</sub>O<sub>3</sub> catalytically and selectively converts methane to methanol in the presence of a strong oxidant (H<sub>2</sub>SeO<sub>4</sub>) in H<sub>2</sub>SO<sub>4</sub> as a solvent,<sup>12</sup> however the mechanism of this transformation is not well understood (possible redox cycles are shown in Scheme E.1; see Chapter 2 for more in-depth background). Further studies are required to determine what the active species is (or are) and what steps are involved in the catalytic cycle(s) in order to

better understand how these catalysts work, as well as to aid in the design of better catalysts.

### Scheme E.1



Recent studies have examined the mechanism of the functionalization step (where  $\text{MeX}$  is released).<sup>23</sup> Using  $(\text{Idipp})\text{AuMe}$ , it was found that this species could be oxidized to form the unprecedented simple monoalkyl  $\text{Au}(\text{III})$  complex,  $(\text{Idipp})\text{AuI}_2\text{Me}$  (see Chapter 1). This complex slowly decomposes into  $\text{MeI}$  and  $(\text{Idipp})\text{AuMe}$ ; kinetics experiments demonstrate that this occurs primarily via reductive elimination (See Chapter 2), in contrast to the related Shilov system which follows a nucleophilic attack pathway. This step is relevant to *either* proposed redox catalytic cycle in Scheme E.1. Using this same ligand framework, is it possible to study the oxidation and C-H activation steps?

### E.3 Results and Discussion

#### E.3.1 Oxidation

Cyclic voltammograms were recorded for both (Idipp)AuCl and (Idipp)AuMe; unfortunately, for both complexes, the results were inconclusive. No oxidation event was observed in the solvent window (acetonitrile) for (Idipp)AuCl. The oxidation curve for (Idipp)AuMe was not reversible, even at faster scan rates or with added KI to help stabilize the intermediate. However, from the experiments described in Chapters 1 and 2, it was established that (Idipp)AuMe is easier to oxidize than (Idipp)AuCl. (Idipp)AuMe is readily oxidized by I<sub>2</sub>, whereas (Idipp)AuX is not; (Idipp)AuI and (Idipp)AuBr both require the stronger oxidant, Br<sub>2</sub>. (Idipp)AuCl reacts readily with Cl<sub>2</sub>; the corresponding reaction with Br<sub>2</sub> was not tested. While quantitatively, it is unclear what the exact redox potentials are, it is certain that (Idipp)AuMe is easier to oxidize from this reactivity scale. This information might indicate that a good C-H activation catalyst design based on Au should follow the Au(I)-pathway—this would require less harsh reaction conditions. Nevertheless, under the conditions that allow the catalytic Periana system<sup>12</sup> to work, it is clear that the reaction *does* require the harsh oxidant, which may indicate that the “easy” pathway may not be the functional pathway. It is possible that both of these pathways are functional, but vary by catalyst and reaction conditions.

#### E.3.2 Investigations into C-H activation

Neither the studies done on the oxidation nor the experiments that determined the mechanism of the functionalization step give any insight into whether Au(I) or Au(III) is

the more likely species to carry out the C-H activation step, or how this step is occurring. DFT calculations done on the Periana system indicate that either Au(I) or Au(III) could be involved in activating the C-H bonds, but it was postulated that under the harshly oxidizing conditions of the reaction Au(III) was the more likely candidate. While this is most likely for this specific system, it is possible that other Au-based systems operate differently; there is certainly no unanimous agreement for the mechanism in the literature.

The cationic Au(I) and Au(III) species were targeted to test the C-H activation step, as these complexes should be more active toward electrophilic C-H activation.  $[(\text{Idipp})\text{Au}(\text{NCMe})][\text{PF}_6]$  has been previously reported,<sup>24</sup> and while no analogous Au(III) cations have been synthesized, in situ generation was considered an alternative for these experiments if they could not be directly isolated.

In the case of Au(I), several methods of halide abstraction were attempted ( $\text{AgPF}_6$ ,  $\text{AgBF}_4$ ,  $\text{Ag}_2\text{O}$ ) in benzene or in a mixture of benzene and acetonitrile, with or without heat (up to 60 °C); the acetonitrile cation is known<sup>24</sup> and C-H activation of benzene is typically easier than for alkanes due to its ability to coordinate to the complex through the  $\pi$ -system first. However, while abstraction of the halide was successful in all cases as demonstrated by the formation of  $\text{AgCl}$  precipitate, the reaction of the subsequent species appeared (by  $^1\text{H}$  NMR spectroscopy) to result in disproportionation of the ligand to generate  $[(\text{Idipp})_2\text{Au}][\text{X}]$  (this reactivity had been previously observed with other NHCs, see Appendix F). Similarly,  $(\text{Idipp})\text{AuOTf}^{25}$  (where  $\text{OTf} = \text{CF}_3\text{SO}_3^-$ ) appeared to have the same reactivity when heated in benzene.

Results starting from Au(III) were more promising. Reactions using AgPF<sub>6</sub> or AgOTf in benzene or a mixture of benzene and acetonitrile showed both Au(I) and Au(III) products (as determined by approximate chemical shifts of the supporting ligand resonances in the <sup>1</sup>H NMR spectrum) and PhBr was detected by GC-MS; solubility problems prevented the use of AgBF<sub>4</sub>. Whether the reactions were run at room temperature, at 60 °C, with or without triethylamine (added after the other reagents were allowed to mix to help drive the reaction forward by soaking up any proton generated from the C-H activation), and regardless of the two solvent compositions, the final products always appeared to eventually go to a 1:1 mixture of (Idipp)AuBr<sub>3</sub> and (Idipp)AuBr by <sup>1</sup>H NMR spectroscopy. Because there are no other NMR handles on these molecules, following the reaction is quite difficult; definitive identification of the ligands other than the NHC on the Au-center is not possible. As the reaction progresses, the resonances shift, as opposed to one complex clearly turning into another. Spectra from a typical reaction are shown in Figure E.1. In this case, <sup>19</sup>F NMR displayed 2 peaks that similarly shifted over the course of the reaction. The initial complex formed could not be identified by mass spectroscopy either; several crystallizations were set up, and in one case using benzene layered with pentane, crystals of (Idipp)AuBr<sub>2</sub>OTf were obtained (Figure E.2). A balanced reaction cannot be expressed for the observed products and their apparent distributions, so clearly something complicated is occurring that cannot be easily monitored. Exchange of the ligands may be occurring between the complexes, making it even more difficult to be certain of the identities of the complexes in solution.

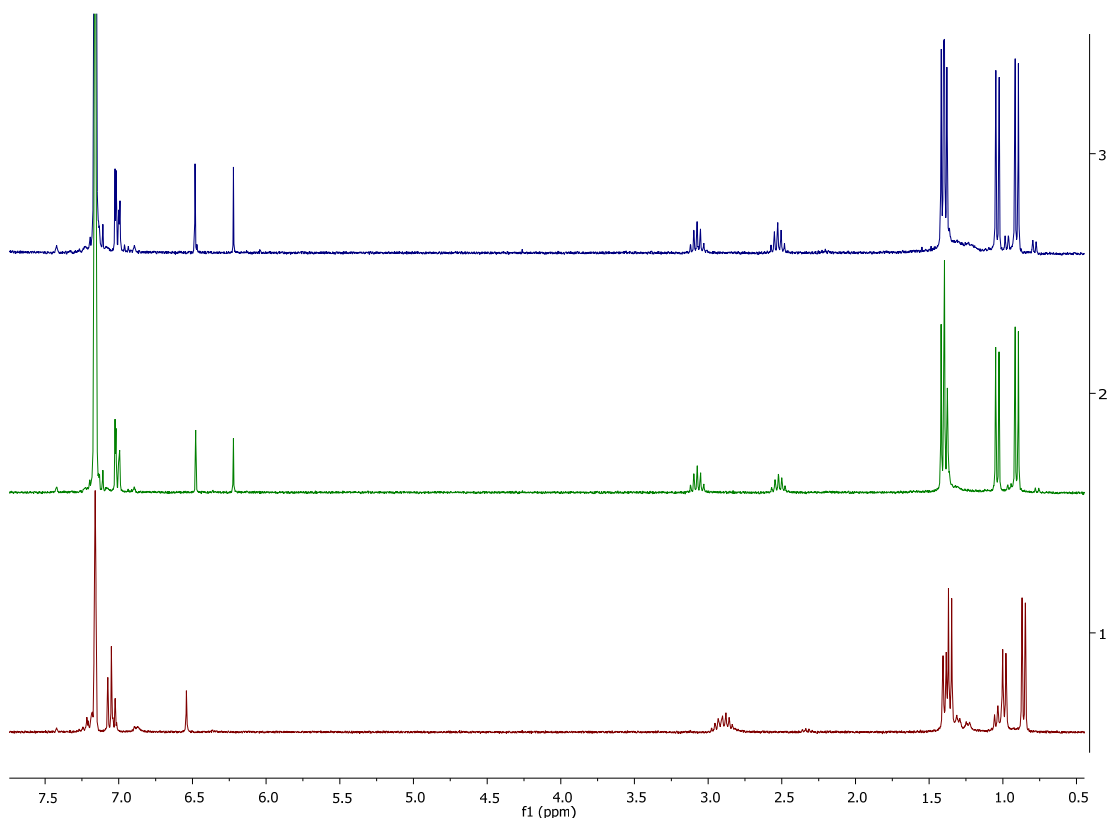


**Figure E.1**  $^1\text{H}$  NMR spectra of the reaction of  $(\text{Idipp})\text{AuBr}_3$  and  $\text{AgOTf}$  in  $\text{C}_6\text{D}_6$  over time (red = 15 min, green = 5 days, blue = 9 days); blue spectrum (top) matches resonances for pure  $(\text{Idipp})\text{AuBr}_3$  and  $(\text{Idipp})\text{AuBr}$  while green and red spectra do not.

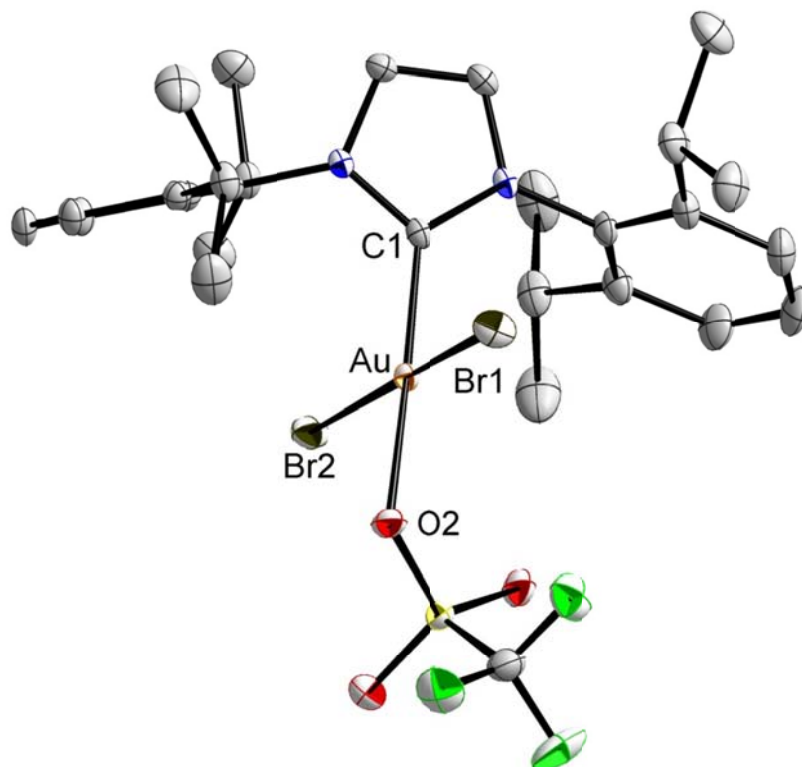


**Figure E.2** Anisotropically refined thermal ellipsoid representation of (Idipp)AuBr<sub>2</sub>OTf; hydrogen atoms have been omitted for clarity. Au-C1 Å; Au-Br1 Å; Au-Br2 Å; Br1-Au-C1 180.000°; Br2-Au-C1 180.000°; O2-Au-C1 180.000°; O2-Au-Br1 180.000°; Br2-Au-O2 180.000°

To quantify the C-H activation product, PhBr, a comparison was made between a GC-MS spectrum of the reaction mixture and one of the same mixture spiked with a known amount of PhBr. For room temperature reactions, the yields were generally about 1-3%, depending on which Ag-salt was being used (AgPF<sub>6</sub> ~ 1%, AgOTf ~ 3%). For a reaction

of (Idipp)AuCl with AgPF<sub>6</sub> in benzene at 80 °C for 12 hours, the yield increased to about 15%. The low yield further complicates determining how the product is formed.

One major caveat for all of these reactions, however, is that Ag-salts in the presence of Br<sub>2</sub> (without Au) will generate PhBr. To test whether or not there was any participation of the Au-complex in the reaction described above, (Idipp)AuOTf was oxidized with just under one equivalent of Br<sub>2</sub> so that there was no Ag in the reaction and all of the Br<sub>2</sub> should be consumed upon reaction with the Au-complex. This reaction looked identical to that carried out with (Idipp)AuBr<sub>3</sub> and AgOTf, both in yield and by <sup>1</sup>H NMR spectroscopy.

In an attempt to make a Au complex with more NMR handles, (Idipp)AuF<sub>2</sub>Me was synthesized. Abstraction of the methyl moiety with B(C<sub>6</sub>F<sub>5</sub>)<sub>3</sub> was attempted in CD<sub>2</sub>Cl<sub>2</sub> and in CD<sub>3</sub>CN; the reaction in CD<sub>2</sub>Cl<sub>2</sub> generated multiple unidentifiable products while in CD<sub>3</sub>CN, no reaction was apparent. Also, if [Ph<sub>3</sub>C][B(C<sub>6</sub>F<sub>5</sub>)<sub>4</sub>] was reacted with (Idipp)AuF<sub>2</sub>Me in CD<sub>2</sub>Cl<sub>2</sub>, no reaction was observed. If instead [Ph<sub>3</sub>C][B(C<sub>6</sub>F<sub>5</sub>)<sub>4</sub>] was used in CD<sub>3</sub>CN, the reaction quickly changed from oily yellow (indicative of the trityl cation) to clear and colorless upon mixing. By <sup>1</sup>H NMR, the Au product appeared to be Au(I); crystallization attempts did not generate crystals suitable for X-ray crystallography and mass spectroscopy only identified the [(Idipp)Au]<sup>+</sup> fragment. GC-MS of the organic fraction shows some Ph<sub>3</sub>CMe, along with other unidentified Ph<sub>3</sub>C-containing fragments. Small peaks are observed in the <sup>19</sup>F NMR spectrum; they do not match the spectrum of (Idipp)AuF or the starting (Idipp)AuF<sub>2</sub>Me. While this reaction is interesting, in general,



characterizing these complexes makes it difficult to work out what is occurring in any of these reactions.

#### E.4 Conclusions

From these experiments, it is impossible to distinguish between the Au(I) and Au(III) cycles. It was evident from past experiments that (Idipp)AuMe is easier to oxidize than (Idipp)AuX, which may imply that it is more favorable to follow C-H activation at a Au(I)-center. However, it was also implied from the above work that the Au(III)-species was the more likely to carry out the C-H activation step under the conditions examined, followed by fast reductive coupling to regenerate a Au(I) species. It seems that both pathways are possible and that the reaction mechanism is determined by the specific Au-complex and reaction conditions.

#### E.5 Experimental

**General considerations.** (Idipp)AuMe,<sup>23</sup> (Idipp)AuOTf<sup>25</sup> and (Idipp)AuF<sub>2</sub>Me<sup>26</sup> were prepared according to the literature procedures. Deuterated solvents were purchased from Cambridge Isotope Laboratories. Before use, each was subjected to three freeze-pump-thaw cycles, then stored over alumina overnight. All other chemicals and solvents were used as received, without further purification. X-ray diffraction experiments were carried out in the Beckman Institute Crystallographic Facility on a Bruker KAPPA APEXII X-ray diffractometer. <sup>1</sup>H and <sup>13</sup>C NMR spectra were obtained on a Varian 300 MHz instrument. GC/MS analyses were performed on an HP model 6890N chromatograph equipped with a

30 m x 25 mm x 0.40  $\mu$ m HP5-1 column and equipped with an HP 5973 mass selective EI detector. Experiments were carried out as described in the text.

## E.6 References

1. Labinger, J. A.; Bercaw, J. E., *Nature*, **2002**, *417*, 507-514.
2. Arndtsen, B. A.; Bergman, R. G.; Mobley, T. A.; Peterson, T. H., *Acc. Chem. Res.*, **1995**, *28*, 154-162.
3. Crabtree, R. H., *Chem. Rev.*, **1995**, *95*, 987-1007.
4. Shilov, A. E.; Shul'pin, G. B., *Chem. Rev.*, **1997**, *97*, 2879-2932.
5. Stahl, S. S.; Labinger, J. A.; Bercaw, J. E., *Angew. Chem. Int. Ed.*, **1998**, *37*, 2181-2192.
6. de Graaf, P. W. J.; Boersma, J.; van der Kerk, G. J. M., *J. Organomet. Chem.*, **1976**, *105*, 399-406.
7. Frúctos, M. R.; de Frémont, P.; Nolan, S. P.; Díaz-Requejo, M. M.; Perez, P. J., *Organometallics*, **2006**, *25*, 2237-2241.
8. Mo, F. Y.; Yan, J. M.; Qiu, D.; Li, F.; Zhang, Y.; Wang, J. B., *Angew. Chem. Int. Ed.*, **2010**, *49*, 2028-2032.
9. Hashmi, A. S. K.; Salathe, R.; Frost, T. M.; Schwarz, L.; Choi, J. H., *Applied Catalysis A-General*, **2005**, *291*, 238-246.
10. Hashmi, A. S. K.; Schafer, S.; Wolfe, M.; Gil, C. D.; Fischer, P.; Laguna, A.; Blanco, M. C.; Gimeno, M. C., *Angew. Chem. Int. Ed.*, **2007**, *46*, 6184-6187.
11. Höffmann-Roder, A.; Krause, N., *Org. Biomol. Chem.*, **2005**, *3*, 387-391.

12. Jones, C. J.; Taube, D.; Ziatdinov, V. R.; Periana, R. A.; Nielsen, R. J.; Oxgaard, J.; Goddard, W. A., *Angew. Chem. Int. Ed.*, **2004**, *43*, 4626-4629.
13. Kar, A.; Mangu, N.; Kaiser, H. M.; Tse, M. K., *J. Organomet. Chem.*, **2009**, *694*, 524-537.
14. Kharasch, M. S.; Beck, T. M., *J. Am. Chem. Soc.*, **1934**, *56*, 2057-2060.
15. Kharasch, M. S.; Isbell, H. S., *J. Am. Chem. Soc.*, **1931**, *53*, 3053-3059.
16. Levchenko, L. A.; Kartsev, V. G.; Sadkov, A. P.; Shestakov, A. F.; Shilova, A. K.; Shilov, A. E., *Dokl. Chem.*, **2007**, *412*, 35-37.
17. Levchenko, L. A.; Sadkov, A. P.; Lariontseva, N. V.; Koldasheva, E. M.; Shilova, A. K.; Shilov, A. E., *J. Inorg. Biochem.*, **2002**, *88*, 251-253.
18. Li, Z. G.; Capretto, D. A.; Rahaman, R. O.; He, C., *J. Am. Chem. Soc.*, **2007**, *129*, 12058-12059.
19. Shul'pin, G. B.; Shilov, A. E.; Süß-Fink, G., *Tetrahedron Lett.*, **2001**, *42*, 7253-7256.
20. Xiao, Y. P.; Liu, X. Y.; Che, C. M., *J. Organomet. Chem.*, **2009**, *694*, 494-501.
21. Vicente, J.; Bermúdez, M. D.; Chicote, M. T.; Sanchez-Santano, M. J., *J. Chem. Soc. Chem. Comm.*, **1989**, 141-142.
22. Vicente, J.; Chicote, M. T.; Lozano, M. I.; Huertas, S., *Organometallics*, **1999**, *18*, 753-757.
23. Scott, V. J.; Labinger, J. A.; Bercaw, J. E., *Organometallics*, **2010**, *29*, 4090-4096.
24. de Fremont, P.; Stevens, E. D.; Fructos, M. R.; Diaz-Requejo, M. M.; Perez, P. J.; Nolan, S. P., *Chem. Commun.*, **2006**, 2045-2047.

25. Tsui, E. Y.; Muller, P.; Sadighi, J. R., *Angew. Chem. Int. Ed.*, **2008**, *47*, 8937-8940.
26. Mankad, N. P.; Toste, F. D., *J. Am. Chem. Soc.*, **2010**, *132*, 12859-12861.

## APPENDIX F

### Synthesis of novel (NHC)Au-complexes

#### F.1 Abstract

Several new N-heterocyclic carbenes (NHCs) with the potential to chelate to a bound metal were designed for the study of the mechanism of C-H activation with Au-complexes. The substituents on these novel ligands had weak points that eventually led to the discontinuation of this avenue of research, however, several new (NHC)Au-complexes are reported here; small modifications of the described ligands could make this a viable research project again.

#### F.2 Introduction

In order to study the activation of C-H bonds using Au-catalysts (See Chapters 1 and 2 for more in-depth background), a library of well-defined complexes was designed to examine each step individually. Carbenes were chosen as the supporting ligand platform because they tend to form highly stable complexes<sup>1</sup> and have recently been shown to support both Au(I) and Au(III).<sup>2</sup> The ligands described herein were designed such that the substituents on the NHC could act as potential donors, possibly to help stabilize complexes that might otherwise be too reactive to isolate. These original ligands (Figure F1) were chosen for early studies because their syntheses were straightforward. Related NHCs are known in the literature and could be relevant to the continuation of this study.<sup>3-6</sup>

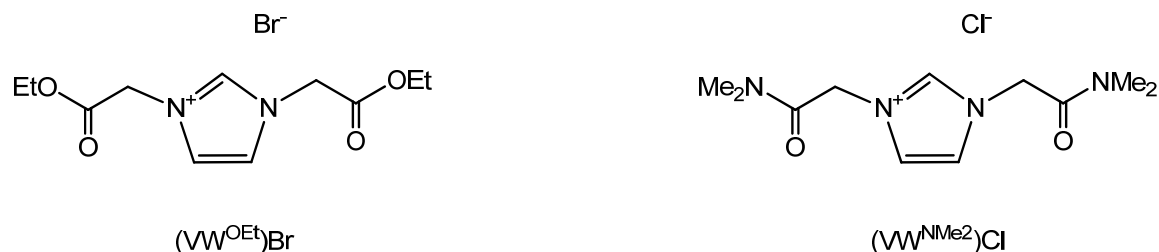


**Figure F.1**  $(\text{VW}^{\text{OEt}})\text{Br}$  and  $(\text{VW}^{\text{NMe}_2})\text{Cl}$

### F.3 Results and Discussion

$(\text{VW}^{\text{OEt}})\text{Br}$  was synthesized according to the literature method;<sup>7</sup>  $(\text{VW}^{\text{NMe}_2})\text{Cl}$  was prepared by an analogous method (Figure F.1). Both ligands were characterized by  $^1\text{H}$  NMR spectroscopy. Metallation of these ligands was achieved by reaction of the ligand with  $\text{Ag}_2\text{O}$  and subsequent transmetallation to  $\text{Au}(\text{SMe}_2)\text{Cl}$  yielding the  $\text{Au}(\text{I})$  complexes cleanly in fair yields (Scheme F.1). One major problem with the generation of these complexes is evident; they are easily reduced to form  $\text{Au}^0$ . This appears to be more of a problem when there is  $\text{Au}(\text{SMe}_2)\text{Cl}$  left at the end of the reaction, so precautions must be taken not to have excess  $\text{Au}$  starting material. Crystals suitable for X-ray diffraction were grown of  $(\text{VW}^{\text{OEt}})\text{AuCl}$  and  $(\text{VW}^{\text{NMe}_2})\text{AuCl}$  (Figures F.2 and F.3).

## Scheme F.1

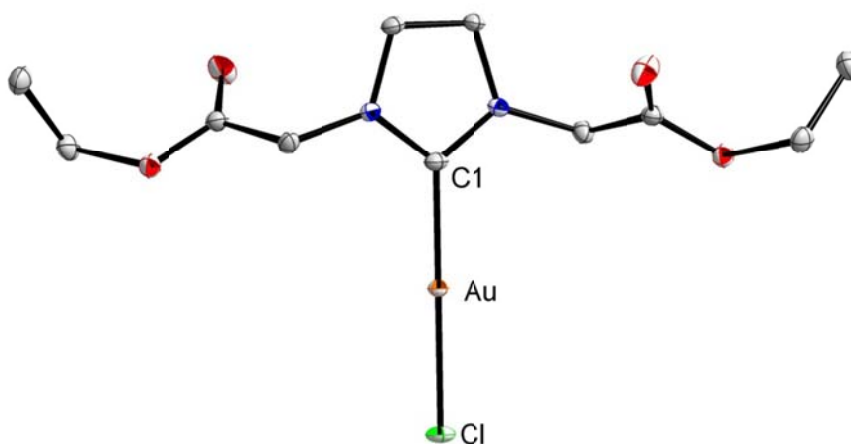
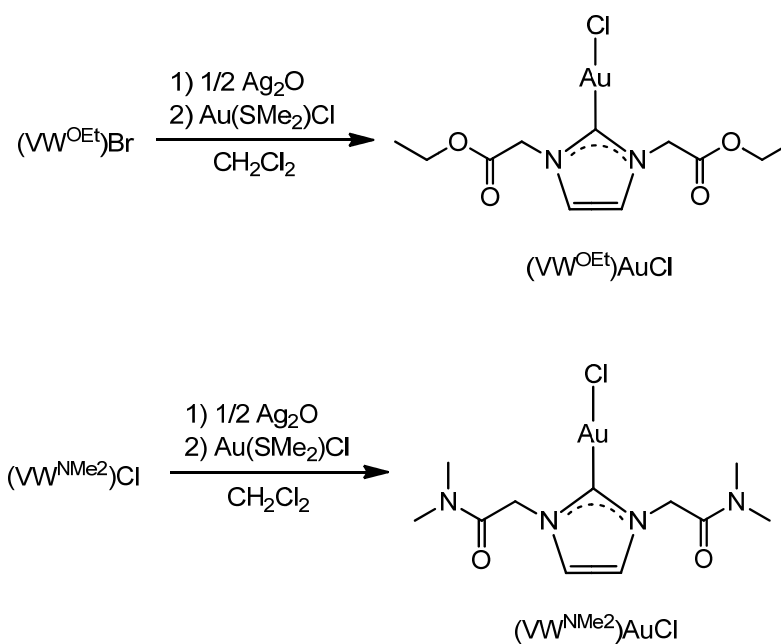


**Figure F.2** Anisotropically refined thermal ellipsoid representation of  $(VW^{OEt})AuCl$ ; hydrogen atoms have been omitted for clarity. Au-Cl1 2.2863 Å; Au-C1 1.9753 Å; Cl1-Au-C1 180.000°

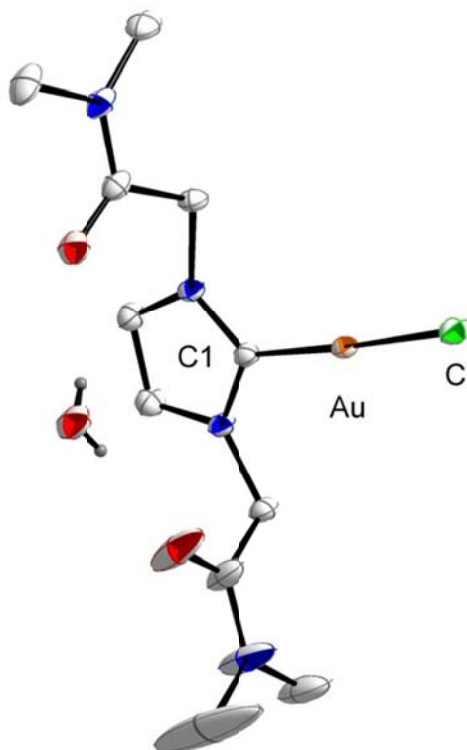


**Figure F.3.** Anisotropically refined thermal ellipsoid representation of (VW<sup>NMe<sub>2</sub></sup>)AuCl with H<sub>2</sub>O molecule shown; hydrogen atoms other than those on H<sub>2</sub>O have been omitted for clarity with the exception of water hydrogen. Au-Cl1 2.2872 Å; Au-C1 1.9689 Å; C1-Au-Cl1 177.059°

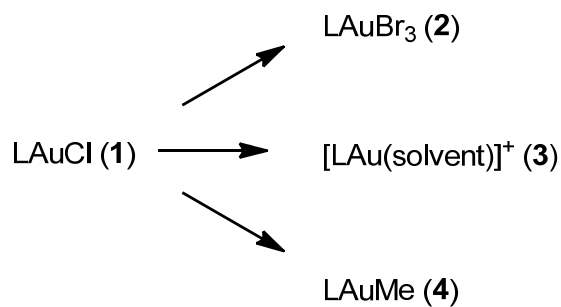
In addition to these new complexes, two common NHCs (Idipp and IPr, where Idipp = 1,3-bis(2,6-diisopropylphenyl)imidazol-2-ylidene) and IPr = 1,3-bis(isopropyl)imidazol-2-ylidene)) were chosen to use as a comparison to the new ligands to determine whether the



chemistry of the new ligands is unique to their design or if it is the same with simple alkyl or phenyl substituents on the NHC.

A number of target molecules were desired that could theoretically be derived from the Au(I) starting materials of type **1** (Scheme F.2). Oxidation of these compounds could give access to the corresponding Au(III) complexes (**2**). Also, halide abstraction could result in the formation of a Au(I) complex with a more accessible binding site, likely to be isolated as a solvento-species (**3**), which could be tested for C-H activation. (This has been accomplished in the Nolan group using (Idipp)AuCl and Ag-salts in acetonitrile.)<sup>8</sup> The synthesis of a Au(I)-alkyl (**4**) is also of interest, as these complexes could be tested for their ability to functionalize the alkyl moiety and thus, as intermediates in the proposed catalytic schemes.

#### Scheme F.1



Attempts to abstract a halide from these complexes were unsuccessful; all resulted in either a black insoluble mixture or disproportionation to form the cationic biscarbene complex. (X-ray diffraction experiments indicated that this complex was likely, but the data sets were of poor quality. This assignment was further supported by similar reactivity

with Au(III), discussed below.) In an attempt to trap the desired cationic species, 1 equivalent each of  $\text{AgPF}_6$ ,  $(\text{VW}^{\text{OEt}})\text{AuCl}$ , and  $\text{PMe}_3$  were allowed to reaction in  $\text{CH}_2\text{Cl}_2$ . Colorless needle crystals were obtained but were identified as disproportionation product,  $[\text{Au}(\text{PMe}_3)_2][\text{PF}_6]$  (a full X-ray diffraction data set was not collected in this case).

By  $^1\text{H}$  NMR spectroscopy, early attempts to alkylate  $(\text{VW}^{\text{OEt}})\text{AuCl}$  and  $(\text{VW}^{\text{NMe}_2})\text{AuCl}$  with  $\text{ZnMe}_2$  showed promise. However, the analogous reaction with  $(\text{Idipp})\text{AuCl}$  was significantly cleaner, so the new ligands were dropped in favor of studying the reactivity of  $(\text{Idipp})\text{AuMe}$  (see Chapters 1 and 2).

Reaction of either  $(\text{VW}^{\text{OEt}})\text{AuCl}$  or  $(\text{VW}^{\text{NMe}_2})\text{AuCl}$  with  $\text{LiBr}$  followed by oxidation with  $\text{Br}_2$  gave clean conversion to the corresponding  $\text{LAuBr}_3$  complexes. Both were characterized by  $^1\text{H}$  NMR spectroscopy and crystals suitable for X-ray crystallography experiments were obtained for  $(\text{VW}^{\text{OEt}})\text{AuBr}_3$  (Figure F.4). With the Au(III)-halides in hand, a similar series of targets were designed with the intent of testing them for C-H activation and functionalization capabilities (Scheme F.3). Here, the donors on the chelating arms could possibly play the role of the solvent shown in Scheme F.3.

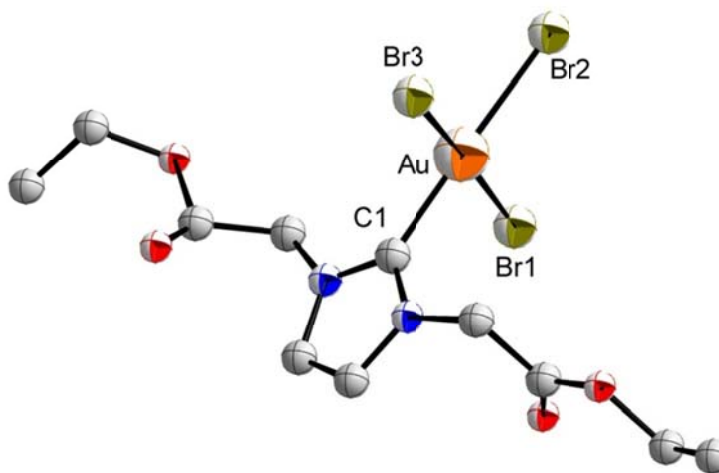
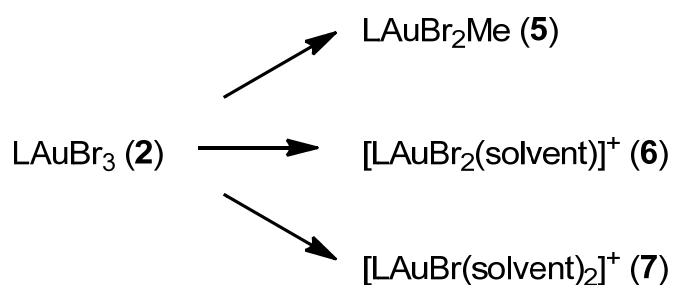


**Figure F.4.** Anisotropically refined thermal ellipsoid representation of  $(VW^{OEt})AuBr_3$ ; hydrogen atoms have been omitted for clarity. Au-C2 2.0075 Å; Au-Br1 2.4208 Å; Au-Br2 2.4264 Å; Au-Br3 2.4455 Å; C2-Au-Br1 85.774°; C2-Au-Br2 90.227°; Br1-Au-Br3 92.913°; Br2-Au-Br3 91.004°

#### Scheme F.2



Similar problems to the Au(I) reactions were encountered with the Au(III) starting materials upon reaction with Ag-salts: either insoluble black solids were formed or disproportionation was observed. For example, the reaction of  $(VW^{OEt})AuBr_3$  with 1

equivalent of  $\text{AgPF}_6$  in a mixture of  $\text{CH}_2\text{Cl}_2$  and acetonitrile was also carried out, filtered, and layered with petroleum ether. Crystals from this reaction were determined to be  $[(\text{VW}^{\text{OEt}})_2\text{AuBr}_2][\text{PF}_6]$  (Figure F.5). Attempts to alkylate  $(\text{VW}^{\text{OEt}})\text{AuBr}_3$  resulted in black precipitate and eventual plating of  $\text{Au}^0$ , with nothing clean observable by NMR spectroscopy.

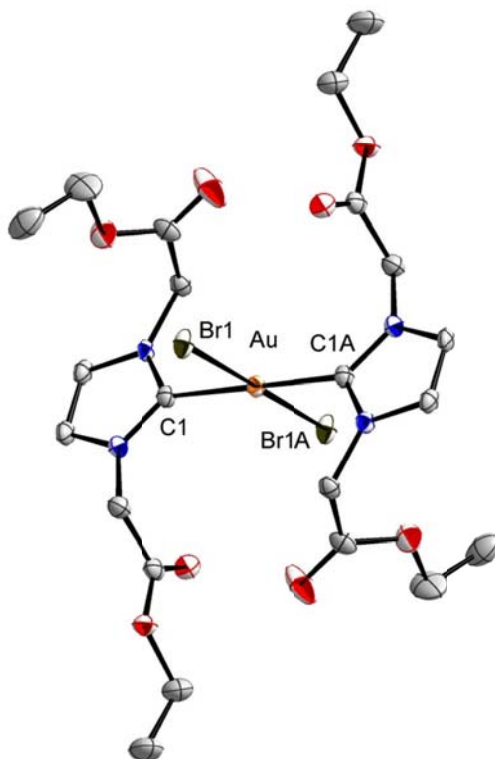


**Figure F.5.** Anisotropically refined thermal ellipsoid representation of  $[(\text{VW}^{\text{OEt}})_2\text{AuBr}_2][\text{PF}_6]$ ; hydrogen atoms and  $\text{PF}_6$  have been omitted for clarity. Au-Br2 2.4254 Å; Au-C4 2.0410 Å; C4-Au-Br2 88.288 °; C4-Au-Br1 91.712 °

Due to early successes with the (Idipp) ligand, further experiments on these potentially chelating NHCs were indefinitely postponed.

#### F.4 Conclusions

Overall, a ligand motif has been designed to aid in the study of potential C-H activation using Au catalysts. Two preliminary versions of this ligand have been successfully metallated and shown to support both Au(I) and Au(III). One potential solution is to remove the reactive carbonyl moieties from future ligands.

#### F.5 Experimental Section

**General considerations.** All chemicals were used as received, without further purification. Sodium-imidazole, potassium *tert*-butoxide, imidazole, 2-bromo-ethylacetate, and 2-chloro-N,N-dimethylacetamide were purchased from Aldrich and Au(SMe<sub>2</sub>)Cl was purchased from Strem. Solvents were dried using the reported procedures by Pangborn et al.<sup>9</sup> X-ray diffraction experiments were carried out in the Beckman Institute Crystallographic Facility on a Bruker KAPPA APEXII X-ray diffractometer. <sup>1</sup>H NMR spectra were recorded on a Varian 300 MHz instrument.

**(VW<sup>OEt</sup>)Br.** In a N<sub>2</sub>-atmosphere glovebox, KO<sup>t</sup>Bu (865 mg, 7.71 mmol) was added to a dry 100 mL Schlenk flask equipped with a stir bar. The flask was brought outside of the glovebox and attached to a Schlenk line. Dry, degassed Et<sub>2</sub>O (50 mL) was added to the KO<sup>t</sup>Bu flask via cannula. Finally, imidazole (500 mg, 7.34 mmol) was added under a steady flow of Ar. (Alternatively, sodium-imidazole can be used in place of this deprotonation step, however yields are somewhat lower.) The reaction was allowed to stir

for 1 hour; at this point, 2-bromo-ethylacetate (0.813 mL, 7.34 mmol) was added under a flow of Ar and this was allowed to stir for another hour. Volatiles were removed in vacuo to give a sticky, colorless goo. The product here was redissolved in 25 mL of THF in a round bottomed flask. Another equivalent of 2-bromo-ethylacetate (0.813 mL, 7.34 mmol) was added; the solution was refluxed (90 °C) for 8 hours. Upon cooling to room temperature, 2 layers were formed; the entire solution was filtered to remove unwanted white solids; volatiles were removed in vacuo from the remaining solution to give a thick yellow liquid in reasonable yield (80%).  $^1\text{H}$  NMR ( $\text{CD}_2\text{Cl}_2$ ):  $\delta$  10.10 (s, 1H), 7.60 (s, 2H), 5.39 (broad, 4H), 4.27 (q, 4H,  $^3J_{\text{HH}} = 6$  Hz), 1.31 (t, 6H,  $^3J_{\text{HH}} = 6$  Hz).

**(VW<sup>NMe2</sup>)Cl.** A procedure analogous to the one described above was used where bromo-ethylacetate replaced with 2-chloro-N,N-dimethylacetamide and the solution was allowed to reflux for 24 hours at 100 °C (60%).  $^1\text{H}$  NMR ( $\text{CD}_3\text{Cl}$ ):  $\delta$  9.69 (s, 1H), 7.51 (s, 2H), 5.51 (s, 4H), 3.14 (s, 6H), 2.93 (s, 6H).

**(VW<sup>OEt</sup>)AuCl.** Under air, (VW<sup>OEt</sup>)Br (783 mg, 2.44 mmol) was dissolved in  $\text{CH}_2\text{Cl}_2$  (20 mL).  $\text{Ag}_2\text{O}$  (282 mg, 1.22 mmol) was added and stirred overnight; volatiles were removed in vacuo to give light grayish brown solids in 90% yield. These solids were redissolved in 15 mL of  $\text{CH}_2\text{Cl}_2$  and  $\text{Au}(\text{SMe}_2)\text{Cl}$  (0.637 mg, 2.16 mmol) was added and stirred for 6 hours; volatiles were removed in vacuo. The resulting solids were redissolved in 25 mL  $\text{CH}_2\text{Cl}_2$ , filtered, and again concentrated in vacuo to give pale yellow solid in 55% yield.  $^1\text{H}$  NMR ( $\text{CD}_3\text{Cl}$ ):  $\delta$  7.11 (s, 2H), 5.00 (broad, 4H), 4.26 (q, 4H,  $^3J_{\text{HH}} = 6$  Hz), 1.31 (t, 6H,  $^3J_{\text{HH}} = 6$  Hz).

**(VW<sup>NMe2</sup>)AuCl.** A procedure analogous to the one described above was used where (VW<sup>NMe2</sup>)Cl was used in place of (VW<sup>OEt</sup>)Br with similar overall yields. <sup>1</sup>H NMR (CD<sub>3</sub>Cl):  $\delta$  7.12 (s, 2H), 5.07 (s, 4H), 3.15 (s, 6H), 3.02 (s, 6H).

**(VW<sup>OEt</sup>)AuBr<sub>3</sub>.** (VW<sup>OEt</sup>)AuCl (220 mg, 0.465 mmol) was dissolved in 10 mL of acetone; LiBr (404 mg, 4.65 mmol) was added and was stirred for 2 hours. Volatiles were removed in vacuo and the resulting white solids taken up in 15 mL of CH<sub>2</sub>Cl<sub>2</sub>. Br<sub>2</sub> (36  $\mu$ L, 0.700 mmol) was added to this slurry and stirred for 5 hours. Volatiles were again removed in vacuo and the yellow solids were extracted with CH<sub>2</sub>Cl<sub>2</sub> until the residual solids were white and all of the Au-complex had been removed. Upon removal of solvent, yellow solids were obtained in 70% yield. <sup>1</sup>H NMR (CD<sub>3</sub>CN):  $\delta$  7.47 (s, 2H), 5.07 (broad, 4H), 4.20 (q, 4H, <sup>3</sup>J<sub>HH</sub> = 6 Hz), 1.26 (t, 6H, <sup>3</sup>J<sub>HH</sub> = 6 Hz).

## F.6 References

1. Herrmann, W. A., *Angew. Chem. Int. Ed.*, **2002**, *41*, 1290-1309.
2. Lin, J. C. Y.; Huang, R. T. W.; Lee, C. S.; Bhattacharyya, A.; Hwang, W. S.; Lin, I. J. B., *Chem. Rev.*, **2009**, *109*, 3561-3598.
3. Samantaray, M. K.; Roy, D.; Patra, A.; Stephen, R.; Saikh, M.; Sunoj, R. B.; Ghosh, P., *J. Organomet. Chem.*, **2006**, *691*, 3797-3805.
4. Arnold, P. L.; Mungur, S. A.; Blake, A. J.; Wilson, C., *Angew. Chem. Int. Ed.*, **2003**, *42*, 5981-5984.
5. Al Thagfi, J.; Dastgir, S.; Lough, A. J.; Lavoie, G. G., *Organometallics*, **2010**, *29*, 3133-3138.

6. Badaj, A. C.; Dastgir, S.; Lough, A. J.; Lavoie, G. G., *Dalt. Trans.*, **2010**, 39, 3361-3365.
7. Fei, Z. F.; Zhao, D. B.; Geldbach, T. J.; Scopelliti, R.; Dyson, P. J., *Chem. Eur. J.*, **2004**, 10, 4886-4893.
8. de Fremont, P.; Stevens, E. D.; Frutos, M. R.; Diaz-Requejo, M. M.; Perez, P. J.; Nolan, S. P., *Chem. Commun.*, **2006**, 2045-2047.
9. Pangborn, A. B.; Giardello, M. A.; Grubbs, R. H.; Rosen, R. K.; Timmers, F. J., *Organometallics*, **1996**, 15, 1518-1520.



## APPENDIX G

### Competitive activation of a methyl C-H bond of dimethylformamide at an Ir center

#### G.1 Abstract

During the synthesis of  $[\text{AsPh}_4][\text{Ir}(\text{CO})_2\text{I}_3\text{Me}]$  by refluxing  $\text{IrCl}_3 \cdot 3\text{H}_2\text{O}$  in DMF (DMF = dimethylformamide) in the presence of aqueous HCl, followed by sequential treatment with  $[\text{AsPh}_4]\text{Cl}$ , NaI, and methyl iodide, and finally recrystallization from methylene chloride/pentane, three crystalline byproducts were obtained:  $[\text{AsPh}_4]_2[\text{Ir}(\text{CO})\text{I}_5]$ ,  $[\text{AsPh}_4]_2[\text{trans-Ir}(\text{CO})\text{I}_4\text{Cl}]$ , and  $[\text{AsPh}_4][\text{Ir}(\text{CO})(\kappa^2\text{-(O,C)-CH}_2\text{NMeCHO})\text{Cl}_2\text{I}]$ . The last of these, whose structure (along with the others) was determined by X-ray diffraction, results from activation of a methyl C-H bond of dimethylformamide, rather than the normally much more reactive aldehydic C-H bond.<sup>1</sup>

#### G.2 Introduction

Dimethylformamide (DMF) is a common and convenient carbonylation reagent in organometallic chemistry.<sup>4-6</sup> The mechanism of these carbonylation reactions has not often been studied in detail, but activation of the aldehydic C-H bond to give a carbamoyl intermediate, followed by C-N bond cleavage (the reverse of either migratory insertion or nucleophilic addition) seems a likely route. Structures resulting from DMF activation at the aldehydic C-H bond have previously been reported. Hidai and coworkers found that *cis*- $[\text{W}(\eta^2\text{-CONMe}_2)(\text{dppe})_2]$  (dppe = diphenylphosphinoethane) can be obtained from DMF and *trans*- $[\text{W}(\text{N}_2)_2(\text{dppe})_2]$  after 20 minutes; on longer reaction it converts to

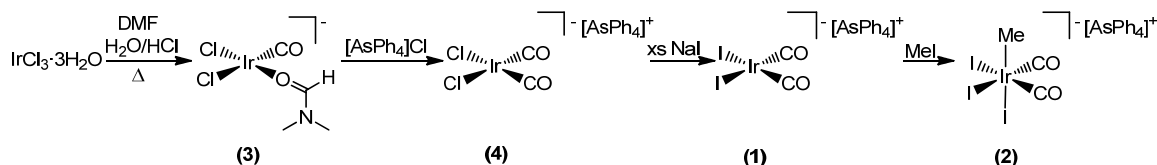
$[\text{W}(\text{CO})(\text{DMF})(\text{dppe})_2]$ .<sup>7</sup> Another decarbonylation intermediate,  $\text{Ru}(\text{H})_2(\text{Cl})(\eta^2\text{-CONMe}_2)(\text{P}^i\text{Pr}_3)_2$ , was generated by reaction of  $\text{Ru}(\text{H})(\text{H}_2)\text{Cl}(\text{P}^i\text{Pr}_3)_2$  with DMF.<sup>8</sup>

The activation of aldehydic C-H bonds at transition metal centers is well known, most prominently in the catalytic decarbonylation of aldehydes.<sup>9</sup> Because this process appears to be relatively facile, reaction at other C-H sites in aldehydes would rarely be expected to be competitive. Indeed, we have found only one example: reaction of  $\text{Rh}(\text{ttp})\text{Cl}$  (ttp = tetrakis-4-tolylporphyrinato) with *p*-methylbenzaldehyde or *p*-tert-butylbenzaldehyde gives (initially) a few percent of  $(\text{ttp})\text{Rh}(\text{CH}_2\text{C}_6\text{H}_5\text{CHO})$  or  $(\text{ttp})\text{Rh}(\text{CH}_2\text{CMe}_2\text{C}_6\text{H}_5\text{CHO})$ , respectively, along with the major product,  $(\text{ttp})\text{Rh}(\text{COAr})$ .<sup>10</sup> To our knowledge there have been no reports of C-H activation of a methyl group of DMF or any closely related species. We report here the structure of an unusual iridium complex resulting from such a reaction.

### G.3 Results and Discussion

Studies in our labs required the synthesis of the iridium carbonyl complexes  $[\text{AsPh}_4][\text{Ir}(\text{CO})_2\text{I}_2]$  (**1**) and  $[\text{AsPh}_4][\text{Ir}(\text{CO})_2\text{I}_3\text{Me}]$  (**2**). Kalck and coworkers reported that decarbonylation of DMF by  $\text{IrCl}_3$  initially formed  $[\text{Ir}(\text{CO})(\text{DMF})\text{Cl}_2]^-$  (**3**), which underwent further transformation to  $[\text{Ir}(\text{CO})_2\text{Cl}_2]^-$ , and was isolated as the  $[\text{AsPh}_4]^+$  salt (**4**).<sup>1</sup> Halide exchange of the latter with NaI or KI in methanol gave **1** in quantitative yields, as monitored by infrared spectroscopy (Scheme 1). In a separate paper, **1** (synthesized by a different route: refluxing  $\text{IrCl}_3$  and NaI in a mixture of 2-methoxyethanol and water while bubbling CO through the solution) was found to react with methyl iodide to give **2**.<sup>11</sup>

## Scheme G.1



In our hands, the reaction of **1** (synthesized via decarbonylation of DMF as in Scheme 1) with MeI gave mainly the expected product **2**, according to infrared spectroscopy. However, on attempted recrystallization of the crude product from a mixture of  $\text{CH}_2\text{Cl}_2$  and pentane two different species were obtained: red needles and a smaller amount of yellow crystals. Both were examined by X-ray crystallography.

A red needle from one such reaction was determined to be a known complex,  $[\text{AsPh}_4]_2[\text{Ir}(\text{CO})\text{I}_5]$  (**5a**), whose structure has been reported.<sup>12, 13</sup> Another needle from a duplicate reaction, surprisingly, turned out to have a different (but closely related) structure:  $[\text{AsPh}_4]_2[\text{trans-Ir}(\text{CO})\text{I}_4\text{Cl}]$  (**5b**). More interesting is the minor yellow product, which was crystallographically determined to be  $[\text{AsPh}_4][\text{Ir}(\text{CO})(\kappa^2\text{-(O,C)-CH}_2\text{NMeCHO})\text{Cl}_2\text{I}]$  (**6**), the product of C-H activation of a methyl group from DMF (Figure 1). As noted above, this appears to be an unprecedented transformation for DMF; the structure demonstrates that the aldehydic C-H bond has remained intact during the methyl C-H activation.

The metallated methyl group in **6** is located *trans* to the iodide ligand, with an Ir-C(3) bond length of 2.0651(11) Å. The aldehydic oxygen is also coordinated to Ir, forming a 5-membered ring; the Ir-O(2) bond distance is 2.0875(9) Å, while the O(2)-C(2) distance is

1.2704(15) Å, somewhat longer than that of unbound, liquid phase DMF (1.24 Å).<sup>14</sup> Otherwise the complex displays fairly typical octahedral geometry, with normal carbonyl Ir-C(1) (1.8221(12) Å) and C(1)-O(1) (1.1455(15) Å) bond lengths, and very small deviations from 90° angles, except for those constrained by the 5-membered ring (C(1)-Ir-C(3) = 95.23(5)°; C3-Ir-I 171.68(3)°).

The origin of **6** is not clear: although there was no evidence of either free or bound DMF in the sample of precursor **1** by IR spectroscopy, trace amounts must have been present. (Formation of **6** was quite reproducible with different batches of the starting material **1**.) One obvious candidate is intermediate **3**, which contains DMF; reaction with MeI could conceivably initiate the observed C-H activation. However, authentic samples of **3** do not react with MeI at all. While the exact mechanism for formation of **6**, specifically the timing of the methyl C-H activation step, remains uncertain, the fact that the latter can compete at all with activation of the much more reactive aldehydic C-H bond is unexpected and intriguing.

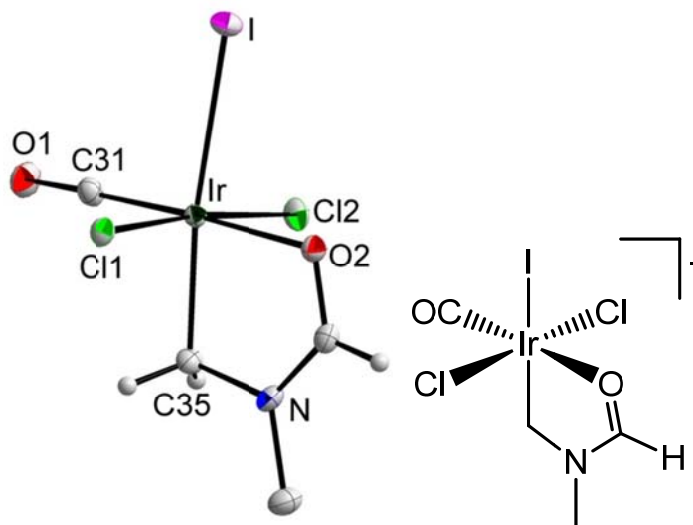


**Figure G.1** Anisotropically refined thermal ellipsoid representation of  $[\text{Ir}(\text{CO})(\kappa^2\text{-CH}_2\text{N}(\text{CH}_3)\text{CHO})\text{Cl}_2\text{I}]^-$ , the anion of **6**. The  $[\text{AsPh}_4]^+$  cation is not shown, and phenyl and methyl hydrogen atoms have been removed for clarity. Selected bond distances and angles: Ir-C1 1.8221(12) Å; Ir-C3 2.0651(11) Å; Ir-I 2.76746(12) Å; C1-Ir-C3 95.23(5) $^\circ$ ; C3-Ir-I 171.68(3) $^\circ$

#### G.4 Conclusions

An unexpected C-H activation of a methyl C-H bond is preferred over the more reactive aldehydic C-H bond, as observed in complex **6**. While attempts to determine the origin of this unusual reactivity were unsuccessful, it is nonetheless a curious example of C-H bond activation and indicates that C-H activation of classically less reactive bonds may occur in the presence of more reactive bonds.

#### G.5 Experimental Section

**General considerations.** All chemicals and solvents were used as received, without further purification.  $\text{IrCl}_3 \cdot 3\text{H}_2\text{O}$  was purchased from Alfa Aesar;  $[\text{AsPh}_4]\text{Cl}$ , MeI,  $\text{CH}_2\text{Cl}_2$ ,

hexanes, and DMF were all purchased from Sigma-Aldrich. Infrared spectra were recorded on a Nicolet 6700 by ThermoFisher Scientific using OMNIC software. X-ray diffraction experiments were carried out in the Beckman Institute Crystallographic Facility on a Bruker KAPPA APEXII X-ray diffractometer.

**[AsPh<sub>4</sub>][Ir(CO)<sub>2</sub>I<sub>2</sub>] (1).** [AsPh<sub>4</sub>][Ir(CO)<sub>2</sub>Cl<sub>2</sub>] (372.0 mg, 0.5296 mmol) was dissolved in methanol and stirred with 5 equivalents of NaI (952.6 mg, 6.355 mmol) for 30 minutes. Volatiles were removed in vacuo. The product was extracted with CH<sub>2</sub>Cl<sub>2</sub>, and volatiles removed again in vacuo to give the desired product in virtually quantitative yield.

**[AsPh<sub>4</sub>][Ir(CO)(κ<sup>2</sup>-(O,C)-CH<sup>2</sup>NMeCHO)Cl<sup>2</sup>I] (6) and [AsPh<sub>4</sub>]<sub>2</sub>[Ir(CO)<sub>4</sub>X] where X = Cl or I (5).** **1** (200 mg, mmol), prepared using the method of decarbonylation of DMF,<sup>2</sup> was reacted with neat MeI (2 mL) for 1 hour. Volatiles were removed in vacuo to give a red-orange solid, whose infrared spectrum matched the literature for [AsPh<sub>4</sub>][Ir(CO)<sub>2</sub>I<sub>3</sub>Me] ( $\nu_{\text{CO}}$  (CH<sub>2</sub>Cl<sub>2</sub>) = 2098, 2046 cm<sup>-1</sup>).<sup>11</sup> The solid was dissolved in approximately 7 mL CH<sub>2</sub>Cl<sub>2</sub>. This solution was layered with hexanes and stored at -36 °C overnight to give red needles (**5**) and trace yellow crystals (**6**) suitable for X-ray diffraction (80 mg total). The infrared spectrum of these crystals displayed only one CO stretch at 2046 cm<sup>-1</sup>, corresponding to **5a**.<sup>12</sup> Crystallographic data have been deposited at the CCDC; the deposition number for **6** is 679443 and for **5b** is 725088.

**Structural data for 6.** Crystals from CH<sub>2</sub>Cl<sub>2</sub>/hexanes; [C<sub>24</sub>H<sub>20</sub>As]<sup>+</sup>[C<sub>4</sub>H<sub>5</sub>NO<sub>2</sub>Cl<sub>2</sub>Ir]<sup>-</sup>, *M* = 872.41; triclinic, space group P-1; *a* = 10.0906(3) Å, *b* = 10.4936(3) Å, *c* = 14.0657(4) Å; α = 90.0840(10)°, β = 107.5460(10)°, γ = 94.2860(10)°; *U* = 1415.63(7) Å<sup>3</sup>; *d*<sub>calc</sub> =

2.047 g/cm<sup>3</sup>;  $T = 100(2)$  K; max  $2\theta$   $^\circ$ ; MoK $\alpha$  radiation ( $\lambda = 0.71073$  Å); 24422 unique reflections were obtained and 19699 with  $I > 2.5\sigma(I)$  were used in the refinement; data was collected on a Bruker KAPPA APEXII X-ray diffractometer. For significant reflections merging  $R$ -value 0.0277; Residuals:  $R_f = 0.0448$  ;  $R_w = 0.0408$  (significant reflections); GooF 1.404.

## G.6 References

- 1) Scott, V. J.; Henling, L. M.; Day, M. W.; Bercaw, J. E.; Labinger, J. A. *Organometallics* **2009**, 28, 4229-4230.
- 2) Serp, P.; Hernandez, M.; Richard, B.; Kalck, P. *Eur. J. Inorg. Chem.* **2001**, 2327.
- 3) Mizobe, Y.; Ishida, T.; Egawa, Y.; Ochi, K.; Tanase, T.; Hidai, M. *J. Coord. Chem.* **1991**, 23, 57.
- 4) Rusina, A.; Vlček, A.A., *Nature* **1965**, 206, 295.
- 5) Collman, J.P.; Sears Jr, J.T.; Kubota, M. *Inorg. Synth.* **1969**, 11, 101.
- 6) Basu, A.; Kasar, T.G.; Sapre, N.Y. *Inorg. Chem.* **1988**, 27, 4539.
- 7) Ishida, T.; Mizobe, Y.; Tanase, T.; Hidai, M. *Chem. Lett.* **1988**, 441; Ishida, T.; Mizobe, Y.; Tanase, T.; Hidai, M. *J. Organomet. Chem.* **1991**, 409, 355.
- 8) Coalter III, J.N.; Huffman, J.C.; Caulton, K.C. *Organometallics* **2000**, 19, 3569.

- 9) See Fristrup, P.; Kreis, M.; Palmelund, A.; Norrby, P.-O.; Madsen, R. *J. Am. Chem. Soc.* **2008**, *130*, 5206-5215; Alaimo, P. J.; Arndtsen, B. A.; Bergman, R. G. *Organometallics* **2000**, *19*, 2130-2143; and references cited therein.
- 10) Haynes, A.; Maitlis, P.M.; Morris, G.E.; Sunley, G.J.; Adams, H.; Badger, P.W.; Bowers, C.M.; Cook, D.B.; Elliott, P.I.P.; Ghaffar, T.; Green, H.; Griffin, T.R.; Payne, M.; Pearson, J.M.; Taylor, M.J.; Vickers, P.W.; Watt, R.J. *J. Am. Chem. Soc.* **2004**, *126*, 2847.
- 11) Chan, K.S.; Lau, C.M. *Organometallics*, **2006**, *25*, 260.
- 12) Malatesta, L.; Naldini, L.; Cariati, F. *J. Chem. Soc.* **1964**, 961.
- 13) Dahm, D.J.; Forster, D. *Inorg. Nucl. Chem. Lett.* **1970**, *6*, 15.
- 14) Ohtaki, H.; Itoh, S.; Yamaguchi, T.; Ishiguro, S.-i.; Rode, B.M. *Bull. Chem. Soc. Jap.* **1983**, *56*, 3406.



## APPENDIX H

### Attempts to increase triptane yields in metal-iodide catalyzed methanol conversion by addition of an external hydride source

#### H.1 Abstract

$\text{ZnI}_2$  and  $\text{InI}_3$  catalyzed methanol conversion is hydrogen deficient; addition of an appropriate external hydride source could theoretically increase the yields of valuable products such as 2,2,3-trimethylbutane (triptane). Finding an appropriate source that can act catalytically under the harsh reaction conditions is a difficult task; attempts to achieve this reactivity is described herein using the Ir-based Cativa catalyst for the  $\text{ZnI}_2$ -based system and methylated cyclohexane for the  $\text{InI}_3$ -based system.

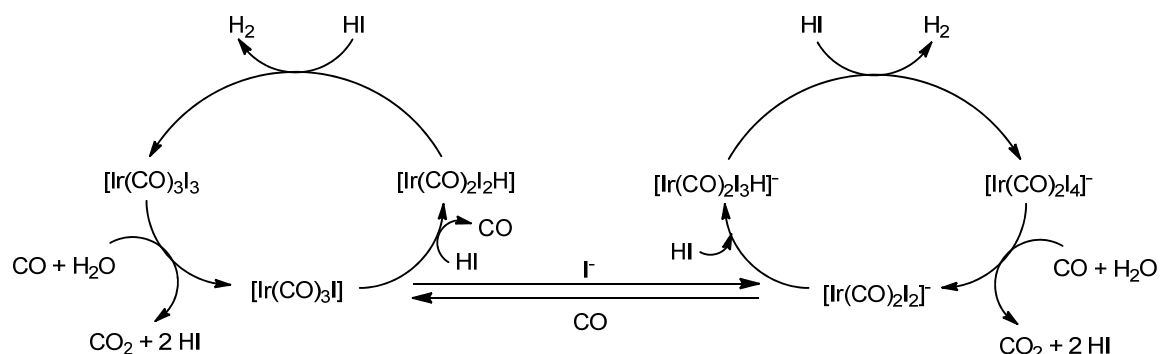
#### H.2 Introduction

$\text{ZnI}_2$  and  $\text{InI}_3$  are known to catalyze the conversion of methanol to 2,2,3-trimethylbutane (common name “triptane”) with surprising selectivity and yields of up to 20% are observed (See Chapter 4 for more in-depth background).<sup>1-3</sup> Previous experiments have demonstrated that adding  $\text{H}_3\text{PO}_2$  and  $\text{H}_3\text{PO}_3$  (6 mol% with respect to methanol) increases the triptane yield up to 36% in some cases.<sup>4</sup> These additives donate a hydride to carbocationic species in solution and are subsequently oxidized to  $\text{H}_3\text{PO}_4$ . There is no simple method of converting  $\text{H}_3\text{PO}_4$  back into either reduced form so  $\text{H}_3\text{PO}_3$  and  $\text{H}_3\text{PO}_2$  only act as stoichiometric hydride donors. Therefore, it is of interest to examine the possibility of

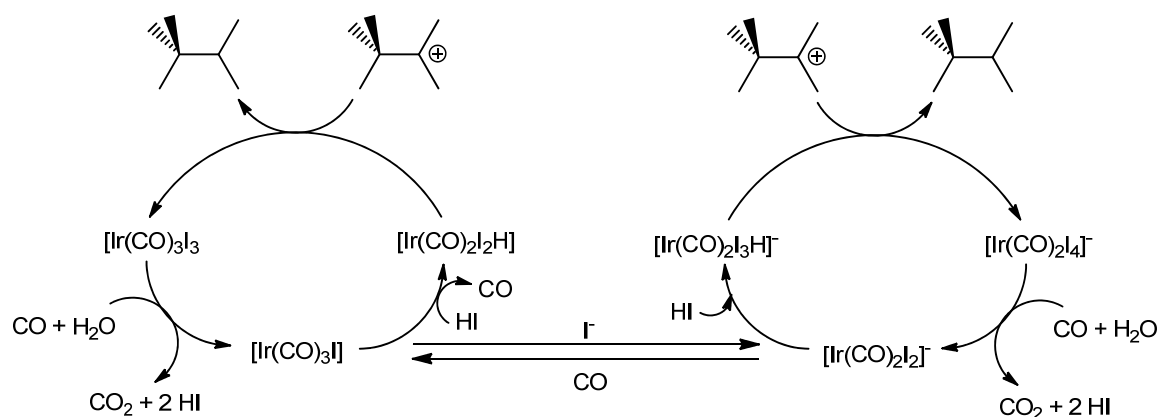
adding a source of hydride that *can* be regenerated under the reaction conditions (a catalytic hydride source). For example, it may be possible to use a metal-complex to donate a hydride and regenerate it under an atmosphere of  $H_2$ . To test this theory, a number of typical hydride donors were utilized as reductants in the triptane reaction (Stryker's reagent ( $[CuH(PPh_3)]_6$ ),  $[Ph_3PNPPh_3][CrH(CO)_5]$ ,  $K[CrH(CO)_5]$ ).<sup>5</sup> Stryker's reagent completely suppressed product formation, presumably because the phosphine is released under the reaction conditions and free bases are known to inhibit  $ZnI_2$ -catalyzed methanol conversion. With the latter two complexes, bubbling was observed immediately upon addition to methanol, presumably from  $H_2$  formation, and no hydrocarbons were formed during the reaction.

With this in mind, a number of restrictions must be placed on the proposed catalyst. First, it must be tolerant to methanol, water, and iodide. It must be stable at high temperatures and under acidic conditions. Furthermore, it should not contain phosphines or amines as ligands which may dissociate to form free bases known to inhibit product formation.<sup>3</sup> The formation of acetic acid from synthesis gas (a mixture of CO and  $H_2$ ) and methanol using an Ir catalyst (the Cativa process) is a catalytic system that operates under *all* of these reaction conditions.<sup>6</sup> Upon inspection of the presumed catalytic cycle, it is seen that a metal-hydride is formed in a side cycle; this species then donates a hydride to generate  $H_2$  (Scheme H.1).<sup>6</sup> If this hydridic species is capable of donating a hydride to carbocations, namely the triptyl cation, this catalyst could be a promising addition to the  $ZnI_2$ -catalyzed methanol conversion system (Scheme H.2).

Scheme H.1



Scheme H.2



### H.3 Results and Discussion

#### H.3.1 $\text{ZnI}_2$ -catalyzed reactions in glass vessels with substoichiometric amount of Ir

$[\text{AsPh}_4][\text{Ir}(\text{CO})_2\text{I}_2]$  is known in the literature and was synthesized following a known procedure.<sup>6,7</sup> One of the preliminary facets to examine was to whether a small amount of the Ir-complexes would perturb the triptane reaction. Experiments were carried out using  $[\text{AsPh}_4][\text{Ir}(\text{CO})_2\text{I}_2]$  and HI, the results of which are shown in Table H.1. The addition of  $[\text{AsPh}_4][\text{Ir}(\text{CO})_2\text{I}_2]$  to the reaction mixture decreases the amount of triptyls formed while

increasing the amount of lighter alkanes; it appears that substoichiometric amounts of either  $[\text{AsPh}_4][\text{Ir}(\text{CO})_2\text{I}_2]$  or  $[\text{AsPh}_4][\text{Ir}(\text{CO})_2\text{I}_3\text{H}]$  (formed in situ) do in fact act as hydride donors. The rate of hydride donation is faster from these species than methylation to form a  $\text{C}_7$  product, resulting in the trapping of lighter alkanes along the growth progression to triptane (Scheme H.3). Aromatic formation appears to increase but this may be due to the decomposition of the cation ( $[\text{AsPh}_4]^+$ ) used in this study.

### Scheme H.3

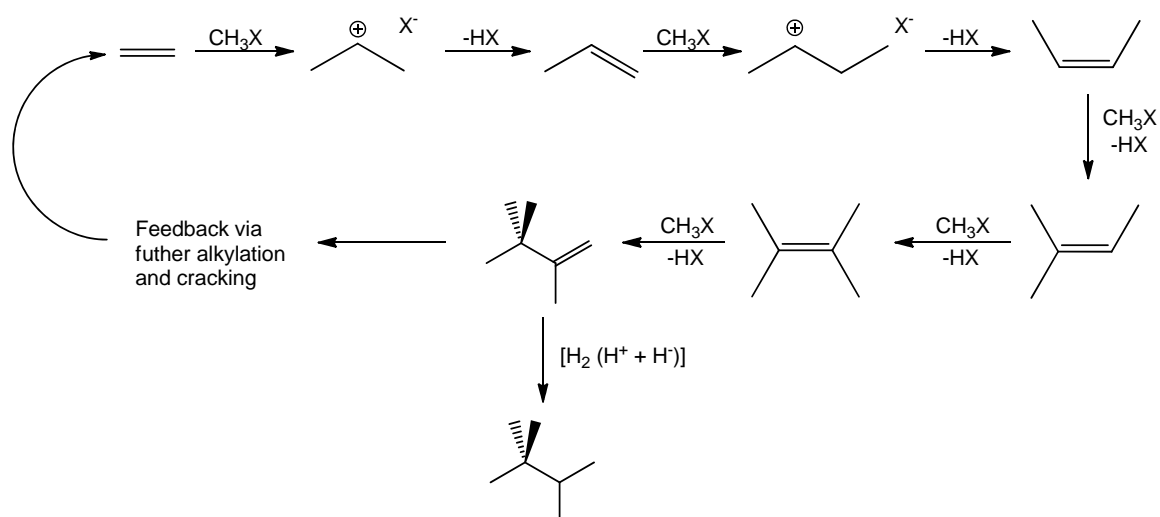


**Table H.1** ZnI<sub>2</sub>-catalyzed methanol conversion in the presence of substoichiometric amounts of [AsPh<sub>4</sub>][Ir(CO)<sub>2</sub>I<sub>2</sub>] and HI

Run <sup>a</sup>	HI <sup>b</sup>	[Ir] <sup>b,c</sup>	Time <sup>d</sup>	DME	C4 <sup>e</sup>	C5 <sup>f</sup>	C6 <sup>g</sup>	Triptyls <sup>h</sup>	Total Alkanes <sup>i</sup>
1	-	-	3	1.3	10.1	8.5	6.9	65.7	91.2
2	-	-	3	3.3	12.3	9	6.1	70.6	98
3	0.5	-	3	0	15.3	11.1	7.1	67.1	100.6
4	0.5	-	3	4.9	10.1	7.8	5.1	70.8	93.8
5	2	-	3	3.1	14	9.2	6.1	69.7	99
6	2	-	3	0	18.8	13.8	8.5	66.9	108
7	-	0.5	8	0	17	15.6	10.9	55.5	99
8	-	0.5	8	0	16.6	16.9	12.5	55.2	101.2
9	0.5	0.5	8	0	16.3	15.4	10.5	56.8	99
10	0.5	0.5	8	6	9.6	10.1	5.2	60.2	85.1
11	0.5	0.5	8	0	12.5	14.4	11.5	55	93.4
12	0.5	0.5	8	0	16.1	16.2	12.9	55.5	100.7
13	1	0.5	8	0	19.6	17.4	12	53.8	102.8
14	1	0.5	8	0	19.9	19.2	13.4	53.2	105.7
15	2	0.5	8	0	15.5	14	10.4	50.5	90.4
16	2	0.5	8	0	20	18	13	49.2	100.2

<sup>a</sup>All runs were carried out using 2.4 g of ZnI<sub>2</sub>, 1 mL of methanol, and 50  $\mu$ L of isopropanol. <sup>b</sup> mol% <sup>c</sup>[AsPh<sub>4</sub>][Ir(CO)<sub>2</sub>I<sub>2</sub>] <sup>d</sup> hours <sup>e</sup> isobutane (mg) <sup>f</sup> isopentane (mg) <sup>g</sup> 2,3-dimethylbutane + 2-methylpentane + and 3-methylpentane (mg) <sup>h</sup> triptane + triptene (mg) <sup>i</sup> C4 + C5 + C6 + triptyls (mg) <sup>j</sup> hexamethylbenzene + pentamethylbenzene + tetramethylbenzene (mg)

Two reactions were done in glass high pressure bombs with Kontes valves in the presence of catalytic quantities of [Ir(CO)<sub>2</sub>I<sub>2</sub>Me]<sub>2</sub>, which eliminates the problem of methylating the counter cation. A reaction containing ZnI<sub>2</sub> (3.76 mmol), MeOH (12.35 mmol), <sup>i</sup>PrOH (0.33 mmol), and [Ir(CO)<sub>2</sub>I<sub>2</sub>Me]<sub>2</sub> (0.3 mol% Ir relative to MeOH) under 1 atm of Ar showed the decomposition of the Ir-catalyst by the formation of Ir-black. The product distribution displayed only slight inhibition of the triptane process (25 mg of triptyls compared with the expected 30 mg), with approximately 12% of the triptyls being triptene (as estimated by GC trace). The same reaction carried out under 1 atm of synthesis gas gave a final reaction mixture that remained bright orange in color and resulted in a

triptyl yield of 27 mg, of which about 9% was triptene (as estimated by GC trace).

Also, only 1.37 mg of 2,3-dimethyl-2-butene is formed under CO/H<sub>2</sub>, whereas the reaction under Ar produced 2.72 mg. There was no indication of methyl acetate being formed under these reaction conditions. Although these are modest differences, with such low catalyst loading and pressure it could be significant.

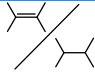
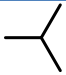
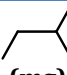
### *H.3.2 ZnI<sub>2</sub>-catalyzed reactions in the Zr-Parr reactor*

The studies done in glass vessels had demonstrated that although this complex affected the product distribution in a standard triptane reaction to display fewer olefins (indicative of hydride transfer), the overall triptane yield was lower, at least in part because of higher aromatic formation; this is likely due to methylation of the phenyl groups on the counter-cation so it was of interest to eliminate [AsPh<sub>4</sub>]<sup>+</sup> from the reaction. Furthermore, it appeared that the hydride was stopping chain growth *before* triptane could be reached; however, the reaction conditions were not catalytic, so it was also of interest to see how the Ir-complexes would affect the product distribution under catalytic conditions (under CO/H<sub>2</sub> pressure).

Attempts to replace the counter-cation with Na<sup>+</sup> or K<sup>+</sup> were all unsuccessfully attempted, however the neutral species, [Ir(CO)<sub>2</sub>I<sub>2</sub>Me]<sub>2</sub> was shown to reduce the amount of olefins observed in a ZnI<sub>2</sub>-catalyzed reaction under one atmosphere of synthesis gas. A reaction was carried out in a 25 mL Zr-reactor. ZnI<sub>2</sub> (45.1 mmol) was dissolved completely in MeOH (148.2 mmol) and <sup>i</sup>PrOH (5.225 mmol). [Ir(CO)<sub>2</sub>I<sub>2</sub>Me]<sub>2</sub> (0.08 mol% relative to MeOH) was added to the solution and put into the 25 mL reactor. The reactor was

pressurized with 500 PSIG of synthesis gas and heated with an oil bath at 220 °C for 22 hours (internal temperature read 160–170 °C, see Section H.3.3). The product distribution of this and other similar reactions done in the Parr bomb are shown in Table H.2. When  $[\text{AsPh}_4][\text{Ir}(\text{CO})_2\text{I}_2]$  was used as the potential hydrogenation catalyst, the triptane yield decreases dramatically, however a substantial amount of methyl acetate was found in the water layer of the final product mixture, showing that the Cativa process is active under these reaction conditions. As compared with  $[\text{AsPh}_4][\text{Ir}(\text{CO})_2\text{I}_2]$ , it is seen that the triptane yield increases modestly when  $[\text{Ir}(\text{CO})_2\text{I}_2\text{Me}]_2$  is used, which is likely indicative of the “wasting” of more methylating equivalents on aromatics formed from decomposition of the counter-cation in the former case. Methyl acetate was still formed in this experiment and it does not appear that the Cativa process can be shut down easily.

**Table H.2**  $\text{ZnI}_2$ -catalyzed methanol conversion in a Parr Reactor

Expt <sup>a</sup>	Pressure (PSIG)	Hydrogenation catalyst	Triptyls (mg)		 (mg)	 (mg)	DME (mg)	PMB + HMB (mg)
<b>1<sup>b</sup></b>	-	-	326.5	0.43	22.6	41.7	39.4	39.3
<b>2<sup>c</sup></b>	-	6 mol% $\text{H}_3\text{PO}_3$	378.2	0.036	48.9	62.5	20.1	141.4
<b>3</b>	500 ( $\text{N}_2$ )	-	309.4	0.25	23.5	60.5	0	63.0
<b>4<sup>c</sup></b>	500 ( $\text{H}_2$ )	2 mol% 10% Pd/C	263.6	0.065	20.0	40.76	0.7	22.6
<b>5</b>	500 ( $\text{CO}/\text{H}_2$ )	4 mol% $[\text{Ir}(\text{CO})_2\text{I}_2]^-$	116.6	0	2.1	14.0	0	90.9
<b>6</b>	500 ( $\text{CO}/\text{H}_2$ )	0.1 mol% $[\text{Ir}(\text{CO})_2\text{I}_2\text{Me}]_2$	143.6	0	7.4	28.9	0	49.0

<sup>a</sup> Reactions were carried out with 14.4 g of  $\text{ZnI}_2$ , 6 mL of methanol and 400 mL of isopropanol for 22 hours (except for reactions that were not pressurized before heating which were run for 8 hours) with the external oil bath set to 220 °C. <sup>b</sup> average of 5 runs. <sup>c</sup> average of 2 runs

### *H.3.3 Notes on working with a Zr-Parr reactor*

A highly corrosion-resistant Zr-reactor was purchased in order to perform these triptane reactions on a large scale and at high pressures. Early experiments indicated that changing from the typically used glass vessels to the reactor caused a dramatic change in the chemistry. GC traces indicated triptane yields of less than 7% for the Zn-system as compared with the normal 20%, and a large increase in the amount of aromatics formed. Additionally, black solids could be isolated from the reaction mixture, which by elemental analysis were found to be more than 45% carbon-based, less than 6% hydrogen, and the rest mainly zinc and iodine.

A number of possible contributors were ruled out: stirring speed, reaction run time, the presence of air, reactant concentration, head space volume, and reactor volume had no effect on the observed chemistry. Shavings from the Zr-stirrer were added to a glass reaction and no perturbation of the typical product distribution was observed, ruling out the possibility that the Zr-surface was changing the chemistry. The accuracy of the thermocouple was confirmed, eliminating the possibility of improper temperature readings. Curiously, pressurizing the reactor with N<sub>2</sub> appeared to increase to amount of black solids isolated from the reaction.

It was suggested that hot spots might be forming inside the reactor, so an experiment was carried out in which an external thermocouple was placed between the heating mantle and the outer wall of the reactor. When the internal thermocouple was set to 200 °C, the heating mantle reached temperatures above 350 °C. To avoid this extra heat input, the



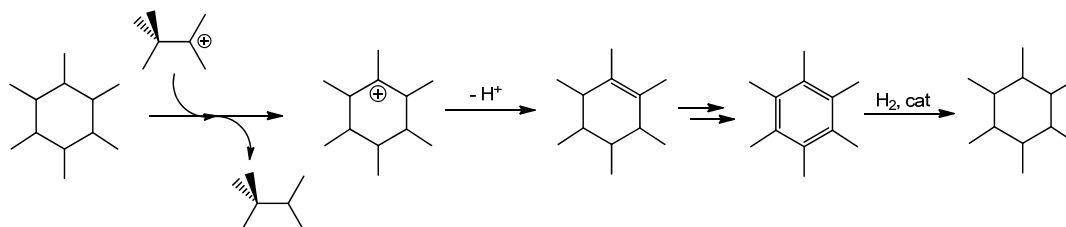
heating mantle was replaced with an oil bath. With the oil bath set to 220 °C and the top of the reactor heavily insulated, the internal temperature (in a reaction using 6 mL of methanol in a 25 mL reactor) reached 165–170 °C. Although it is not expected for a  $\text{ZnI}_2$ -catalyzed reaction to initiate at temperatures below 180 °C, the GC trace showed approximately the expected yield of triptane, with no excess of aromatics. To further confirm the theory that hot spots were the cause of the unusual chemistry being observed, a standard triptane reaction was carried out in a glass vessel at 235 °C. This reaction generated a larger amount of aromatic side products, supporting the theory that the reactor was actually getting hotter than the internal thermocouple was registering. The setup with an oil bath was utilized for all Parr reactor experiments.

#### *H.3.4 Addition of an external hydrogen source to $\text{InI}_3$ -catalyzed MeOH conversion*

It has been previously shown that in a similar fashion to  $\text{ZnI}_2$ ,  $\text{InI}_3$  can catalyze the conversion of methanol to triptane, although there are some significant differences in product distribution.<sup>8</sup> Firstly, the product mixture contains predominantly isoparaffins and aromatics, while the  $\text{ZnI}_2$ -system also produced olefins. This is presumably due to better hydride transfer in the  $\text{InI}_3$ -system. Also, the  $\text{InI}_3$ -catalyzed reaction can be initiated using alkanes, which is not true of the Zn-system. A related proposal for adding an external source of  $\text{H}_2$  to increase alkane yields and reduce aromatic formation can be applied to the  $\text{InI}_3$ -system (where the source is an Ir-H species in the Zn-system). An ideal source of  $\text{H}_2$  would be a compound that could easily be regenerated to close the cycle. In the  $\text{InI}_3$ -system, unlike with  $\text{ZnI}_2$ , it is possible to exploit the fact that alkanes can be activated. In

theory, hexamethylcyclohexane could be used as the source of hydride to form hexamethylbenzene, a known side product of the reaction. Theoretically, hexamethylbenzene could then be removed from the reaction mixture and hydrogenated to regenerate hexamethylcyclohexane (Scheme H.4).

**Scheme H.4**



Preliminary studies were carried out using 1,2,3,5-tetramethylcyclohexane because it is commercially available. Adamantane was also examined both alone and in combination with tetramethylcyclohexane because it is known to facilitate hydride transfer by acting as a shuttle (See Chapter 5). From the results shown in Table H.3 it can be seen that tetramethylcyclohexane successfully initiates the triptane reaction while adamantane does not. Higher concentrations of tetramethylcyclohexane result in slightly higher amounts of lighter alkanes and less triptane. The reactions carried out using both tetramethylcyclohexane and adamantane display even larger amounts of light alkanes and less triptane, showing that the rate of hydride transfer is faster than the rate of methylation to form the  $C_7$  product in this system.

**Table H.3** InI<sub>3</sub>-catalyzed methanol conversion reactions in the presence of 1,2,3,5-tetramethylcyclohexane and adamantane.

Run	Time <sup>a</sup>	Me <sub>4</sub> Cy <sup>b</sup>	Ad <sup>b</sup>	<i>i</i> PrOH <sup>c</sup>	HMB <sup>d</sup>	PMB <sup>d</sup>	Triptane <sup>d</sup>	C6 <sup>e</sup>	C4 <sup>f</sup>	Total Alkanes <sup>g</sup>
1	2	0	0	50	3.5	8.7	20.6	9.4	10	40
2	2	0	0	50	2.4	9	22.8	11.2	11.1	45.1
3	2	0	3	0	0	0	0	0	0	0
4	2	0	3	0	0	0	0	0	0	0
5	2	2.25	0	0	4.6	11.1	19.2	9.4	14.1	42.7
6	2	2.25	0	0	4	13	20.2	10.3	15.9	46.4
7	2	4.5	0	0	4.9	16.8	16.8	10.6	17	44.4
8	2	4.5	0	0	6.2	18.5	16.1	10.7	13.4	40.2
9	2	4.5	0	0	10.1	15.6	17.2	9.8	16.7	43.7
10	2	9.0	0	0	20.4	12.5	14.4	13	23.5	50.9
11	2	2.25	3	0	2.4	12.3	5.4	13.9	20.7	40
12	2	2.25	3	0	13	3.9	9.7	12	14.5	36.2

<sup>a</sup>hours <sup>b</sup>mol % <sup>c</sup>μL <sup>d</sup>mg <sup>e</sup>2,3-dimethylbutane + 2-methylpentane + and 3-methylpentane (mg) <sup>f</sup>isobutane <sup>g</sup>triptane + C6 + C4

#### H.4 Conclusions

The addition of a second catalyst to Zn- and In-based methanol conversions could theoretically cause a dramatic increase in valuable products. While it is obvious that finding a catalyst that can function under the harsh reaction conditions is difficult, it appears that the competing rate of methylation versus hydride transfer is an additional complication. In every case where hydride transfer was successful (where fewer olefins were observed), this transfer occurred too early in the chain growth process, namely before the valuable C<sub>7</sub> product could be built. In the case of the Cativa catalyst under catalytic pressures, the formation of methyl acetate also competed and diverted methanol away from triptane synthesis and toward methyl acetate synthesis. In the end, neither of these systems could be engineered to give better high-value product yields by the addition of these catalysts that are stable under the reaction conditions.

## H.5 Experimental Section

**General considerations.**  $\text{InI}_3$  (purchased from Alfa Aesar),  $\text{ZnI}_2$  (purchased from Sigma-Aldrich), MeOH and other organic compounds were reagent-grade commercial samples used without further purification. GC analyses were performed on an HP model 6890N chromatograph equipped with a 10 m x 0.10 mm x 0.40  $\mu\text{m}$  DB-1 column.  $\text{IrCl}_3 \cdot x\text{H}_2\text{O}$  was purchased from Alfa Aesar and 1,2,3,5-tetramethylcyclohexane was purchased from Sigma Aldrich; both were used without further purification.  $[\text{AsPh}_4][\text{Ir}(\text{CO})_2\text{I}_2]$  and  $[\text{Ir}(\text{CO})_2\text{I}_2\text{Me}]_2$  were prepared according to the literature procedures.

**Glass bomb protocols.** Reactions were performed in thick-walled pressure tubes equipped with Teflon stopcocks (Kontes valves), rated up to 10 bar. The procedure for standard reactions is based on the procedure reported earlier for MeOH-to-hydrocarbon conversions using  $\text{ZnI}_2$  and  $\text{InI}_3$ . In a typical experiment, the tube was equipped with a stir bar and charged with  $\text{ZnI}_2$  (2.4 g, 7.52 mmol), MeOH (1.0 mL, 24.8 mmol), and isopropanol (0.050 mL, 0.65 mmol), if an initiator was required. (If  $\text{InI}_3$  was used as the catalyst it was weighed out in a glove box due to its hygroscopic nature; however the reactions were carried out under an atmosphere of air). If an Ir-complex or 1,2,3,5-tetramethylcyclohexane was utilized as an additive, it was added at this stage; if an atmosphere of gas was to be used, the system was flushed with the appropriate gas, then sealed with the Teflon stopcock. The pressure tube was then placed in a pre-heated oil bath behind a blast shield and stirred at the appropriate temperature for the desired period of

time. After heating, the tube was removed from the bath and allowed to cool to room temperature and then placed in an ice bath. The stopcock was removed and chloroform (1.0 mL), containing a known amount of cyclohexane as an internal standard, was pipetted into the reaction mixture followed by water (0.5 mL). The stopcock was replaced, the mixture was shaken vigorously and the organic layer separated. A small aliquot was diluted with acetone or tetradecane for GC analysis.

**Zr Parr reactor protocols.** The procedure for standard reactions is based on the procedure reported earlier for MeOH-to-hydrocarbon conversions using  $\text{ZnI}_2$  and  $\text{InI}_3$ . In a typical experiment, the tube was equipped with a stir bar and charged with  $\text{ZnI}_2$  (14.4 g, 45.12 mmol), MeOH (6 mL, 148.8 mmol), and iso-propanol (0.40 mL, 5.2 mmol), if an initiator was required. If an Ir-complex was utilized as an additive, it was added at this stage. The Parr reactor was then sealed and pressurized if gas was to be used. The top of the Parr reactor was heavily insulated with glass wool and aluminum foil (not interfering with the stirring mechanism) and an oil bath was placed around the vessel. While stirring the reaction, the oil bath was set to 220 °C and the internal temperature of the vessel read temperatures between 165–170 °C. The reaction was heated at this temperature for the allotted time and then the oil bath was removed, the entire system cooled, and the Parr reactor vented. The reactor was opened and chloroform (3 mL), containing a known amount of cyclohexane as an internal standard, was pipetted into the reaction mixture followed by water (5 mL). This solution was mixed vigorously and the organic layer separated. A small aliquot was diluted with acetone or tetradecane for GC analysis.

## H.6 References

1. Kim, L.; Wald, M. M.; Brandenberger, S. G., *J. Org. Chem.*, **1978**, *43*, 3432-3433.
2. Bercaw, J. E.; Diaconescu, P. L.; Grubbs, R. H.; Hazari, N.; Kay, R. D.; Labinger, J. A.; Mehrkhodavandi, P.; Morris, G. E.; Sunley, G. J.; Vagner, P., *Inorganic Chemistry*, **2007**, *46*, 11371-11380.
3. Bercaw, J. E.; Diaconescu, P. L.; Grubbs, R. H.; Kay, R. D.; Kitching, S.; Labinger, J. A.; Li, X. W.; Mehrkhodavandi, P.; Morris, G. E.; Sunley, G. J.; Vagner, P., *J. Org. Chem.*, **2006**, *71*, 8907-8917.
4. Bercaw, J. E.; Grubbs, R. H.; Hazari, N.; Labinger, J. A.; Li, X. W., *Chem. Commun.*, **2007**, 2974-2976.
5. Hazari, N., In *BP Quarterly Report*, 2007.
6. Haynes, A.; Maitlis, P. M.; Morris, G. E.; Sunley, G. J.; Adams, H.; Badger, P. W.; Bowers, C. M.; Cook, D. B.; Elliott, P. I. P.; Ghaffar, T.; Green, H.; Griffin, T. R.; Payne, M.; Pearson, J. M.; Taylor, M. J.; Vickers, P. W.; Watt, R. J., *J. Am. Chem. Soc.*, **2004**, *126*, 2847-2861.
7. Serp, P.; Hernandez, M.; Richard, B.; Kalck, P., *European Journal of Inorganic Chemistry*, **2001**, 2327-2336.

## APPENDIX I

### Synthesis and characterization of Fe and Co complexes of a new sterically demanding BP<sub>2</sub>pz ligand

#### I.1 Abstract

A series of Fe and Co complexes supported by the bulky [PhBP<sup>tBu</sup><sub>2</sub>(pz<sup>tBu</sup>)]<sup>-</sup> ligand platform are reported herein. Target molecules en route to highly reactive multiply bonded species were synthesized; while this system demonstrates some promising results, more work is required to achieve these goals.

#### I.2 Introduction

Over the last thirty years there has been an increase of research on complexes containing metal-ligand multiple bonds. Until recently, first-row late metal-ligand multiple bonds (Fe, Co, Ni, Cu) were especially rare.<sup>1</sup> These complexes have biological importance as they have been proposed as intermediates in multiple enzymatic pathways. For example, high-valent nitrido and imido species have been proposed as intermediates in the reduction of dinitrogen to ammonia by iron nitrogenases.<sup>2</sup> Furthermore, complexes containing late metal-ligand multiple bonds show promise as atom or group transfer reagents.<sup>3-4</sup>

It was once believed that late metals had an inherent incompatibility with multiply bonded, strong  $\pi$ -donors because these complexes were expected to possess populated antibonding orbitals;<sup>1</sup> however, many examples have appeared recently that contradict this theory. Among the earlier examples of late metal-ligand multiple bonds were Ir-imide and Ir-oxo functionalities which were synthesized by the groups of Bergman (( $\eta^5$ -

$\text{C}_5\text{Me}_5\text{IrNR})^{5-6}$  and Hursthouse  $((\text{mesityl})_3\text{IrO})$ ,<sup>7</sup> respectively. Subsequently, multiple Fe-oxo species were prepared, largely due to their relevance to cytochrome P450 chemistry.<sup>8-13</sup> In 2000, Lee and coworkers reported the first terminal Fe-imide, which existed in an  $\text{Fe}_4$ -cluster.<sup>14</sup> Soon after, terminal amido and imido complexes of Ni were prepared using a bisphosphine chelate as a scaffold<sup>15</sup> and a family of Co and Fe imides were prepared, supported by  $[\text{PhBP}_3]$  ( $[\text{PhBP}_3] = \text{PhB}(\text{CH}_2\text{PPh}_2)_3$ ) (see Figure I.1) and related ligands.<sup>3,16-19</sup> In 1998, an Os-nitride supported by hydrotris(1-pyrazolyl)borate was synthesized<sup>20</sup> and later, in 2004, an Fe-nitride supported by the  $[\text{PhBP}_3]$  ligand platform was reported.<sup>21</sup> Although this is by no means an exhaustive review of the many examples that have appeared over the years, all of these reports demonstrate that under suitable conditions, late-metals can in fact form metal-ligand multiple bonds.

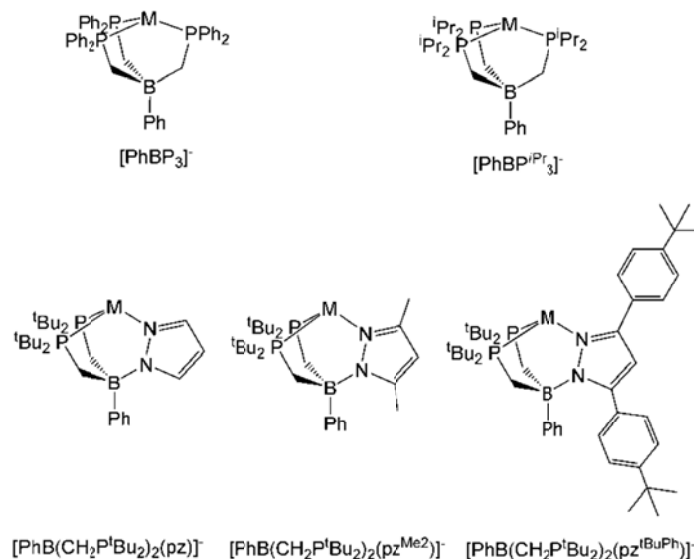
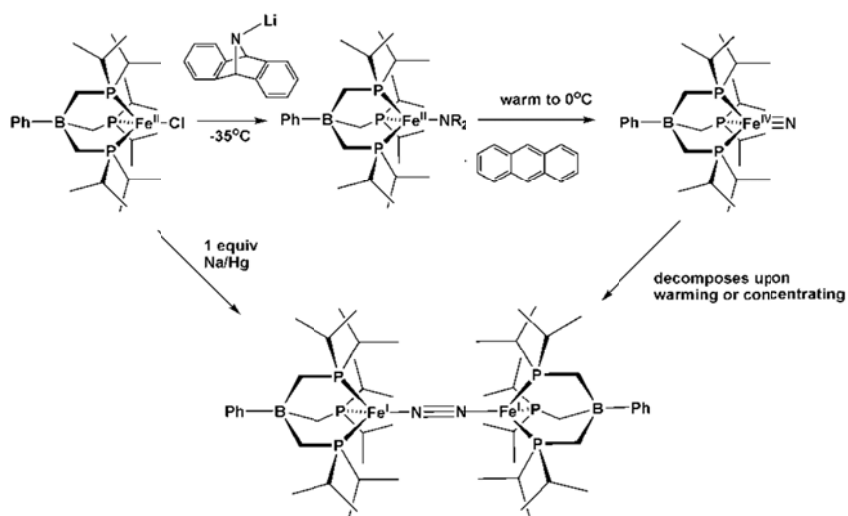


**Figure I.1.** Ligands and the abbreviations used to denote them



A new ligand design with three phosphine donors and a borate backbone was developed in 1999.<sup>22-23</sup> This ligand platform is unique because it has an anionic backbone with three strongly donating phosphine arms which results in a very strong-field ligand. The  $\text{PhBP}^{\text{iPr}}_3$  ( $\text{PhBP}^{\text{iPr}}_3 = \text{PhB}(\text{CH}_2\text{P}^{\text{iPr}}_2)_3$ ) ligand platform was found to support a rare  $\text{Fe(IV)}\equiv\text{N}$  at low temperatures,<sup>21</sup> however, under vacuum or upon warming to room temperature, the complex reductively couples to form an  $\text{Fe(I)}\text{-N}_2\text{-Fe(I)}$  bridged complex (Scheme I.1).<sup>21</sup>

**Scheme I.1**<sup>21</sup>



In order to prevent this coupling from occurring, a new ligand platform was designed containing two phosphine arms and one pyrazole donor (See Figure I.1). The 3-position on the pyrazole moiety is relatively simple to modify and this makes it easy to increase the steric bulk around the fourth coordination site on the metal center, whereas changing the steric bulk of phosphine derivatives is typically much more difficult. Although the original design of this ligand aimed to prevent the dimerization of a nitride complex, it was also

hoped that this ligand might provide a scaffold to access other high-valent multiply bonded species (such as oxos or carbynes) that had not yet been realized using  $[\text{PhBP}^{\text{iPr}}_3]\text{M}$  ( $\text{M} = \text{Fe}$  or  $\text{Co}$ ) as a platform (Figure I.1). In addition it was of interest to see how small changes to the ligand donor set would affect the reactivity of the resulting Fe and Co complexes and test if other novel coordination complexes could be prepared. Unfortunately a nitride was never successfully synthesized using the  $[\text{PhBP}^{\text{tBu}}_2(\text{pz}')] \text{ ligand platform, although several novel mononuclear Fe(IV)-imides were realized using them.}^{18-19}$

The Fe(III) imides  $[\text{PhBP}^{\text{tBu}}_2(\text{pz})]\text{FeNAd}$  and  $[\text{PhB}(\text{CH}_2\text{P}^{\text{tBu}}_2)_2(\text{pz}^{\text{Me}_2})]\text{FeNAd}$  underwent a reversible oxidation event at  $-0.72 \text{ V}$  at  $500 \text{ mV/s}$  and at  $-0.77 \text{ V}$  at  $100 \text{ mV/s}$  (vs  $\text{Fc}/\text{Fc}^+$ ), respectively.<sup>19</sup> The corresponding reduction event was irreversible in both of these complexes. It was subsequently shown that both ligands support Fe(III)-imides that can be successfully oxidized at low temperatures to form the first stable mononuclear Fe(IV)-imides (Figure I.2).<sup>18-19</sup>

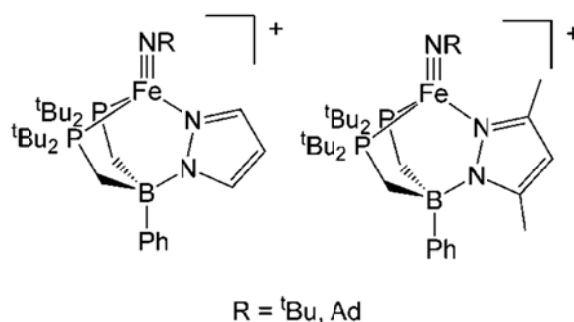
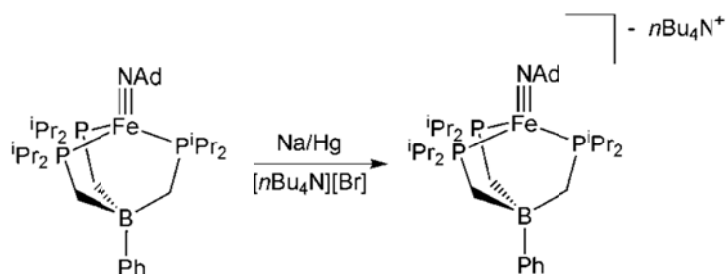


**Figure I.2.** Fe(IV)-imides supported by  $[\text{PhBP}^{\text{tBu}}_2(\text{pz}')] \text{ ligand platform.}^{18-19}$

In contrast, both Co(IV) and Fe(IV) imides have been elusive using the trisphosphinoborate ligand platform.<sup>17</sup> Although a stable Fe(III) imide was synthesized, the redox chemistry proved to be incompatible with obtaining an Fe(IV) imide as  $[\text{PhBP}^{\text{iPr}}_3]\text{Fe}$

$\equiv\text{NAd}$  displays an irreversible oxidation event at  $-0.45\text{ V}$  vs.  $\text{Fc}/\text{Fc}^+$ .<sup>17</sup> On the other hand, a reversible II/III couple ( $-1.79\text{ V}$  vs.  $\text{Fc}/\text{Fc}^+$ ) was observed and an Fe(II)-imide anion was synthesized utilizing these ligands (Scheme I.2),<sup>17</sup> demonstrating some of the differences between trisphosphinoborate ligands and the related pyrazole ligands.

**Scheme I.2**



The aim of this work was to expand on previous chemistry from the Peters group and synthesize a new ligand with a *tert*-butyl substituent on the pyrazole arm (Figure I.3) to increase the steric bulk surrounding the fourth coordination site.

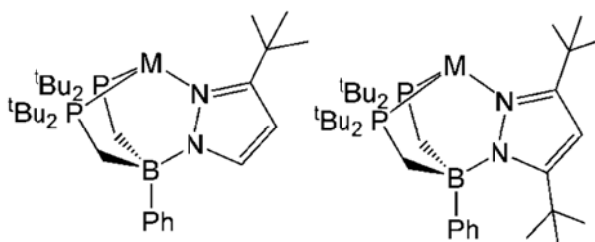


**Figure I.3** New ligand design

By more efficiently blocking the fourth coordination site, it was hoped that different ligand substitution patterns would be observed as compared with the parent ligands and that this might result in dramatically different reactivity toward substrates leading to multiply-bonded species. At this stage, it was unclear how this new ligand would affect the

electronic properties of the complexes in comparison to the parent ligands. In general, adding donating alkyl groups makes reduction potentials more negative, as evidenced by the shift from - 2.25 V for  $[\text{PhB}(\text{CH}_2\text{P}^t\text{Bu}_2)_2(\text{pz})]\text{FeCl}$  to -2.48 V for  $[\text{PhB}(\text{CH}_2\text{P}^t\text{Bu}_2)_2(\text{pz}^{\text{Me}_2})]\text{FeCl}$  (vs  $\text{Fc}/\text{Fc}^+$ ).<sup>18-19</sup> However, it is uncertain whether changing from a methyl substituent to a *tert*-butyl substituent will have a significant effect on the electronic properties. The synthesis of this new ligand was developed based on the previous synthesis of the related ligands in the same family and the chemistry of its coordination compounds as potential precursors to interesting metal-ligand multiply-bonded species was examined.

### I.3 Results and Discussion

#### I.3.1 Ligand synthesis

The first pyrazole that was selected to prepare a more sterically bulky ligand was 3,5-di-*tert*-butylpyrazole (Figure I.4). This compound was selected ahead of 3-*tert*-butylpyrazole because it was immediately available from commercial sources; however, it proved to be incompatible for this chemistry. Once deprotonated (See Scheme I.3), 3,5-di-*tert*-butylpyrazole failed to react with  $\text{PhB}(\text{CH}_2\text{P}^t\text{Bu}_2)_2$ . A molecular mechanics model (using Chem3D) (Figure I.5) showed a steric clash between the 5-*tert*-butyl group and the phenyl group on the borane; thus, the target ligand could not be synthesized.

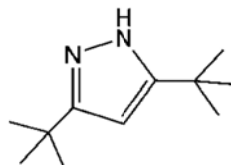


**Figure I.4.** 3,5-di-*tert*-butylpyrazole

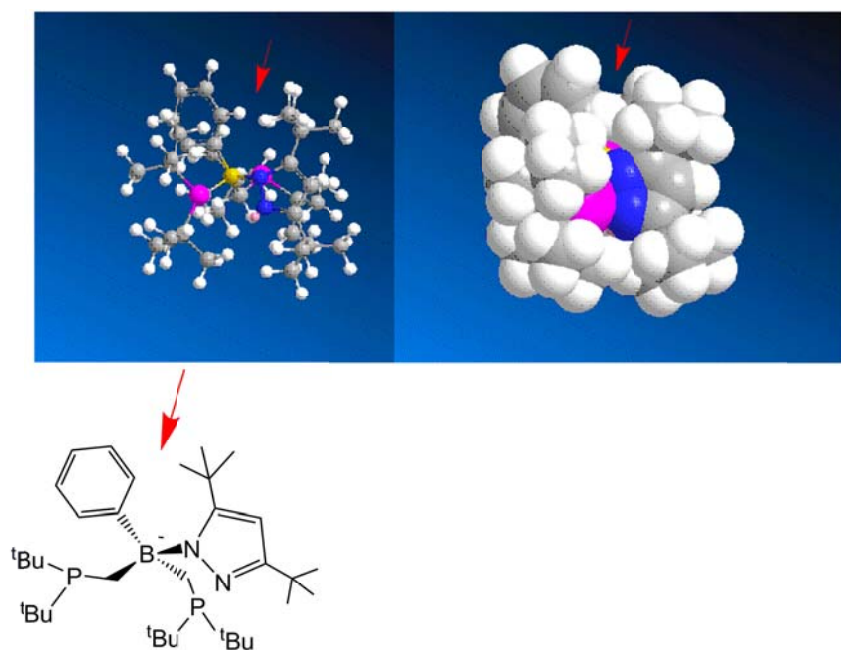
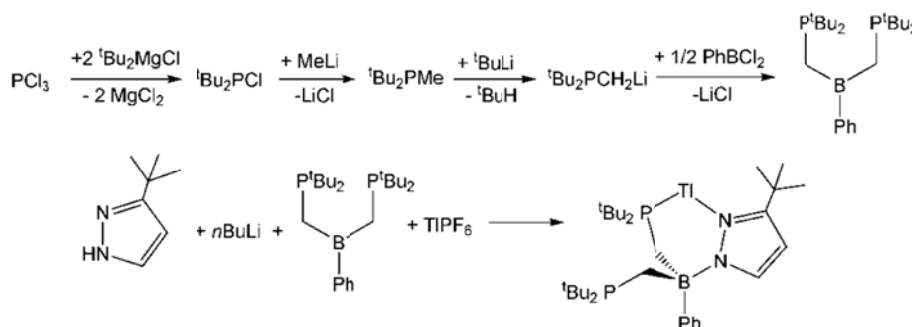


**Figure I.5.** MM2 energy minimization of  $[\text{PhBP}^{\text{tBu}}_2(\text{pz}^{\text{tBu}2})]^-$  and steric clash between 5-*tert*-butyl on the pyrazole and the phenyl substituent on the borane

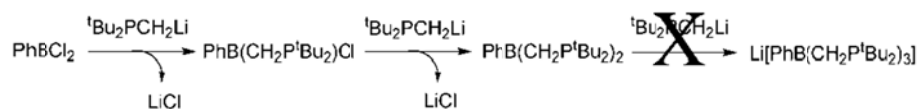
After the unsuccessful synthesis using 3,5-di-*tert*-butylpyrazole, a synthesis with 3-*tert*-butylpyrazole was attempted, and  $[\text{PhB}(\text{CH}_2\text{P}^{\text{tBu}}\text{Bu}_2)_2(\text{pz}^{\text{tBu}})]^-$  was successfully obtained (Scheme I.3).

## Scheme I.3



In the synthesis of the diphosphenoborane, it is important that the substituents on the phosphine are *tert*-butyl groups; these bulky groups prevent the addition of a third equivalent of  $\text{Li}[\text{CH}_2\text{P}^t\text{Bu}_2]$  to  $\text{PhB}(\text{CH}_2\text{P}^t\text{Bu}_2)_2$  (Scheme I.4). Additionally, the large groups prevent any appreciable amount of adduct formation between the borane and phosphine in solution, allowing for the pyrazole arm to be introduced effectively.<sup>18-19</sup>

## Scheme I.4



An interesting trend is seen in the NMR spectra collected of Tl-salts of  $[\text{PhBP}^t\text{Bu}(\text{pz})]^-$ ,  $[\text{PhBP}^t\text{Bu}(\text{pz}^{\text{Me}_2})]^-$ ,  $[\text{PhBP}^t\text{Bu}(\text{pz}^t\text{BuPh})]^-$ , and  $[\text{PhBP}^t\text{Bu}(\text{pz}^t\text{Bu})]^-$ , which are generated using analogous procedures to the one shown in Scheme I.3. The  $^{31}\text{P}$  NMR spectra show different degrees of fluxionality of the phosphine arms in solution. At room temperature,  $\text{Tl}[\text{PhBP}^t\text{Bu}_2(\text{pz})]$  and  $\text{Tl}[\text{PhBP}^t\text{Bu}_2(\text{pz}^{\text{Me}_2})]$  show only a very broad signal at 35 ppm in the  $^{31}\text{P}$  NMR spectrum due to rapid exchange of the phosphines.<sup>19</sup> When cooled to  $-40^\circ\text{C}$ , the two arms can be distinguished as one bound to Tl and one unbound (Figure I.6).<sup>19</sup>

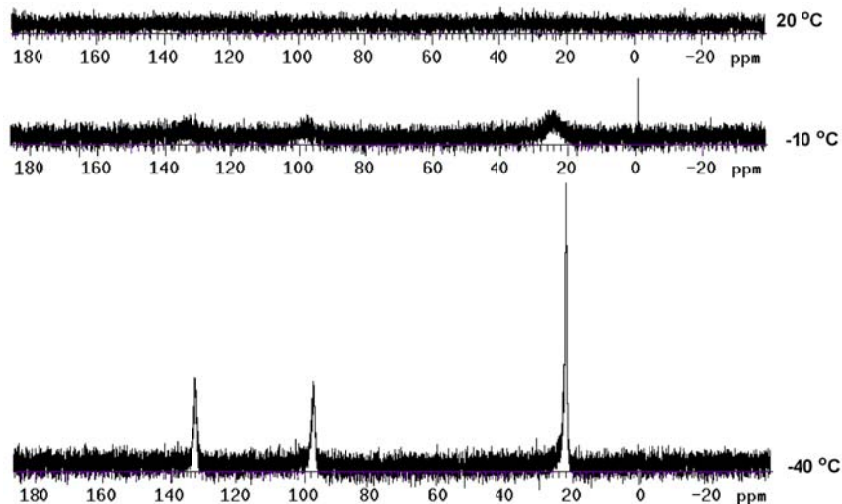


**Figure I.6.** Variable temperature NMR of  $\text{Tl}[\text{PhBP}^{\text{tBu}}_2(\text{pz})]^{19}$

$\text{Tl}[\text{PhBP}^{\text{tBu}}_2(\text{pz}^{\text{tBuPh}})]$  shows 2 signals at room temperature ( $\delta$  113 ( $^1J_{\text{Tl-P}} = 3790$  Hz),  $\delta$  27.5) displaying less rapid exchange of the arms. At room temperature,  $\text{Tl}[\text{PhBP}^{\text{tBu}}_2(\text{pz}^{\text{tBu}})]$  also displays 2 strong signals for the two different phosphines ( $\delta$  117.9 ( $^1J_{\text{Tl-P}} = 4438$  Hz),  $\delta$  24.7), indicating that the phosphine arms are no longer switching rapidly on the NMR time scale, presumably because of the increase in steric bulk (Figure I.7).

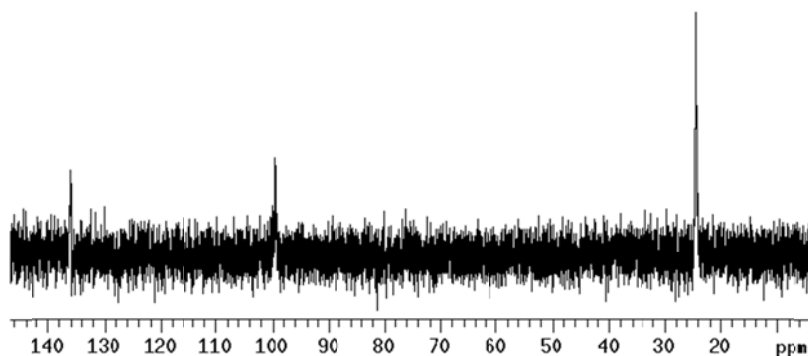
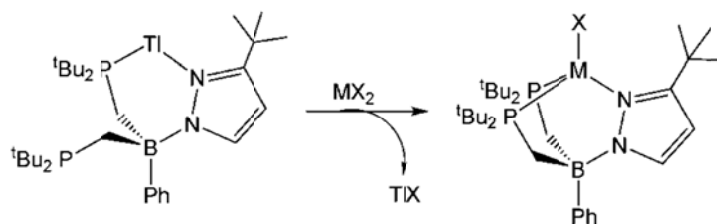


**Figure I.7.**  $^{31}\text{P}$  NMR spectra of  $\text{Tl}[\text{PhBP}^{\text{tBu}}_2(\text{pz}^{\text{tBu}})]$  at room temperature

### I.3.2 $[\text{PhBP}^{\text{tBu}}_2(\text{pz}^{\text{tBu}})]\text{Metal(II)-Halide complexes}$

Reaction of  $\text{Tl}[\text{PhBP}^{\text{tBu}}_2(\text{pz}^{\text{tBu}})]$  with  $\text{FeCl}_2$ ,  $\text{CoI}_2$ , or  $\text{CoCl}_2$  gives conversion in modest yields to the corresponding metal-halide complexes accompanied by loss of  $\text{TlX}$  (Scheme I.5).

#### Scheme I.5



All three complexes were determined to be high-spin using an Evans Method solution magnetic moment determination ( $\mu_B = 5.01$  ( $[\text{PhBP}^{\text{tBu}}_2(\text{pz}^{\text{tBu}})]\text{FeCl}$ ), 4.16 ( $[\text{PhBP}^{\text{tBu}}_2(\text{pz}^{\text{tBu}})]\text{CoCl}$ ), and 4.08 ( $[\text{PhBP}^{\text{tBu}}_2(\text{pz}^{\text{tBu}})]\text{CoI}$ ), with 4 unpaired electrons for the



Fe-complex and 3 unpaired electrons for each Co-complex. Each of the complexes was characterized using cyclic voltammetry and displayed irreversible reduction events at -2.35 V for  $[\text{PhBP}^{\text{tBu}}_2(\text{pz}^{\text{tBu}})]\text{FeCl}$ , -1.56 V for  $[\text{PhBP}^{\text{tBu}}_2(\text{pz}^{\text{tBu}})]\text{CoI}$ , and -1.85 V for  $[\text{PhBP}^{\text{tBu}}_2(\text{pz}^{\text{tBu}})]\text{CoCl}$  versus  $\text{Fc}/\text{Fc}^+$ , respectively. In comparison to  $[\text{PhBP}^{\text{tBu}}_2(\text{pz})]^-$  complexes and  $[\text{PhBP}^{\text{tBu}}_2(\text{pz}^{\text{Me2}})]^-$  complexes, it is seen that the new ligand is presumably similarly electron-releasing, however this cannot be stated with confidence because of the irreversible nature of the observed reduction events (Table I.1). It is notable that for the new Co-complexes, the reduction event is irreversible,<sup>19</sup> whereas for  $[\text{PhBP}^{\text{tBu}}_2(\text{pz})]\text{CoI}$  and  $[\text{PhBP}^{\text{tBu}}_2(\text{pz}^{\text{Me2}})]\text{CoI}$  the reduction events are reversible.

**Table I.1** Reduction Potentials of  $[\text{PhBP}^{\text{tBu}}_2(\text{pz}')]\text{MX}$

Complex	Redox Potential (vs $\text{Fc}/\text{Fc}^+$ )
$[\text{PhBP}^{\text{tBu}}_2(\text{pz}^{\text{tBu}})]\text{FeCl}$	Irrev. -2.35
$[\text{PhBP}^{\text{tBu}}_2(\text{pz}^{\text{tBu}})]\text{CoI}$	Irrev. -1.56
$[\text{PhBP}^{\text{tBu}}_2(\text{pz}^{\text{tBu}})]\text{CoCl}$	Irrev. -1.85
$[\text{PhBP}^{\text{tBu}}_2(\text{pz})]\text{FeCl}$	Irrev. -2.25
$[\text{PhBP}^{\text{tBu}}_2(\text{pz})]\text{CoI}$	Rev. -1.56
$[\text{PhBP}^{\text{tBu}}_2(\text{pz}^{\text{Me2}})]\text{FeCl}$	Irrev. -2.48
$[\text{PhBP}^{\text{tBu}}_2(\text{pz}^{\text{Me2}})]\text{CoI}$	Rev. -1.64

$[\text{PhBP}^{\text{tBu}}_2(\text{pz}^{\text{tBu}})]\text{FeCl}$  was also characterized using X-ray crystallography (Figure I.8). In contrast,  $[\text{PhBP}^{\text{tBu}}_2(\text{pz})]\text{FeCl}$  has been characterized as a dimer in the solid state; the monomeric structure of  $[\text{PhBP}^{\text{tBu}}_2(\text{pz}^{\text{tBu}})]\text{FeCl}$  demonstrates that the ligand has sufficient steric bulk to prevent dimerization. The structure of  $[\text{PhBP}^{\text{tBu}}_2(\text{pz}^{\text{tBu}})]\text{FeCl}$  can be compared with that of  $[\text{PhB}(\text{P}^{\text{tBu}}_2)_2(\text{pz}^{\text{tBuPh}})]\text{FeCl}$ ,<sup>19</sup> which is also a monomer, and it can be seen that the bond distances and angles are similar in the two complexes (Table I.2).

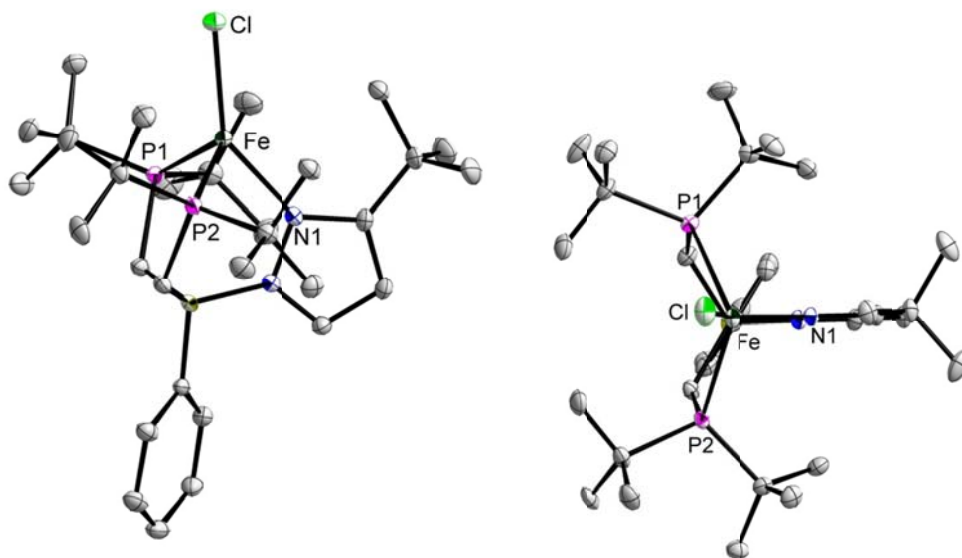


**Figure I.8.** Anisotropically refined thermal ellipsoid representation of  $[\text{PhBP}^{\text{tBu}}_2(\text{pz}^{\text{tBu}})]\text{FeCl}$ ; 2 molecules of toluene and hydrogen atoms omitted for clarity. Fe-N 2.1057(0.0020) Å; Fe-P1 2.4900(0.0009) Å; Fe-P2 2.4787(0.0011) Å; Fe-Cl 2.2645(0.0010) Å; N1-Fe-Cl 141.87(0.06) $^\circ$ ; P1-Fe-P2 112.44(0.04) $^\circ$ ; P1-Fe-N1 88.11(0.06) $^\circ$ ; N1-Fe-P2 87.20(0.06) $^\circ$

**Table I.2** Bond Lengths and Angles for  $[\text{PhB}(\text{CH}_2\text{P}^{\text{tBu}}\text{Bu}_2)_2(\text{pz}^{\text{tBuPh}})]\text{FeCl}$

Bond	Length/Angle
Fe-N	2.1138 (0.0049) Å
Fe-Cl	2.2360 (0.0021) Å
Fe-P1	2.4685 (0.0019) Å
Fe-P2	2.24625 (0.0021) Å
P1-Fe-P2	114.33 (0.07) $^\circ$
P1-Fe-N	87.83 (0.14) $^\circ$
P2-Fe-N	88.49 (0.15) $^\circ$
Cl-Fe-N	139.25 (0.16) $^\circ$

### I.3.3 [ $\text{PhBP}^{\text{tBu}}_2(\text{pz}^{\text{tBu}})]\text{Metal(I)} \text{ Complexes}$

The binding of  $\text{N}_2$  to first-row metal centers is still somewhat rare.<sup>23-24</sup> Despite this, species of this sort are proposed as intermediates in both biological and industrial nitrogen fixation processes and isolation of such complexes is key to determining if they are viable intermediates. Reduction of  $[\text{PhBP}^{\text{iPr}}_3]\text{FeCl}$  or  $[\text{PhBP}^{\text{iPr}}_3]\text{CoI}$  with Na/Hg amalgam or Mg results in the binding of  $\text{N}_2$  as the fourth ligand.<sup>23</sup> In the case of Mg,  $\{[\text{PhBP}^{\text{iPr}}_3]\text{Fe}(\text{N}_2)\} \{\text{MgCl}(\text{THF})_4\}$  and  $\{[\text{PhBP}^{\text{iPr}}_3]\text{Co}(\text{N}_2)\}_2 \{\text{Mg}(\text{THF})_4\}$  are formed, whereas when Na/Hg amalgam is used, the products are  $\{[\text{PhBP}^{\text{iPr}}_3]\text{Fe}\}_2(\mu\text{-N}_2)$  and  $\{[\text{PhBP}^{\text{iPr}}_3]\text{Co}\}_2(\mu\text{-N}_2)$ .<sup>23</sup> Reduction of  $[\text{PhB}(\text{CH}_2\text{P}^{\text{tBu}}_2)(\text{pz}^{\text{tBu}})]\text{FeCl}$  and  $[\text{PhBP}^{\text{tBu}}_2(\text{pz}^{\text{tBu}})]\text{CoCl}$  with Na/Hg amalgam gave no isolable products, which is not surprising given the irreversible nature of the I/II couple. However, reduction of  $[\text{PhBP}^{\text{tBu}}_2(\text{pz}^{\text{tBu}})]\text{CoI}$  with Na/Hg amalgam gave a three-coordinate, planar Co(I) complex where the pyrazole arm is no longer coordinated to the Co-center but rather to a  $\text{Na}^+$  ion (Figure I.9). The data set was of poor quality due to twinning, however was sufficient enough to identify the complex.

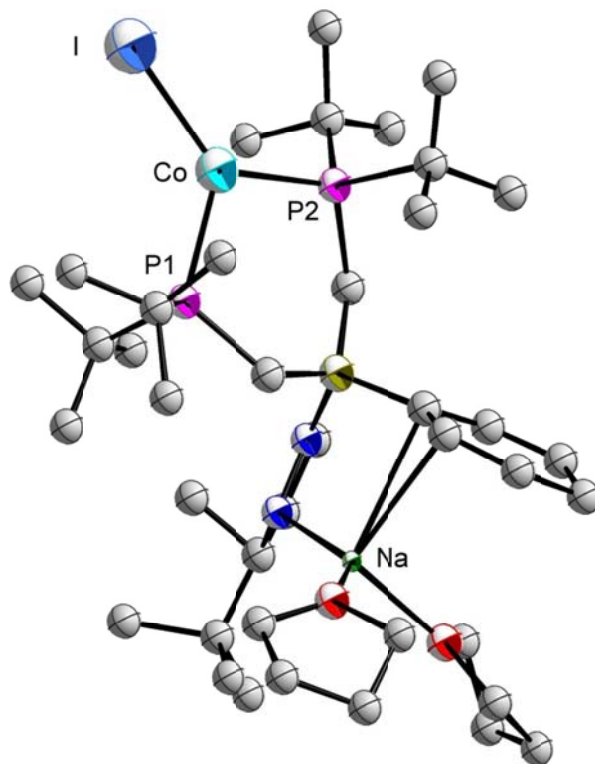


**Figure I.9.** Isotropically refined thermal ellipsoid representation of  $\kappa^2$ -[PhBP<sup>tBu</sup><sub>2</sub>(pz<sup>tBu</sup>)]CoNaI; hydrogen atoms have been omitted for clarity. No bond length and angles are reported due to poor quality of the data set.

An Evans Method solution magnetic moment determination showed that this complex is also high-spin, with  $\mu_B = 2.81$ , corresponding to 2 unpaired electrons. This is not the first time this geometry has been seen for this type of ligand: in an attempt to reduce [PhBP<sup>tBu</sup><sub>2</sub>(pz)]Co(dbabh) (dbabh = 2,3:5,6-dibenzo-7-aza bicyclo[2.2.1]hepta-2,5-diene), a similar structure with an amide in place of the iodide was observed (Figure I.10).<sup>25</sup>

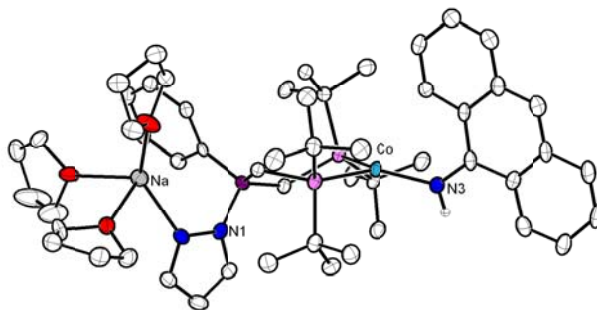
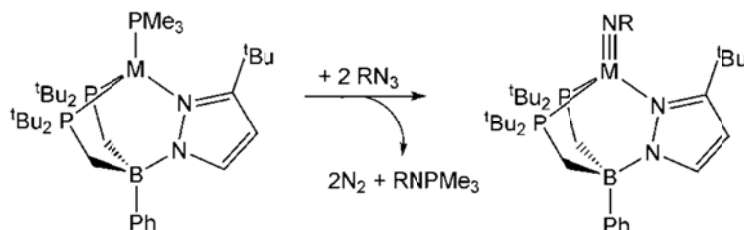


**Figure I.10.**  $\{\kappa^2\text{-[PhBP}^{\text{tBu}}_2(\text{pz})]\text{CoNH}(\text{anthr})\} \{\text{Na}(\text{THF})_3\}^{25}$

One of the strategies used to obtain a M(III)-imide is by “NR” group transfer from an azide to the corresponding M(I) complex (Scheme I.6).<sup>3</sup>

**Scheme I.6**

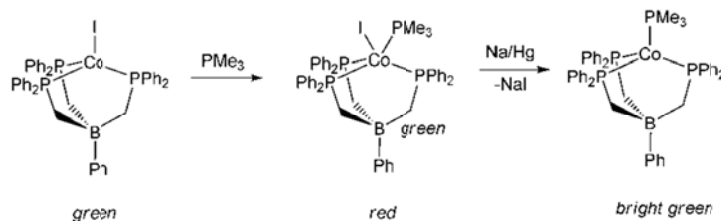


$[\text{PhBP}^{\text{tBu}}_2(\text{pz}^{\text{tBu}})]\text{CoNaI}$  appeared to react cleanly as a Co(I) complex: reaction with  $^{\text{tBu}}\text{N}_3$  gave a diamagnetic complex which was identified as  $[\text{PhBP}^{\text{tBu}}_2(\text{pz}^{\text{tBu}})]\text{CoN}^{\text{tBu}}$  by analogy with similar known complexes of this type, which are diamagnetic and display comparable  $^{31}\text{P}$  NMR signals ( $\delta$  81.1).<sup>3,19</sup>

The  $\text{PMe}_3$  capped species  $[\text{PhBP}_3]\text{CoPMe}_3$  was synthesized by reducing a mixture of the Co(II)-I precursor with Na/Hg amalgam in the presence of  $\text{PMe}_3$ . In this case, the intermediate  $[\text{PhBP}_3]\text{CoI}(\text{PMe}_3)$  adduct could be isolated and characterized.<sup>3</sup> The

formation of this species was clearly observed by color change;  $[\text{PhBP}_3]\text{CoI}$  is green,  $[\text{PhBP}_3]\text{CoI}(\text{PMe}_3)$  is red, and  $[\text{PhBP}_3]\text{Co}(\text{PMe}_3)$  is bright green (Scheme I.7).<sup>3</sup>

### Scheme I.7



The reduction of  $[\text{PhBP}_3]\text{FeCl}$  with Na/Hg amalgam in the presence of  $\text{PPh}_3$  gives  $[\text{PhBP}_3]\text{FePPh}_3$  in good yield.<sup>16</sup> Similarly, reduction of  $[\text{PhBP}^{\text{tBu}}_2(\text{pz}^{\text{tBu}})]\text{FeCl}$  with Na/Hg amalgam in the presence of  $\text{PMe}_3$  gave the  $\text{Fe(I)-PMe}_3$  capped species in good yield. No evidence for  $[\text{PhBP}^{\text{tBu}}_2(\text{pz}^{\text{tBu}})]\text{FeCl}(\text{PMe}_3)$  was observed, likely indicating that the ligand is too sterically bulky to form a 5-coordinate species. An Evans Method determination on  $[\text{PhBP}^{\text{tBu}}_2(\text{pz}^{\text{tBu}})]\text{FePMe}_3$  established that  $\mu_B = 3.90$ , indicating a high-spin configuration. The lime-green complex was characterized using electrochemistry and displayed a quasi-reversible redox event at  $-1.23 \text{ V}$  versus  $\text{Fc}/\text{Fc}^+$ , which became increasingly reversible at faster scan rates (Figure I.11A).

Reduction of  $[\text{PhBP}^{\text{tBu}}_2(\text{pz}^{\text{tBu}})]\text{CoCl}$  with Na/Hg amalgam in the presence of  $\text{PMe}_3$  also gave relatively clean conversion to the  $\text{PMe}_3$ -capped species. Again, no evidence was observed for the formation of the  $\text{Co(II)}$  adduct  $[\text{PhBP}^{\text{tBu}}_2(\text{pz}^{\text{tBu}})]\text{Co}(\text{Cl})(\text{PMe}_3)$ . The turquoise compound was analyzed using electrochemistry. In a similar fashion to  $[\text{PhBP}^{\text{tBu}}_2(\text{pz}^{\text{tBu}})]\text{FePMe}_3$ , a partially reversible redox event was observed at  $-0.90 \text{ V}$  versus  $\text{Fc}/\text{Fc}^+$ , which also became more reversible with faster scan rates (Figure I.11B).

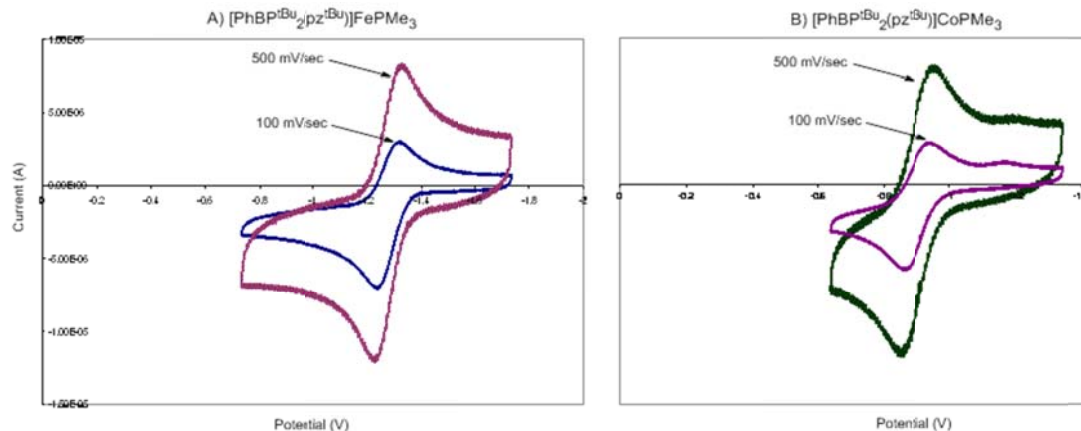


**Figure I.11.** Cyclic voltammetry of A)  $[\text{PhBP}^{\text{tBu}}_2(\text{pz}^{\text{tBu}})]\text{FePMe}_3$  and B)  $[\text{PhBP}^{\text{tBu}}_2(\text{pz}^{\text{tBu}})]\text{CoPMe}_3$  in THF containing 0.4 M TBAPF<sub>6</sub> using a glassy carbon electrode as the working electrode, a Pt wire as the auxiliary electrode, and Ag/AgNO<sub>3</sub> in THF as the reference electrode; plotted vs Fc/Fc<sup>+</sup>

$[\text{PhBP}^{\text{tBu}}_2(\text{pz}^{\text{tBu}})]\text{CoPMe}_3$  was characterized by X-ray diffraction (Figure I.12). A comparison to related Co(I) complexes with other ligand platforms is not possible because none were characterized using X-ray crystallography, however, the solid-state structure of  $[\text{PhBP}^{\text{tBu}}_2(\text{pz}^{\text{Me}_2})]\text{FePMe}_3$  has been elucidated and a broad comparison can be made. The P3-Fe-N bond angle in this complex is significantly less (124.04°) than in  $[\text{PhBP}^{\text{tBu}}_2(\text{pz}^{\text{tBu}})]\text{CoPMe}_3$  (134.38°), presumably because the *tert*-butyl substituent is more sterically demanding. Although  $[\text{PhBP}^{\text{tBu}}_2(\text{pz}^{\text{tBu}})]\text{CoPMe}_3$  was successfully characterized both by single crystal X-ray diffraction and elemental analysis, the <sup>1</sup>H NMR spectrum always contained many more peaks than were expected and these peaks always appeared in the same ratio. The sample was examined using low-temperature NMR, which showed

that at low temperature in toluene- $d_8$ , the expected number of peaks could be observed. It is probable that this is due to lability of an arm of the ligand, most likely the pyrazole arm, at room temperature in benzene- $d_6$ . (Figure I.13).

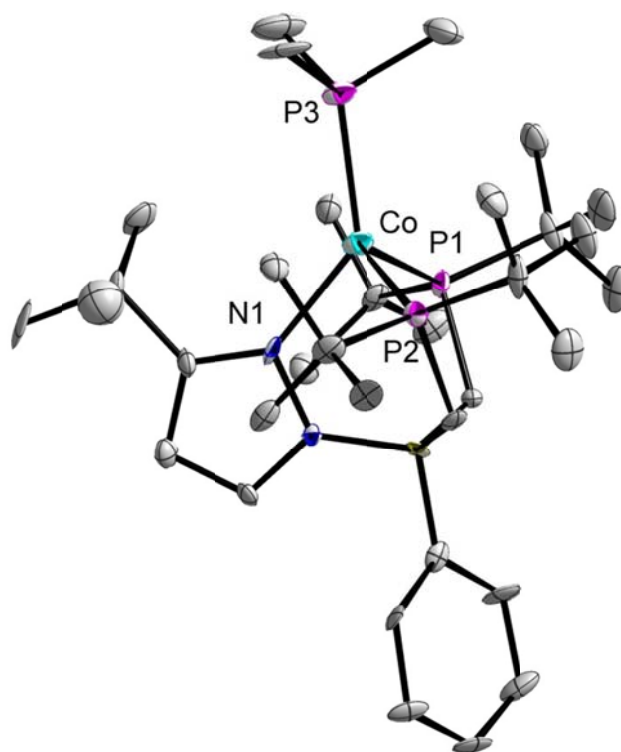


**Figure I.12.** Anisotropically refined thermal ellipsoid representation of  $[\text{PhBP}^{\text{tBu}}_2(\text{pz}^{\text{tBu}})]\text{CoPMe}_3$ ; hydrogen atoms have been omitted for clarity. Co-N1 2.0736(0.0057) Å; Co-P1 2.4260(0.0020) Å; Co-P2 2.4300(0.0020) Å; Co-P3 2.2693(0.0021) Å; N1-Co-P3 134.38 (0.15)°; P1-Co-P2 113.00(0.07)°; P1-Co-N1 89.83(0.15)°; N1-Co-P2 90.51 (0.15)°



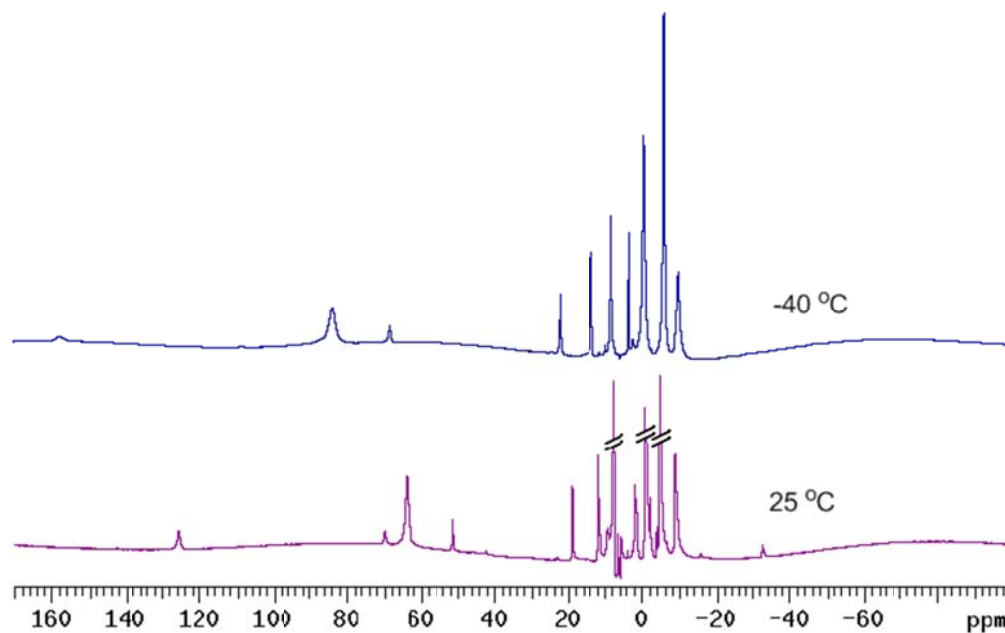


**Figure I.13.**  $^1\text{H}$  NMR spectra of  $[\text{PhBP}^{\text{tBu}}_2(\text{pz}^{\text{tBu}})]\text{CoPMe}_3$  at 25 °C ( $\text{C}_6\text{D}_6$ ) and -40 °C (toluene- $d_8$ )

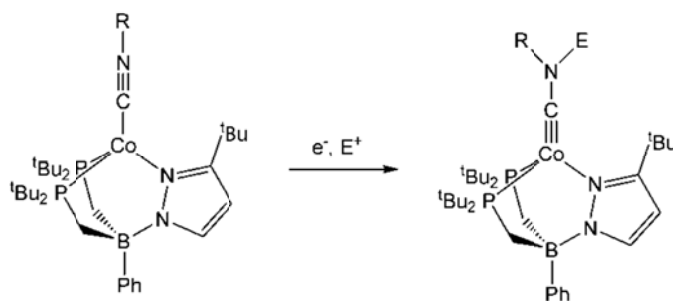
Interestingly, when the same protocol used to obtain  $[\text{PhBP}^{\text{tBu}}_2(\text{pz}^{\text{tBu}})]\text{CoPMe}_3$  was used starting with  $[\text{PhBP}^{\text{tBu}}_2(\text{pz}^{\text{tBu}})]\text{CoI}$ , the reaction gave a much lower yield of the desired product. A second dark blue compound is formed as a byproduct, which X-ray diffraction experiments indicated was most likely to be  $\text{Co(I)(PMe}_3)_3$ , demonstrating that the ligand is more likely to fall off during this reaction using the Co-I starting material than with the Co-Cl complex.

#### *1.3.4 Investigations toward an Fe-carbyne complex*

A potential precursor to a carbyne complex is the mono-isonitrile species  $[\text{PhBP}^{\text{tBu}}_2(\text{pz}^{\text{tBu}})]\text{Co(CNR)}$ , which could be converted to the carbyne via a pathway similar

to that in (Scheme I.8). In an attempt to synthesize a Co-carbyne precursor,  $[\text{PhBP}^{\text{tBu}}_2(\text{pz}^{\text{tBu}})]\text{CoPMe}_3$  was treated with  $\text{CNR}$ , where  $\text{R} = \text{tBu}$  or Ad (Ad = adamantyl). This reaction gave clean conversion to a paramagnetic, tetrahedral Co(I) complex, where instead of the desired exchange of  $\text{PMe}_3$  for isocyanide, the pyrazole arm is displaced (Figure I.14). The desired molecule was also targeted by reduction of  $[\text{PhBP}^{\text{tBu}}_2(\text{pz}^{\text{tBu}})]\text{CoCl}$  in the presence of isocyanide, but this reaction gave no identifiable products (Scheme I.9).

### Scheme I.8



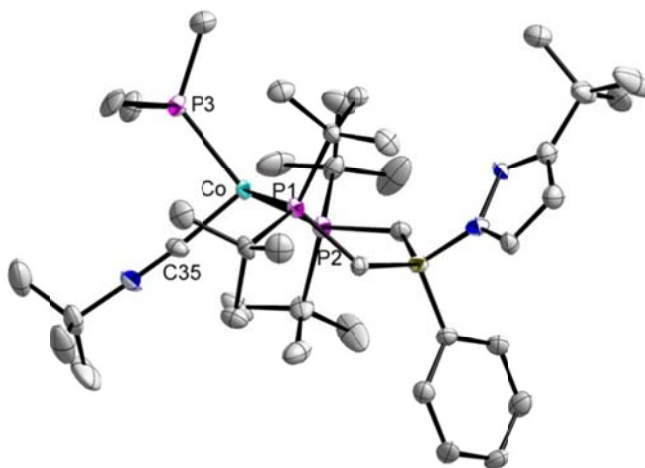
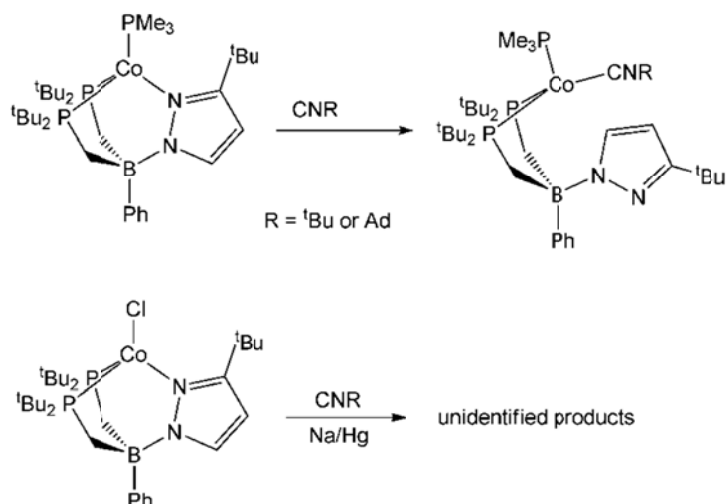


**Figure I.14.** Anisotropically refined thermal ellipsoid representation of  $\kappa^2$ -[PhBP<sup>tBu</sup><sub>2</sub>(pz<sup>tBu</sup>)]Co(PMe<sub>3</sub>)(CN<sup>tBu</sup>); 2 molecules of pentane and hydrogen atoms have been omitted for clarity. Co-C35 1.8707(0.0100) Å; Co-P1 2.3151(0.0032) Å; Co-P2 2.3515(0.0033) Å; Co-P3 2.2884(0.0033) Å; C35-Co-P1 103.08(0.32)°; C35-Co-P2 109.32(0.31)°; C35-Co-P3 91.86(0.33)°; P1-Co-P2 100.45(0.12)°; P1-Co-P3 115.02(0.12)°; P2-Co-P3 133.28(0.11)°

Scheme I.9



### I.3.5 Metal(III)-imide synthesis

One straightforward method of obtaining a M(III)-imide is by group transfer from an alkyl azide to the corresponding M(I) precursor (refer to Scheme I.6). This is the standard procedure used in the Peters' group to synthesize M(III)-imides.<sup>3,16-18</sup> Reaction of  $[\text{PhBP}^{\text{tBu}}_2(\text{pz}^{\text{tBu}})]\text{FePMe}_3$  with  $^t\text{BuN}_3$  gave conversion to  $[\text{PhBP}^{\text{tBu}}_2(\text{pz}^{\text{tBu}})]\text{FeN}^t\text{Bu}$  in modest yield. This compound was characterized by single crystal X-ray diffraction (Figure I.15). This complex is very similar to  $[\text{PhBP}^{\text{tBu}}_2(\text{pz})]\text{FeNAd}$  and  $[\text{PhBP}^{\text{tBu}}_2(\text{pz}^{\text{Me}_2})]\text{FeNAd}$  with an Fe-N bond length of 1.6255 (0.0088) Å and an Fe-N-C bond angle of 168.79 (0.31)°. <sup>19</sup> It is also structurally analogous to  $[\text{PhBP}_3]\text{FeN-}p\text{-tolyl}$ , where the Fe-N-C angle is 169.96(2)° and Fe-N bond length is 1.6578 Å. <sup>16</sup> All of these related Fe(III)-imide complexes are low-spin with  $S = 1/2$ , as determined using the Evans' method or SQUID magnetometry. <sup>16-18</sup> This unusual low-spin tetrahedral Fe(III) arrangement is presumably

due to the strong  $\pi$ -donation from the imide functionality, resulting in high-lying  $d_{xz}$  and  $d_{yz}$  based orbitals.<sup>16</sup> By analogy, it is expected that this new complex will also be low-spin.

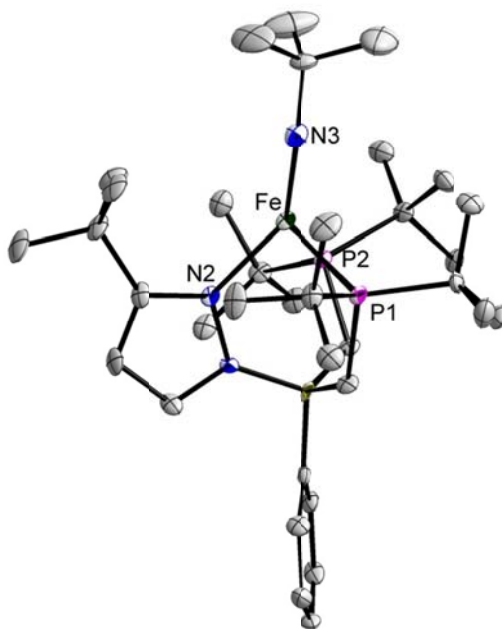


**Figure I.15.** Anisotropically refined thermal ellipsoid representation of  $[\text{PhBP}^{\text{tBu}}_2(\text{pz}^{\text{tBu}})]\text{FeN}^{\text{tBu}}$ ; solvent and hydrogen atoms have been omitted for clarity. Fe-N3 1.7312(0.0040) Å; Fe-N2 2.0327(0.0040) Å; Fe-P2 2.5931(0.0034) Å; Fe-P3 2.3986(0.0038) Å; C10-N3-Fe1 168.79(0.31)°; N2-Fe-N3 140.66(0.15)°; N2-Fe-P2 90.85(0.12)°; P2-Fe-P3 103.86(0.09)°; P3-Fe-N2 88.60(0.12)°

$[\text{PhBP}^{\text{tBu}}_2(\text{pz}^{\text{tBu}})]\text{CoN}^{\text{tBu}}$  was cleanly synthesized from  $[\text{PhBP}^{\text{tBu}}_2(\text{pz}^{\text{tBu}})]\text{CoPMe}_3$  and  $^{\text{tBu}}\text{N}_3$ . This complex is diamagnetic, as are similar Co(III)-imides,<sup>3</sup> and was characterized

by  $^1\text{H}$  and  $^{31}\text{P}$  NMR spectroscopy. This compound was also characterized by X-ray diffraction experiments, however the data set was of poor quality due to a shift in the crystal position during data collection and only connectivity could be determined (not shown). The complex was examined using cyclic voltammetry, but it did not display clean electrochemistry and no obvious oxidation peak was identified. As nothing constructive could be determined from the electrochemistry, oxidation of  $[\text{PhBP}^{\text{tBu}}_2(\text{pz}^{\text{tBu}})]\text{CoN}^{\text{tBu}}$  with  $\text{FcB}(\text{Ar}_\text{F})_4$  ( $\text{B}(\text{Ar}_\text{F})_4 = \text{B}\{3,5-(\text{CF}_3)_2\text{-C}_6\text{H}_3\}_4$ ) and  $\text{FcPF}_6$  at different temperatures were attempted to obtain a Co(IV)-imide, however, all attempts resulted in multiple unidentifiable products.

#### *1.3.6 Synthesis of $[\text{PhBP}^{\text{tBu}}_2(\text{pz}^{\text{tBu}})]\text{FeOSiPh}_3$*

$[\text{PhBP}^{\text{tBu}}_2(\text{pz}^{\text{tBu}})]\text{FeOSiPh}_3$  was made from  $[\text{PhBP}^{\text{tBu}}_2(\text{pz}^{\text{tBu}})]\text{FeCl}$  and  $\text{TiOSiPh}_3$ , as a precursor to an Fe(III) or Fe(IV)-oxo complex. It was characterized by single crystal X-ray diffraction and the connectivity was determined (Figure I.16).

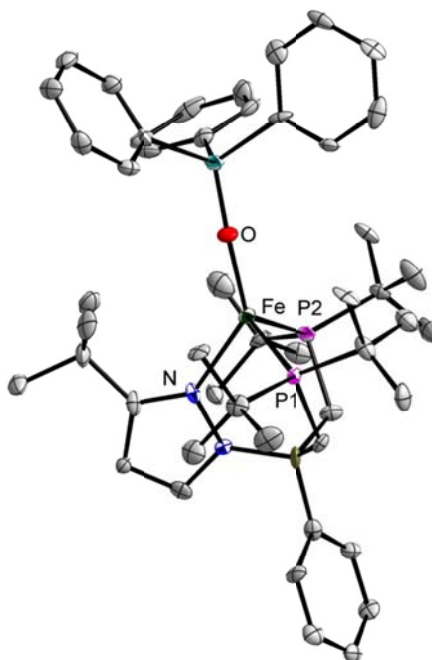
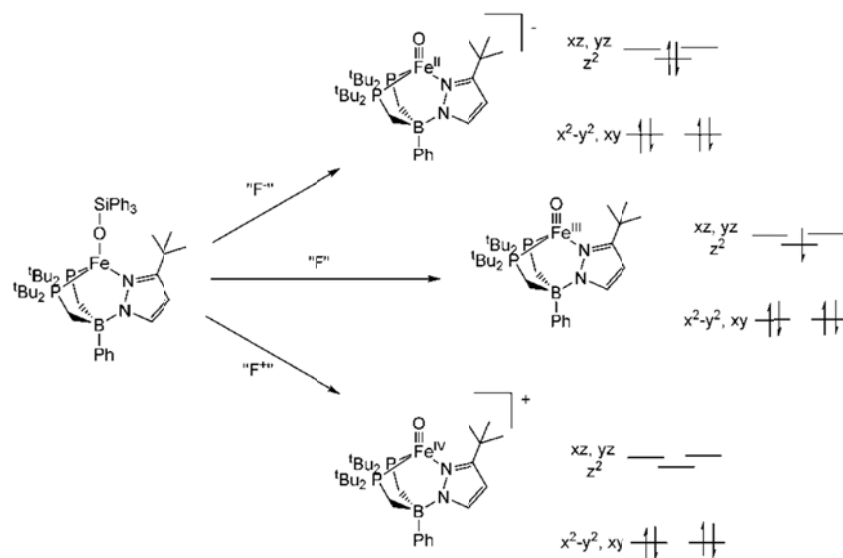


**Figure I.16.** Anisotropically refined thermal ellipsoid representation of  $[\text{PhBP}^{\text{tBu}}_2(\text{pz}^{\text{tBu}})]\text{FeOSiPh}_3$ ; solvent and hydrogen atoms have been omitted for clarity. Fe-O1 1.9710(0.0060) Å; Fe-N1 2.0832(0.0067) Å; Fe-P1 2.5432(0.0043) Å; Fe-P2 2.5457(0.0033) Å; Fe-O1-Si 162.25(0.39)°; N1-Fe-O1 133.32(0.25)°; N1-Fe-P1 88.04(0.19)°; P1-Fe-P2 109.93(0.12)°; P2-Fe-N1 89.04(0.19)°

When  $[\text{PhBP}^{\text{tBu}}_2(\text{pz}^{\text{tBu}})]\text{FeOSiPh}_3$  was treated with a fluoride source such as NaF to prepare an Fe(II)-oxo, no reaction was observed. It is expected that the molecular orbital diagram of the target molecule should be somewhat similar to that calculated for  $[\text{PhBP}^{\text{iPr}}_3]\text{FeN}$ .<sup>21</sup> In this complex, the separation between the lower-lying non-bonding orbitals and the  $\text{dz}^2$  orbital was calculated to be nearly 4 eV, so placing electrons in these

higher orbitals should be highly unfavorable.<sup>21</sup> Thus it might be expected that it is unfavorable to form an Fe(II)O species, which places two electrons in a highly antibonding orbital. If an  $F^\bullet$  source was used, this would go through an Fe(III) with one electron destabilizing the system. In an attempt to bypass these possibly unstable intermediates (Scheme I.10),  $[\text{PhBP}^{\text{tBu}}_2(\text{pz}^{\text{tBu}})]\text{FeOSiPh}_3$  was reacted with  $F^+$  sources (N-fluorobenzene-sulfonamide and 1-fluoro-2,4,6-trimethylpyridinium tetrafluoroborate).<sup>26</sup> Both of these cases, no reaction was observed, even at temperatures up to 60 °C. Despite this, other routes to bypass these intermediates are feasible and should be examined.

**Scheme I.10**

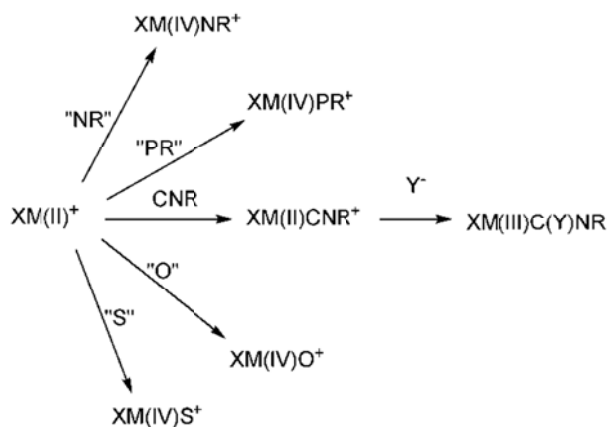


### I.3.7 Cationic complexes

A cationic M(II) complex would be a useful precursor to many target molecules as shown in Scheme I.11 and the electrochemistry of  $[\text{PhBP}^{\text{tBu}}_2(\text{pz}^{\text{tBu}})]\text{M-PMe}_3$  gives hope for isolating this type of complex.



Scheme I.11



In an attempt to make this type of complex,  $[\text{PhBP}^{\text{tBu}}_2(\text{pz}^{\text{tBu}})]\text{FePMe}_3$  was mixed at low temperature with  $\text{FcB}(\text{Ar}_\text{F})_4$ , ( $\text{B}(\text{Ar}_\text{F})_4 = \text{B}\{3,5\text{-(CF}_3)_2\text{-C}_6\text{H}_3\}_4$ ) in THF. To our surprise,  $\text{PMe}_3$  is labile under the reaction conditions and is replaced by THF, resulting in the clean formation of  $\{[\text{PhBP}^{\text{tBu}}_2(\text{pz}^{\text{tBu}})]\text{Fe}(\text{THF})\}[\text{BArF}]$ , the structure of which is shown in Figure I.17. This unexpected ligand replacement may be beneficial as THF should be more easily substituted than a phosphine. Preliminary results show that this complex does not react with either alkyl azides or iodosylbenzene to give the corresponding Fe(IV)-imide and Fe(IV)-oxo species.

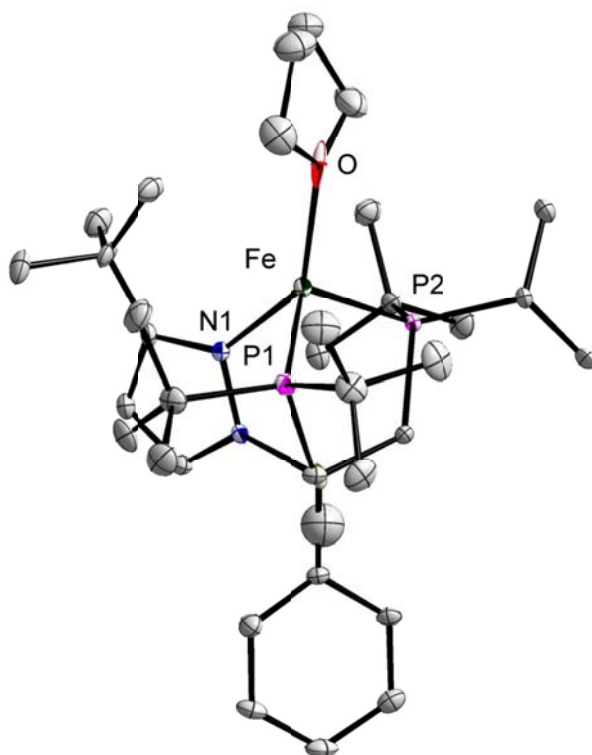


**Figure I.17.** Anisotropically refined thermal ellipsoid representation of  $\{[\text{PhBP}^{\text{tBu}}_2(\text{pz}^{\text{tBu}})]\text{Fe}(\text{THF})\}\{\text{B}(\text{Ar}_\text{F})_4\}$ ; hydrogen atoms and  $\{\text{B}(\text{Ar}_\text{F})_4\}$  have been omitted for clarity. Fe-O 2.1441(0.0040) Å; Fe-N1 2.0604(0.0037) Å; Fe-P1 2.4921(0.0020) Å; Fe-P2 2.4829(0.0021) Å; O-Fe-N1 138.40(0.13) $^\circ$ ; N1-Fe-P1 90.67(0.12) $^\circ$ ; P1-Fe-P2 115.31(0.05) $^\circ$ ; P2-Fe-N1 89.17(0.12) $^\circ$

#### I.4 Conclusions

In this work an array of Fe and Co complexes with the new sterically bulky ligand  $[\text{PhBP}^{\text{tBu}}_2(\text{pz}^{\text{tBu}})]$  were prepared. A number of Fe(II) and Co(II) halide species were synthesized and their electrochemistry reported. These complexes could be reduced to

form  $M(I)\text{-PMe}_3$  complexes in the presence of  $\text{PMe}_3$ , which displayed reversible oxidation events. The  $\text{PMe}_3$  capped complexes were precursors to  $M(III)\text{-imides}$ , which were made as a means to access  $M(IV)\text{-imides}$ . Although the  $M(IV)\text{-imides}$  have not yet been prepared using this synthetic strategy, the test reactions were not exhaustive and many other options are still available. Furthermore, cyclic voltammetry should be carried out on the Fe-derivative to determine whether or not another  $\text{Fe(IV)-imide}$  is feasible. As a possible precursor to and  $\text{Fe(IV)-oxo}$ , an  $\text{Fe(II)-siloxide}$  was synthesized. Among others, a possible route that would utilize this  $\text{Fe(II)}$  precursor to get to the target molecule would be to first oxidize the species, then test for reactivity toward  $\text{F}^+$ ,  $\text{F}$ , and  $\text{F}^-$  sources. Cyclic voltammetry should be carried out to determine whether an  $\text{Fe(III)-siloxide}$  cation is a feasible pathway. Finally, a novel  $\text{Fe(II)}$  cation has been made and a  $\text{Co(II)}$  cation proposed. Both of these complexes could be valuable precursors to many unique complexes containing metal-ligand multiple bonds as displayed in **Scheme 11**. Overall, the complexes prepared in this work form a series of promising precursors to different multiply-bonded species.

## I.5 Experimental Section

**General considerations.** All syntheses were carried out under an  $\text{N}_2$  atmosphere using standard glovebox and Schlenk techniques unless otherwise noted. Benzene, toluene, petroleum ether, diethyl ether, THF, and acetonitrile were sparged with  $\text{N}_2$ , then passed through an activated alumina column. Deuterated benzene was purchased from Cambridge Isotope Laboratories, Inc., and degassed by multiple freeze-pump-thaw cycles, then stored

over molecular sieves. Solvents were tested for moisture and O<sub>2</sub> using a standard solution of sodium benzophenone ketyl in THF.  $\text{Ti}[\text{PhBP}^{\text{tBu}}_2(\text{pz})]$  was prepared according to the literature method.<sup>19</sup> NMR spectra were recorded on Varian Mercury 300 MHz instruments. <sup>1</sup>H and <sup>13</sup>C NMR chemical shifts were referenced to internal residual protio solvent. <sup>31</sup>P NMR chemical shifts were externally referenced to 85% H<sub>3</sub>PO<sub>4</sub> in D<sub>2</sub>O. IR spectra were recorded on a Bio-Rad Excalibur FTS 3000 spectrometer using Win-IR Pro software. X-ray diffraction experiments were carried out in the Beckman Institute Crystallographic Facility on a Bruker Smart 1000 CCD diffractometer. Electrochemical measurements were carried out in a glovebox under an N<sub>2</sub> atmosphere using a CH Instruments electrochemical analyzer. A glassy carbon electrode, platinum wire, and Ag/AgNO<sub>3</sub> in THF were used as the working, auxiliary, and reference electrodes. UV-Vis spectra were recorded on a Cary 50 Bio UV-visible spectrophotometer. Elemental analyses were done by Desert Analytics, Tucson, AZ.

**$\text{Ti}[\text{PhBP}^{\text{tBu}}_2(\text{pz}^{\text{tBu}})]$  (1).** Solid 3-*tert*-butyl pyrazole (0.486 g, 3.91 mmol) was dissolved in Et<sub>2</sub>O (125 mL) in a 250 mL Erlenmeyer flask and then cooled to -78 °C. At this temperature, *n*BuLi (2.69 mL, 1.6 M solution in hexanes, 4.30 mmol) was added dropwise with stirring, and the solution was allowed to warm to room temperature and stirred for 1 hour.  $\text{PhB}(\text{CH}_2\text{P}^{\text{tBu}}\text{Bu}_2)_2$  (1.59 g, 3.91 mmol) was dissolved in 30 mL of Et<sub>2</sub>O and added to the reaction mixture, which was then stirred for 18 hours. This was followed by the addition of TIPF<sub>6</sub> (1.37 g, 3.91 mmol) dissolved in 30 mL of THF, and the reaction mixture was stirred for an additional hour. The reaction mixture was then filtered through

Celite and the volatiles were removed in vacuo. The remaining solids were washed with MeCN (2 x 12 mL), petroleum ether (5 mL), and dried in vacuo to give a white powder (1.18 g, 1.61 mmol, 41%).  $^1\text{H}$  NMR (300 MHz,  $\text{C}_6\text{D}_6$ ):  $\delta$  8.08 (br, 2H, *o*-Ph), 7.26 (br, 1H, *p*-Ph), 7.1-7.0 (br, 2H, *m*-Ph), 6.71 (br, 1H, pz-3), 6.20 (s, 1H, pz-4), 1.74 (m, 4H,  $\text{CH}_2$ ), 1.42 (d, 18H,  $^3J_{\text{P-H}} = 9.9$  Hz,  $^t\text{Bu-P}$ ), 1.33 (s, 9H,  $^t\text{Bu-pz}$ ), 1.21 (d, 18H,  $^3J_{\text{P-H}} = 11.4$ ,  $^t\text{Bu-P}$ ), 0.85 (d, 18H,  $^3J_{\text{P-H}} = 10.2$ ,  $^t\text{Bu-P}$ ) 0.76 (d, 18H,  $^3J_{\text{P-H}} = 11.4$ ,  $^t\text{Bu-P}$ ).  $^{31}\text{P}\{^1\text{H}\}$  NMR (121.5 MHz,  $\text{C}_6\text{D}_6$ ):  $\delta$  117.9 (d, 1P,  $^1J_{\text{Ti-P}} = 4438$  Hz, coordinated), 24.7 (s, 1P, uncoordinated). Anal. Calcd. for  $\text{C}_{31}\text{H}_{56}\text{BN}_2\text{P}_2\text{Ti}$ : C, 50.73; H, 7.69; N, 3.82. Found: C, 50.55; H, 7.39; N, 3.78.

**[PhBP $^t\text{Bu}_2(\text{pz}^{t\text{Bu}})]\text{FeCl}$  (2).** Solid (1) (0.500 g, 0.681 mmol) was dissolved in 10 mL of THF.  $\text{FeCl}_2$  (0.086 g, 0.68 mmol) was added to the stirring solution as a slurry (5 mL THF) and the reaction mixture was allowed to stir for 12 hours. The resulting cloudy white mixture was filtered through Celite to remove  $\text{TiCl}$  and the volatiles were removed in vacuo. The remaining solids were extracted with 15 mL of benzene, filtered, and the solution was lyophilized. The resulting solids were then extracted with 12 mL of toluene and the solution filtered. The solution was concentrated in vacuo and placed in the freezer at  $-35$   $^\circ\text{C}$  overnight to give colorless crystals (0.25 g, 0.41 mmol, 60%).  $^1\text{H}$  NMR (300 MHz,  $\text{C}_6\text{D}_6$ ):  $\delta$  227.3, 57.7, 24.9, 13.6, 12.7, 12.4, 5.0, -2.8, -31.4. Evans Method ( $\text{C}_6\text{D}_6$ , 295 K): 5.01  $\mu\text{B}$ . UV-Vis ( $\text{C}_6\text{H}_6$ ):  $\lambda_{\text{max}}$ , nm, ( $\epsilon$ ): 367 (1277), 872 (211). Anal. Calcd. for  $\text{C}_{31}\text{H}_{56}\text{BClFeN}_2\text{P}_2$ : C, 59.97; H, 9.09; N, 4.51. Found: C, 60.08; H, 9.05; N, 4.64.

**[PhBP<sup>t</sup>Bu<sub>2</sub>(pz<sup>tBu</sup>)]CoI (3).** Solid (1) (0.535 g, 0.729 mmol) was dissolved in 10 mL of THF. CoI<sub>2</sub> (0.228 g, 0.729 mmol) was added to the stirring solution as a slurry (5 mL THF) and the reaction mixture was allowed to stir for 12 hours. The resulting greenish yellow mixture was filtered through Celite to remove yellow TII and the volatiles were removed in vacuo. The remaining solids were extracted with 15 mL of benzene, filtered, and the solution was lyophilized. These solids were extracted with 12 mL of toluene and the solution filtered. The solution was concentrated in vacuo and placed in the freezer at -35 °C overnight to give dark green crystals (0.427 g, 0.595 mmol, 82%). <sup>1</sup>H NMR (300 MHz, C<sub>6</sub>D<sub>6</sub>): δ 75.1, 47.4, 21.8, 21.4, 11.5, 10.1, 4.0, -2.6, -30.8. Evans Method (C<sub>6</sub>D<sub>6</sub>, 295 K): 4.16 μ<sub>B</sub>. UV-Vis (C<sub>6</sub>H<sub>6</sub>): λ<sub>max</sub>, nm, (ε): 365 (2549), 463 (392), 592 (488), 659 (482), 709 (346), 871 (150).

**[PhBP<sup>t</sup>Bu<sub>2</sub>(pz<sup>tBu</sup>)]CoCl (4).** Solid (1) (0.500 g, 0.681 mmol) was dissolved in 10 mL of THF. CoCl<sub>2</sub> (0.089 g, 0.68 mmol) was added to the stirring solution as a slurry (5 mL THF) and the reaction mixture was allowed to stir for 12 hours. The cloudy blue mixture was filtered through Celite to remove white TiCl and the volatiles were removed in vacuo. The remaining solids were extracted with 15 mL of benzene, filtered, and the solution was lyophilized. These solids were extracted with 12 mL of toluene and the solution filtered. The solution was concentrated in vacuo and placed in the freezer at -35 °C overnight to give colorless crystals (0.165 g, 2.63 mmol, 39%). <sup>1</sup>H NMR (300 MHz, C<sub>6</sub>D<sub>6</sub>): δ 74.6, 48.9, 18.3, 10.5, 9.1, 8.9, 5.4, 2.1, -18.4. Evans Method (C<sub>6</sub>D<sub>6</sub>, 295 K): 4.08 μ<sub>B</sub>. UV-Vis

(C<sub>6</sub>H<sub>6</sub>):  $\lambda_{\text{max}}$ , nm, ( $\epsilon$ ): 416 (386), 569 (475), 608 (476), 703 (408), 873 (341). Anal.

Calcd. for C<sub>31</sub>H<sub>56</sub>BClCoN<sub>2</sub>P<sub>2</sub>: C, 59.67; H, 9.05; N, 4.49. Found: C, 59.60; H, 9.27; N, 4.49.

**[PhBP<sup>t</sup>Bu<sub>2</sub>(pz<sup>tBu</sup>)]FePMe<sub>3</sub> (5).** Solid (2) (0.150 g, 0.242 mmol) was dissolved in 10 mL of THF and PMe<sub>3</sub> (75.0  $\mu$ L, 0.725 mmol) was added to this solution. The solution was added to a stirring Na/Hg amalgam (0.5%, 0.0061 g Na, 1.22 g Hg, 0.26 mmol) in 5 mL of THF. The reaction mixture was stirred for 3 hours, filtered through Celite and the volatiles were removed in vacuo. The remaining solids were extracted with petroleum ether (20 mL) and the solution filtered. The solution was concentrated and stored overnight at -35 °C to give lime-green crystals (0.088 g, 0.13 mmol, 55%). <sup>1</sup>H NMR (300 MHz, C<sub>6</sub>D<sub>6</sub>):  $\delta$  219.3, 58.0, 36.1, 16.3, 12.5, 10.7, 8.9, 2.0, -22.9, -41.8. Evans Method (C<sub>6</sub>D<sub>6</sub>, 295 K): 3.90  $\mu$ B. Anal. Calcd. for C<sub>34</sub>H<sub>65</sub>BCoN<sub>2</sub>P<sub>3</sub>: C, 61.74; H, 9.90; N, 4.24. Found: C, 61.94; H, 10.12; N, 4.41.

**[PhBP<sup>t</sup>Bu<sub>2</sub>(pz<sup>tBu</sup>)]CoPMe<sub>3</sub> (6).** Solid (4) (0.150 g, 0.240 mmol) was dissolved in 10 mL of THF and PMe<sub>3</sub> (74.7  $\mu$ L, 0.721 mmol) was added to this solution. The solution was added to a stirring Na/Hg amalgam (0.5%, 0.0061 g Na, 1.22 g Hg, 0.26 mmol) in 5 mL of THF. The reaction mixture was stirred for 3 hours, filtered through Celite and the volatiles were removed in vacuo. The remaining solids were extracted with petroleum ether (20 mL) and the solution filtered. The solution was concentrated and stored overnight at -35 °C to give teal crystals (0.089 g, 0.13 mmol, 56%). <sup>1</sup>H NMR (300 MHz, C<sub>6</sub>D<sub>6</sub>, -45.33 °C):  $\delta$

155.5, 81.9, 66.8, 20.9, 12.3, 12.0, 2.1, -1.9, -7.0, -11.1. Anal. Calcd. for  $C_{34}H_{65}BCoN_2P_3$ : C, 61.45; H, 9.86; N, 4.22. Found: C, 61.21; H, 9.50; N, 4.09.

**[PhBP<sup>t</sup>Bu<sub>2</sub>(pz<sup>tBu</sup>)]CoNaI (7).** Solid (3) (0.155 g, 0.216 mmol) was dissolved in 10 mL of THF. This solution was added to a stirring Na/Hg amalgam (0.5%, 0.0130 g Na, 2.60 g Hg, 0.24 mmol) in 5 mL of THF. The reaction mixture was stirred for 2 hours, filtered through Celite and the volatiles were removed in vacuo. The remaining solids were dissolved in a minimal amount of THF (2.5 mL). This solution was layered with petroleum ether (5 mL) and stored at -35 °C overnight to give line-green crystals (0.11 g, 70 %). <sup>1</sup>H NMR (300 MHz, C<sub>6</sub>D<sub>6</sub>): δ 140.1, 65.6, 19.0, 11.7, 8.0, 5.6, 0.2, -2.9, -7.8. Evans Method (C<sub>6</sub>D<sub>6</sub>, 295 K): 2.81 μ<sub>B</sub>. Anal. Calcd. for  $C_{31}H_{56}BCoINa_2P_2$ : C, 50.43; H, 7.64; N, 3.79. Found: C, 49.35; H, 7.93; N, 3.36.

**[PhBP<sup>t</sup>Bu<sub>2</sub>(pz<sup>tBu</sup>)]CoN<sup>t</sup>Bu (8).** Solid (6) (0.179 g, 0.269 mmol) was dissolved in 15 mL of C<sub>6</sub>H<sub>6</sub>. Neat <sup>t</sup>BuN<sub>3</sub> (0.053 g, 0.54 mmol) was added to the solution and stirred for 1 hour. The solution was then lyophilized to give a dark blue-purple powder. Crystals suitable for X-ray diffraction were grown from a petroleum ether/toluene mixture (0.097 g, 55%). <sup>1</sup>H NMR (300 MHz, C<sub>6</sub>D<sub>6</sub>): δ 7.87 (d, 2H, <sup>3</sup>J<sub>H-H</sub> = 6.6 Hz, *o*-PhB), 7.44 (t, 2H, <sup>3</sup>J<sub>H-H</sub> = 7.5 Hz, *m*-PhB), 7.29 (m, 1H, <sup>3</sup>J<sub>H-H</sub> = 6.9, *p*-PhB), 6.9 (br, 1H, pz-3), 6.14 (d, 1H, <sup>3</sup>J<sub>H-H</sub> = 2.4 Hz, pz-4), 1.92 (s, 9H, <sup>t</sup>Bu), 1.48 (d, 18H, <sup>3</sup>J<sub>P-H</sub> = 11.7 Hz, <sup>t</sup>Bu), 1.14 (d, 18H, <sup>3</sup>J<sub>P-H</sub> = 11.1 Hz, <sup>t</sup>Bu), 0.97 (s, 9H, <sup>t</sup>Bu), 0.46 (m, 4H, CH<sub>2</sub>). <sup>31</sup>P{<sup>1</sup>H} NMR (121.5 MHz, C<sub>6</sub>D<sub>6</sub>): δ 81.1. Anal. Calcd. for  $C_{35}H_{65}BCoN_3P_2$ : C, 63.73; H, 9.93; N, 6.37. Found: C, 63.73; H, 10.03; N, 6.34.



**[PhBP<sup>t</sup>Bu<sub>2</sub>(pz<sup>tBu</sup>)]FeOSiPh<sub>3</sub> (9).** Solid (2) (0.233 g, 0.375 mmol) was dissolved in 40 mL of THF. TIOSiPh<sub>3</sub> was added as a slurry in 10 mL of THF and the mixture was stirred overnight. The resulting milky solution was filtered through Celite and the volatiles were evaporated in vacuo. The resulting solids were extracted with toluene, filtered, and the solution was concentrated in vacuo. The resulting solution was then layered with petroleum ether and stored at -35 °C overnight to give white crystals suitable for X-ray diffraction (0.098 g, 42%). *Partially characterized by:* <sup>1</sup>H NMR (300 MHz, C<sub>6</sub>D<sub>6</sub>): δ 58.1, 35.0, 32.4, 29.4, 15.9, 15.3, 12.6, 9.3, 5.4, 1.0, 02.9, -13.1, -30.8, -38.0, -131.5.

**{[PhBP<sup>t</sup>Bu<sub>2</sub>(pz<sup>tBu</sup>)]Fe(THF)}{BArF-24} (10).** Solid (5) (0.100g, 0.151 mmol) was dissolved in 8 mL of THF and cooled to -35 °C. FcBArF-24 (0.159 g, 0.151 mmol) was dissolved, separately, in 8 mL of THF and also cooled to -35 °C. The two solutions were mixed thoroughly and the volatiles were removed in vacuo immediately. The remaining yellow oil was washed with petroleum ether (3 x 5 mL) and then redissolved in 4 mL of THF. This solution was then layered with 12 mL of petroleum ether and left at -35 °C for 48 hours to yield yellow crystals suitable for x-ray diffraction (0.076 g, 33%). *Partially characterized by:* <sup>1</sup>H NMR (300 MHz, C<sub>6</sub>D<sub>6</sub>): δ 94.0, 82.2, 59.4, 42.6, 25.1, 22.8, 17.6, 11.0, 9.0, 8.0, 3.5, 1.4, -33.7. Anal. Calcd. for C<sub>35</sub>H<sub>65</sub>BCoN<sub>3</sub>P<sub>2</sub>: C, 52.92; H, 5.04; N, 1.84. Found: C, 52.77; H, 5.39; N, 2.02.

**[PhBP<sup>t</sup>Bu<sub>2</sub>(pz<sup>Me2</sup>)]CoI (11).** Solid Tl[PhBP<sup>t</sup>Bu<sub>2</sub>(pz<sup>Me2</sup>)] (0.500 g, 0.681 mmol) was dissolved in 10 mL of THF. CoI<sub>2</sub> (0.089 g, 0.68 mmol) was added to the stirring solution as a slurry (5 mL THF) and the reaction mixture was allowed to stir for 12 hours. The

cloudy green mixture was filtered through Celite to remove yellow TII and the volatiles were removed in vacuo. The remaining solids were extracted with 15 mL of benzene, filtered, and the solution was lyophilized. These solids were extracted with 12 mL of toluene and the solution filtered. The solution was concentrated in vacuo and placed in the freezer at -35 °C overnight to give dark green crystals. *Partially characterized by:*  $^1\text{H}$  NMR (300 MHz,  $\text{C}_6\text{D}_6$ ):  $\delta$  65.1, 48.9, 33.6, 22.5, 19.1, 10.9, 8.6, 7.9, -31.2.

## I.6 References

- 1) Nugent, W.A.; Mayer, J.M. *Metal-Ligand Multiple Bonds*; John Wiley and Sons: New York, 1988.
- 2) Costas, M.; Mehn, M.P.; Jensen, M.P.; Que, L., Jr. *Chem. Rev.*, **2004**, *104*, 939.
- 3) Jenkins, D.M.; Betley, T.A.; Peters, J.C. *J. Am. Chem. Soc.*, **2002**, *124*, 11238.
- 4) Woo, L.K. *Chem. Rev.*, **1993**, *93*, 1125.
- 5) Glueck, D.S.; Hollander, F.J.; Bergman, R.G. *J. Am. Chem. Soc.*, **1989**, *111*, 2719.
- 6) Glueck, D.S.; Wu, J.; Hollander, F.J.; Bergman, R.G. *J. Am. Chem. Soc.*, **1991**, *113*, 2041.
- 7) Hay-Motherwell, R.S.; Wilkinson, G.; Hussain-Bates, B.; Hursthouse, M.B. *Polyhedron*, **1993**, *12*, 2009.
- 8) MacBeth, C.A.; Golombek, A.P.; Young, V.G. Jr.; Yang, C.; Kuczera, K.; Hendrich, M.P.; Borovik, A.S. *Science*, **2000**, *289*, 938.
- 9) Lange, S.J.; Miyake, H.; Que, L. Jr. *J. Am. Chem. Soc.*, **1999**, *121*, 6330.
- 10) Meunier, B.; de Visser, S.P.; Shaik, S. *Chem. Rev.*, **2004**, *104*, 3947.

- 11) Gross, Z.; Nimri, S. *Inorg. Chem.*, **1994**, *33*, 1731.
- 12) De Oliveira, F.T.; Chanda, A.; Banerjee, D.; Shan, X.; Mondal, S.; Que, L, Jr.; Bominaar, E.L.; Münck, E.; Collins, T.J. *Science*, **2007**, *315*, 835.
- 13) Bukowski, M.R.; Koehntop, K.D.; Stubna, A.; Bominaar, E.L.; Halfen, J.A.; Münck, E.; Nam, W.; Que, L., Jr. *Science*, **2005**, *310*, 1000.
- 14) Verma, A.K.; Nazif, T.N.; Achim, C.; Lee, S.C. *J. Am. Chem. Soc.*, **2000**, *122*, 11013.
- 15) Mindiola, D.J.; Hillhouse, G.L. *J. Am. Chem. Soc.*, **2001**, *123*, 4623.
- 16) Brown, S.D.; Betley, T.A.; Peters, J.C. *J. Am. Chem. Soc.*, **2003**, *125*, 322.
- 17) Brown, S.D.; Peters, J.C. *J. Am. Chem. Soc.*, **2005**, *127*, 1913.
- 18) Thomas, C. M.; Mankad, N. P.; Peters, J. C. *J. Am. Chem. Soc.*, **2006**, *128*, 4956.
- 19) Thomas, C.M. “Novel Reactivity at Iron Centers Supported by Poly(phosphino)borate Ligands.” Thesis: *Doctor of Philosophy*, California Institute of Technology, Pasadena, CA, May 8, 2006.
- 20) Crevier, T.J.; Lovell, S.; Mayer, J.M. *J. Am. Chem. Soc.*, **1998**, *120*, 6607.
- 21) Betley, T. A.; Peters, J. C. *J. Am. Chem. Soc.*, **2004**, *126*, 6252.
- 22) Peters, J.C.; Feldman, J.D.; Tilley, T.D. *J. Amer. Chem. Soc.*, **1999**, *121*, 9871.
- 23) Barney, A.A.; Heyduk, A.F.; Nocera, D.G. *Chem. Commun.* **1999**, 2379.
- 24) Betley, T.A.; Peters, J.C. *J. Am. Chem. Soc.*, **2003**, *125*, 10782.
- 25) MacKay, B.A.; Fryzuk, M.D. *Chem. Rev.*, **2004**, *104*, 385.
- 26) Thomas, C.M.; Peters, J.C. *Unpublished results*.

- 27) Hull, K.L.; Anani, W.Q.; Sanford, M.S. *J. Am. Chem. Soc.*, **2006**, *128*, 7134.

